

Design, Synthesis, Characterization and Application of Fluorescent Organic Nanoparticles for Live *In Vitro/In Vivo* Bioimaging

A THESIS
SUBMITTED FOR THE DEGREE OF
DOCTOR OF PHILOSOPHY
IN CHEMISTRY

BY
E. RAMANJANEYA REDDY



Dr. Reddy's Institute of Life Sciences
University of Hyderabad Campus
Gachibowli, Hyderabad 500 046, India

December 2015

Dedicated to 2014 Nobel Laureates



Eric Betzig



Stefan W. Hell



William E. Moerner

Table of contents

	Page No.
Declaration	i
Certificate	ii
Acknowledgements	iii
Synopsis	v
Abbreviations	xi
General information	xv
Chapter 1: Introduction to Fluorescent Nano-Bioimaging	1-26
1.1 Introduction to bioimaging	3
1.2 Historical perspective of bioimaging and fluorescence microscope	4
1.3 Introduction to fluorophore	6
1.4 Advantages of fluorescence microscope	12
1.5 Areas of improvement of fluorescent bioimaging	13
1.6 Classification of fluorophores	14
1.7 Model organisms for <i>in vivo</i> imaging studies	17
1.8 Layout of the thesis	20
1.9 References	22
Chapter 2: Selective Multicolour Imaging of Zebrafish Muscle Fibres Using Fluorescent Organic Nanoparticles	27-64
2.1 Abstract	29
2.2 Introduction	29
2.3 Results and discussion	31
2.4 Optical properties of PPy and GPy	33
2.5 Photophysics of pyrene excimers formation	36
2.5.1 PPy excimer formation studies	37
2.6 Morphology studies	40
2.7 Comparative optical studies of PPy bulk and PPy nanoparticles	41
2.8 Applications of PPy FONS for bioimaging	43
2.9 Photostability studies of PPy nanoparticles	44
2.10 Conclusions	46

2.11 Experimental section	47
2.11.1 Materials and methods	47
2.11.2 Nanoparticles preparation for biological studies	47
2.11.3 Nanoparticles preparation for SEM and AFM studies	47
2.11.4 Nanoparticles exposure to cells	48
2.11.5 Nanoparticles exposure to zebrafish embryos	48
2.11.6 PPy and GPy synthesis	48
2.12 References	52
2.13 Appendix	55
2.14 NMR spectra of synthesized compounds	59

Chapter 3: Red Fluorescent Organic Nanoparticles for

Real Time *In Vitro* and *In Vivo* Bioimaging

3.1 Abstract	67
3.2 Introduction	67
3.3 Results and discussion	69
3.4 Photophysical properties of Cy-Red	73
3.4.1 Overcoming of Cy-Red solubility issue	73
3.4.2 Optical properties	74
3.4.3 Photostability studies of Cy-Red fluorophore	76
3.5 Morphology and stability studies	77
3.6 Application of Cy-Red FONs for bioimaging	80
3.6.1 Toxicity studies of nano-Cy-Red	80
3.6.2 DNA binding study	81
3.6.3 Mouse macrophage, human oral cancer and metastatic breast cancer cells staining	82
3.6.4 Tracking transplanted cells in live animal	84
3.6.5 Yeast staining	86
3.7 Conclusions	88
3.8 Experimental section	89
3.8.1 Materials and methods	89
3.8.2 Improvement of Cy-Red solubility	90
3.8.2.1 Salt formation using hydrobromic acid	90

3.8.2.2 Complexation with citric acid	90
3.8.3 Nanoparticle preparation for biological studies	90
3.8.4 Nanoparticles preparation for SEM and AFM studies	90
3.8.5 Nanoparticles stability by dynamic light scattering studies	91
3.8.6 Nanoparticles exposure to yeast cells	91
3.8.6.1 Nano-Cy-Red and calcofluor staining	91
3.8.6.2 Nano-Cy-Red and DAPI staining	91
3.8.7 Nanoparticles exposure to mouse macrophage cells	92
3.8.8 Nanoparticles exposure to oral cancer cells	92
3.8.9 Nanoparticles exposure to metastatic breast cancer cells	92
3.8.10 Nanoparticles exposure to zebrafish embryos	92
3.8.11 Nano-Cy-Red in tracking cancer cells using zebrafish as a model organism	93
3.8.12 Differentiation of cell nature by flow cytometry	93
3.8.13 Preparation of red fluorescent tag	94
3.8.14 Cy-Red synthesis (route-I)	96
3.8.15 Cy-Red synthesis (route-II)	99
3.9 References	103
3.10 Appendix	106
3.10.1 Cytotoxicity evaluation against mouse macrophage cells	106
3.10.2 Differentiation of stained and unstained cells using flow cytometry	106
3.10.3 Transplantation of MDA-MB-231 cells in zebrafish embryos	107
3.11 NMR spectra of synthesized compounds	108

Chapter 4: Novel Fluorescent 3, 5 and 5'-Substituted Nucleosides

Derivatives with Selective Antibacterial Activity	119-192
4.1 Abstract	121
4.2 Introduction	121
4.3 Results and discussion	123
4.4 Optical studies	129
4.5 Evaluation of anti-mycobacterial properties	132
4.6 Cytotoxicity evaluation against host cells	133

4.7 Antibacterial studies	133
4.8 Bacterial staining and microscopy studies using 2.4	134
4.9 Investigation of the mechanism of antibacterial activity of 2.4	136
4.10 Docking study of 2.4 with Taq DNA Pol	139
4.11 Examination of binding ability of 2.4 to Taq DNA Pol	140
4.12 Morphology studies	144
4.13 Conclusions	145
4.14 Experimental section	146
4.14.1 Materials and methods	146
4.14.2 Nanoparticles preparation for biological studies	146
4.14.3 Nanoparticles preparation for SEM and AFM studies	147
4.14.4 <i>In vitro</i> anti-mycobacterial assay (<i>Mtb</i> pathogenic <i>H37Rv</i>)	147
4.14.5 Cytotoxicity assay	147
4.14.6 Bacterial MIC assay	147
4.14.7 Bacterial growth assay	148
4.14.8 Bacterial staining protocol	148
4.14.9 Effect of 2.4 on polymerase chain reaction	148
4.14.10 Docking study	149
4.14.11 Synthesis of fluorescent intermediates	149
4.14.12 Synthesis of 3-substituted uridine analogue	152
4.14.13 Synthesis of 3-substituted thymidine analogue	154
4.14.14 Synthesis of 5-substituted cytidine analogue	157
4.14.15 Synthesis of 5'-substituted adenosine analogue	162
4.14.16 Synthesis of 9-substituted guanine analogue	164
4.15 References	167
4.16 Appendix	169
4.16.1 <i>In vitro</i> anti-mycobacterial studies of various nucleosides	169
4.16.2 <i>In vitro</i> cytotoxicity assay of human monocytic cell lines	170
4.16.3 Toxicity study on various bacterial cell lines	170
4.17 NMR spectra of synthesized compounds	171

Chapter 5: 1,8-Naphthyridine-Based Boronic Acid as Fluorescent Chemo Sensor for Hg²⁺ and D-Fructose	193-238
5.1 Abstract	195
5.2 Introduction	195
5.3 Results and discussion	197
5.3.1 Synthesis of naphthyridine-boronic acid (1.1)	197
5.3.2 Photophysical properties of 1.1	201
5.3.3 Examination of binding abilities of 1.1 to metal ions	202
5.3.4 Examination of binding abilities of 1.1 to monosaccharides	206
5.3.5 Competitive sensing of Hg ²⁺ and D-monosaccharides	212
5.4 Conclusions	213
5.5 Experimental section	214
5.5.1 Materials and methods	214
5.5.2 Buffer preparation for fluorescence studies	214
5.5.3 Sample preparation for fluorescence binding studies with metal ions	214
5.5.4 Stoichiometry determination using Jobs plot	215
5.5.5 Sample preparation for fluorescence binding studies with D-monosaccharides	215
5.5.6 Sample preparation for fluorescence binding studies of D-fructose at various pH solutions	215
5.5.7 Sample preparation for competitive fluorescence binding studies with D-monosaccharides	215
5.5.8. Synthesis of target compound 1.1	216
5.6 References	226
5.7 Appendix	229
5.7.1 NMR spectra of synthesized compounds	229
Curriculum Vitae	239
List of Publications in Peer Reviewed Journals	241
Presentations in Conferences and Symposiums	243

DECLARATION

I, hereby, declare that the matter embodied in this thesis is the result of research investigation carried out by me at the Dr. Reddy's Institute of Life Sciences, University of Hyderabad Campus, Hyderabad, India, under the supervision of Dr. Marina Rajadurai.

In keeping with the general practice of reporting scientific observations, due acknowledgements have been made wherever the work described is based on the findings of other investigators. Any omission, which might have occurred by oversight or error, is regretted.

Dr. Reddy's Institute of Life Sciences
University of Hyderabad Campus
December 2015

E. Ramanjaneya Reddy

CERTIFICATE

This is to certify that the thesis entitled “*Design, Synthesis, Characterization and Application of Fluorescent Organic Nanoparticles for Live In Vitro/In Vivo Bioimaging*” being submitted by **Mr. E. Ramanjaneya Reddy** to the University of Hyderabad for the award of ***Doctor of Philosophy in Chemistry*** has been carried out by him under my supervision and the same has not been submitted elsewhere for a degree. I am satisfied that the thesis has reached to the standard of fulfilling the requirements of the regulations relating to the nature of the degree.

Dr. Marina Rajadurai
(Research Supervisor)
Department of Organic and Medicinal Chemistry
Dr. Reddy's Institute of Life Sciences (DRILS)
University of Hyderabad Campus
Gachibowli, Hyderabad 500 046
Telangana, India
Tel.: +91 40 66571500
Fax: +91 40 66571581
E-mail: Marinar@drils.org

Acknowledgements

It is difficult to overstate my gratitude to my supervisor Dr. Marina Rajadurai for her excellent support, guidance and caring throughout my Ph.D. I am indebted to her for the freedom she gave me in carrying out my research and the time she spent in trying to explain various facts and concepts. My association with her is a memorable one.

I sincere gratitude to Prof. Rajadurai Chandrasekhar (School of Chemistry, University of Hyderabad) for his support and numerous consultations throughout my Ph.D programme. It would not have been possible to start nor finish my Ph.D without the two of you and I am forever grateful.

I honourably thank to my teachers who worked in Dr. Reddy's Institute of Life Sciences, first of all, our former director Prof. Javed Iqbal along with founder Dr. K. Anji Reddy, Dr. A. Venkateswarulu (present director) who gave me this place for doing my research. I would like to thank also Prof. Prabhat Arya, Prof. Manojit Pal, Dr. Rajamohan Reddy, Dr. Neelima, Prof. Parimal Mishra, Dr. Prasanjit Mitra, Dr. Kishore Parsa, Dr. Devyani Halder, Dr. Kiranam Chatti, Dr. Ritta Mathew, Dr. Puskar Kulkarni and Dr. Aarti Sevilimedu for their excellent teaching and advises whenever I needed in my Ph.D career.

I am truly thankful to my doctoral committee member, Prof. Faiz Ahmed Khan (IIT, Hyderabad) for his critical evaluation and valuable suggestions.

I would like to thank my labmates and colleagues namely G. Narendar Reddy, D. Balakrishna, N.V. Ratnam, V. Devendram, D. Kavita, S. Ghouse, B. Sunandana, M. Ravikumar, B. Surendar, Balamurgan, Y.S. L.V Narayana, N. Chandrasekhar Reddy, B. Ajay Kumar, Supratim Basak, Pramiti Hui, D. Krishna, U. Ramudu, V. Radhika, O. Anjana and friends namely Ch. Srinivas, A. Madhu, D. Bhanudas, G. Shivakrishna Reddy, J. Ravikumar, M. Naveen, J. Srinivas, K. Saidulu, K. Mahendar, G. Jagan, A. Raju, B. Prasad, S. Rajinikanth and Alinakhi not only for wonderful discussions in chemistry, but also for providing the friendly environment for me during entire Ph.D career.

I gratefully thank my roommates Rajagopal Rao, Rajagopal Reddy, Nagaprasad Reddy, D. P. Anna (TPR lab), Katha Rajasekhar Reddy, D. Subramanyam, Aleem, Ashin,

Anand Rao, Siva Reddy, Pavan Kumar Reddy, D. Siva Rama Krishna and Gopi for their excellent training in cooking, personal life, and behalf of sharing their wonderful lovely environment providing to me throughout my Ph.D career.

I extend my gratitude to my school teachers Venu sir, Murali sir, and my college lecturers Dr. Obul Reddy, Dr. Ramachandraiah and Dr. Murali, for their loving affection and constant encouragement till now.

My special thank all my friends at different levels of S.S.C (M. Anjaneyulu, G. Prudvinath Reddy and Maheswar Reddy). Intermediate (V. Chandrasekhar Reddy, S. Dadapeer and Siva), Undergraduate level (Balu, Ramesh, Sunil), M.Sc (D. Subramanyam, Narendar, Chandu, Narshima Reddy, Nagaraju) and my Ph.D friends Naganna, Boss, Ramireddy, Harsha, Apparao Annaiah from IICT, Daman, Gonu (IITM), Siviah (IITB), Nagaraju (CLRI), Nagendar (NCL Pune dorling), Malli sir (S.V.U), Ramesh (S.K.U), Ramakrishna (Assistant Prof in Narayana Junior college), Gangadhar (A.U), Suresh (IISc Banglore), Srinu (KCK lab), N. Krishna Reddy, Nagarjuna, Ugendar, Ashin, Sashi (From HCU) for their valuable loving affection throughout my carrer.

It is my great pleasure to acknowledge the support extended by Analytical, Finance and Accounts, Purchase, Project & Maintenance and Human Resource departments at Dr. Reddy's Institute of Life Sciences.

I humbly thank CSIR for fellowship, DST for funding, HCU for registration and Dr.Reddy's Institute of Life Sciences for infrastructure throughout my Ph.D programme.

Last but not least, many thanks to my family members who encouraged me and supports financially throughout my career: E. Linga Reddy (father), E. Lakshmi Devi (mother), E. Vijaya Lakshmi (wife), E. Siva Shankar Reddy (babai), E. Sidda Reddy (uncle), B. Sumalika & Satya (sisters), K. Siva Bharathi, K. Gowri Shankar (bava) and brothers (E. Siva Mohan Reddy, B. Praneeth Kumar Reddy and V. Bhargav Reddy).

I thank the Almighty for giving me the strength and patience to work through all these years, so that today I can stand proud with my head held high.

Dr. Reddy's Institute of Life Sciences
December 2015

E. Ramanjaneya Reddy

Synopsis

In this thesis, preparation of novel fluorescent organic nano-materials for long-term *in vitro* and *in vivo* bioimaging applications is described. Fluorescent organic nanoparticles (FONs) were prepared from organic chromophores based on naturally occurring nitrogen containing heterocycles, including nucleobases and nucleosides, connected to fluorescent moieties through a long and flexible aliphatic linker. The primary goal was to synthesize novel fluorescent organic molecules with improved properties, from readily available biocompatible materials and convert them into FONs via bottom-up approach. Characterization of these nanoparticles was carried out using modern methods employed in nanotechnology, e.g. scanning electron microscope (SEM), dynamic light scattering (DLS), atomic force microscope and confocal fluorescence microscope (CFM). FONs prepared in this work were resistant to bleaching/fading, were water soluble, biocompatible, easy to use and were shown to be excellent bioimaging reagents. Biological activity of the FONs was tested using different cell lines and model organisms, including mouse macrophage cells, cancer cells, yeast, zebrafish embryos and various bacterial cell lines, and utilization for *in vivo* and *in vitro* molecular bioimaging was demonstrated. In addition, a novel fluorescent chemosensor for toxic heavy metals was also designed and examined.

The thesis entitled, “**Design, Synthesis, Characterization and Application of Fluorescent Organic Nanoparticles for Live *In Vitro/In Vivo* Bioimaging**” contains five chapters:

CHAPTER 1

Introduction to Fluorescent Nano-Bioimaging

Chapter 1 contains a detailed discussion on the subject of bioimaging, and covers the historical perspective, recent developments and applications of bioimaging. This chapter also presents basic concepts of fluorescence and evolution of the fluorescent microscope, including areas of improvement of fluorescence bioimaging. Additionally, this chapter includes a detailed discussion of the properties and major characteristics of fluorophores. Advantages and drawbacks of the main fluorophore families, including biological or natural fluorophores, quantum dots, fluorescent organic molecules and FONs are presented. History and advances in the development

of the FONs family is covered more comprehensively. Finally, a brief description of the most popular small model organisms commonly used for *in vivo* bioimaging studies is also included.

CHAPTER 2

Selective Multicolour Imaging of Zebrafish Muscle Fibres Using Fluorescent Organic Nanoparticles

(*ChemBioChem* **2012**, 13, 1889-1894)

Chapter 2 reveals the design, synthesis, characterization and *in vitro/in vivo* bioimaging applications of multicolour emitting FONs. Multicolour and biocompatible FONs were prepared from novel chromophores (**PPy** and **GPy**), composed of purine derivatives connected to pyrene by 12 carbons aliphatic chain. Both chromophores were synthesized via simple and straightforward synthetic route involving copper catalyzed (3+2) cycloaddition as a key reaction. FONs were prepared from **PPy** and **GPy** via bottom-up approach, and their photophysical properties and morphology were fully investigated by UV-Vis and fluorescence spectroscopy, SEM, AFM and CFM. It was found that multicolour FONs were able to penetrate into human breast cancer cells and zebrafish embryos. They were nontoxic, biocompatible and exhibited specificity for muscular tissues of zebrafish embryos. The multicolour imaging potential of the pyrene containing FONs can be exploited to overcome tissue autofluorescence, which often occur in many biological samples.

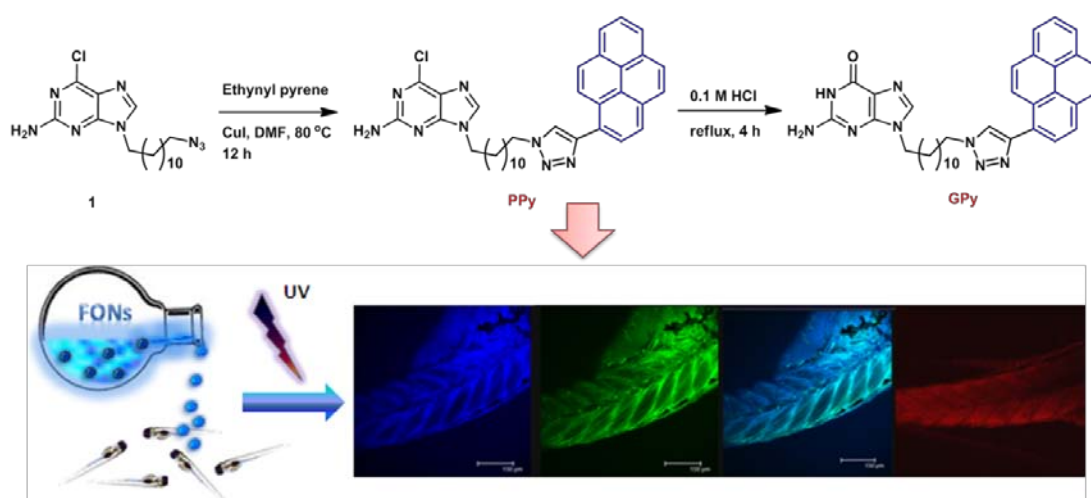


Figure 1: Synthesis and application of pyrene containing guanine analogues (**PPy** and **GPy**)

PPy and **GPy** nanoparticles were resistant to bleaching or fading, easy to use and could be utilized as an excellent reagent for the study of neuromuscular changes in zebrafish embryos. This study demonstrated, for the first time, the utilization possibility of FONs for zebrafish *in vivo* whole body fluorescent imaging.

CHAPTER 3

Red Fluorescent Organic Nanoparticles for Real Time *In Vitro* and *In Vivo* Bioimaging

(*ChemNanoMat* **2015**, *1*, 567-576)

This chapter describes the design, synthesis, characterization and *in vitro/in vivo* bioimaging applications of red FONs. Novel highly efficient FONs based on red fluorescent compound (**Cy-Red**), which was synthesized using click chemistry approach from cytosine moiety connected to 4,7-di(thiophene-2-yl)benzo[c][1,2,5]thiadiazole via long (12 carbons) aliphatic chain. Although **Cy-Red** was almost insoluble in most of the common organic solvents and water, nanonization effectively converted it into water soluble nanoparticles (**nano-Cy-Red**), suitable for biological experiments.

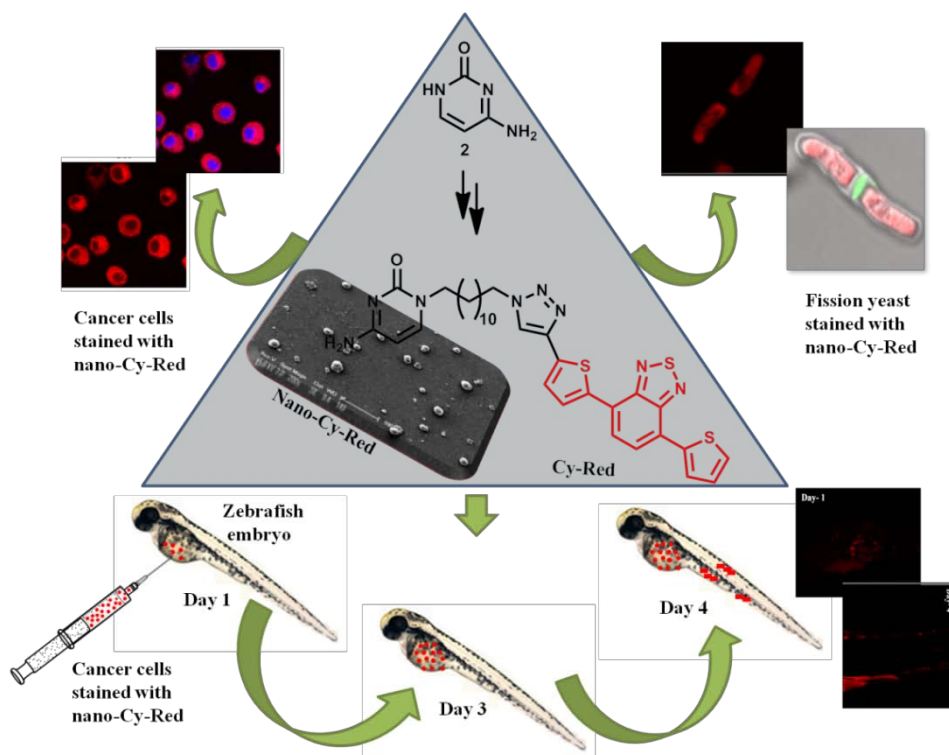


Figure 2: Synthesis, characterization and application of **nano-Cy-Red** for long-term real time *in vitro* and *in vivo* visualization

The photophysical properties and morphology of **nano-Cy-Red** were fully investigated by UV-Vis and fluorescence spectroscopy, SEM, AFM, DLS, CFM and fluorescence microscope. It was found that novel **nano-Cy-Red** nanoparticles are nontoxic, biocompatible and were able to penetrate into mouse macrophage cells, oral cancer cells and yeast. More importantly, they retained in living cells for several generations, serving as a cytoplasmic stain. Taking advantage of this property, the **nano-Cy-Red** dye was exploited for direct *in vivo* visualization of cancer cell migration upto 72 h post transplantation in zebrafish embryos.

CHAPTER 4

Novel Fluorescent 3, 5 and 5'- Substituted Nucleosides Derivatives with Selective Antibacterial Activity

(*J. Med. Chem.* 2015 submitted)

Chapter 4 discloses the synthesis of various 3, 5 and 5'- substituted nucleosides and evaluation of their *in vitro* inhibitory activity against gram-positive/gram-negative bacteria and *Mycobacterium tuberculosis* (Mtb, pathogenic H37Rv). One of the tested compounds, 3-substituted pyrene alkyl uridine **3** showed mycobacterium inhibitory activity in MTT assay at MIC₅₀ = 62 µM, without significant cytotoxic effect against host macrophages. Compound **3** also showed selective inhibitory activity against gram-positive bacteria, but was non-toxic to gram-negative bacteria at all concentrations tested. This work hypothesizes that bactericidal activity of active compound **3** stems from its ability to disrupt DNA replication. In support of this mechanism, a) it was demonstrated that active compound **3** inhibits polymerase chain reaction (PCR) *in vitro*; b) fluorescent properties of the compound **3** were utilized to perform microscopy studies in different bacteria, showing that selectivity of compound **3** is limited by cell permeability; c) *in vitro* binding studies and fluorescence measurements were used to establish direct binding of compound **3** to enzyme; and finally, d) molecular modeling studies demonstrated a good fit of this compound within the active site of Taq DNA polymerase enzyme (Taq DNA Pol). SEM, AFM and Tyndal scattering of light revealed that compound **3** exist in the form of solution stable nanoparticles. The uniform shape and size of nanoparticles was confirmed by SEM and the average diameter was *ca.* 250-300 nm, which was small enough to penetrate into micro organisms. Thus, 3-substituted pyrene alkyl uridine **3**

is a novel, potent, narrow spectrum antibacterial compound which can be used to target Mtb as well as gram-positive bacteria.

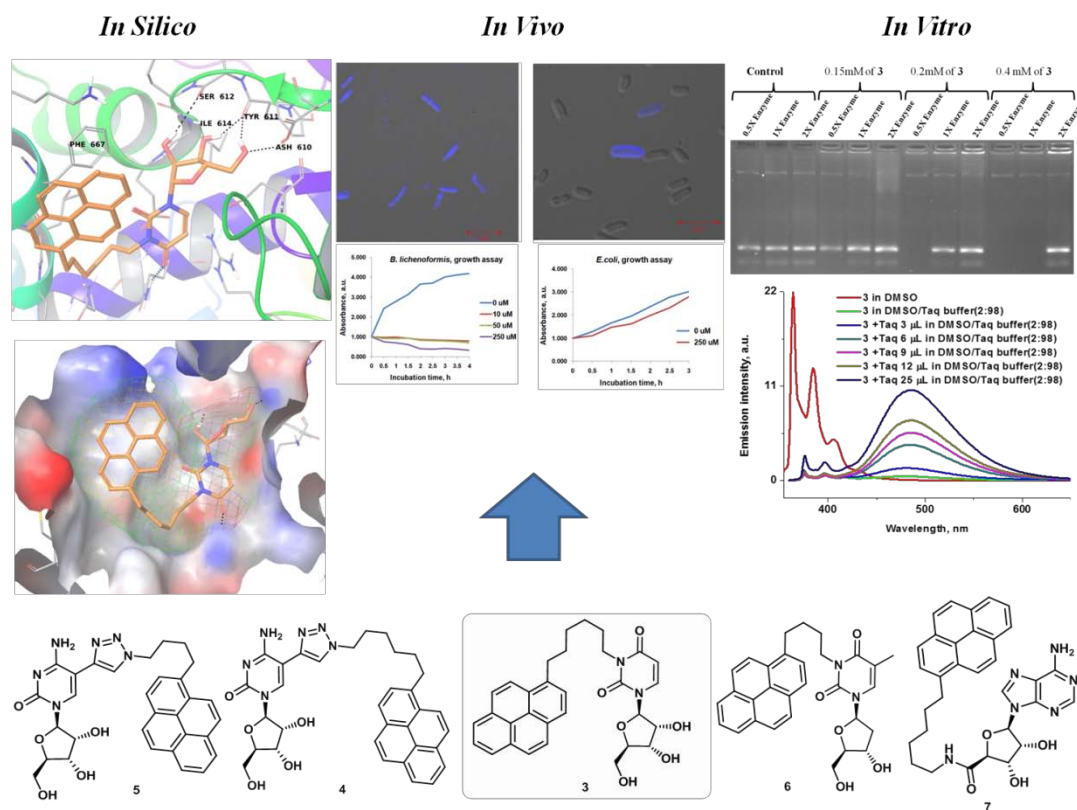


Figure 3: Biological evaluation of various 3, 5 and 5'-substituted nucleosides, and *in-vitro*, *in vivo*, and *in silico* mechanistic studies of lead compound **3**

CHAPTER 5

1,8-Naphthyridine-Based Boronic Acid as Fluorescent Chemosensor for Hg^{2+} and D-Fructose

(Manuscript under preparation)

Chapter 5 presents the design and synthesis of novel fluorescent chemosensor **8** [(2-(((5-(7-acetamido-1,8-naphthyridin-2-yl)thiophen-2-yl)methyl)(methyl)amino)methyl)phenyl)boronic acid], its fluorescence properties, and interaction with various metal ions and monosaccharides. Compound **8** displayed highly selective fluorescence quenching upon interaction with Hg^{2+} , possibly by means of photo induced electron transfer (PET) mechanism. The binding stoichiometry of the naphthyridine-boronic acid- Hg^{2+} complex and the association constant was determined. It was found that in the presence of D-fructose at physiological concentration, the sensitivity of

chemosensor **8** towards Hg^{2+} improved by at least 7 fold, perhaps as result of the cooperative binding of both D-fructose and mercury ion to the sensor. To the best of our knowledge, this dual D-fructose-mercury chemosensor is the first example, where boronic acid–diol complexation is utilized for enhancement of the sensor's sensitivity towards toxic metal ion. The utility of compound **8** is in applications in food industry, e.g. for detection of mercury contamination of high fructose corn syrup, or in estimation of mercury in polluted biological samples and underground water.

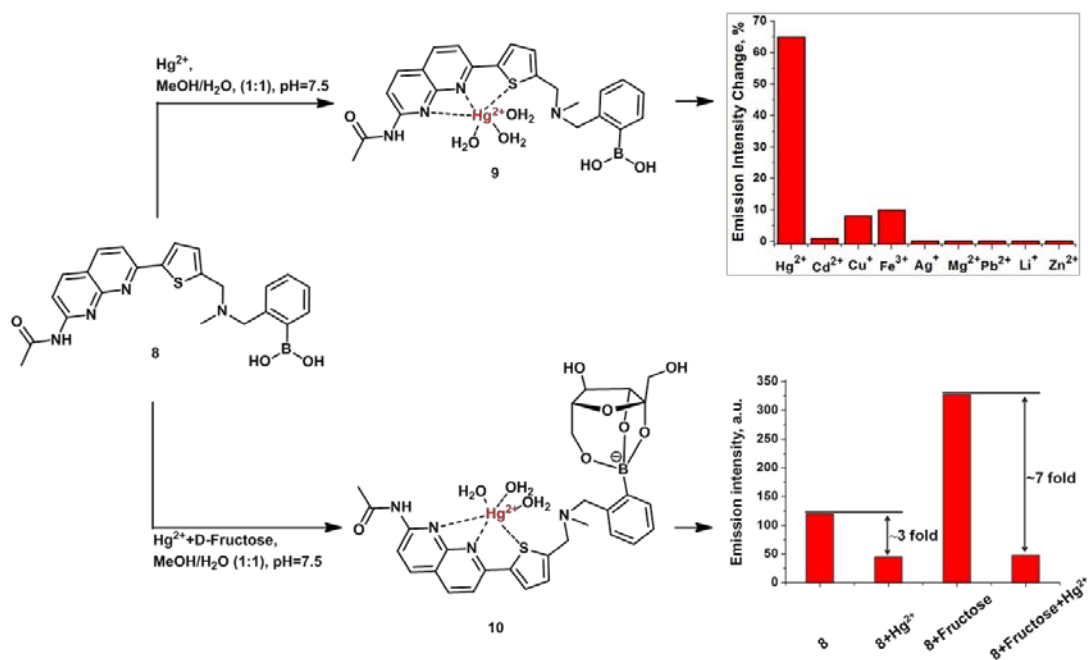


Figure 4: PET based fluorescent chemosensor **8**, proposed binding modes and its fluorescence properties with Hg^{2+} in presence and absence of D-fructose

ABBREVIATIONS

Φ_f	:	Relative quantum yield
δ	:	NMR chemical shift reported in ppm
λ	:	Wavelength
ε	:	Molar extinction coefficient
π - π	:	pi-pi
λ_{ex}	:	Excitation wavelength
λ_{em}	:	Emission maxima
$\Delta\lambda$:	Difference in absorption and emission maxima
μM	:	Micromolar
μL	:	Microlitre
μm	:	Micrometer
Ac	:	Acetyl
AcOH	:	Acetic acid
ACN	:	Acetonitrile
Ac ₂ O	:	Acetic anhydride
AFM	:	Atomic force microscope
AIBN	:	Azobisisobutyronitrile
AIQ	:	Aggregation induced quenching
AlCl ₃	:	Aluminum chloride
Aq. NH ₃	:	Aqueous ammonia
BIAB	:	Bis(acetoxy)iodobenzene
<i>B.l.</i>	:	<i>Bacillus licheniformis</i>
Boc	:	<i>t</i> -butyloxy carbonyl
BSA	:	Bovine serum albumin
Bu ₃ SnCl	:	Tributyl tin chloride
CAM	:	Camera
CCl ₄	:	Carbon tetra chloride
CDCl ₃	:	Deuterated chloroform
CFM	:	Confocal fluorescence microscope
CH ₃ NH ₂	:	Methyl amine
Con. H ₂ SO ₄	:	Concentrated sulfuric acid
CSA	:	Camphorsulfonic acid

CuI	:	Copper iodide
CuSO ₄ .5H ₂ O	:	Copper sulphate pentahydrate
DAPI	:	4',6-diamidino-2-phenylindole
DCM	:	Dichloromethane
DLS	:	Dynamic light scattering
DMF	:	Dimethylformamide
DMAP	:	4-Dimethylaminopyridine
DMEM	:	Dulbecco's modified Eagle's medium
DMSO	:	Dimethylsulphoxide
DNA	:	Deoxyribonucleic acid
dNTP	:	Deoxyribonucleotide triphosphate
D ₂ O	:	Deuterium oxide
dpf	:	Days post fertilization
EDCI	:	1-Ethyl-3-(3-dimethylaminopropyl)carbodiimide
EGFP	:	Enhanced green fluorescent protein
EtOAc	:	Ethyl acetate
Et ₂ O	:	Diethyl ether
Et ₃ N or TEA	:	Triethylamine
<i>E. coli</i> or <i>E.c.</i>	:	<i>Escherichia coli</i>
ES	:	Electron spray
FBS	:	Fetal bovine serum
FITS	:	Fluorescein isothiocyanate
FONs	:	Fluorescent organic nanoparticles
Fe(ClO ₄) ₃ .6H ₂ O	:	Iron perchlorate hexahydrate
FESEM	:	Field emission scanning electron microscope
GFP	:	Green fluorescent protein
H ₂	:	Hydrogen
H ₂ O	:	Water
HCl	:	Normal hydrochloric acid
HgCl ₂	:	Mercury chloride
HIO ₃	:	Iodic acid
h	:	Hour
hpf	:	Hours post fertilization
hpi	:	Hours post injection

HPLC	:	High-performance liquid chromatography
h ν	:	Light
I ₂	:	Iodine
ICG	:	Indocyanine green
KCl	:	Potassium chloride
K ₂ CO ₃	:	Potassium carbonate
KOH	:	Potassium hydroxide
KHMDS	:	Potassium hexamethyldisilazane
KH ₂ PO ₄	:	Potassium phosphate monobasic
MeI	:	Methyl iodide
MeOH	:	Methanol
mM	:	millimolar
Mp	:	Melting point
Mtb	:	Mycobacterium tuberculosis
n-BuLi	:	n-Butyl lithium
NH ₄ Cl	:	Ammonium chloride
Na ₂ CO ₃	:	Sodium carbonate
NaHCO ₃	:	Sodium bicarbonate
Na ₂ HPO ₄	:	Sodium phosphate dibasic
Na ₂ SO ₄	:	Sodium sulphate
NaH	:	Sodium hydride
NaHCO ₃	:	Sodium bicarbonate
NaHSO ₃	:	Sodium bisulfite
NaBH ₄	:	Sodium borohydride
NBS	:	N-Bromo succinimide
NIR	:	Near-infrared
nm	:	Nanometer
nM	:	Nanomolar
NMR	:	Nuclear magnetic resonance
NaN ₃	:	Sodium azide
Me	:	Methyl
MeOH	:	Methanol
MP	:	Melting point
MRI	:	Magnetic resonance imaging

PBS	:	Phosphate buffer solution
PCR	:	Polymerase chain reaction
PET	:	Photo induced electron transfer
<i>P.e.</i>	:	<i>Paenibacillus elgii</i>
POCl ₃	:	phosphorus oxychloride
PTSA	:	<i>para</i> -toluene sulfonic acid
Pd/C	:	10% Palladium on carbon
PdCl ₂ (PPh ₃) ₂	:	Bis(triphenylphosphine) palladium(II) dichloride
PDB	:	Protein data bank
RNA	:	Ribonucleic acid
RT	:	Room temperature
R _f	:	Retardation factor
SEM	:	Scanning electron microscope
<i>S.m.</i>	:	<i>Serratia marcescens</i>
Taq	:	<i>Thermus aquaticus</i>
Taq DNA Pol	:	Taq DNA polymerase
TBDMS-Cl	:	tert-butyldimethylsilyl chloride
TBAF	:	Tetra-n-butylammonium fluoride
TEM	:	Transmission electron microscope
TEMPO	:	2,2,6,6-Tetramethylpiperidinyloxy
TFA	:	Trifluoroacetic acid
THF	:	Tetrahydrofuran
TLC	:	Thin layer chromatography
TMS-Acetylene	:	Trimethyl silyl acetylene
UV	:	Ultraviolet
UV-Vis	:	Ultraviolet-visible
WHO	:	World health organization
YES	:	Yeast extract plus supplements

General Information

Nuclear Magnetic Resonance Spectroscopy:

^1H and ^{13}C NMR spectra were recorded on a Varian 400 MHz NMR spectrometer. Spectra were recorded using the solvent peaks as the internal standard.

Mass Spectrometry:

Mass spectra and LC-MS were recorded using electron impact, chemical ionization or electron spray ionization techniques, on Micro Mass VG-7070H.

Infrared Spectroscopy:

FT-IR spectra were recorded on a Bruker (Alpha) spectrometer. Solid samples were recorded as KBr pellets and liquid samples as thin films between NaCl plates.

Solvents Distillation:

DMF, DCM, MeOH and THF were dried immediately prior to use according to standard procedures: dimethylformamide, dichloromethane was distilled under N_2 from CaH_2 , methanol was distilled under N_2 over Mg and tetrahydrofuran was distilled under N_2 over Na. All solvents were removed by evaporation under reduced pressure.

Melting Point:

Melting temperatures of solids were determined using Büchi made electro-thermal melting point apparatus and values reported are uncorrected.

Thin Layer Chromatography/Flash Column Chromatography:

Thin layer chromatography (TLC) was carried out on aluminum sheets coated with silica gel 60F₂₅₄ (Merck, 1.05554) and the spots were visualized with UV light at 254 nm or alternatively by staining with aqueous basic potassium permanganate or ceric ammonium molybdate or ninhydrin. Flash column chromatography was performed using silica gel (Merck, 60A, 230-400 Mesh).

High-performance Liquid Chromatography:

High-performance liquid chromatography was carried out on Agilent-1200 instrument using X-BRIDGE C-18 150×4.6mm 5 μ column.

Elemental Analysis:

Elemental analysis was carried out on a Thermo Finnigan Flash EA-1112 series CHNS analyzer.

Single Crystal X-ray Diffraction Data Collection, Solution and Refinement:

The X-ray intensity data of crystals were collected on a Bruker Nonius SMART APEX CCD area detector system equipped with a graphite monochromator and a MoK α fine-focus sealed tube ($\lambda = 0.71073 \text{ \AA}$) operated at 1750 W power (50 kV, 35 mA). All data were collected at 298 K. The detector was placed at a distance of 6.003 cm from the crystal; exposure time (10-20 sec/frame) was set based on the data quality. The frames were integrated with the Bruker SAINT Software package using a narrow-frame integration algorithm. Data were corrected for absorption effects using the multi-scan technique (SADABS). The structure was solved and refined using the direct method analysis in Bruker SHELXTL Software Package.

Absorption Spectroscopy:

Absorption spectra were recorded on a Cary-100, Varian double beam spectrophotometer.

Fluorescence Spectroscopy:

Steady state fluorescence emission and excitation spectra were recorded on a Jobin Yvon Horiba model Fluoromax-3 spectrofluorimeter.

Scanning Electron Microscopy:

SEM and FESEM images were recorded on a Philips XL30 ESEM and a HITACHI S-4300SE/N FESEM respectively using beam voltages of 20 kV. The samples were fixed on aluminum platforms using carbon tapes; a conducting connection was made between samples and aluminum platform by silver paint. Samples were coated with a thin layer (3-5 nm) of sputtered gold prior to imaging.

Atomic Force Microscopy:

Atomic Force Microscopy (AFM) imaging was carried out on NT-MDT Model Solver Pro M microscope using a class 2R laser of 650 nm wavelength having maximum output of 1 mW. All calculations and image processing was carried out by a software NOVA 1.0.26.1443 provided by the manufacturer. The images were recorded in a semi-contact mode using a noncontact mode tip purchased from NT-MDT, Moscow. The dimensions of the tip are as

follows: Cantilever length = 95 (± 5) μm , Cantilever width 30 (± 5) μm , and Cantilever thickness = 1.5-2.5 μm , Resonate frequency = 140-390 kHz, Force constant = 3.1-37.6 N/m, Chip size = 3.4 \times 1.6 \times 0.3 mm, Reflective side = Au, Tip height = 14-16 μm , Tip curvature radius = 10 nm, and Aspect ratio 3:1-5:1.

Dynamic Light Scattering:

The size of the aggregates was determined by dynamic light scattering technique using a Malvern Zeta size Instrument (NanoZS90, Malvern, U.K.). The laser light source (He-Ne) has a single wavelength of 633 nm and the detector was Avalanche photodiode. Before measurement, the scattered cell (DTS1060) was rinsed with biocompatible solution and equilibrated for 180 s in the system. The measurement was carried at 25 $^{\circ}\text{C}$ with a scattering angle of 90 $^{\circ}$.

Confocal Laser Scanning Microscopy:

The luminescence behavior of the samples was observed with a Leica Laser scanning confocal microscope, Germany [model No - TCS – SP2 (spectral confocal microscope)] equipped with an Acousto-Optical Beam Splitter (AOBS) emission filter. The wavelength and amplitude of the ultrasound can be changed (programmed) to deflect certain band of wavelength and its amount passing through the field to collect emissions in high efficiency. The topographic structural data were directly coupled with the spectroscopic properties of the specimen. The emission spectral curves were recorded in XY λ (spectral scan mode) scan mode, and the images were recorded in XYT mode (time scan mode). Argon-ion Laser (Power- 280 mW) was used as UV excitation source. Scanning was done by a 20.0X optical lens, later it was further magnified by a factor 3.45 using digital magnification by the Leica confocal software (LCS). The data were recorded with a (Continuous scan) scanning speed of 400 Hz (image lines per second) with a scan format of 512 pixel \times 512 pixel resolution. The active emission colors were detected using the different color detection channels of the photomultiplier tube (PMT). The pinhole size was 36 μm and six frames were taken to make an average of the final frame.

1

Introduction to Fluorescent Nano- Bioimaging

1.1. Introduction to Bioimaging:

Molecular live-cell bioimaging is one of the advanced interdisciplinary areas of the translational biomedical research. Bioimaging is a non-invasive tool, allowing visualization of the biological processes in real time without disturbing its physical structure.¹ Moreover, it provides the three dimensional structure of the observed specimen from outside and makes available information about specific intracellular events, such as changes in receptors kinetics, molecular and cellular signaling,² protein-protein interactions³ and movement of the molecules through membrane.⁴ Depending on the type of source used for imaging, bioimaging techniques can be classified as X-ray imaging, ultrasonography, magnetic resonance imaging (MRI), positron emission tomography (PET), computed tomography (CT), fluorescence molecular imaging, *etc.*

Among the methods listed above, fluorescence molecular bioimaging has a special place. Since its discovery in the 16th century, light microscope plays central role in studying dynamic processes in living cells and is remaining one of the most significant imaging tools.^{5a} Continuous improvements of optics hardware and digital imaging sensors made it a very powerful instrument. However, it is discovery of green fluorescent protein (GFP) and evolution of small fluorescent molecular probes that helped to overcome limitations and advanced optical microscope sensitivity enough to illuminate specific biological targets and processes, both *in vitro* and *in vivo*.

Compared with conventional imaging methods, which are deeply obsessed with either low spatial resolution or costly equipment, fluorescence imaging exhibits distinct advantages such as high sensitivity, high selectivity and non-invasive *in vivo* imaging without radiopharmaceuticals.^{5b-c} Fluorescence imaging offers visualizing biological process such as genetic expression and biological information transmission at the molecular level, and tracing the real-time physiological processes *in vivo* via staining tissue, cells, or cellular compartments with fluorescent dyes.⁶ Moreover, fluorescence techniques provide not only direct visualization using biomarkers, but also have ability to detect intrinsically non-fluorescent species or parameters such as the pH value and activity of enzymes.⁷

1.2. Historical Perspective of Bioimaging and Fluorescence Microscope:

An active use of the microscope for research begun in 1660th -1670th in England, the Netherlands and Italy. Antonie van Leeuwenhoek's discovery of the red blood cells and spermatozoa attracted broad attention of research community to a microscope-assisted visualization.^{8a} In late 17th century optical microscopes were used for seeing microorganisms. However, optical microscopes had poor resolution, contrast, and sensitivity, as well as optical aberrations and immense noise. In 1873, Ernst Abbe proposed an equation which gives a maximum resolution of an optical microscope. According to the Abbe's equation the resolution could never become better than 0.2 micrometers. Invention of the fluorescent microscopes helped to improve specificity, resolution and contrast. The first fluorescence microscope was developed between 1911 and 1913 by German physicists Otto Heimstaedt and Heinrich Lehmann. They used ultraviolet light as a source of excitation, which resulted in increased resolution of microscope (as per Abbe's equation).^{8b} In the very beginning, fluorescent microscope was employed to observe autofluorescence in bacteria, animal's and plant's tissue. Subsequently, cells and tissues were labeled with fluorescent dyes for selective imaging. For example, in 1940s fluorescent microscope become very popular with the invention of immunofluorescence technique,⁹ by Albert Coons and Melvin Kaplan. In this technique fluorescent molecules are chemically bound to antibodies that can couple with a specific protein in a cell or tissue, thus providing good contrast and high specificity towards targeted object. In 1994, Chalfie *et al.* succeeded in expressing of a prokaryotic and eukaryotic cells with the help of GFP, which shows strong green fluorescence when excited by UV-light.¹⁰ This was a landmark evolution in the field, fostering a whole new class of tagging methods. The conventional methods which are used for monitoring gene expression and protein distribution require an additional co-factors or substrates from outside, but the use of GFP requires only irradiation of UV-light. The important impact of this work in cell and molecular biology led to the awarding of Noble Prize in Chemistry in 2008 to Martin Chalfie, Osamu Shimomura and Roger Y. Tsien for the development of GFP. The winners of Noble prize in chemistry- 2014, Eric Betzig, Stefan W. Hell and William E. Moerner, have taken optical microscope onto new level with help of fluorescent molecules. They converted microscope into nanoscope using stimulated

emission depletion process. Super resolution image is provided by selectively deactivated fluorophore except for that in a nanometer sized volume. Using this technique super imposition of nanometer range provides resolution far better than Abbe's diffraction limit (**Figure 1**).¹¹ With these new developments in the field of molecular bioimaging, biologists have got unprecedented tool which helps to visualize sub-cellular components and processes both structurally and functionally. Nevertheless, the scope of improvement lays in development of new, better fluorescent probes with higher quantum yields, longer fluorescence life time and better photostability.

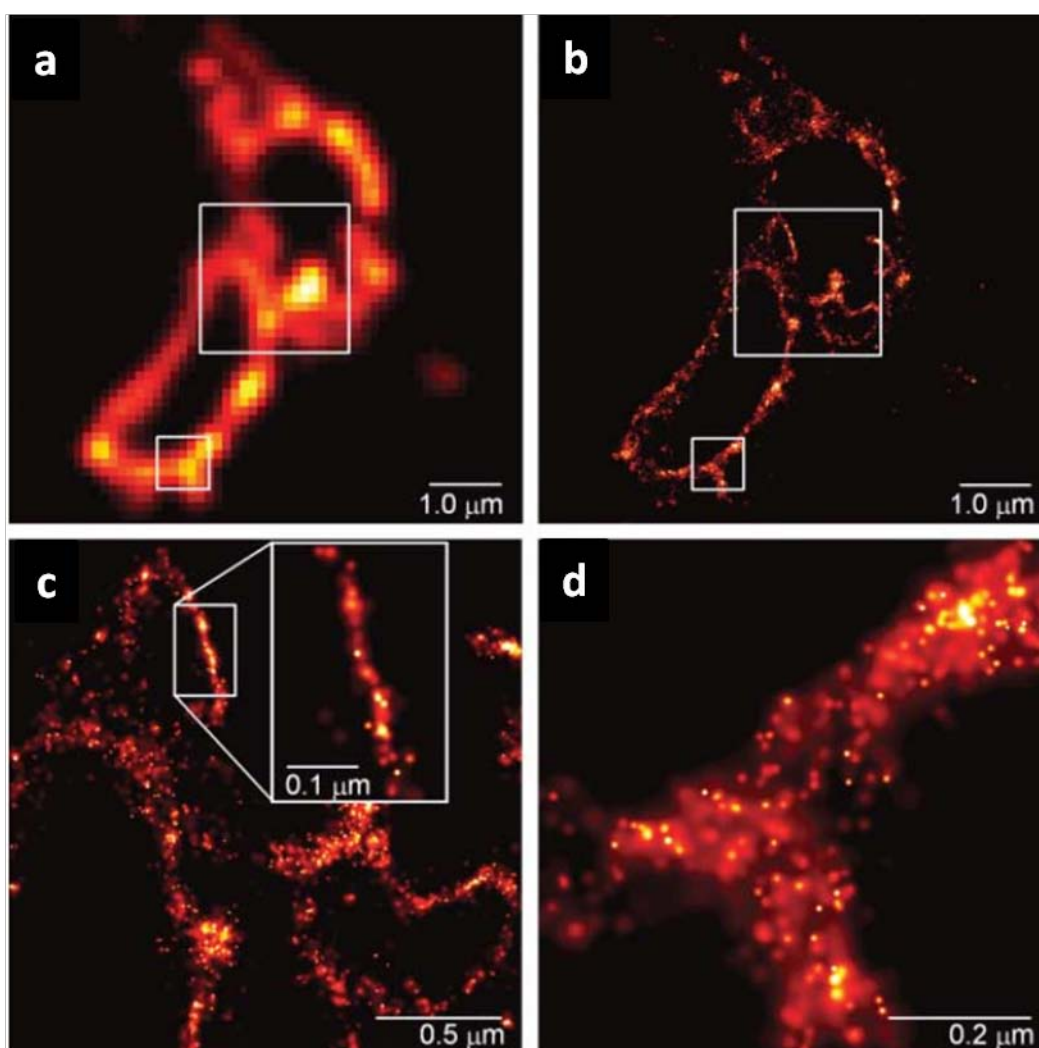


Figure 1: Image of lysosome membranes; a) with conventional microscope, b) with super resolution microscope, c) and d) are higher magnification views using super resolution microscope (note the scale division of 0.2 micrometres, equivalent to Abbe's diffraction limit (adapted from reference 11a)

1.3. Introduction to Fluorophore:

In order to employ fluorescent microscope highly efficiently, one needs fluorescent probes of specific qualities. The earliest example of the phenomenon of fluorescence was observed in 1565, when Spanish physician and botanist Nicolas Monardes discovered a bluish colour of water when it comes in contact with Mexican wood.¹² Due to its strange property, it becomes well known in Europe from 16th to 18th century. Cups made from the Mexican wood (**Figure 2a**) were given as gifts to royalty and were thought to have great medicinal properties. In 1603, a Vincenzo Casciarolo discovered a stone named as a Lapis Solaris (**Figure 2b**) which emits a purple-blue in the dark. In 1850 the term fluorescence was first named by George Gabriel Stokes after observed the phenomenon that the emitted light has longer wavelengths than that of excited light. In 1871 Adolph Von Baeyer synthesized a fluorescent dye from phthalic anhydride and resorcinol named as Fluorescein. Famous GFP was isolated from *Aequorea Victoria* jellyfish by Shimomura, Johnson and Saiga in 1962 (**Figure 2d**).¹³

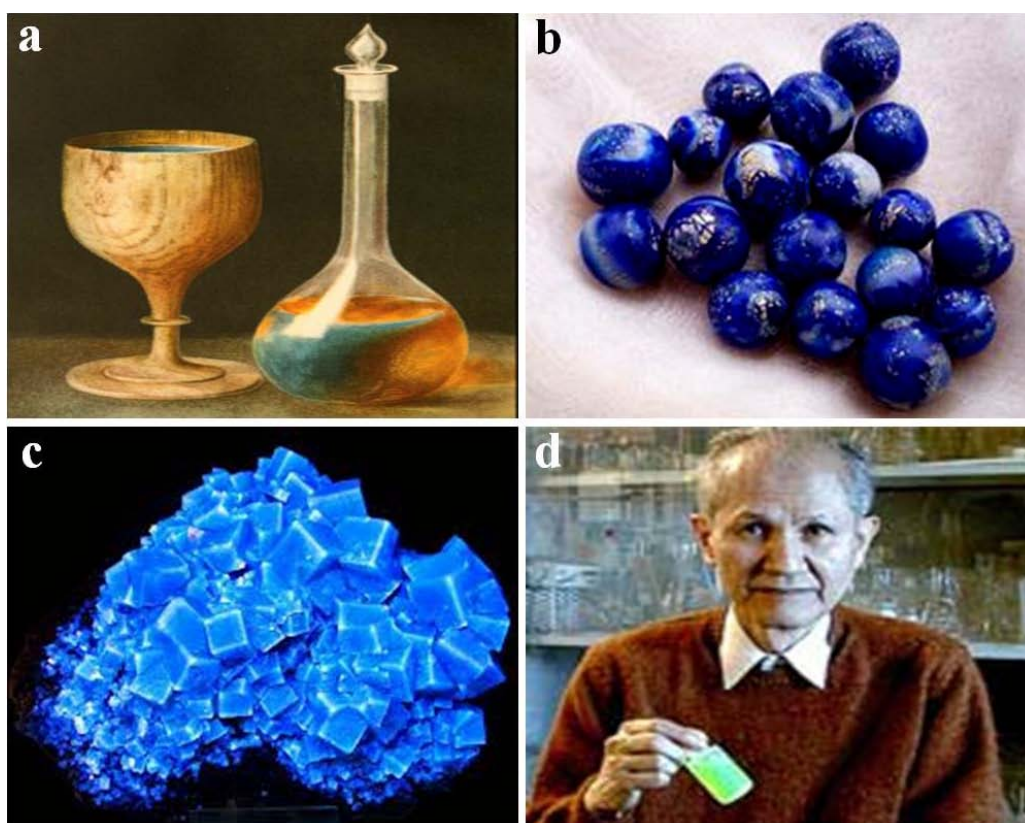


Figure 2: Discovery of fluorescence (past to present) a) from Mexican wood, b) from Lapis Solaris, c) from fluorites and d) GFP isolated from jellyfish *Aequorea Victoria* (adapted from reference 12 and 13)

Fluorophore is a molecule that has the ability to re-emit light upon light excitation. Compared with other molecules, fluorophores react distinctly to light: a photon of excitation light is absorbed by an electron of a fluorescent particle, which raises the energy level of electron to an excited state. During this short excitation period, some of the energy is being lost as result of molecular collisions or transfer to a proximal molecule, the remaining energy is emitted as a photon, while the electron relaxes back to the ground state. Naturally, the emitted photon usually carries less energy and has a longer wavelength than the excitation photon. If a molecule absorbs energy in the form of electromagnetic radiation, there are a several routes by which it can return to the ground state. The Jablonski diagram (**Figure 3**) shows a varying relaxation process for an electronically excited state molecule.

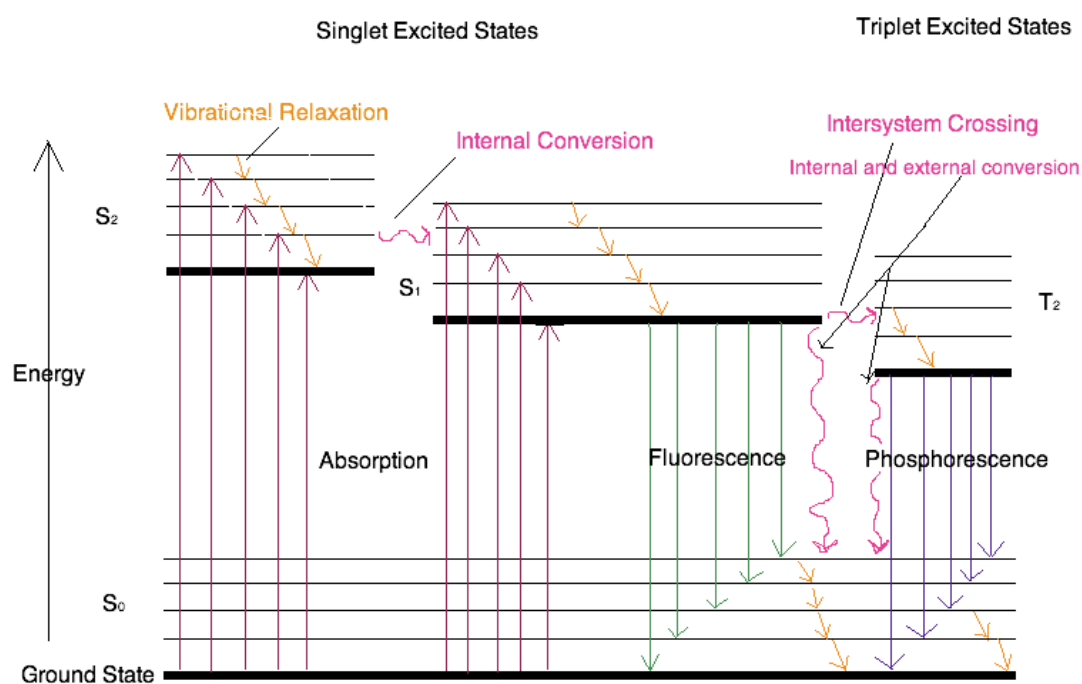


Figure 3: Illustration of various relaxation processes of an electronically excited state molecule by Jablonski diagram (adapted from reference 14)

Molecule excited to its singlet excited state may either have internal conversion to the singlet state that relax to the ground state and cause fluorescence, or have intersystem crossing to the triplet state that relax to the ground state, thus causing phosphorescence.¹⁴ The excitation and emission of a photon is cyclic process, and can continue until the fluorophore is irreversibly damaged. Each fluorophore has unique characteristic optical properties which are varying from one fluorophore to another due to several factors, such as: extended π conjugation, solvent polarity,

attractive forces between two molecules, aggregation of molecules, steric hindered rotations, chemical nature of chromophore and binding strength. The main characteristic properties of a fluorophore are:

1. Excitation and emission wavelengths;
2. Extinction coefficient or molar absorption value;
3. Quantum yield;
4. Fluorescence life time;
5. Stokes shift;
6. Photostability.

1) Excitation and Emission Wavelengths. The excitation of the molecule or atom happens when absorption of light either in ultraviolet or visible region promotes a valence electron of an atom or molecule from its ground state to an excited state with preservation of the electron's spin. For example, a pair of electrons occupying the same electronic ground state has opposite spins and are said to be in a singlet spin state. A photon of excitation light absorbed by one of the electrons in singlet ground state promotes to its singlet excited state. The excited states are not stable and an electron in the excited state will spontaneously return to the ground state after a short period of time (**Figure 3**). The names for above described processes are: deactivation and relaxation or decay. If the energy, which was absorbed during the excitation process, releases in the form of a photon (emission of the photon), it results in fluorescence.¹⁵

2) Molar Extinction Coefficient. Molar extinction coefficient is a measure of how strongly a chemical species absorbs light at a given wavelength. According to Beer-Lambert law, the absorbance is directly proportional to the concentration of the sample and also proportional to the length of the light path. Therefore,

$$A \propto cl \quad \dots\dots\dots (1)$$

$$A = \epsilon cl \quad \dots\dots\dots (2)$$

where A is absorbance, c is concentration and l is width of the cuvette. The molar extinction coefficient values usually represented by $\text{Lmol}^{-1}\text{cm}^{-1}$. In order to determine the molar extinction coefficient values Beer's Law plot is to be drawn (concentration over absorbance), where determination of the slope gives the molar extinction coefficient, ($\epsilon \times l$). The molar extinction coefficient value is important in order to find

the exact concentration of an analyte, for example protein.¹⁶ Larger molar extinction coefficient values reflect better optical properties of the fluorophores.

3) Quantum Yield. The fluorescence quantum yield (Φ_f) is calculated as the ratio of photons absorbed to photons emitted through fluorescence (**Equation 3**). In other words, the quantum yield gives the probability of the excited state being deactivated by fluorescence or non-radiative mechanism.

$$\Phi_f = \text{Photons emitted/Photons absorbed} \quad \dots\dots\dots (3)$$

In general, the value Φ_f of any fluorophore is always less than one (0 to 1), except for a few cases, like photo-induced process, where the value Φ_f is greater than one. Williams *et al.* found the most consistent method for recording Φ_f by using a relative method,^{17a} which involves the use of well characterized standard samples (for example quinine sulphate) with known Φ_f values. He assumed that solutions of the standard and test samples with identical absorbance at the same excitation wavelength are absorbing the same number of photons. Hence, a ratio of the integrated fluorescence intensities of the two solutions (recorded under identical wavelength) will yield the ratio of the quantum yield values. Since Φ_f for the standard sample is known, and the quantum yield of the unknown is calculated by the following equation (**Equation 4**). Quantum yield has no units; high quantum yield is most desirable in bioimaging applications, as it can ensure high signal-to-noise ratio, thus providing higher quality of imaging.

$$\dots\dots\dots (4)$$

4) Fluorescence Life Time. Absorption of light by fluorophore results in a formation of an electronically excited state. After some time the species return to the ground state. The relaxation processes of fluorophore might be via: a) inter system crossing (vibrational relaxation), b) fluorescence (radiative process), or c) non-radiative process. The fluorescence life time (τ) is a measure of the average time a molecule spends in the excited state before relaxing back to the ground state (**Figure 4**)

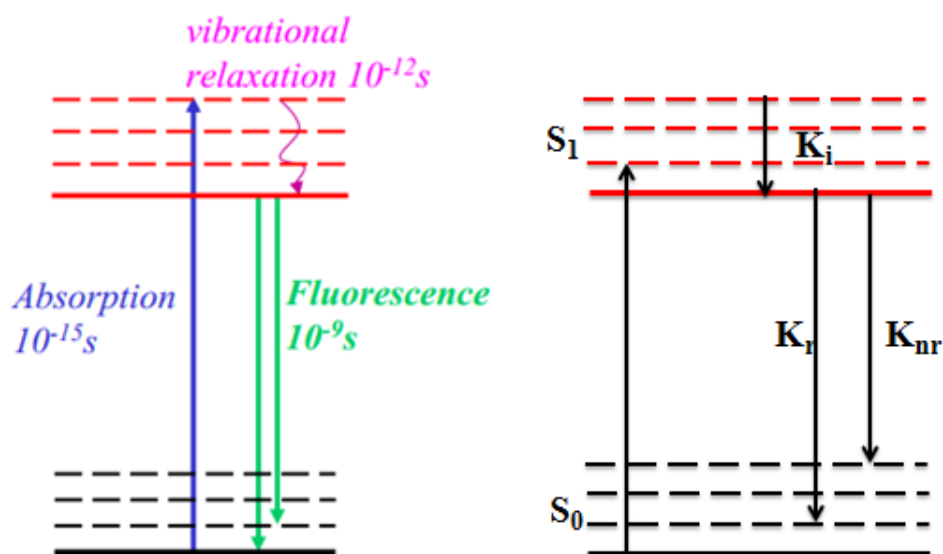


Figure 4: Pictorial representation of relaxation process (adapted from reference 14)

The absorption process $S_0 \rightarrow S_1$ and vibrational relaxation $S_1 \rightarrow S_1$ (inter system crossing) processes happen on a much faster timescale than the fluorescence emission ($S_1 \rightarrow S_0$). Thus the time it takes to return to the ground state S_0 only depends on the time spend in the lowest vibrational state of S_1 . K_r is the rate coefficient for the $S_1 \rightarrow S_0$ transition through fluorescent emission, K_{nr} is the rate coefficient for the $S_1 \rightarrow S_0$ transition through non-radiative relaxation mechanism and K_i is the rate coefficient for the $S_1 \rightarrow S_1$ through intersystem crossing. Therefore fluorescence life time is a sum of all relaxed transitions (**Equation 5**).

$$\tau = 1/K_r + K_{nr} + K_i \quad \dots\dots\dots$$

(5)

The contribution of K_i is negligible due to rapid relaxation by internal conversion occurs on the picosecond time scale, and hence can be ignored. Therefore,

$$\tau = 1/K_r + K_{nr} \quad \dots\dots\dots$$

(6)

Fluorescence life time depends on surrounding environment properties, like pH, ions concentration, binding strength, proximity of the energy acceptors, but is independent on the concentration of probe.^{17b,c} This can be an important advantage for imaging of cells and tissues where probe concentration may not be uniform.

5) Stokes Shift. Stokes described for the first time the phenomenon of fluorescence in 1852, in his famous paper “On the change of refrangibility of light”. Based on his experience, he came up with the idea that some materials, like fluorspar and uranium glass, have a power to convert invisible radiation (shorter wavelength) into visible one (longer wavelength). On the honor of his efforts the difference between the positions of the band maximum of the absorbance and emission of the fluorophore named as a Stokes shift (**Figure 5**).^{18a} The shift occurs due to internal conversion, which results in partial loss of the absorbed photon energy. Large Stokes shift is very important for high sensitivity of fluorescence microscope. The presence of the red shift gives the possibility to use additional optical filters in order to block the excitation source from reaching the detector so that fluorescence detection is measured against a low background.¹⁹

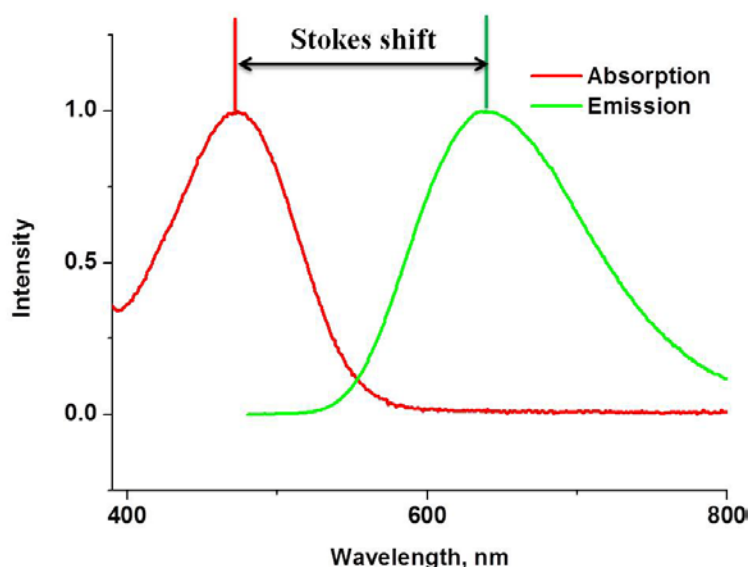


Figure 5: Pictorial representation of absorption, emission and Stokes shift (adapted from reference 18b)

6) Photostability. Photobleaching is the photochemical reaction of fluorophore on components of the local environment, which results in permanent loss of fluorescence property due to photoinduced chemical damage²⁰ of a fluorophore or the covalent modifications of fluorophore by surrounding molecules.²¹ The accurate mechanism of photobleaching is not known, but experts assumed that transition of excited singlet state to excited triplet state, which is relatively long-lived and chemically reactive. There are numerous ways to reduce photobleaching: a) minimizing exposure time of illumination on fluorophore, b) irradiating at longer wavelengths, or/and c) avoiding

of exposure to oxygen to prevent molecular interactions with it in reactive triplet excited state, which can be achieved either by passing nitrogen gas or using antioxidants.^{22a} Obviously, the fluorophore which can undergo high number of photon emission cycles are highly desirable.

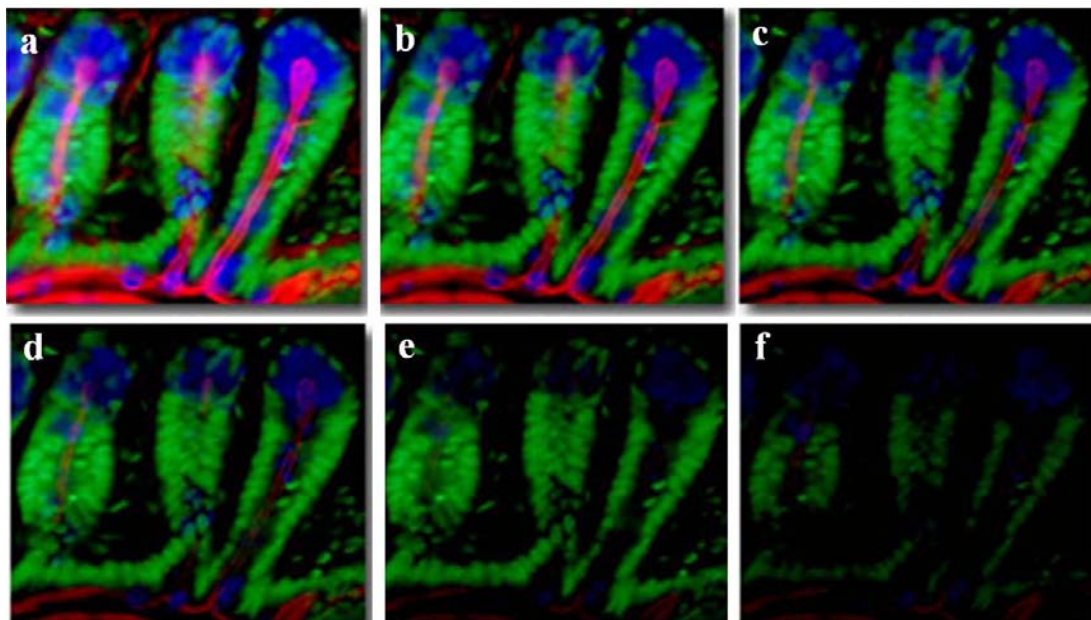


Figure 6: A typical example of photobleaching observed in a series of digital images captured at different time points for a multiply stained cryostat thin section of mouse intestine. a) at 0 min, b) at 2 min, c) at 4 min, d) at 6 min, e) at 8 min, f) at 10 min (adapted from reference 22b)

1.4. Advantages of Fluorescence Microscope:

The fundamental properties of fluorescence are extensively used in biological imaging for understanding of molecular recognition events. Compared with other techniques fluorescence offers much safer and more convenient procedures. In addition to that, fluorescence offers advantages of high sensitivity, selectivity, versatility of molecular probes, and high signal-to-noise ratio.

1) High Sensitivity. Fluorescence offer high sensitivity towards analyte, and its detection limit lays in the nano-molar range. For example, Weiying Lin *et al.* discovered a highly sensitive fluorescent for benzenethiols in environmental solutions and living cells and its detection limit was in the nanomolar range.²³

2) High Selectivity. Among available existing fluorophores, one can choose highly selective probe to differentiate events of cells and micro organisms on the subcellular

level, as well as to recognize metal ions, anions and molecules in analyzed sample. For example, DAPI is a staining agent for selective recognition of nuclei,²⁴ which is routinely used to discriminate between cytoplasm and nuclei. Another example, Ye Won Choi and co-workers developed a chemosensor for selective recognition of mercury ions even by naked eye.²⁵ Li Fu and co-workers developed a highly selective BODIPY dyes for recognition of fluoride anions.²⁶

3) High Versatility. Great numbers of fluorescent probes are available as cellular and molecular biology tools for understanding of the fundamental aspects of life.²⁷ One of the recent examples is versatile fluorescence probes developed in group of B. Imperiali for protein kinase activity.²⁸ The probe was designed in such a way, that by changing the kinase recognition motif in the peptide sequence it can target and recognize any desired kinase.

4) Stokes Shift. One of the major contributors in high resolution and increased sensitivity of microscope imaging is a large Stokes shift of the fluorescent molecule. It provides extremely high sensitivity for fluorescence imaging experiments.²³ Larger Stokes shift helps to reduce interference as it eliminates spectral overlap between absorption and emission. Such dyes in general give stronger signal and have reduced fluorescence quenching, which is advantageous for biological imaging.

1.5. Areas of Improvement of Fluorescence Bioimaging:

Although fluorescence microscope possesses numerous definite benefits over other microscope techniques, there is still scope for improvement. For example, difficulty to obtain clear image for the objects exhibiting autofluorescence, or in case when signal is also coming from non-specific binding parts. Some of the disadvantages and ways to overcome them are listed below.

1) Blurring. Fluorescence images may not be clear for deeper tissues imaging or thick samples (>1-2 cm) due to optical sectioning or refraction of light.²⁹ This can be overcome by use of either red to near infra-red light or use of transparent/semi-transparent model organisms, e.g. zebrafish.

2) Bleaching. Photoinduced chemical damage of a fluorophore or the covalent and non-covalent modifications of fluorophore by surrounding molecules may lead to

fluorescence quenching.³⁰ This problem can be solved by protecting molecule in excited state from interactions or reduce an exposure time of illumination.

3) Autofluorescence. Autofluorescence often interferes during fluorescent imaging, especially when the signals of interest are very dim, resulting in loss of images clarity. This problem can be solved by using of fluorophores with large Stokes shift or multi-colour fluorophores.

4) Toxicity. Sometimes chemical interference may cause cytotoxicity, in this case, special care should be taken to select non-toxic chromophores suitable for particular experiment.

1.6. Classification of Fluorophores:

Fluorophores can be classified into four types, based on their nature, size and chemical composition:

1. Biological fluorophores or natural fluorophores;
2. Quantum dots;
3. Fluorescent organic molecules;
4. Fluorescent organic nanoparticles (FONs).

1) Biological Fluorophores. GFP was the first biological fluorophore used in molecular and cellular biology. In 1962 Shimomura, Johnson and Saiga isolated a GFP from *Aequorea Victoria* jellyfish.¹³ In 1994, Chalfie *et al.* succeeded in expressing of GFP in a prokaryotic and eukaryotic cells, resulted in a strong green fluorescence when excited by UV-light.¹⁰ GFP has excitation wavelength at 395 nm and emission wavelength at 475 nm and quite good fluorescence quantum yield of $\Phi_f = 0.79$. In order to improve its physical and biochemical properties, new versions of GFP were engineered through mutagenesis. In 1995, Roger Y. Tsien³¹ described an S65T point mutation that increased the fluorescence intensity and photostability of GFP, labeled as enhanced green fluorescent protein (EGFP). Later T203Y mutation of GFP resulted in yellow fluorescent protein.³² Undoubtedly the family of GFP fluorophores is very useful tool for biological studies, which does not require any cofactors or substrates. However, the problem of overexpression, which may lead to generation of novel phenotypes, must be taken into consideration and special attention has to be paid do not alter the natural function of the fused to GFP proteins.³³

2) Quantum Dots. Quantum dots (QDs) are tiny nanocrystals of a semiconducting material with diameters in the range of 2-10 nm.³⁴ In general, quantum dots are composed from the elements in the periodic groups of II-VI, III-V or IV-VI, for example CdTe, InP, *etc.* In comparison with conventional fluorescent probes, quantum dots have substantial advantages, such as bright fluorescence, narrow emission, broad band excitation, photostability and extended half-life. Unique size of quantum dots allow them to penetrate in any part of the body making them suitable for such bio-medical applications as medical imaging, biosensors, *in vivo* and *in vitro* imaging, *etc.*³⁵ However, quantum dots have they own limitations, examples of which are poor solubility in aqueous medium and often high toxicity, which results in requirement of additional surface coating with non-toxic materials.³⁶

3) Fluorescent Organic Molecules: Organic fluorophores based on small molecules are powerful tools of visualization of biological events in living cells and organisms. Their diversity, easy synthesis, good colour tunability and high quantum yields are definite advantages for both bio-medical and biological research, yet there is still demand for development of molecular probes which combine best properties of the fluorophores. For example, Fluorescein, Rhodamine, and cyanine dyes show bright fluorescence and high quantum yield. However, these fluorophores have poor photostability.³⁷ Indocyanine green (ICG) is a stable and clinically approved dye, but its aqueous solubility of it is poor.³⁸ Currently BODIPY based dyes are widely used as a fluorescent labels and probes for bioimaging, nevertheless these fluorophores also have poor aqueous solubility and small Stokes shift.³⁹

4) Fluorescent Organic Nanoparticles. In order to overcome the disadvantages of organic chromophores for bioimaging, fluorescent organic molecules are converted into FONs. This is an effective strategy to minimize photobleaching, improve quantum efficiency and increase its aqueous solubility and biocompatibility. Over bulk chromophores, FONs have the following advantages for both *in vivo* and *in vitro* experiments:

- a) good biocompatibility and penetrability;
- b) high photobleaching threshold;
- c) high quantum yields;
- d) high signal to noise ratios;

e) they are easy to prepare, relatively inexpensive and easy to handle.

Zero dimensional organic nanoparticles (when all dimensions of nanoparticle are in nanoscale) have already found wide applications in optoelectronic nanodevices, bio/chemical sensing, immunofluorescent labeling, diagnostics, drug delivery, monitoring systems, and *in vitro* /*in vivo* imaging.⁴⁰ For the first time, FONs have been made in 1992 from π -conjugated organic molecules by Nakanishi and co-workers through reprecipitation method.⁴¹ Later in 1997, perylene and phthalocyanine nanoparticles were prepared in the same group and their photophysical properties were shown to be much different from that of bulk samples.⁴² Similarly, pyrazoline nano-crystals reported by Yao *et al.* were exhibiting optical properties divergent from bulk pyrazoline.⁴³ Although the reprecipitation method is well accepted as a cheap and efficient way to fabricate organic nanoparticles, formation of stable nanoparticles is an issue. The method of improvement came from Yao's group, where they used a water soluble polymer (poly(vinyl alcohol), PVA) as a protective and stabilizing agent to obtain a stable nanoparticles suspension.⁴⁴ In 2006, Latterini *et al.* synthesized perylene nanoparticles by reprecipitation method under various experimental conditions and showed that their spectral properties are markedly different from those of bulk perylene.⁴⁵ Latter, Baba *et al.* applied perylene nanocrystals for *in vitro* fluorescence confocal imaging of living cells.⁴⁶ In 2008, Jinsang Kim *et al.* reported dual colour self assembled organic nanoparticles and their application in targeted immune fluorescent labeling.^{40e} Nanoparticles with very interesting properties were reported in 2012 by N. D. Pradeep Singh *et al.* Prepared in his group perylene-3-yl-methanol FONs had four important functions: a) nano-carriers for drug delivery, b) photo-triggers for drug release, c) fluorescent chromophores for cell imaging and d) detectors for real time-monitoring of drug release.

Fluorescent imaging of thicker tissues is difficult with visible range wavelengths. Hence, one photon imaging using fluorescent organic nanoparticles is efficient only for surface tissues or transparent animals. However, *in vitro* fluorescent imaging of thicker samples is possible with dye possessing good two-photon absorption and the corresponding excitation in the far infrared region. In order to increase spatial resolution and high penetration in bioimaging, in 2011 Blanchard-Desce *et al.* prepared dipolar and octupolar triphenyl amine based FONs in aqueous

medium. The developed FONs were successfully utilized for two photon imaging on living *Xenopus laevis* tadpoles.⁴⁸ Similarly, in 2014 Chuang-Feng Chen *et al.* prepared multicolour FONs based on tetrahydro[5]helicene moiety and used for HeLa cell imaging.⁴⁹

Among all FONs, ones with red/ near-infrared emission are more preferable for biomedical applications due to reduced light scattering, minimal auto fluorescence interference from biological samples, and ability to illuminate thicker samples as result of their longer excitation and emission wavelengths. In 2014 Yen Wei *et al.* reported a new class of red FONs, which were good imaging agents for A549 cells and had excellent solubility in water and biocompatibility.⁵⁰ Another fascinating work was reported by Ben Zhong Tang *et al.* who prepared aggregation-induced red to near infrared emissive organic nanoparticles as effective and photo stable fluorescent probes for long term cell tracing studies.⁵¹

Thus, fluorescent organic probes are powerful tool for both basic biology and translational biomedical research.⁵² Development of FONs with high quantum yield, large Stokes shift, good photostability and impermeability remains to be very appealing area which is rapidly expanding. Among FONs, red /near infrared nano-dyes attract bigger interest due to their less harmful effect on the biological samples and lesser interference of autofluorescence. One of the limitations of the fluorescence microscope is inability to obtain clear image for deeper or thick samples (due to optical sectioning or refraction of light). However this problem can be easily addressed by usage of either red/near-infra-red light or transparent/semi-transparent model organisms, like zebrafish.

1.7. Model Organisms for *In Vivo* Imaging Studies:

Biological phenomena on laboratory level are usually studied using model non-human organisms, expecting that discoveries made with their help will be translated into understanding of biological processes in humans. Investigations of the cellular functions, developmental pathways and diagnosis of disease on the early stages of research are made on small model organisms, such as *xenopus*, *drosophila*, zebrafish, mouse, yeast and *E. coli*.

1) Zebrafish: For the last ten years, zebrafish (*Danio rerio*) has become a popular model system for the study of vertebrate development. The ability to acquire and

quantitatively analyze microscope data of living biological organisms is crucial in many areas of life sciences. In many model systems, light scattering and light absorption ambiguous the view of the inside of the specimen. Zebrafish offer the exciting opportunity to study development and function in a highly complex vertebrate model system by live imaging as the embryos are small enough to fit completely within the working distance of optical microscope. The embryos and larvae of this species are of small size, optically transparent, they have external fertilization and rapid embryo development (**Figure 7**). Apart from that, they are cost effective, easy to maintain, have high fecundity and shares the majority of the same genes as humans.⁵³ Zebrafish rapid development and exceptionally high optical clarity in embryonic and larval stages make it simple for quantitative investigation using live imaging approaches.^{54a} Zebrafish embryos can be labeled effortlessly with fluorescent dyes by just immersion in medium. After treatment and a brief wash followed by anesthetization, embryos can be transferred and oriented in correct the position on glass slides for visualization under optical microscope. A high resolution images with smaller signal to noise ratio can be easily captured facilitating quick collection of live imaging data.

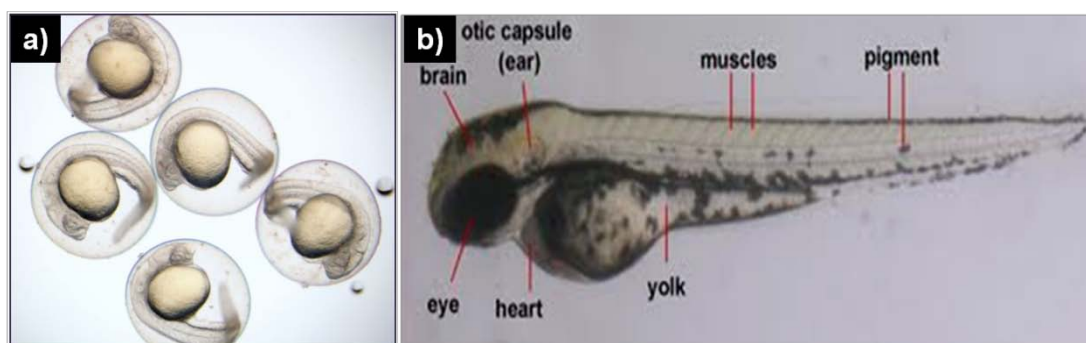


Figure 7: a) 2-day old zebrafish larvae still inside the egg shell, b) pictorial representation of zebrafish larva at 2 days post-fertilization (adapted from reference 54b)

2) Yeast: Yeast is a eukaryotic microorganism, which is particularly attractive as a model organism due to its small size, ease of culturing and short life cycle. Yeast can exist in both haploid and diploid stages (**Figure 8a** and **8b**), and its genomes shares 50 genes with human disease.⁵⁵ Apart from that, it is relatively cheap *in vivo* model. In yeast, the two most important species namely, budding or brewer's yeast *Saccharomyces cerevisiae* (*S. cerevisiae*), and the fission yeast *Schizosaccharomyces pombe* (*S. pombe*) are commonly employed as a models for biomedical research in

molecular biology laboratory. *S. cerevisiae* entered laboratories as a model system in early 1900s, when Ojvind Winge and Carl Lindegren begun their experiments.⁵⁷ Later in 1990, fission yeast was used as model system to study basic principles of a cell that can be applied to understand more complex organisms like mammals and in particular humans.⁵⁸ Budding and fission yeast are still used to study cellular processes such as growth, cell division, and morphogenesis using live cell fluorescence microscope.⁵⁹

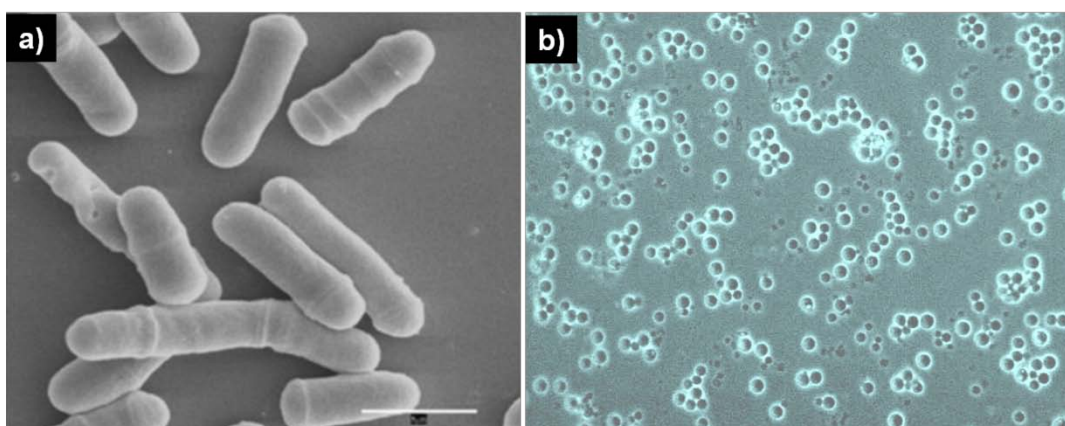


Figure 8: Pictorial representation of a) *S. pombe* and b) *S. cerevisiae* (adapted from reference 56)

3) *Escherichia coli* (*E. coli*): *E. coli* is a unicellular prokaryotic microorganism (**Figure 9**), and is another very attractive model organism. This small single celled organism reproduces and grows very rapidly, it is cheap and easy to maintain, its complete genome is studied and is easy to manipulate.⁶⁰ In 1940, *E. coli* adopted as a model organism to understand mechanisms of molecular genetics such as DNA replication and protein synthesis. Now *E. coli* is also used to study dynamic cellular processes such as growth, cell division, morphogenesis and gene expression using live cell fluorescence microscope.¹⁰

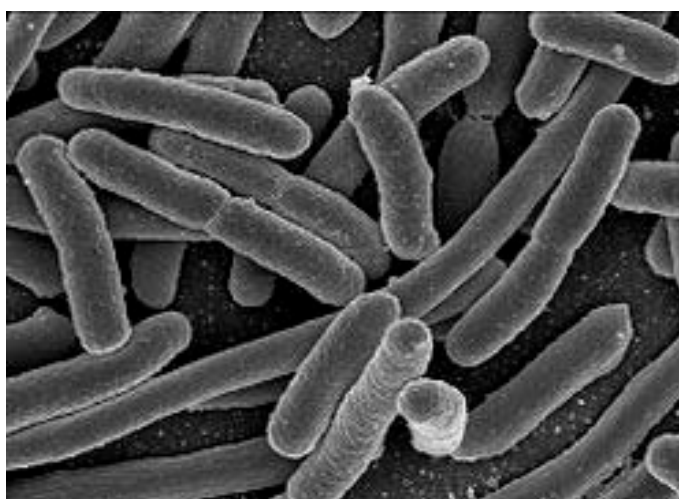


Figure 9: SEM images of *E. coli* (adapted from reference 61)

4) *Xenopus*: In *xenopus*, the two species namely, *xenopus laevis* and *xenopus tropicalis* are widely employed in basic cell and molecular biology studies. Among them *Xenopus laevis* embryos and their eggs are a popular model system for *in vivo* imaging studies.⁵³ They are attractive due to large abundant eggs that are easily manipulated, ready accessibility to any developmental stage and availability at low cost. *Xenopus* genome is similar to that of human, which makes it an ideal vertebrate model organism for *in vivo* imaging studies.⁶² Individual cells in *xenopus* embryos are larger than those in other vertebrate models, and therefore are more suitable for imaging cell behaviour and subcellular processes.⁶³ They are also easy to manipulate, and easy to stain with fluorescent dyes by means of targeted micro injections.⁶⁴ Such manipulations do not require highly trained personnel due to big size of the embryos and their large number available.

5) *Drosophila*: *Drosophila* is a multicellular eukaryotic organism and it is also very attractive as a model organism, due to its small size, short life cycle, high fecundity, cost effectiveness and effortless maintenance. Moreover, its genome (61%) and its protein sequence (51%) almost similar to that of human genome.⁶⁵ In addition to that, *Drosophila* larva possesses translucent skin surface which is very convenient property for live imaging.⁶⁶

Among all model organisms described above, zebrafish, yeast and *E. coli* were successfully employed in this work for bioimaging using FONs.

1.8. Layout of the Thesis:

In this thesis, preparation of the novel fluorescent organic nano-materials for long-term *in vitro* and *in vivo* bioimaging applications is described. FONs were prepared from organic chromophores based on naturally occurring nitrogen containing heterocycles including nucleobase and nucleosides, connected to fluorescent moieties through long and flexible aliphatic linker. The primary goal was to synthesize novel fluorescent organic molecules with improved properties from readily available bio-compatible materials and convert them into FONs using bottom-up approach. Characterization of those nanoparticles was carried out using modern methods employed in nanotechnology, e.g. scanning electron microscope (SEM), dynamic light

scattering (DLS), atomic force microscope and confocal fluorescent microscope (CFM). Biological activity of FONs was tested using different cell lines and model organisms, including mouse macrophage cells, cancer cells, yeast, zebrafish embryos and various bacterial cell lines, and utilization for *in vivo* and *in vitro* molecular bio-imaging was demonstrated. On the other hand, a novel fluorescent chemosensor for toxic heavy metals was designed and examined in this work as well.

In summary of aspects involved in thesis,

Chapter 1 contains a brief introduction to bioimaging, historical perspective of bioimaging, introduction to fluorophore and its recent developments and applications for bioimaging. Evolution of the fluorescent microscope/ nanoscope is covered in the Chapter 1 as well. Finally, brief description of the most popular small model organisms commonly used for *in vivo* bioimaging studies is also included.

Chapter 2 comprises the synthesis and characterization of multi-colour FONs based on **PPy** and **GPy** fluorescent chromophores, their physical-chemical characterization and mechanism of the nanoparticles formation. The use of **PPy** and **GPy** based FONs for the real-time *in vivo* whole-body fluorescent imaging of zebrafish was demonstrated for the first time.

Chapter 3 reports the synthesis of **Cy-Red** (cytosine-4,7-di(thiophene-2-yl)benzo[c][1,2,5]thiadiazole) - the novel biocompatible, non-toxic and highly efficient chromophore with large Stokes shift and high quantum yield. Although the organic molecule **Cy-Red** was almost insoluble, nanonization effectively converted it into well soluble in water as FONs (**nano-Cy-Red**). Chapter 3 describes broad range of applications of **nano-Cy-Red** in real life long-term *in vitro/in vivo* imaging, which includes staining of mouse macrophage, cancer cells and fission yeast, and direct *in vivo* visualization of cancer cell migration up to 72 h post transplantation in zebrafish embryos.

Chapter 4 describes the synthesis of various 3, 5 and 5-pyrene alkyl substituted nucleosides via simple, rapid and economical protocols. The evaluation of antibacterial activity of novel nucleoside derivatives helped to identify potent lead compound **2.4** with high activity against both gram-positive bacteria and *Mycobacterium tuberculosis*, without significant cytotoxic effect against host macrophages. The mechanism of action via disruption of the bacterial DNA replication is proposed, and a series of the experiments leading to its conformation is

presented. Morphology studies of FONs based on compound **2.4** are described as well.

Chapter 5 comprises multiple efforts to synthesize the novel fluorescent chemosensor based on naphthyridine-boronic acid through the short and efficient synthetic route. Final compound was shown to be highly sensitive specifically towards Mercury ion, with much improved sensitivity in the presence of D-fructose at physiological concentration. This finding is especially important in food industry, *e.g.* for detection of mercury contamination of high fructose corn syrup, or in estimation of mercury in polluted biological samples and underground water.

1.9. Reference:

- (1) (a) Ciobanu, L.; Pennington, C. H. *Solid. State. Nucl. Mag.* **2004**, 25, 138. (b) Milka, V. I.; V. I. R.; P. A. B. *J. Optoelectron. Adv. Mat.* **2012**, 14, 559.
- (2) Qian, Y.-Z.; Shipley, J. B.; Levasseur, J. E.; Kukreja, R. C. *J. Mol. Cell. Cardiol.* **1998**, 30, 1163.
- (3) Shi, Y.; Wu, J. *J. Struct. Funct. Genomics.* **2007**, 8, 67.
- (4) Eils, R.; Athale, C. *J. Cell. Boil.* **2003**, 161, 477.
- (5) (a) Stephens, D. J.; Allan, V. J. *Science* **2003**, 300, 82. (b) Pichler, B. J.; Kolb, A.; Nägele, T.; Schlemmer, H.-P. *J. Nucl. Med.* **2010**, 51, 333. (c) Bar-Shalom, R.; Yefremov, N.; Guralnik, L.; Gaitini, D.; Frenkel, A.; Kuten, A.; Altman, H.; Keidar, Z.; Israel, O. *J. Nucl. Med.* **2003**, 44, 1200.
- (6) (a) Schäferling, M. *Angew. Chem. Int. Ed.* **2012**, 51, 3532. (b) Yao, J.; Yang, M.; Duan, Y. *Chem. Rev.* **2014**, 114, 6130.
- (7) (a) Guo, Z.; Park, S.; Yoon, J.; Shin, I. *Chem. Soc. Rev.* **2014**, 43, 16. (b) Shao, J.; Sun, H.; Guo, H.; Ji, S.; Zhao, J.; Wu, W.; Yuan, X.; Zhang, C.; James, T. D. *Chem. Sci.* **2012**, 3, 1049. (c) Liu, Y.; Chen, M.; Cao, T.; Sun, Y.; Li, C.; Liu, Q.; Yang, T.; Yao, L.; Feng, W.; Li, F. *J. Am. Chem. Soc.* **2013**, 135, 9869. (d) Banerjee, S.; Veale, E. B.; Phelan, C. M.; Murphy, S. A.; Tocci, G. M.; Gillespie, L. J.; Frimannsson, D. O.; Kelly, J. M.; Gunnlaugsson, T. *Chem. Soc. Rev.* **2013**, 42, 1601. (e) Li, Y.; Zhang, G.; Yang, G.; Guo, Y.; Di, C. a.; Chen, X.; Liu, Z.; Liu, H.; Xu, Z.; Xu, W.; Fu, H.; Zhang, D. *J. Org. Chem.* **2013**, 78, 2926.
- (8) (a) Leeuwenhoek A van. *Arcana Natura Detecta*, Delphis, Batav, **1695**. (b) Ellinger, P. *Biol. Rev.* **1940**, 15, 323.

- (9) Monardes, N. *J. Immunol.* **1942**, 45, 159.
- (10) M.Chalfie, Y. T.; Euskirchen, G.; Ward, W.; Prasher, D.C. *Science*, **1994**, 263, 801.
- (11) (a) Fölling, J.; Belov, V.; Riedel, D.; Schönle, A.; Egner, A.; Eggeling, C.; Bossi, M.; Hell, S. W. *Chem.Phys. Chem.* **2008**, 9, 321. (b) Fernandez-Suarez, M.; Ting, A. Y. *Nat. Rev. Mol. Cell Biol.* **2008**, 9, 929.
- (12) Monardes, N., *Dos Libros/El* **1565**.
- (13) Shimomura, O.; Johnson, F. H.; Saiga, Y. *J. Cell. Physio.* **1962**, 59, 223.
- (14) Zimmermann, J.; Zeug, A.; Roder, B. *Phys. Chem. Chem. Phys.* **2003**, 5, 2964.
- (15) Frangioni, J. V. *Curr. Opin. Chem. Biol.* **2003**, 7, 626.
- (16) Pace, C. N.; Vajdos, F.; Fee, L.; Grimsley, G.; Gray, T. *Protein Sci.* **1995**, 4, 2411.
- (17) (a) Williams, A. T. R.; Winfield, S. A.; Miller, J. N. *Analyst* **1983**, 108, 1067. (b) Calleja, V.; Ameer-Beg, S. M.; Vojnovic, B.; Woscholski, R.; Downward, J.; Larijani, B. *Bio. chem. J.* **2003**, 372, 33. (c) Lin, H.-J.; Herman, P.; Lakowicz, J. R. *Cytometry Part A* **2003**, 52A, 77.
- (18) (a) Stokes, G. G. *Philos. T. Roy. Soc.* **1852**, 142, 463. (b) Reddy, E. R.; Yellanki, S.; Medishetty, R.; Konada, L.; Alamuru, N. P.; Haldar, D.; Parsa, K. V. L.; Kulkarni, P.; Rajadurai, M. *ChemNanoMat* **2015**, DOI: 10.1002/cnma.201500108.
- (19) (a) Rihn, S.; Retaillieu, P.; De Nicola, A.; Ulrich, G.; Ziessel, R. *J. Org. Chem.* **2012**, 77, 8851. (b) Chen, Y.; Zhao, J.; Guo, H.; Xie, L. *J. Org. Chem.* **2012**, 77, 2192. (c) Xu, Z.; Liao, Q.; Wu, Y.; Ren, W.; Li, W.; Liu, L.; Wang, S.; Gu, Z.; Zhang, H.; Fu, H. *J. Mater. Chem.* **2012**, 22, 17737. (d) Shcherbakova, D. M.; Hink, M. A.; Joosen, L.; Gadella, T. W. J.; Verkhusha, V. V. *J. Am. Ceram. Soc.* **2012**, 134, 7913.
- (20) Zheng, Q.; Blanchard, S. In *Encyclopedia of Biophysics*; Roberts, G. K., Ed.; Springer Berlin Heidelberg, 2013.
- (21) Bou-Abdallah, F.; Chasteen, N. D.; Lesser, M. P. *BBA-Gen. Subjects* **2006**, 1760, 1690.
- (22) Hemmateenejad, B.; Shamsipur, M.; Khosousi, T.; Shanehsaz, M.; Firuzi, O. *Analyst* **2012**, 137, 4029.
- (23) Lin, W.; Long, L.; Tan, W. *Chem. Commun.* **2010**, 46, 1503.
- (24) Kapuscinski, J. *Biotech. Histochem.* **1995**, 70, 220.

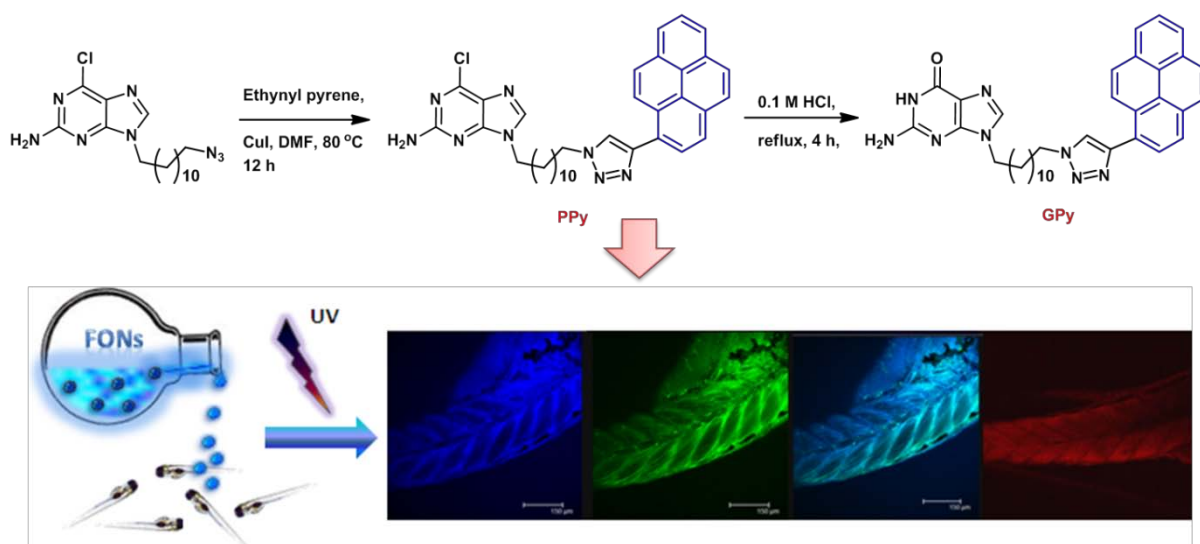
- (25) Choi, Y. W.; You, G. R.; Lee, M. M.; Kim, J.; Jung, K.-D.; Kim, C. *Inorg. Chem. Commun.* **2014**, *46*, 43.
- (26) Fu, L.; Wang, F.-F.; Gao, T.; Huang, R.; He, H.; Jiang, F.-L.; Liu, Y. *Sens. Actuators, B: Chemical*.
- (27) Zhang, J.; Campbell, R. E.; Ting, A. Y.; Tsien, R. Y. *Nat. Rev. Mol. Cell. Biol.* **2002**, *3*, 906.
- (28) Shultz, M. D.; Imperiali, B. *Journal of the American Chemical Society* **2003**, *125*, 14248.
- (29) Sreejith, S.; Divya, K. P.; Ajayaghosh, A. *Angew. Chem. Int. Ed.* **2008**, *47*, 7883.
- (30) (a) Yum, K.; Ahn, J.-H.; McNicholas, T. P.; Barone, P. W.; Mu, B.; Kim, J.-H.; Jain, R. M.; Strano, M. S. *ACS Nano* **2012**, *6*, 819. (b) Su, H.; Chen, X.; Fang, W. *Anal. Chem.* **2014**, *86*, 891.
- (31) Heim, R.; Cubitt, A. B.; Tsien, R. Y. *Nature* **1995**, *373*, 663.
- (32) Tsien, R. Y. *Annu. Rev. Biochem.* **1998**, *67*, 509.
- (33) Clyne, P. J.; Brotman, J. S.; Sweeney, S. T.; Davis, G. *Genetics* **2003**, *165*, 1433.
- (34) Ekimov, A. I. O., A. A. *J. Exp. Theor. Phys. Lett.* **1981**, *34*, 345.
- (35) Medintz, I. L.; Uyeda, H. T.; Goldman, E. R.; Mattoussi, H. *Nat. Mater.* **2005**, *4*, 435.
- (36) (a) Bruchez, M.; Moronne, M.; Gin, P.; Weiss, S.; Alivisatos, A. P. *Science* **1998**, *281*, 2013. (b) Pinaud, F.; Michalet, X.; Bentolila, L. A.; Tsay, J. M.; Doose, S.; Li, J. J.; Iyer, G.; Weiss, S. *Biomaterials* **2006**, *27*, 1679.
- (37) (a) Eggeling, C.; Volkmer, A.; Seidel, C. A. M. *Chem. Phys. Chem* **2005**, *6*, 791. (b) Panchuk-Voloshina, N.; Haugland, R. P.; Bishop-Stewart, J.; Bhalgat, M. K.; Millard, P. J.; Mao, F.; Leung, W.-Y.; Haugland, R. P. *J. Histochem. Cytochem.* **1999**, *47*, 1179.
- (38) Soper, S. A.; Mattingly, Q. L. *J. Am. Chem. Soc.* **1994**, *116*, 3744.
- (39) Loudet, A.; Burgess, K. *Chem. Rev.* **2007**, *107*, 4891.
- (40) (a) An, B.-K.; Gierschner, J.; Park, S. Y. *Acc. Chem. Res.* **2012**, *45*, 544. (b) Choi, J. W., N.S. *Biomedical Engineering-From theory to applications (Ed.: R. Fazel-Rezai)* **2011**, 299. (c) An, B.-K.; Kwon, S.-K.; Jung, S.-D.; Park, S. Y. *J. Am. Chem. Soc.* **2002**, *124*, 14410. (d) Cui, W.; Lu, X.; Cui, K.; Wu, J.; Wei, Y.; Lu, Q. *Langmuir* **2011**, *27*, 8384. (e) Kim, H.-J.; Lee, J.; Kim, T.-H.;

- Lee, T. S.; Kim, J. *Adv. Mater.* **2008**, *20*, 1117(f) Kaeser, A.; Schenning, A. P. H. *J. Adv. Mater.* **2010**, *22*, 2985.
- (41) Hitoshi, K.; Hari Singh, N.; Hidetoshi, O.; Shuji, O.; Hiro, M.; Nobutsugu, M.; Atsushi, K.; Katsumichi, O.; Akio, M.; Hachiro, N. *Jpn. J. Appl. Phys.* **1992**, *31*, L1132.
- (42) (a) Hitoshi, K.; Hirokazu, K.; Shuji, O.; Hidetoshi, O.; Hiro, M.; Hachiro, N. *Jpn. J. Appl. Phys.* **1996**, *35*, L221. (b) Komai, Y.; Kasai, H.; Hirakoso, H.; Hakuta, Y.; Okada, S.; Oikawa, H.; Adschiri, T.; Inomata, H.; Arai, K.; Nakanishi, H. *Mol. Cryst. Liq. Cryst. A* **1998**, *322*, 167.
- (43) Fu, H.-B.; Yao, J.-N. *J. Am. Chem. Soc.* **2001**, *123*, 1434.
- (44) Xie, R.; Xiao, D.; Fu, H.; Ji, X.; Yang, W.; Yao, J. *New J. Chem.* **2001**, *25*, 1362.
- (45) Latterini, L.; Roscini, C.; Carlotti, B.; Aloisi, G. G.; Elisei, F. *Phys. Status Solidi A* **2006**, *203*, 1470.
- (46) Koichi, B.; Hitoshi, K.; Akito, M.; Hidetoshi, O.; Hachiro, N. *Jpn. J. Appl. Phys.* **2009**, *48*, 117002.
- (47) Vijayakumar, C.; Sugiyasu, K.; Takeuchi, M. *Chem. Sci.* **2011**, *2*, 291.
- (48) Parthasarathy, V.; Fery-Forgues, S.; Campioli, E.; Recher, G.; Terenziani, F.; Blanchard-Desce, M. *Small* **2011**, *7*, 3219.
- (49) Li, M.; Feng, L.-H.; Lu, H.-Y.; Wang, S.; Chen, C.-F. *Adv. Funct. Mater.* **2014**, *24*, 4405.
- (50) Zhang, X.; Zhang, X.; Yang, B.; Zhang, Y.; Wei, Y. *ACS Appl. Mater. Interfaces* **2014**, *6*, 3600.
- (51) Li, K.; Qin, W.; Ding, D.; Tomczak, N.; Geng, J.; Liu, R.; Liu, J.; Zhang, X.; Liu, H.; Liu, B.; Tang, B. Z. *Sci. Rep.* **2013**, *3*.
- (52) Terai, T.; Nagano, T. Pfluger. *Eur. J. Phycol.* **2013**, *465*, 347.
- (53) Fleming, A.; Rubinsztein, D. C. *Biochim. Biophys.* **2011**, *1812*, 520.
- (54) (a) Antoine, T. E.; Jones, K. S.; Dale, R. M.; Shukla, D.; Tiwari, V. *Zebrafish* **2014**, *11*, 17. (b) Kimmel, C. B.; Ballard, W. W.; Kimmel, S. R.; Ullmann, B.; Schilling, T. F. *Dev. dynam.* **1995**, *203*, 253.
- (55) Mell, J. C.; Burgess, S. M. In *eLS*; John Wiley & Sons, Ltd, 2001.
- (56) Tang, Z. *Nature Education* **2010**, *3*, 56.
- (57) Mortimer, R. K. *Genome Research* **2000**, *10*, 403.
- (58) Piel, M.; Tran, P. T. *Curr. Biol.* **19**, R823.

- (59) Rines, D. R.; Thomann, D.; Dorn, J. F.; Goodwin, P.; Sorger, P. K. *Cold. Spring. Harb. Protoc.* **2011**, 2011, pdb.top065482.
- (60) Blattner, F. R.; Plunkett, G.; Bloch, C. A.; Perna, N. T.; Burland, V.; Riley, M.; Collado-Vides, J.; Glasner, J. D.; Rode, C. K.; Mayhew, G. F.; Gregor, J.; Davis, N. W.; Kirkpatrick, H. A.; Goeden, M. A.; Rose, D. J.; Mau, B.; Shao, Y. *Science* **1997**, 277, 1453.
- (61) Hartmann, M.; Berditsch, M.; Hawecker, J.; Ardakani, M. F.; Gerthsen, D.; Ulrich, A. S. *Antimicrob. Agents Chemother.* **2010**, 54, 3132.
- (62) Tan, M. H.; Au, K. F.; Yablonovitch, A. L.; Wills, A. E.; Chuang, J.; Baker, J. C.; Wong, W. H.; Li, J. B. *Genome Res.* **2013**, 23, 201.
- (63) Kieserman, E. K.; Lee, C.; Gray, R. S.; Park, T. J.; Wallingford, J. B. *Cold. Spring. Harb. Protoc.* **2010**, pdb.prot5427.
- (64) Cohen, S.; Au, S.; Panté, N. *J. Vis. Exp.* **2009**, 1106.
- (65) Reiter, L. T.; Potocki, L.; Chien, S.; Gribskov, M.; Bier, E. *Genome Res.* **2001**, 11, 1114.
- (66) Mishra, B.; Ghannad-Rezaie, M.; Li, J.; Wang, X.; Hao, Y.; Ye, B.; Chronis, N.; Collins, C. A. **2014**, e50998.

2

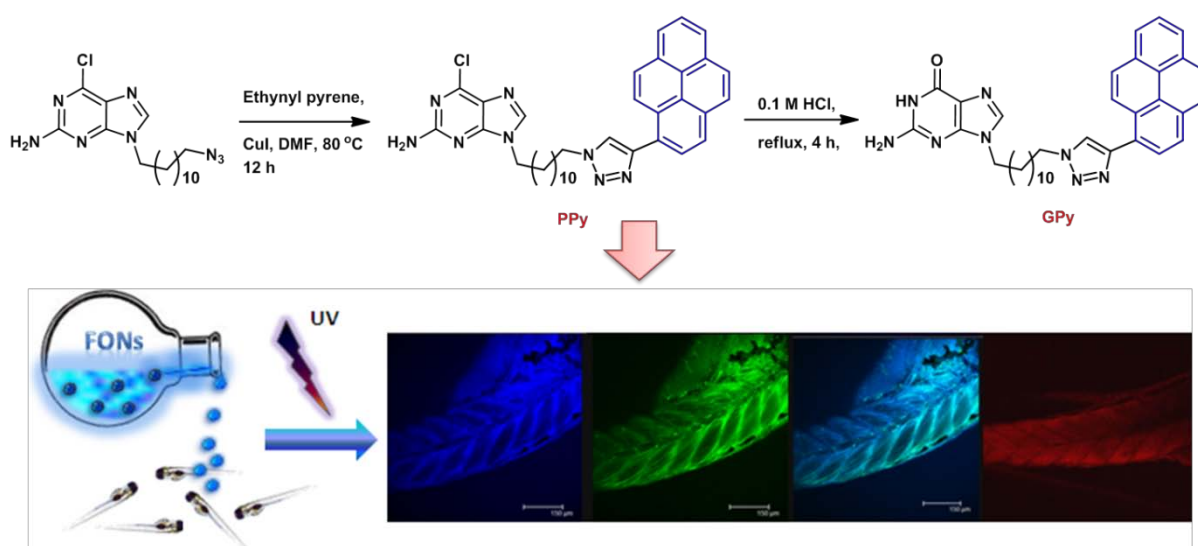
Selective Multicolour Imaging of Zebrafish Muscle Fibres Using Fluorescent Organic Nanoparticles



*This chapter partly adapted from: **E. Ramanjaneya Reddy**, Rakesh Kumar Banote, Kiranam Chatti, Puskar Kulkarni and Marina S. Rajadurai* *ChemBioChem* **2012**, 13, 1889-1894.

2

Selective Multicolour Imaging of Zebrafish Muscle Fibres Using Fluorescent Organic Nanoparticles



*This chapter partly adapted from: **E. Ramanjaneya Reddy**, Rakesh Kumar Banote, Kiranam Chatti, Puskar Kulkarni and Marina S. Rajadurai* *ChemBioChem* **2012**, 13, 1889-1894.

2.1. Abstract:

This chapter describes novel multi colour FONs (**PPy** and **Gpy**) prepared from pyrene containing guanine analogs through an efficient Cu-catalyzed alkyne-azide (3+2) cycloaddition.¹ Their photophysical properties and morphology were fully investigated by UV-Vis and fluorescence spectroscopy, SEM, AFM and CFM studies. This work demonstrates that multicolour FONs were able to penetrate into human breast cancer cells and zebrafish embryos, they were nontoxic, biocompatible and exhibited specificity towards muscular tissues of zebrafish embryos. Tissue autofluorescence occur in many biological samples,² and it is challenging task to correctly select chromophore of specific properties, which is not masked by natural autofluorescence, especially when multiply-labeled specimens are used. This work displays effective use of multicolour imaging using pyrene containing FONs to overcome the issue of high background noise arising from sample autofluorescence. **PPy** and **GPy** nanoparticles were resistant to bleaching or fading and were easy to use. This chapter proposes a potential application of **PPy** and **GPy** FONs as an excellent reagent for the study of neuromuscular changes in zebrafish embryos. This study demonstrated for the first time the utilization possibility of **PPy** FONs for the *in vivo* whole body multicolour fluorescent imaging of zebrafish embryos.

2.2 Introduction:

The design and preparation of FONs from organic molecules is one of the rapidly emerging fields of organic-based nanoscience. FONs can be exploited in the broad range of potential applications in optoelectronic nano-devices, (bio-)chemical sensing, drug delivery and monitoring systems, diagnostics, immunofluorescent labelling and *in vitro/ in vivo* imaging.³⁻⁷ Particularly for fluorescent imaging studies, fluorescent proteins, organic dyes and probes have been widely used in all areas of biology and preclinical research for the visualization of cellular and subcellular biological processes.⁸ Among fluorescence-based imaging agents, organic dyes are of rising interest, because of their diversity, easy synthesis, good colour tunability and high quantum yield, although poor photostability is an issue.^{7b} On the other hand, FONs are very attractive candidates for fluorescent imaging, as they offer definite advantages over bulky organic chromophores, such as easy cellular uptake,⁹ size-dependent fluorescent properties¹⁰ and longer fluorescence lifetime.^{4c}

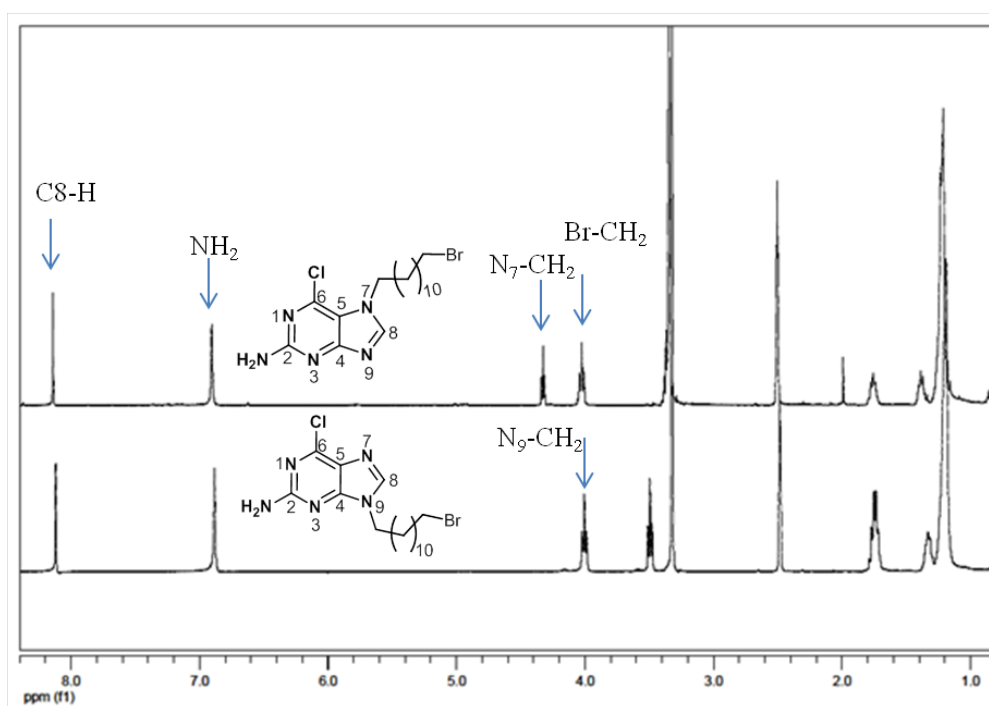
Although the nature of the organic fluorophores does not allow them to generate fluorescent signals at significant tissue depths (>1-2 cm), this limitation can be overcome by using either fluorescence imaging with near-infrared (NIR) light¹¹⁻¹² or by taking advantage of small animals with transparent tissues, for example frog (*Xenopus* frog) or zebrafish (*Danio rerio*) embryos. Zebrafish is particularly attractive model for fundamental and preclinical research because of an exceptional combination of experimental and genetic advantages, such as the significant similarity between zebrafish and human genomes, high fecundity, external fertilization, rapid embryo development and optical transparency of embryos. An additional advantage is the straight forward generation of a zebrafish mutant for modeling a particular human disease; for example, human muscular dystrophies show very similar cellular pathology to that of zebrafish muscle degeneration.¹³ These qualities make zebrafish an ideal research model for studying early development, understanding the pathogenesis of human disease and providing systems for developing and testing new therapies.

Though there is a number of reports available on zebrafish tissues fluorescent imaging, including green fluorescent protein expression, quenched fluorescent protein (EnzChek), phospholipid (PED6), antibody labeling and staining with fluorescent small molecules,¹⁴ however, until now there are no reports of whole-body imaging with FONs. FONs based on purine scaffolds seem particularly promising because substituted purines, pyrimidines and their tautomers have high biological activity and are the most widely distributed nitrogen-containing heterocycles in nature. This thesis proposes that the use of non-toxic FONs self-assembled from biologically active molecules and carrying chromophoric tags with high quantum yield and broad emission could be useful for cell/tissue/organism multicolour imaging, and for biological processes visualization in zebrafish embryos.

Particularly, this chapter reports the synthesis of a novel pyrene-based blue chromophore linked to biologically active guanine analogues, **PPy** and **GPy**, and their self-assembly in DMSO/H₂O to form solution-stable, blue emissive, biocompatible, nontoxic FONs. Their photophysical properties and the results of SEM, AFM and CFM studies are also presented here. Finally, this chapter demonstrates the use of FONs as an excellent technique for *in vivo* whole-body fluorescent imaging of zebrafish, and in particular for the selective imaging of muscle fibres.

2.3. Results and Discussion:

The target guanosine analogues, 6-chloro-7-(12-(4-(pyren-1-yl)-1H-1,2,3-triazol-1-yl)dodecyl)-7H-purin-2-amine (**PPy**) and 2-amino-7-(12-(4-(pyren-1-yl)-1H-1,2,3-triazol-1-yl)dodecyl)-1H-purin-6(7H)-one (**GPy**) were synthesized from commercially available 6-chloro-7H-purin-2-amine (**1.1**) in four steps according to **Scheme 1A**. At the first step, N-alkylation of 6-chloro-7H-purin-2-amine (**1.1**) with 3 equiv of 1,12-dibromododecane (**1.2**) in the presence of anhydrous potassium carbonate gave N9-alkylated purine **1.3** in 53% yield. Such low yield can be explained by the fact that alkylation of purines is not regiospecific, and product mixtures usually contain significant amounts of N7-substituted product and unutilized material.¹⁵ The two regio-isomers, N7 and N9-alkylated purines have been characterized by ¹H NMR, where they exhibit characteristic shift differences in the spectra that were used to distinguish the products in mixtures.¹⁵ Specifically, the signals of N9-CH₂ and Br-CH₂ for the N9-isomer shifted upfield relative to the corresponding N7-CH₂ and Br-CH₂ for the N7-isomer (**Figure 1**). At the next step, reaction of N9-substituted purine **1.3** with sodium azide formed the azide precursor **1.4** in good yield. Subsequent 1,3- dipolar Huisgen cycloaddition reaction of **1.4** with 1-ethynylpyrene (**1.8**)¹⁶ under “click reaction” conditions in presence of CuSO₄·5H₂O/Sodium ascorbate in water/DMF (2:1) gave purine connected to fluorescent pyrene unit *via* triazole-alkyl linker (compound **1.5** or **PPy**). ¹H NMR spectroscopy confirmed the formation of a five-membered triazole ring by exhibiting a C_{triazole}-H proton at 8.23 ppm and disappearance of the terminal acetylene proton at 3.63 ppm (see page no 61). Subsequently, treatment of **PPy** with 0.1N HCl under reflux condition produced the corresponding guanine derivative carrying alkylated pyrene triazolyl compound **GPy** in a reasonable 52% yield. FTIR spectroscopy clearly confirmed the formation of carbonyl group by displaying a band at 1567 cm⁻¹. Additionally, the ¹H NMR spectrum showed a peak at 10.7 ppm in DMSO-*d*₆ (see page no 62), thus confirming the presence of an N-H proton. EI-MS spectrometry revealed an *m/z* value of 586, corresponding to **GPy**. Apart from that 1-decyl-4-(pyren-1-yl)-1H-1,2,3-triazole (**1.9**) was prepared from 1-azidodecane¹⁷ (**1.7**) through a click reaction with 1-ethynylpyrene (**1.8**) in 81% yield and was used for photophysical studies (**Scheme 1B**).

Scheme 1: Synthesis of fluorescent guanosine analogues **PPy** and **Gpy****Figure 1:** Stacked spectra of N7 and N9- alkylated purine regio-isomers in $\text{DMSO-}d_6$

2.4. Optical Properties of PPy and GPy:

For the exploitation of organic compounds for biological studies, the preferred biocompatible solvent mixture is DMSO/H₂O (2:98); hence, photophysical properties of **PPy** and **GPy** were examined in both solvents DMSO and DMSO/H₂O. **Figures 2** and **3** show the solution-state optical absorption and emission properties of **PPy** and **GPy**. In DMSO, **PPy** and **GPy** displayed nearly identical absorbance maxima (350 nm and 353 nm, respectively). Fluorescent emission spectra ($\lambda_{\text{ex}} = 350$ nm) exhibited similar fluorescence bands, with a maximum at 389 nm and a shoulder at 409 nm for both compounds. Due to high solubility of **PPy**, its optical absorption and emission properties in various solvents were also studied. It was found that in chloroform **PPy** forms strong J-aggregates²⁵ which was indicated by a band shift from 350 nm to 365 nm in absorption spectrum (**Figure A1**, see page no. 55) and a band is shift from 387 nm to 408 nm in emission spectrum (**Figure A2**, see page no. 55). The solution-state quantum yield of **GPy** ($\Phi_f = 0.221$) was slightly weaker than that of **PPy** ($\Phi_f = 0.257$). The new chromophore **PPy** had Stokes shift of 39 nm, while **PPy** FONs had even large Stokes shift of 135 nm, which is also an indication of the formation of J-type molecular aggregates. Although the target compound for preparation of FONs was **GPy**, its precursor **PPy** found to be more convenient to use for all further biological and morphological studies, as it had better solubility, slightly higher quantum yield, larger Stokes shift, while maintaining structural similarity to **GPy** and nearly identical optical properties.

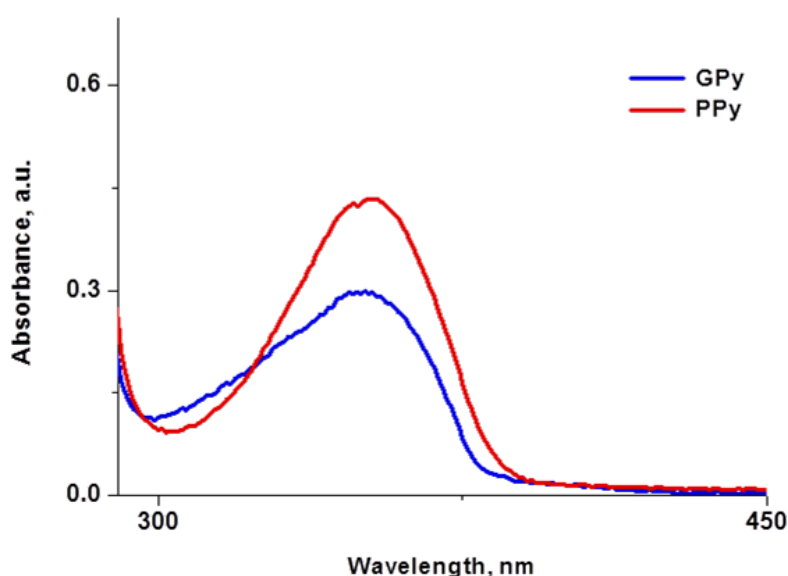


Figure 2: UV-Vis absorption spectra of **PPy** and **GPy** in DMSO at 10^{-5} M

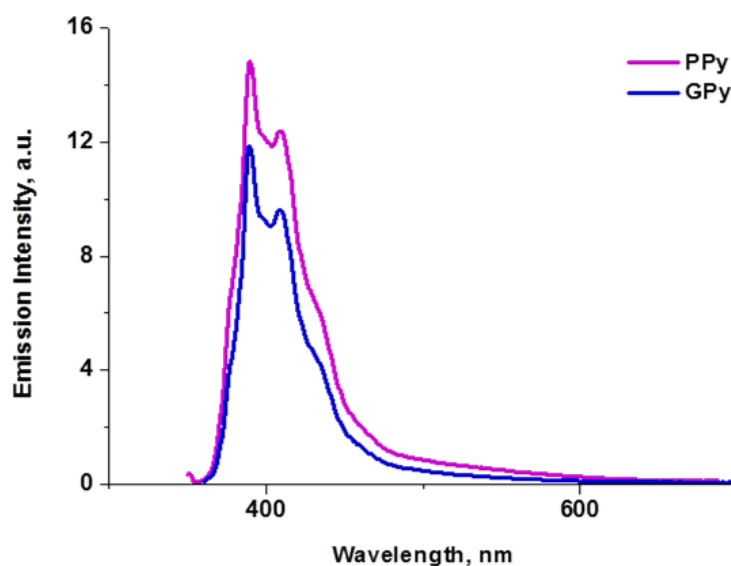


Figure 3: Emission spectra of **PPy** and **GPy** in DMSO ($\lambda_{\text{ex}} = 350$ nm) at 10^{-5}M

While preparing solutions of **PPy** in DMSO/water for biological investigations, it was noted that addition of water to the DMSO solution of **PPy** results a new optical absorption bands with red shift and high extinction coefficients in the region 230-270 nm. Interestingly, the bathochromic shift was increasing with increasing water content (50 to 98%, **Figure 4**). In addition to that **PPy** shows a visual bathochromic shift and increasing quenching of fluorescence as the percentage of water in solution was increasing (**Figure 5a** and **5b**), although the same concentration was maintained in all examined solutions.

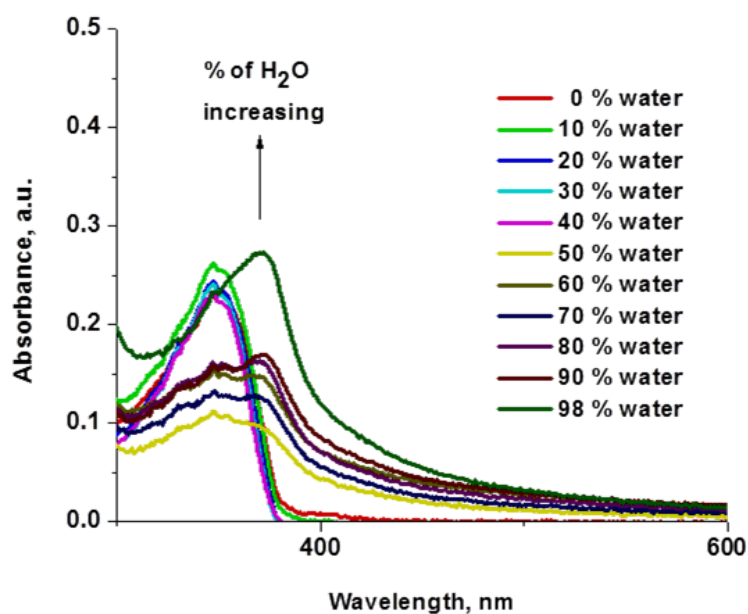


Figure 4: Absorbance spectra of **PPy** in DMSO/H₂O solutions at 10^{-5}M

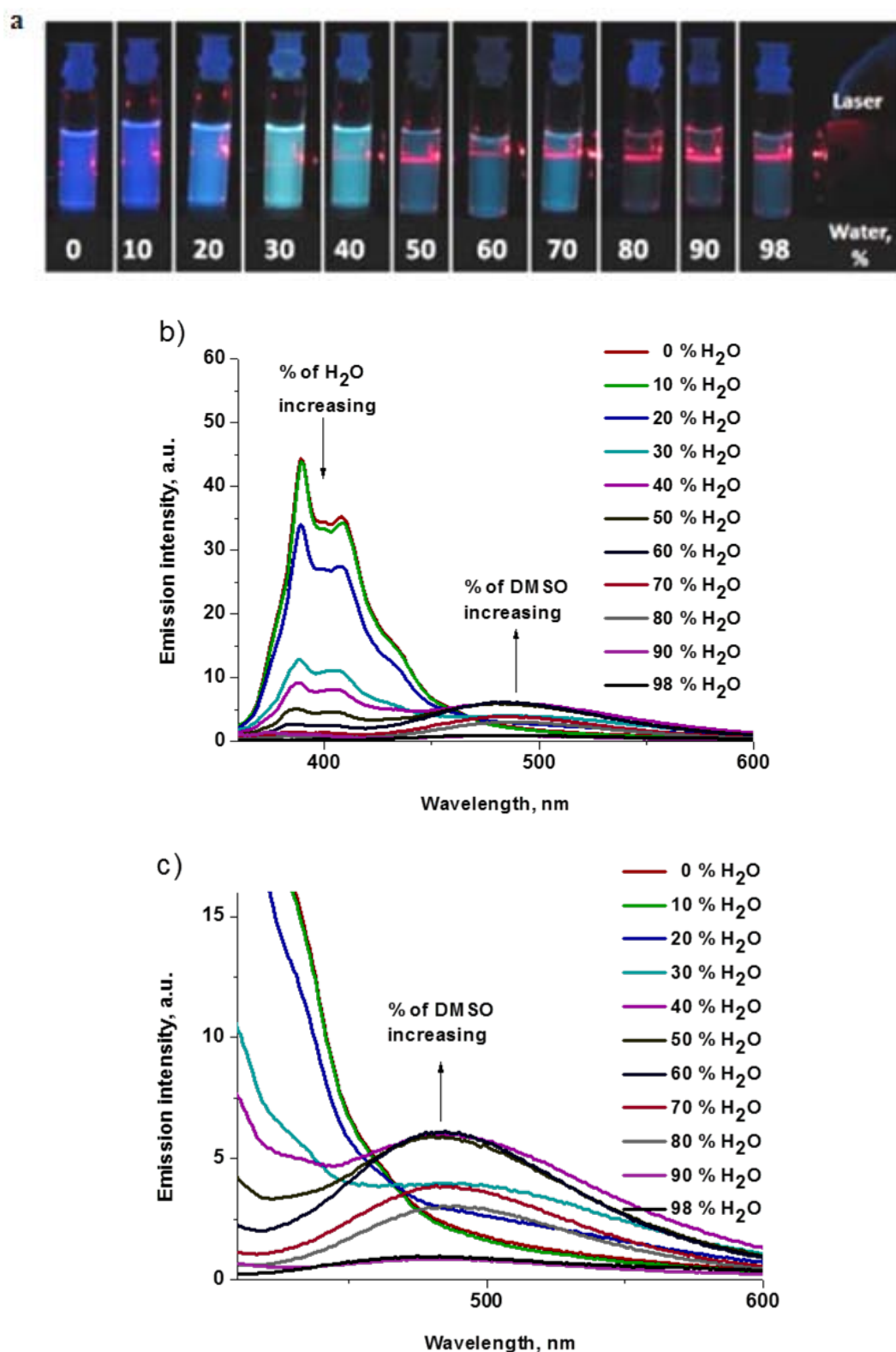


Figure 5: Fluorescence properties of **PPy** in DMSO/H₂O solutions at 10^{-5} M, a) fluorescence quenching and Tyndall effect observed as result of nanoparticles formation of **PPy** in DMSO solution after addition of water ($\lambda_{\text{ex}} = 350$ nm), b) emission spectra of **PPy** nanoparticles obtained at different DMSO/H₂O ratios and c) expanded low-energy part of figure 5b

Laser irradiation of a series of solutions containing **PPy** in DMSO/H₂O at different ratios showed a clear onset of Tyndall scattering in samples containing more than 30% H₂O. Importantly, pronounced scattering was observed at the biologically preferred concentration (DMSO/H₂O (2:98); **Figure 5a** extreme right), whereas in 100% DMSO no scattering was displayed (**Figure 5a** extreme left). The presence of Tyndal scattering indicated the formation of solution-stable nanoparticles in DMSO/H₂O solution of **PPy**. To investigate the formation of **PPy**-based FONs, optical and ¹H NMR spectroscopy studies were performed. Surprisingly, the observed red shift and fluorescence quenching of **PPy** at different DMSO/H₂O ratios found to be associated with the appearance of a new broad fluorescent band (400-700 nm) of lower intensity centered at 485 nm (**Figure 5b** and **5c**). This observed low-energy optical shift of **PPy** could be associated with the formation of excited-state dimers (excimers).^{18a}

2.5. Photophysics of Pyrene Excimers Formation:

According to Birks, an excimer is a dimer which is associated in an electronic excited state and which is dissociative in its ground state.¹⁹ Requirement for an excimer formation is an interaction of an electronically excited state molecule with a ground state molecule. The two molecules must be sufficiently far apart when light is absorbed, so that the excitation is localized on one of them. Excimer formation was observed in the course of a study of anthracene derivatives in water by Suzuki and Tazuke, indicated by rather unusual patterns in the absorption and emission spectra of these molecules.²⁰ Furthermore, the excitation spectra observed for anthracene derived monomer and excimer emissions differed in shape and in wavelengths of band maxima. To explain these effects Suzuki and Tazuke assumed that the anthracene molecule associate as dimers or higher aggregates.²¹ In general, the characteristic features of excimers are

- a) the wavelength of an excimers emission is always larger than that of the excited monomers emission;
- b) the bands in the spectrum observed for the excimers are broadened;
- c) the peak-to-valley ratio of excimer emission (P_E) is always smaller than that of monomer emission (P_M);
- d) if the differences of wavelengths between the excimer emission and monomer emission is positive, it is preassociated excimer or static excimer.

Many aromatic molecules can form an excimer but among them, pyrene has achieved stardom status. This is largely due to the fact that the 0-0 transition between the lowest vibrational energy levels of the E_0 and E_1 electronic states is symmetry forbidden in the case of pyrene and the excited pyrene relaxes to the lowest vibrational levels of the ground state (E_0) by fluorescence on longer fluorescence life time compared with normal photophysical processes. An excimer formation by **PPy** molecules, observed in the course of this work, was also attributed to the presence of pyrene unit in **PPy** scaffold.

2.5.1. PPy Excimer Formation Studies:

Excimer formation is a concentration dependent phenomenon.²² In majority of the experiments the concentration of **PPy** in pure organic solvents was kept very low (10 μ M). Hence, the typical red-shifted fluorescence band corresponding to excimer was not observed. At higher concentrations (100 μ M, 500 μ M and 1mM) the fluorescence emission spectra clearly showed strong fluorescence quenching (disappearance of the bands with maxima at 390 and 409 nm) and the appearance of a new red-shifted emission band at 510 nm (**Figure 6**), thus indicating molecular aggregation or excimer formation.

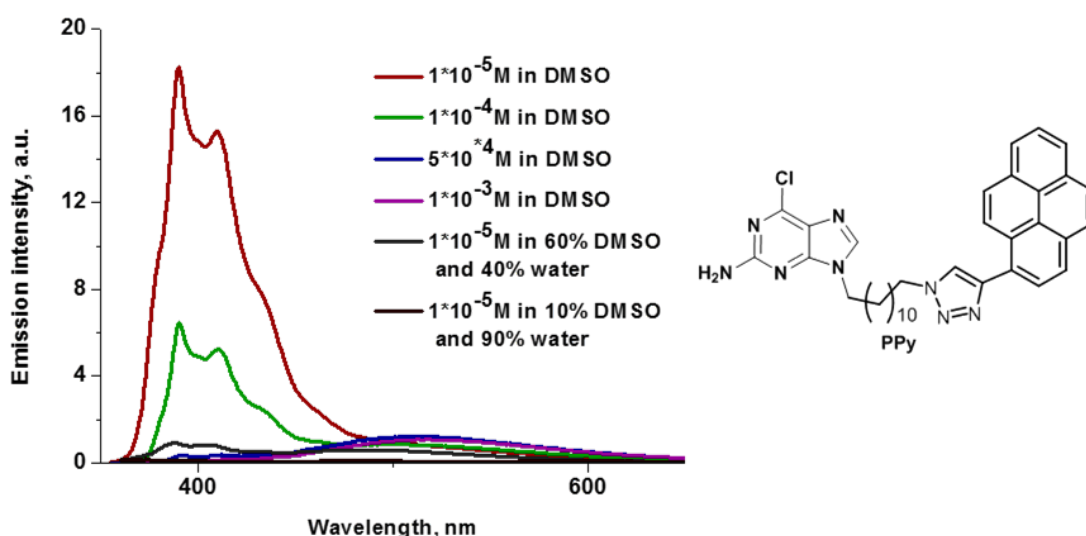


Figure 6: Emission spectra of **PPy** in DMSO and DMSO/H₂O at various concentrations ($\lambda_{\text{ex}} = 350$ nm)

Further investigation showed that in **PPy**-DMSO/H₂O systems only static excimers were formed. Strong evidence of preassociated excimer formation was obtained with

excitation spectra recorded at $\lambda_{\text{ex}} = 350$ nm for 10 μM PPy solutions. Emission maximum observed were $\lambda_{\text{em}} = 388$ nm for monomer and $\lambda_{\text{em}} = 488$ nm for excimer. The peak-to-valley ratio of the excimer (P_{E}) was significantly smaller than that of the monomer (P_{M}), with a positive $\Delta\lambda$, thus indicating pyrene preassociation^{18b-d} ($\Delta\lambda = 100$ nm). In order to investigate the contributions of pyrene and purine units in the aggregation process, the concentration dependent photophysical properties of isolated model fragments **1.3** and **1.9** (Scheme 1) were compared with PPy in DMSO and DMSO/H₂O solutions (Figures 6-8).

The fluorescence emission spectrum of **1.9** ($\lambda_{\text{ex}} = 350$ nm) showed optical behavior similar to that of PPy (Figure 7): as the concentration of **1.9** in DMSO was increased (10 μM - 1 mM) fluorescence bands with maxima at 389 nm and 409 nm disappeared and a new broad red-shifted fluorescent band appeared with maximum centered at around 498 nm. In DMSO/H₂O, upon increasing the water content from 40 to 90%, similar effects were observed, thus demonstrating the formation of aggregates (Figure 7). In contrast, a DMSO solution of **1.3** showed no such effects, neither with increasing concentration nor with addition of water (Figure 8).

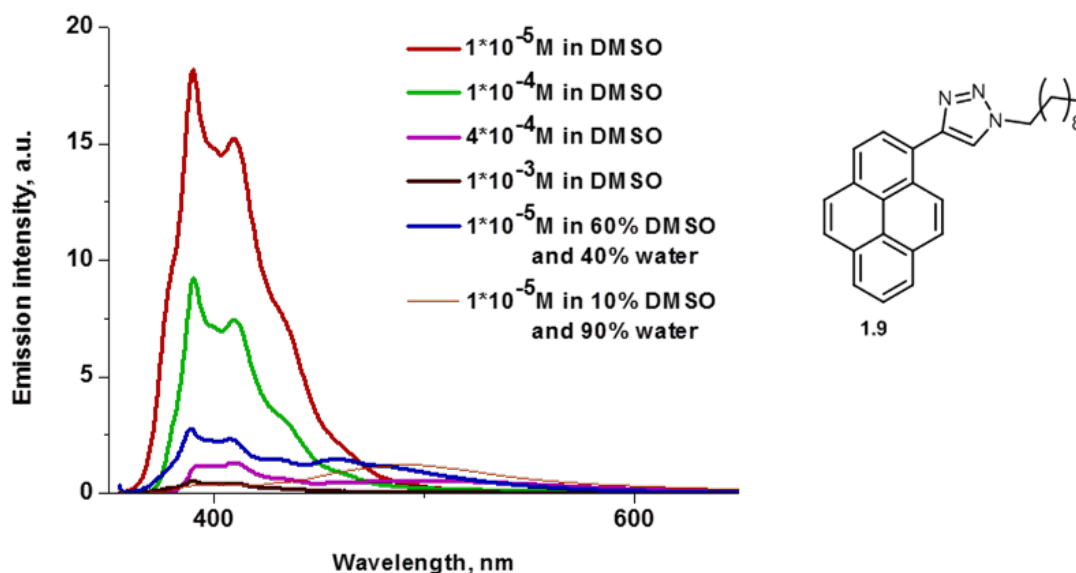


Figure 7: Emission spectra of compound **1.9** in DMSO and DMSO/H₂O at different concentrations ($\lambda_{\text{ex}} = 350$ nm)

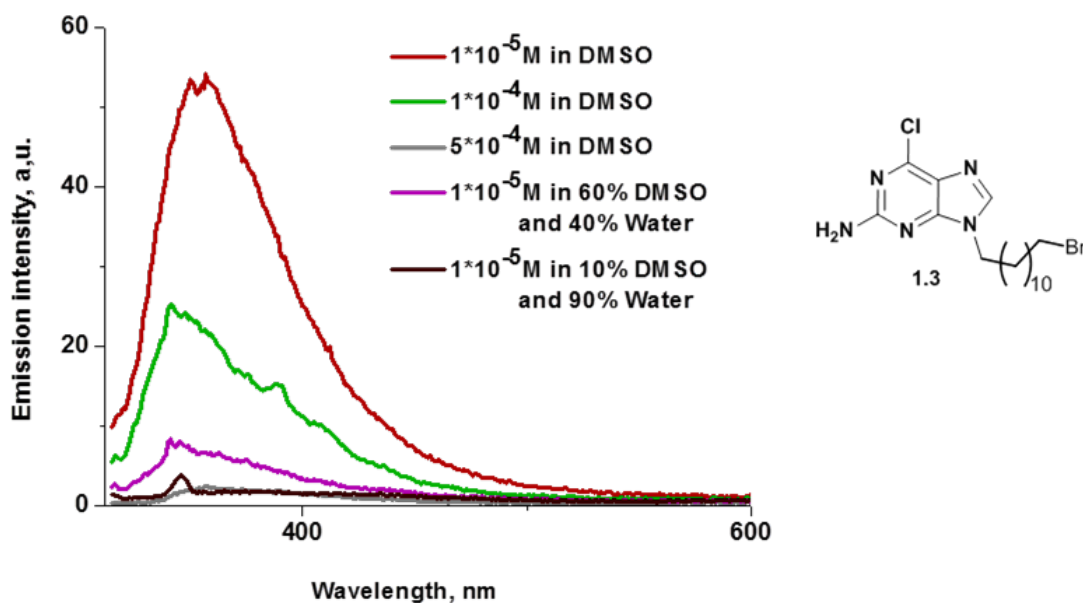


Figure 8: Emission spectra of compound **1.3** in DMSO and DMSO/H₂O at different concentrations ($\lambda_{\text{ex}} = 350$ nm)

Addition of water to the DMSO solution of **PPy** resulted in characteristic excimer emission at 485 nm (**Figure 6**) and the Tyndall effect (**Figure 4a**). These observations strongly supported the postulation that the formation of solution stable FONs is driven by intermolecular pyrene-pyrene π - π stacking-mediated self assembly of **PPy**. In order to confirm it, ¹H NMR titration studies of DMSO-*d*₆ solutions of **PPy** with D₂O were performed.

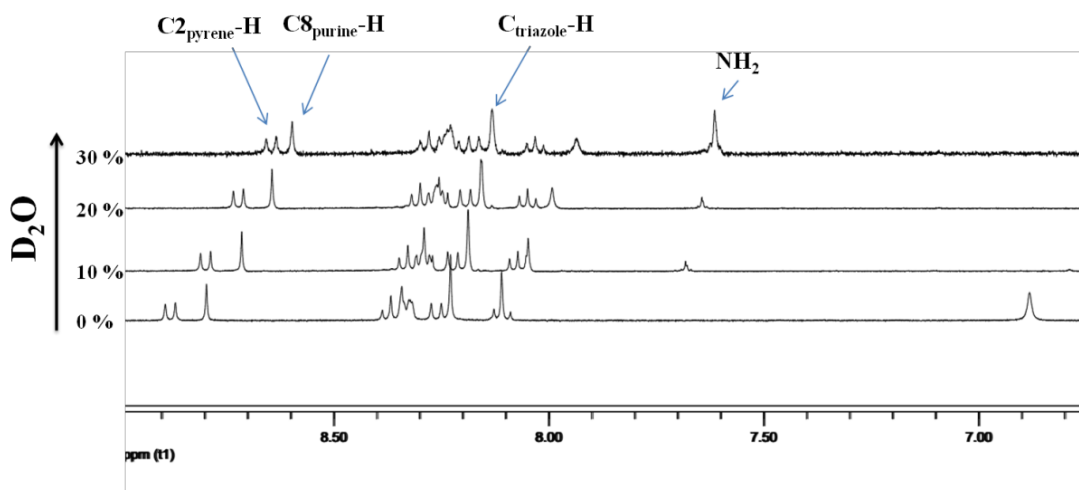


Figure 9: Stack ¹H NMR spectra of **PPy** in DMSO-*d*₆ alone and gradual increase of D₂O (0, 10, 20 and 30%)

As **Figure 9** shows, the titration spectra exhibited an upfield chemical shift of the C_{triazole}-H aromatic protons (8.23, 8.19, 8.15 and 8.12 ppm for 0, 10, 20 and 30% addition of D₂O to DMSO-*d*₆ solutions, respectively), as well as C8_{purine}-H and C2_{pyrene}-H. This observation clearly supports the theory of aggregation of **PPy** molecules through supramolecular interactions and formation of solution-stable nanoparticles.

2.6. Morphology Studies:

In order to investigate the morphology of **PPy**-based FONs formed in DMSO/H₂O (2:98), SEM and AFM investigation were performed. For the SEM study the sample was prepared using reprecipitation method. For that, DMSO solution of compound **PPy** (60 µL, *c* ~ 2.5 mM) was rapidly injected into water (3 mL) leading to the formation of **PPy** FONs and then immediately drop-casting a solution containing **PPy** FONs on clean silica substrate. Supporting with the earlier studies (Tyndall scattering and ¹H NMR titration), the SEM micrographs revealed a narrow distribution of **PPy**-based FONs (**Figure 10a**). AFM was also utilized to estimate nanoparticles size and morphology. Topographical analysis of noncontact-mode AFM images of the **PPy** nanoparticles showed the average widths from 100 to 200 nm and heights in the range 70 to 80 nm (**Figure 10b, 10c and 10d**). In addition to that self assembled structures of **PPy** in various solvents were studied using SEM. Self assembly is driven by interactions of molecules through π - π interactions, hydrogen bonding and Van der Waals forces, which lead to the formation of nano/micro structures. The nano/micro structures not only depend on supramolecular interactions, but also on the nature of the solvent,²⁷ concentration,²⁸ chain length (hydrophobicity)²⁹ and the nature of the surface.³⁰ In the case reported in this chapter from nano to micro structures were observed in various solvents. For example, in DCM **PPy** forming microspheres with 3 micron size (**Figure A3a-b**, see page no 56). In case of acetone **PPy** forms sheet like structures with 10 micron size, while in acetone/water it forms 1 micron size spindles (**Figure A3c-d**, see page no 56). In case of THF **PPy** form nanoparticles with average size of 350 nm and in THF/water forms porous type structures (**Figure A3e-f**, see page no 56). In case of DMF solvent **PPy** form micron size particles, which further aggregate into micro structures with flower like morphology (**Figure A3g-h**, see page no 56).

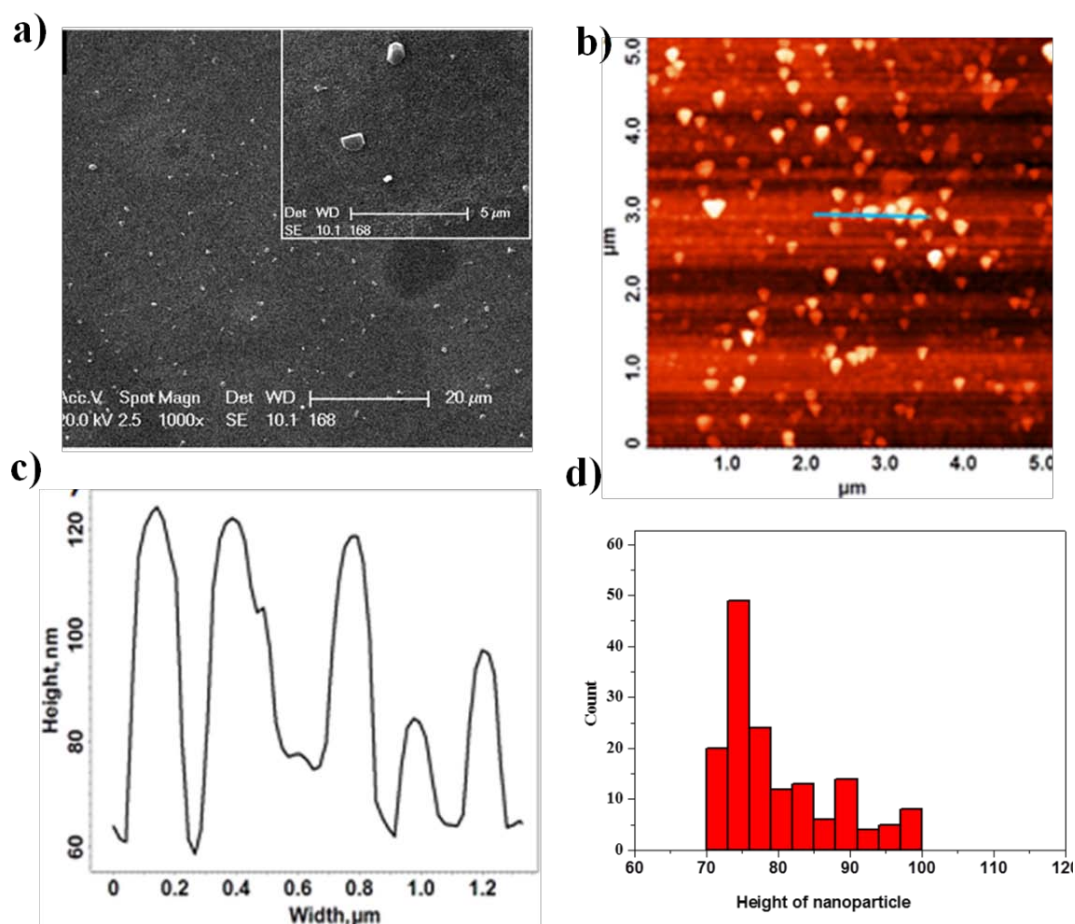


Figure 10: a) SEM micrographs of **PPy** nanoparticles obtained from DMSO/H₂O (2:98); inset shows close-up image of the nanoparticles; b) non-contact mode AFM image of **PPy** nanoparticles; c) height and length profile (selected nanoparticles in b); height and count of **PPy** nanoparticles (selected from b)

2.7. Comparative Optical Studies of PPy Bulk and PPy Nanoparticles:

The solid-state photophysical properties of **PPy** bulk powder showed emission with a band splitting in two maxima (500 nm and 573 nm). **PPy** FONs were studied using confocal fluorescent microscope displayed a broad emission spectrum (410-700 nm with maximum at 500 nm; **Figure 11**), similar to that of the **PPy** FONs suspension in DMSO/H₂O (**Figure 4b**). Bulk PPy compound in solid state displayed broad emission in the range of 400-700 nm. As result, for the **PPy** nanoparticles blue, green and red emission can be observed in the corresponding filters *via* fluorescent microscope and confocal fluorescent microscope (**Figure12**).

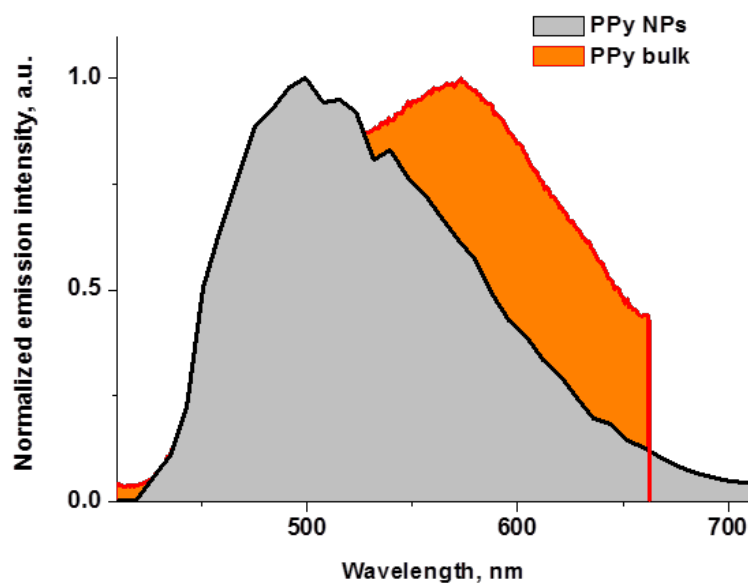


Figure 11: Solid-state emission spectra of bulk (compound **PPy**) and nanoparticles (CFM data)

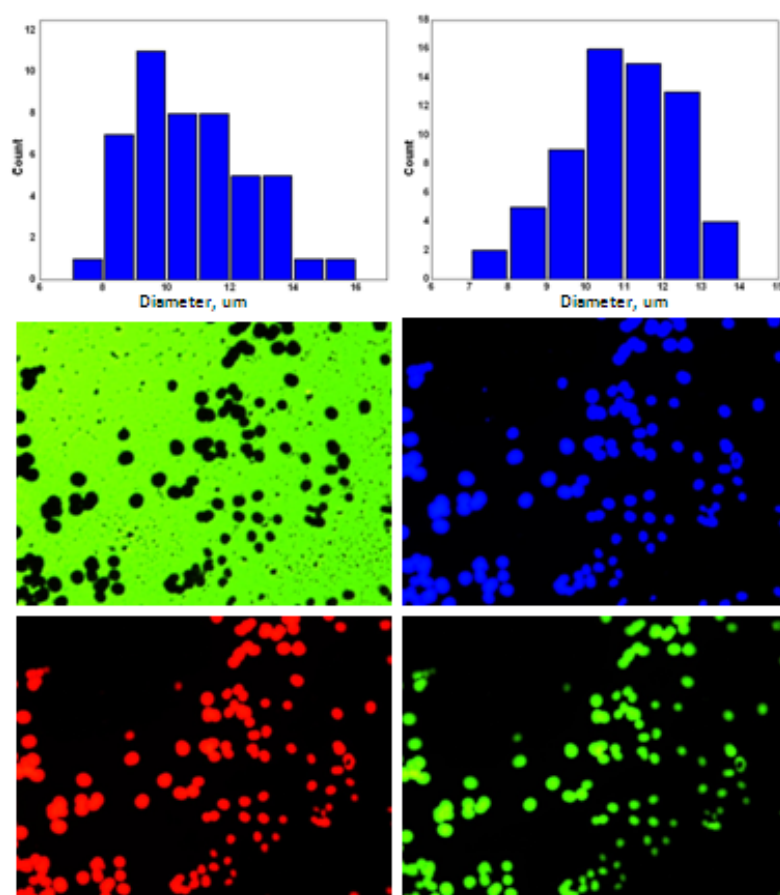


Figure 12. Fluorescent microscopy images of **PPy** nano/micro structures obtained in DMSO/H₂O solutions recorded with blue filter ($\lambda_{em}=400-440$ nm); green filter ($\lambda_{em}=480-550$ nm); and Texas red filter ($\lambda_{em}=600-650$ nm)

2.8. Application of PPy FONs for Bioimaging:

In order to investigate the utility of **PPy** FONs as a fluorescent dye for *in vitro* experiments, human metastatic breast cancer cells (MDAMB-231) were treated with 100 μ M **PPy** nanoparticles and incubated for 4 h. The samples were studied and photographed with an upright fluorescence microscope in bright field and fluorescence mode. The **PPy** FONs incubated cells showed a clear blue intracellular fluorescence (**Figure 13**), whereas in control cells (treated with only 2% DMSO solution) did not show any fluorescence (**Figure A4**, see page no 57). During the imaging experiments the cells remained viable and no noticeable toxicity or side effects were observed. Therefore, **PPy** based FONs are nontoxic at tested concentration (100 μ M) and cell-permeable and could be used for the imaging of biological processes in living cells.

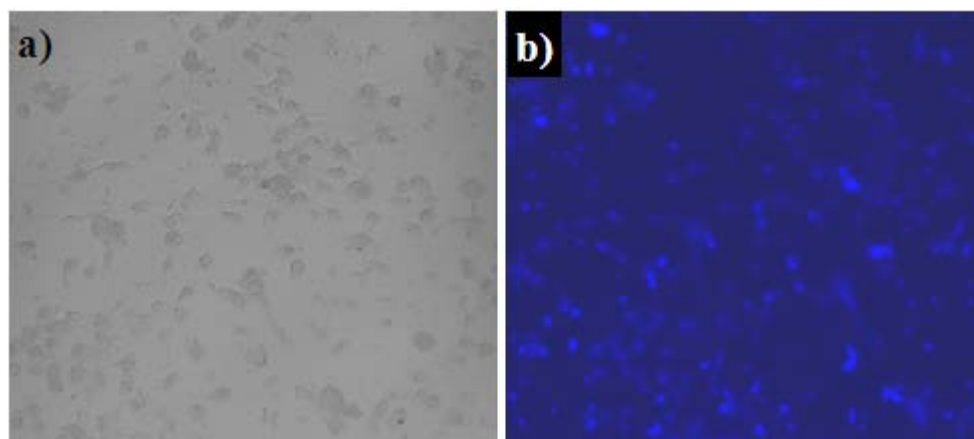


Figure 13: Fluorescent microscopy images of a) bright field image of cells treated with **PPy**; b) fluorescence image of cells shown in figure 13a (λ_{ex} =365 nm, λ_{em} =445 nm)

Finally, the toxicity and permeability of **PPy**- and **GPy**- based FONs were investigated using zebrafish embryos. Zebrafish embryos (24 hpf) were treated with **PPy** and **GPy** nanoparticles at different concentration (50 μ M, 5 μ M, 500 nM, 50 nM and 5 nM in 2% DMSO) for 48-144 h. Interestingly, there was no any negative effect on the development or survival of FONs treated zebrafish at any concentration or exposure time. Additionally, for confocal fluorescent microscopic studies the embryos were treated with 50 μ M **PPy** or **GPy** nanoparticles for 120 h, followed by washing and fixing with paraformaldehyde. Upon excitation with argon ion UV laser (356/365 nm) both **PPy** and **GPy** treated embryos selectively showed fluorescence in muscle

fibres **Figure 14**), where as untreated embryos did not exhibited fluorescence (**Figure A6**, see page no 58). Interestingly, the **PPy** treated embryos displayed equally clear images with a blue-violet filter set ($\lambda_{em}=400-440$ nm) and with a green filter set ($\lambda_{em}=480-550$ nm), commonly used for biological studies, and a slightly less clear image with a red filter set ($\lambda_{em}=600-650$ nm; **Figure A6**, see page no 58). Thus, the broad and intense emission of **PPy** FONs could be efficiently exploited in the areas of muscle biology and pathophysiology, particularly for the study of neuromuscular disorders.

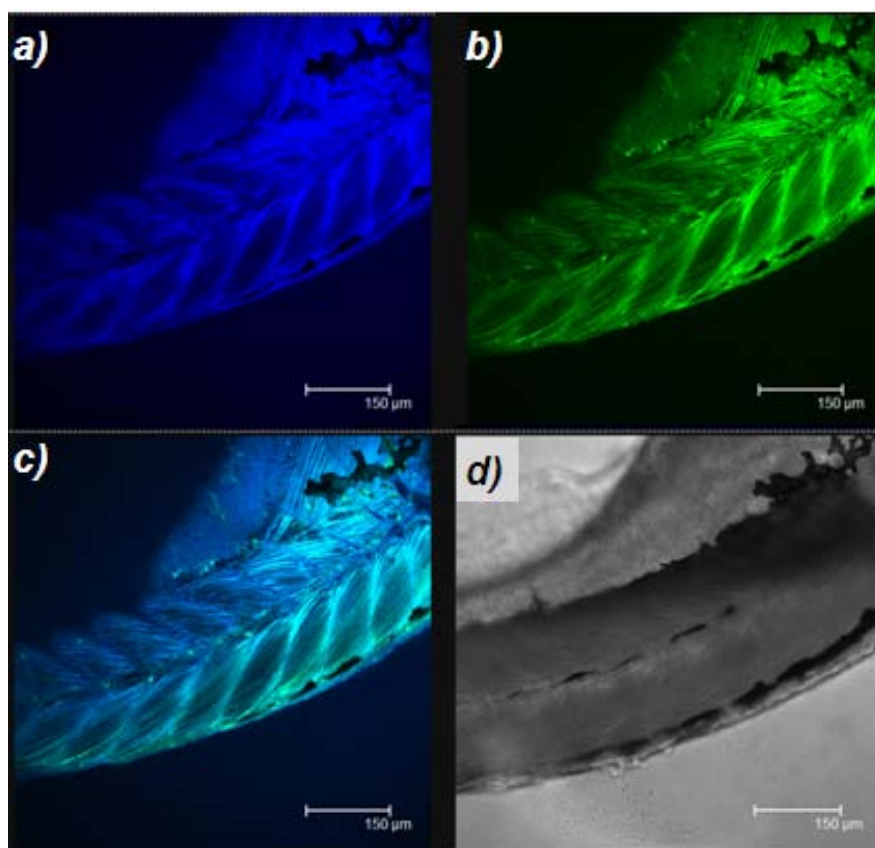


Figure 14: Laser scanning confocal microscopy images (λ_{ex} : Ar ion UV laser 356/365 nm) of zebrafish embryos treated with **PPy** nanoparticles: a) image recorded with blue-violet filter ($\lambda_{em}=400-440$ nm); b) image recorded with green filter ($\lambda_{em}=480-550$ nm); c) overlap images represented on (a) and (b); d) bright field image before excitation

2.9. Photostability Studies of PPy Nanoparticles:

It is very well known that majority of organic fluorophores are prone to photobleaching;⁶ however, the presented **PPy** and **GPy** FONs showed no

photobleaching or fading effect throughout the imaging experiments. The emission spectra recorded for the **PPy** solutions in different solvents showed negligible intensity decrease (**Figure 15 and 16**) even after overnight treatment with UV light (254 nm, 8W, 760 $\mu\text{W}/\text{cm}^2$, 20 h). Moreover, **PPy** treated zebrafish embryos exposed to continuous UV-treatment for 5 h also showed good fluorescent signal, verifying high photostability of **PPy** FONs. Images of zebrafish embryos captured at different time intervals of UV-treatment show negligible intensity decrease (**Figure 17**).

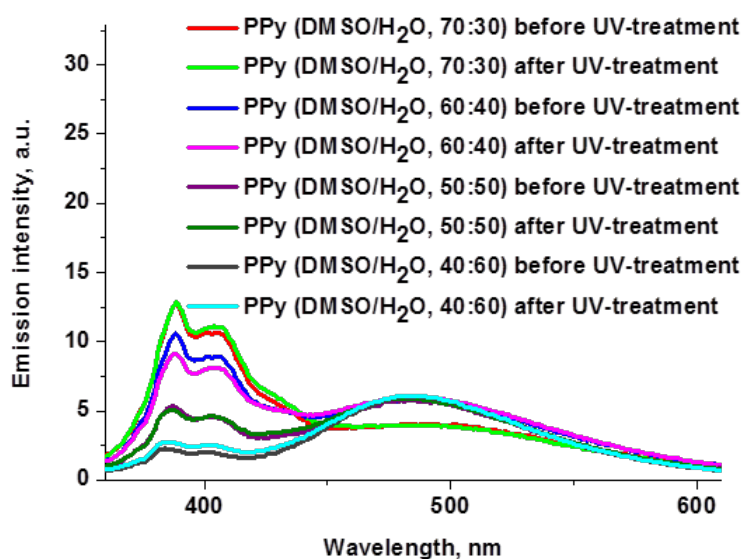


Figure 15: Emission spectra of **PPy** solutions in DMSO/H₂O obtained before and after UV treatment (λ_{ex} =254 nm, 8W, 760 $\mu\text{W}/\text{cm}^2$) for 20 h

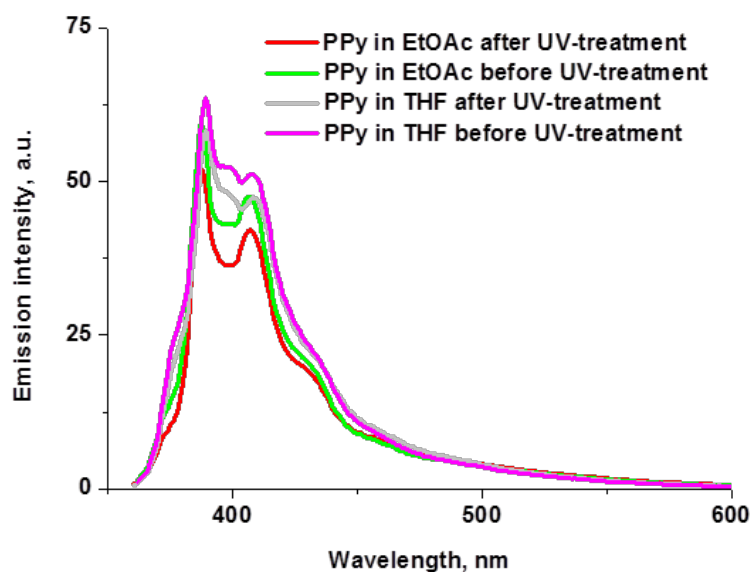


Figure 16: Emission spectra of **PPy** solutions in pure organic solvents obtained before and after UV treatment (254 nm, 8W, 760 $\mu\text{W}/\text{cm}^2$) for 20 h

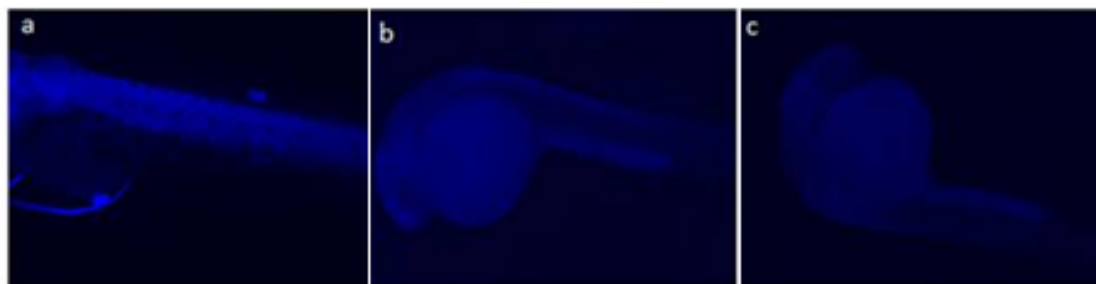


Figure 17: Fluorescent microscopy images of zebrafish embryos treated with **PPy** solutions in DMSO/H₂O ($\lambda_{\text{ex}}=365$ nm, $\lambda_{\text{em}}=445$ nm); a) before UV-treatment; b) after UV-treatment (254 nm, 8W, 760 $\mu\text{W}/\text{cm}^2$) for 3 h; c) after continuous UV-treatment (254 nm, 8W, 760 $\mu\text{W}/\text{cm}^2$) for 5 h

2.10. Conclusions:

In conclusion, in this chapter two blue-emitting fluorescent guanine analogues (**PPy** and **GPy**) were designed and synthesized through simple and straightforward route using effective 1, 3-dipolar Huisgen cycloaddition. Stable FONs based on **PPy** and **GPy** were successfully prepared in biocompatible solvent mixture (DMSO/H₂O; 2:98) *via* reprecipitation method. Their photophysical properties and morphology were fully investigated by UV-Visible and fluorescence spectroscopy, SEM, AFM and CFM studies. The ability of **PPy** and **GPy** FONs to penetrate into human breast cancer cells and zebrafish embryos was examined. Interestingly, both **PPy**- and **GPy**-based FONs showed selective multicolour illumination of the zebrafish muscle fibres under UV-light. This work proposes that multicolour imaging potential of the presented **PPy** and **GPy** nanoparticles can be exploited to overcome autofluorescence in many biological samples. As demonstrated here, both FONs were nontoxic and remarkably good stains, particularly specific for muscular tissues, thus providing more comprehensible visualization of muscle fibres architecture. Developed in this chapter novel chromophores were resistant to bleaching or fading, easy to use and could be utilized for the study of neuromuscular changes in zebrafish embryos. This result demonstrates an innovative and technologically important bio-nanotechnology method to generate multicolour imaging of cancer cells and muscle tissues.

2.11. Experimental Section:

2.11.1. Materials and Methods:

All reactions were carried out under an inert atmosphere with dry solvents, unless otherwise stated. Syringes and needles for the transfer of reagents were dried at 100 °C and allowed to cool in desiccators over P₂O₅ before use. Reactions were monitored by thin layer chromatography (TLC) on silica gel plates (60 F254), using UV light detection. Merck silicagel (particle size 100-200 mesh) was used for column chromatography. For UV-Vis and fluorescence measurements spectroscopic grade solvents were used.

The materials 2-amino-6-chloropurine, 1,12-dibromododecane, and paraformaldehyde were purchased from Sigma Aldrich. Commercial reagents (NaN₃, Sodium Ascorbate, K₂CO₃, CuSO₄ and HCl) were purchased from Merck, Loba Chemie and Rankem and were used as received. The solvents were distilled and dried before reactions and for extracting purposes.

2.11.2. Nanoparticles Preparation for Biological Studies:

1.5 mg of compound **PPy**/**GPy** was taken in a sample vial and dissolved in 1 mL of DMSO. Then 60 µL of the above solution was rapidly injected into 2940 µL of millipore water to obtain the final concentration of nanoparticles 50 µM in 2% DMSO. Prepared nanoparticles were used for the fluorescent imaging studies immediately.

2.11.3. Nanoparticles Preparation for SEM and AFM Studies:

Nanoparticles were prepared by two methods;

a) 1.5 mg of compound **PPy** or **GPy** was taken in a sample vial and dissolved in 1 mL of DMSO. Then 60 µL of the above solution was rapidly injected into 2.94 mL of millipore water to obtain the final concentration of nanoparticles 50 µM in 2% DMSO. Prepared nanoparticles were dispersed on a clean glass slide by a capillary for SEM and AFM studies.

b) 1 mg of compound **PPy** was dissolved in 3 mL of DCM/acetone/THF/DMF respectively and left for 0.5 h and one drop of the solution was dispersed on a clean glass slide by capillary for SEM analysis. In other case 1mg/2mL of THF containing PPy solution was rapidly injected to 1 mL of millipore water and the sample vial was left for 1 h without disturbing. One drop of the solution was dispersed on a clean glass slide by a capillary for SEM analysis.

2.11.4. Nanoparticles Exposure to Cells:

1.5×10^6 MDAMB-231 (human metastatic breast cancer) cells were seeded on glass cover slips in 6-well plates, in DMEM (Dulbecco's modified Eagle's medium) supplemented with 10% FBS (Fetal Bovine Serum) and antibiotics (Penicillin-Streptomycin). After allowing them to adhere (overnight) at 37 °C in 5% CO₂, 100 µM of **PPy** nanoparticles and equivalent volume of vehicle (2% DMSO) were added to the cells and incubated for 4 h. The cells were washed with PBS (Phosphate-buffered Saline), and the cover slips were mounted on glass slides using 50% Glycerol in PBS. The slides were examined and photographed with an upright fluorescence microscope using a 10x objective and 10 x eyepieces in bright field and fluorescence modes.

2.11.5. Nanoparticles Exposure to Zebrafish Embryos:²⁴

At 24 hours post fertilization (hpf), embryos were de-chlorinated using 50 µg/mL Proteinase-K (Sigma-Aldrich) for 5 minutes. All embryos were immersed (6 embryos/well) into 24 well culture plates containing 500 µL of **PPy** or **GPy** at different concentrations (50 µM, 5 µM, 500 nM, 50 nM, 5 nM) for treatment. Control embryos were incubated in 2% DMSO. The complete study was carried out for 24, 48, 72, 96, 120 and 168 h. On the respective time points the embryos were washed with 1X PBS (phosphate buffer saline) thrice for 5 min each and fixed in 4% paraformaldehyde in PBS, pH 7.0 for 4 h at room temperature. Then embryos were used for fluorescent observations under confocal fluorescence or optical fluorescence microscope.

2.11.6. PPy and GPy Synthesis:

7-(12-Bromododecyl)-6-chloro-7H-purin-2-amine (1.3):

Anhydrous K₂CO₃ (1.22 g, 8.84 mmol) was added to a stirred suspension of 2-amino-6-chloropurine **1.1** (0.5 g, 2.948 mmol) in dry DMF (10 mL) under nitrogen at room temperature. After 30 min, a solution of 1, 12- dibromododecane **1.2** (2.90 g, 8.84 mmol) in DMF (4 mL) was added, and the reaction mixture was stirred for 24 h. DMF

was removed under reduced pressure, and the crude residue was then purified using column chromatography on silica gel with hexane/ethylacetate (1:3) as eluent to yield **1.3** as a white solid (0.6 g, 53%). Mp: 78-79 °C. TLC (hexane/EtOAc (1:1)): R_f = 0.31. IR (KBr): 3426, 3333, 3212, 3074, 3039, 2924, 2852, 1645, 1608, 1562, 1468, 1354, 1229 cm^{-1} . ^1H NMR (DMSO- d_6 , 400 MHz) δ : 1.20 (14H, m), 1.32 (2H, m), 1.74 (4H, m), 3.49 (2H, t), 4.0 (2H, t), 6.88 (2H, brs), 8.11 (1H, s). ^{13}C NMR (DMSO- d_6 , 100 MHz) δ : 26.3, 27.9, 28.5, 28.8, 29.2, 32.6, 35.6, 43.4, 123.7, 143.6, 149.7, 154.5, 160.1. MS (EI, 70eV): m/z $[\text{M}]^+$ calcd for $\text{C}_{17}\text{H}_{27}\text{BrClN}_5$: 416.79, found 418.1 $[\text{M} + \text{H}]^+$. Anal. Calcd for $\text{C}_{17}\text{H}_{27}\text{BrClN}_5$: C, 48.99; H, 6.53; N, 16.80; found: C, 48.85; H, 6.41; N, 16.61.

7-(12-Azidododecyl)-6-chloro-7H-purin-2-amine (1.4):

Compound **1.3** (0.6 g, 1.44 mmol) and sodium azide (0.28 g, 4.32 mmol) were dissolved in dry DMF (10 mL) and were stirred at room temperature for 12 h. DMF was removed under reduced pressure, and the crude residue was then purified using column chromatography on silica gel with hexane/ethylacetate (1:3) as eluent to yield **1.4** as a yellowish solid (0.42 g, 77%). Mp: 60-62 °C. TLC (hexane/EtOAc (1:1)): R_f = 0.36. IR (KBr): 3431, 3331, 3212, 3075, 3040, 2924, 2855, 2094, 1647, 1608, 1561, 1468 cm^{-1} . ^1H NMR (DMSO- d_6 , 400 MHz) δ : 1.19 (16H, m), 1.48 (2H, m), 1.73 (2H, m), 3.27 (2H, t), 4.0 (2H, t), 6.87 (2H, brs), 8.11 (1H, s). ^{13}C NMR (DMSO- d_6 , 100 MHz) δ : 26.3, 26.5, 28.6, 28.8, 28.9, 29.2, 29.3, 43.4, 51.0, 123.7, 143.7, 149.7, 154.5, 160.1. MS (EI, 70eV): m/z $[\text{M}]^+$ calcd for $\text{C}_{17}\text{H}_{27}\text{ClN}_8$: 378.2, found 379.2 $[\text{M} + \text{H}]^+$. Anal. Calcd for $\text{C}_{17}\text{H}_{27}\text{ClN}_8$: C, 53.89; H, 7.18; N, 29.57; found: C, 53.76; H, 7.10; N, 29.65.

6-Chloro-7-(12-4-(pyren-1-yl)-1H-1,2,3-triazol-1-yl)dodecyl)-7H-purin-2-amine (1.5/PPy):

A mixture of 1-ethynylpyrene **1.8** (0.30 g, 1.33 mmol), **1.4** (0.42 g, 1.11 mmol), sodium ascorbate (0.052 g, 0.26 mmol), CuSO₄ (0.0055 g, 0.022 mmol) in a 1:1 mixture of DMF and H₂O (20 mL) was stirred at 80 °C for 12 h. After cooling solvents were removed under vacuum and the crude residue was then purified by column chromatography on silica gel with hexane/ethylacetate (3:7) as eluent to yield **PPy** as a yellowish solid (0.20 g, 31%). Mp: 165-167 °C. TLC (EtOAc): R_f = 0.43. IR (KBr): 3488, 3296, 3171, 3088, 2923, 2851, 1615, 1567, 1516, 1458, 1403, 1363, 1213 cm⁻¹. ¹H NMR (DMSO-*d*₆, 400 MHz) δ : 1.28 (16H, m), 1.69-1.73 (2H, m), 1.97 (2H, m), 3.98 (2H, t), 4.52 (2H, t), 6.88 (2H, brs), 8.10 (1H, t), 8.30 (7H, m), 8.79 (1H, s), 8.87 (2H, d). ¹³C NMR (CDCl₃, 100 MHz) δ : 26.5, 28.9, 29.3, 29.3, 29.3, 29.5, 30.3, 43.7, 50.5, 122.7, 124.7, 124.8, 125.0, 125.2, 125.3, 126.0, 127.1, 127.3, 127.7, 128.1, 128.5, 130.8, 131.2, 131.3, 142.3, 147.3, 151.1, 153.7, 158.9. MS (EI, 70eV): *m/z* [M]⁺ calcd for C₃₅H₃₇ClN₈: 605.17, found 605.3 [M]⁺. Anal. Calcd for C₃₅H₃₇ClN₈: C, 69.46; H, 6.16; N, 18.52; found: C, 69.32; H, 6.23; N, 18.41.

2-amino-7-(12-(4-(pyren-1-yl)-1H-1,2,3-triazol-1-yl)dodecyl)-1H-purin-6(7H)-one (1.6/GPy):

Compound **PPy** (0.2g 0.33 mmol) was refluxed in 0.1M HCl (40 mL) for 6h. After cooling and neutralization with aq. KOH, the product precipitated as a grey solid, which was filtered and analyzed without further purification (0.09 g, 52%). Mp: 296-

298 °C. IR (KBr): 3486, 3317, 3158, 2925, 2851, 1689, 1626, 1600, 1467, 1414, 1176, 1053 cm^{-1} . ^1H NMR ($\text{DMSO-}d_6$, 400 MHz) δ : 1.20 (14H, m), 1.66 (2H, m), 1.97 (2H, m), 3.87 (2H, t), 4.50 (2H, t), 6.51 (2H, brs), 7.88 (1H, s), 8.08 (1H, t) 8.27 (7H, m) 8.78 (1H, s), 8.86 (1H, d) 10.67 (1H, s). ^{13}C NMR ($\text{DMSO-}d_6$, 100 MHz) δ : 26.3, 28.8, 28.8, 29.3, 29.6, 30.1, 43.3, 50.0, 124.3, 124.7, 125.5, 125.9, 126.8, 126.9, 127.4, 127.7, 127.8, 128.0, 128.1, 128.3, 128.4, 130.7, 130.9, 131.3, 146.5, 154.2, 156.7. MS (EI, 70eV): m/z $[\text{M}]^+$ calcd for $\text{C}_{35}\text{H}_{38}\text{BrN}_8\text{O}$: 586.3, found 587.3 $[\text{M}+\text{H}]^+$. Anal. Calcd for $\text{C}_{35}\text{H}_{38}\text{N}_8\text{O}$: C, 71.65; H, 6.53; N, 19.10; found: C, 71.48; H, 6.61; N, 19.25.

1-Ethynylpyrene (1.8):¹²

1-Bromopyrene (2.0 g, 3.57 mmol), $\text{PdCl}_2(\text{PPh}_3)_2$ (100 mg, 0.14 mmol), PPh_3 (74.6 mg, 0.28 mmol) and CuI (54.3 mg, 0.28 mmol) were mixed under nitrogen, in THF (20 mL) and triethylamine (60 mL). Then trimethylsilylacetylene (414 mg, 4.2 mmol) was added and the system was heated for 6 h at 90 °C. The reaction mixture was cooled to room temperature and filtered. The filtrate was collected and the solvent removed under reduced pressure. The residue was dissolved in n-hexane. The remaining solid was filtered off and the filtrate was collected. Then the solvent was removed and a yellow oily was obtained. The yellow oil was dissolved in diethyl ether (20 mL). Then methanol (40 mL) and potassium carbonate (3.2 g) were added. The system was stirred at room temperature for 3 h. The mixture was filtered and the filtrate was evaporated and the crude residue was purified by column chromatography on silicagel using n-hexane/DCM= 50:1, v/v as an eluent (9:1), to yield **1.8** as a cinereous powder (0.6 g, 40%). Spectroscopic data matches with the one from the reported procedure. ^1H NMR (CDCl_3 , 400 MHz) δ : 3.61 (1H, s), 7.97 (2H, m), 8.03 (2 H, m), 8.11 (4H, m), 8.54 (d, 1H).

(1-Decyl-4-(pyren-1-yl)-1H-1,2,3-triazole) (1.9):

Compound **1.7** (0.05 g, 0.27 mmol) and 1-ethynyl pyrene **1.8** (0.073 g, 0.324 mmol) were dissolved in dry DMF (1.5 mL). To the reaction mixture copper iodide (0.0051 g, 0.027 mmol) was added and heated at 80 °C for 12 h under nitrogen atmosphere. Solvents were removed under high vacuum and DCM (5 mL) was added, the resulting suspension was filtered through celite in order to remove inorganic salts. The filtrate was concentrated under reduced pressure, and the crude product was then purified using flash column chromatography on silicagel using hexane/ethyl acetate (9:1) as an eluent, to yield **1.9** as a white solid (0.09 g, 81% yield). Mp: 108-110 °C. TLC (hexane/ethyl acetate (4:1)): $R_f = 0.32$. IR (KBr): 3867, 3626, 3095, 3044, 2922, 2851, 2722, 2427, 2322, 1917, 1853, 1790, 1746, 1641, 1595, 1457, 1369, 1321, 1218, 1176, 1057, 724 cm^{-1} . ^1H NMR (CDCl_3 , 400 MHz) δ : 0.87 (3H, t), 1.36 (14H, m), 2.05 (2H, m), 4.52 (2H, t), 7.94 (1H, s), 8.02 (1H, t), 8.18 (7 H, m) 8.70 (1H, d). ^{13}C NMR ($\text{DMSO}-d_6$, 100 MHz) δ : 14.1, 22.6, 26.6, 29.0, 29.2, 29.4, 29.5, 30.4, 31.8, 50.5, 124.6, 124.7, 124.8, 125.0, 125.3, 126.2, 127.0, 127.1, 127.4, 127.6, 127.9, 127.9, 128.2, 128.5, 130.8, 131.2, 131.3, 147.2; MS (EI, 70eV): m/z $[\text{M}]^+$ calcd for $\text{C}_{28}\text{H}_{31}\text{N}_3$: 409.2, found 410.0 $[\text{M}+\text{H}]^+$.

2.12. References:

- (1) Huisgen, R. *Angew. Chem. Int. Ed.* **1963**, 75, 604.
- (2) Xing, Y.; Smith, A. M.; Agrawal, A.; Ruan, G.; Nie, S. *Int. J. Nanomedicine* **2006**, 1, 473.
- (3) (a) An, B.-K.; Gierschner, J.; Park, S. Y. *Acc. Chem. Res.* **2012**, 45, 544. (b) Martin, C. R.; Kohli, P. *Nat. Rev. Drug Disc.* **2003**, 2, 29. (c) Choi, J. W., N.S. *Biomedical Engineering-From theory to applications* (Ed.: R. Fazel-Rezai) **2011**, 299. (d) Köstler, S.; Ribitsch, V. In *Nanotechnologies for the Life Sciences*; Wiley-VCH Verlag GmbH & Co. KGaA, **2007**. (e) Rajadurai, M. S. S., Z. B.; Kuchkina, N. V.; Rusanov, A. L.; Mullen, K. *Russ. Chem. Rev.*

- 2007**, 76, 821. (f) An, B.-K.; Kwon, S.-K.; Jung, S.-D.; Park, S. Y. *J. Am. Chem. Soc.* **2002**, 124, 14410.
- (4) (a) Wang, L. X., T.; Liu, J.; Wang, L.; Chen, H.; Dong, L.; Bain, G. *Spectrochim. Acta Part A* **2005**, 62, 565. (b) Li, H.; Xu, J.; Yan, H. *Sens. Actuators, B*: **2009**, 139, 483. (c) Wang, L.; Dong, L.; Bian, G.; Xia, T.; Chen, H.; Wang, L.; Cao, Q.; Li, L. *Anal. Lett.* **2004**, 37, 1811. (d) Shifrina, Z. B.; Rajadurai, M. S.; Firsova, N. V.; Bronstein, L. M.; Huang, X.; Rusanov, A. L.; Muellen, K. *Macromolecules* **2005**, 38, 9920.
- (5) (a) Sreejith, S.; Carol, P.; Chithra, P.; Ajayaghosh, A. *J. Mater. Chem.* **2008**, 18, 264. (b) Jana, A.; Devi, K. S. P.; Maiti, T. K.; Singh, N. D. P. *J. Am. Chem. Soc.* **2012**, 134, 7656. (c) Cui, W.; Lu, X.; Cui, K.; Wu, J.; Wei, Y.; Lu, Q. *Langmuir* **2011**, 27, 8384.
- (6) (a) Chandrasekhar, N.; Chandrasekar, R. *Angew. Chem. Int. Ed.* **2012**, 51, 3556. (b) Chandrasekhar, N.; Chandrasekar, R. *Chem. Commun.* **2010**, 46, 2915. (c) Narayana, Y. S. L. V.; Chandrasekar, R. *Chem. Phys. Chem* **2011**, 12, 2391. (d) Basak, S.; Chandrasekar, R. *Adv. Funct. Mater.* **2011**, 21, 667.
- (7) (a) Jiang, S.; Gnanasammandhan, M. K.; Zhang, Y. *J. R. Soc. Interface* **2010**, 7, 3. (b) Kim, H.-J.; Lee, J.; Kim, T.-H.; Lee, T. S.; Kim, J. *Adv. Mater.* **2008**, 20, 1117. (c) Kaeser, A.; Schenning, A. P. H. *J. Adv. Mater.* **2010**, 22, 2985. (d) Kumar, M.; George, S. J. *Nanoscale* **2011**, 3, 2130.
- (8) Ntziachristos, V. *Annu. Rev. Biochem. Eng.* **2006**, 8, 1.
- (9) Dos Santos, T.; Varela, J.; Lynch, I.; Salvati, A.; Dawson, K. A. *Small* **2011**, 7, 3341.
- (10) Fu, H.-B.; Yao, J.-N. *J. Am. Chem. Soc.* **2001**, 123, 1434.
- (11) Sreejith, S.; Divya, K. P.; Ajayaghosh, A. *Angew. Chem. Int. Ed.* **2008**, 47, 7883.
- (12) Ghoroghchian, P. P.; Therien, M. J.; Hammer, D. A. *Wiley Interdisciplinary Reviews: Nanomedicine and Nanobiotechnology* **2009**, 1, 156.
- (13) Lieschke, G. J.; Currie, P. D. *Nat. Rev. Genet.* **2007**, 8, 353.
- (14) (a) Hama, K.; Provost, E.; Baranowski, T. C.; Rubinstein, A. L.; Anderson, J. L.; Leach, S. D.; Farber, S. A. *Am. J. Physiol Gastrointest*, **2009**. (b) Du, S. J.; Gao, J.; Anyangwe, V. *Comp. Biochem. Physiol. B: Biochem. Mol. Biol.* **2003**, 134, 123. (c) Watanabe, K.; Nishimura, Y.; Oka, T.; Nomoto, T.; Kon, T.;

- Shintou, T.; Hirano, M.; Shimada, Y.; Umemoto, N.; Kuroyanagi, J. *BMC Neurosci* **2010**, *11*, 116.
- (15) (a) Kjellberg, J.; Johansson, N. G. *Tetrahedron* **1986**, *42*, 6541. (b) Geen, G. R.; Grinter, T. J.; Kincey, P. M.; Jarvest, R. L. *Tetrahedron* **1990**, *46*, 6903.
- (16) Wu, W.; Wu, W.; Ji, S.; Guo, H.; Zhao, J. *Eur. J. Inorg. Chem.* **2010**, *44*, 4470.
- (17) Díaz, L.; Bujons, J.; Casas, J.; Llebaria, A.; Delgado, A. *J. Med. Chem.* **2010**, *53*, 5248.
- (18) (a) Duhamel, J. *Polymers* **2012**, *4*, 211. (b) Winnik, F. M. *Chem. Rev.* **1993**, *93*, 587. (c) Kumar, M.; George, S. J. *Chem. Eur. J.* **2011**, *17*, 11102. (d) Dabrowski, M. J.; Schrag, M. L.; Wienkers, L. C.; Atkins, W. M. *J. Am. Chem. Soc.* **2002**, *124*, 11866.
- (19) Birks, J. B. *Rep. Prog. Phys.* **1975**, *38*, 903.
- (20) (a) Suzuki, Y.; Tazuke, S. *Macromolecules* **1980**, *13*, 25, (b) Suzuki, Y.; Tazuke, S. *Macromolecules* **1981**, *14*, 1742.
- (21) Chandross, E. A.; Ferguson, J.; McRae, E. G. *J. Chem. Phys.* **1966**, *45*, 3546.
- (22) Turro, N. J.; Kuo, P. L. *Langmuir* **1986**, *2*, 438.
- (23) Satsoura, D.; Leber, B.; Andrews, D. W.; Fradin, C. *Chem. Phys. Chem* **2007**, *8*, 834.
- (24) Westerfield, M. *The Zebrafish Book. A Guide for the Laboratory Use of Zebrafish (Danio rerio)*, 4th ed., University of Oregon Press, Eugene, **2000**.
- (25) E.E. Jelley, *Nature* **138** (1936) 1009.
- (26) (a) Trixler, F.; Markert, T.; Lackinger, M.; Jamitzky, F.; Heckl, W. M. *Chem. Eur. J.* **2007**, *13*, 7785. (b) Maitra, U.; Vijay Kumar, P.; Chandra, N.; J. D'Souza, L.; D. Prasanna, M.; R. Raju, A. *Chem. Commun.* **1999**, 595.
- (27) Kastler, M.; Pisula, W.; Wasserfallen, D.; Pakula, T.; Müllen, K. *J. Am. Chem. Soc.* **2005**, *127*, 4286.
- (28) Rabani, E.; Reichman, D. R.; Geissler, P. L.; Brus, L. E. *Nature* **2003**, *426*, 271.
- (29) Schoonbeek, F. S.; van Esch, J. H.; Wegewijs, B.; Rep, D. B. A.; de Haas, M. P.; Klapwijk, T. M.; Kellogg, R. M.; Feringa, B. L. *Angew. Chem. Int. Ed.* **1999**, *38*, 1393.
- (30) Palermo, V.; Morelli, S.; Simpson, C.; Mullen, K.; Samori, P. *J. Mater. Chem.* **2006**, *16*, 266.
-

2.13. Appendix:

A1. Solvatochromism Studies of PPy:

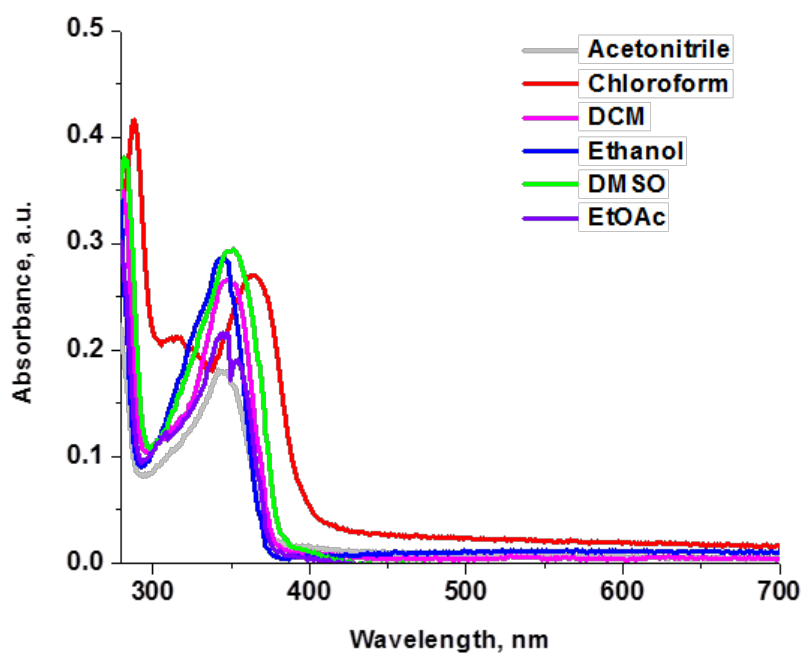


Figure A1: UV-Vis absorption spectra of **PPy** in various solvents

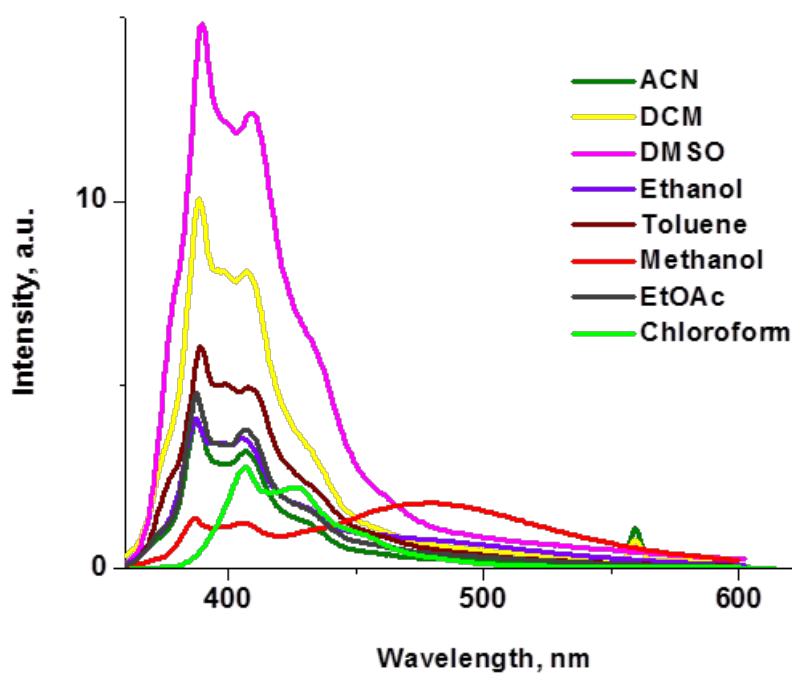


Figure A2: Fluorescence emission spectra of **PPy** in various solvents

A3. SEM Images of PPy:

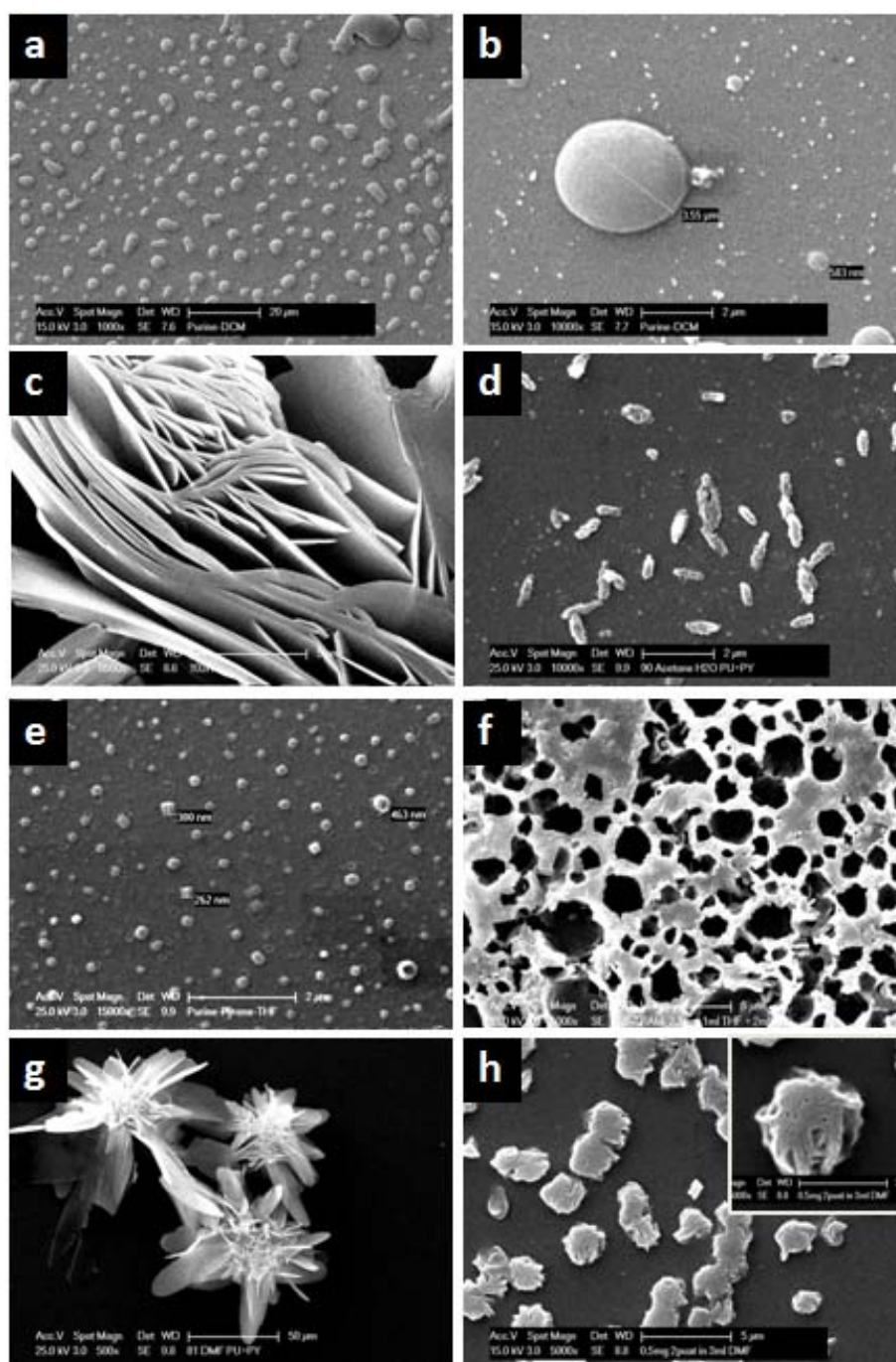


Figure A3: SEM micrographs of nano- and sub-microstructures of **PPy** obtained from different solvents: (a) from DCM (scale bar is 20 μm), (b) closer look at the same sample (scale bar is 2 μm), (c) from acetone (scale bar is 5 μm), (d) from acetone/water generated by CAM (scale bar is 2 μm), (e) from THF (scale bar is 2 μm), (f) from THF/water generated by CAM (scale bar is 5 μm), (g) from DMF (scale bar is 50 μm) and (h) nanoparticles observed in the same sample (scale bar is 5 μm), the insert shows a single particle at bigger scale (scale bar is 2 μm).

A4. Fluorescence Microscopy Images of MDA-MB-231 (Human Metastatic Breast Cancer) Cells

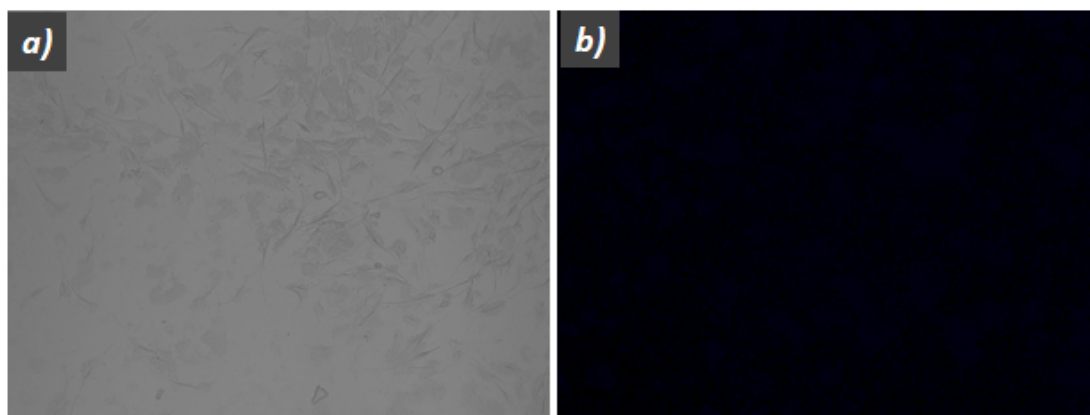


Figure A4: Fluorescent microscope images ($\lambda_{\text{ex}} = 365 \text{ nm}$, $\lambda_{\text{em}} = 445 \text{ nm}$) show no auto-fluorescence for control cells: a) bright field image of untreated cells; b) fluorescent image of untreated cells shown in (a).

A5. Confocal Fluorescence Microscope Images of PPy Nanoparticles:

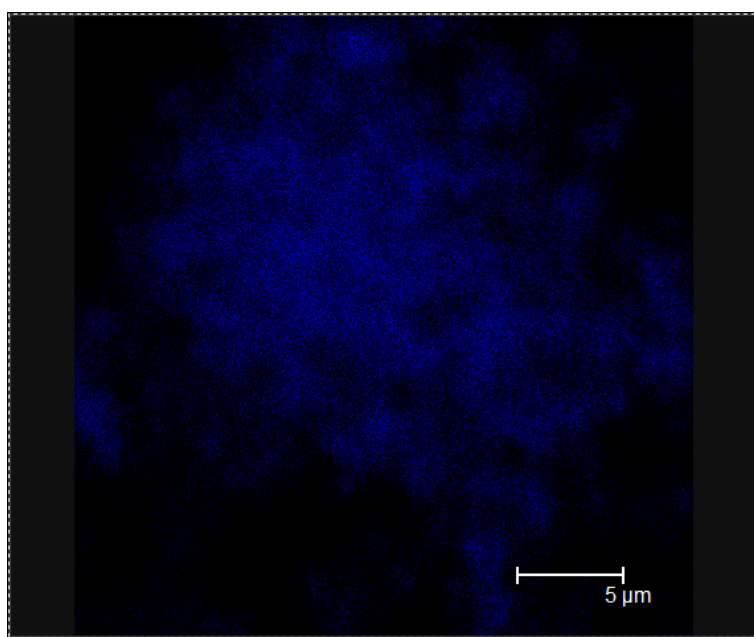


Figure A5: Confocal fluorescent microscope images ($\lambda_{\text{ex}} = 350 \text{ nm}$) of nanoparticles obtained from **PPy** in DMSO/H₂O (2:98) solutions.

A6. Laser Scanning Fluorescence Microscopy Images of Zebrafish Embryos Treated With PPy and GPy:

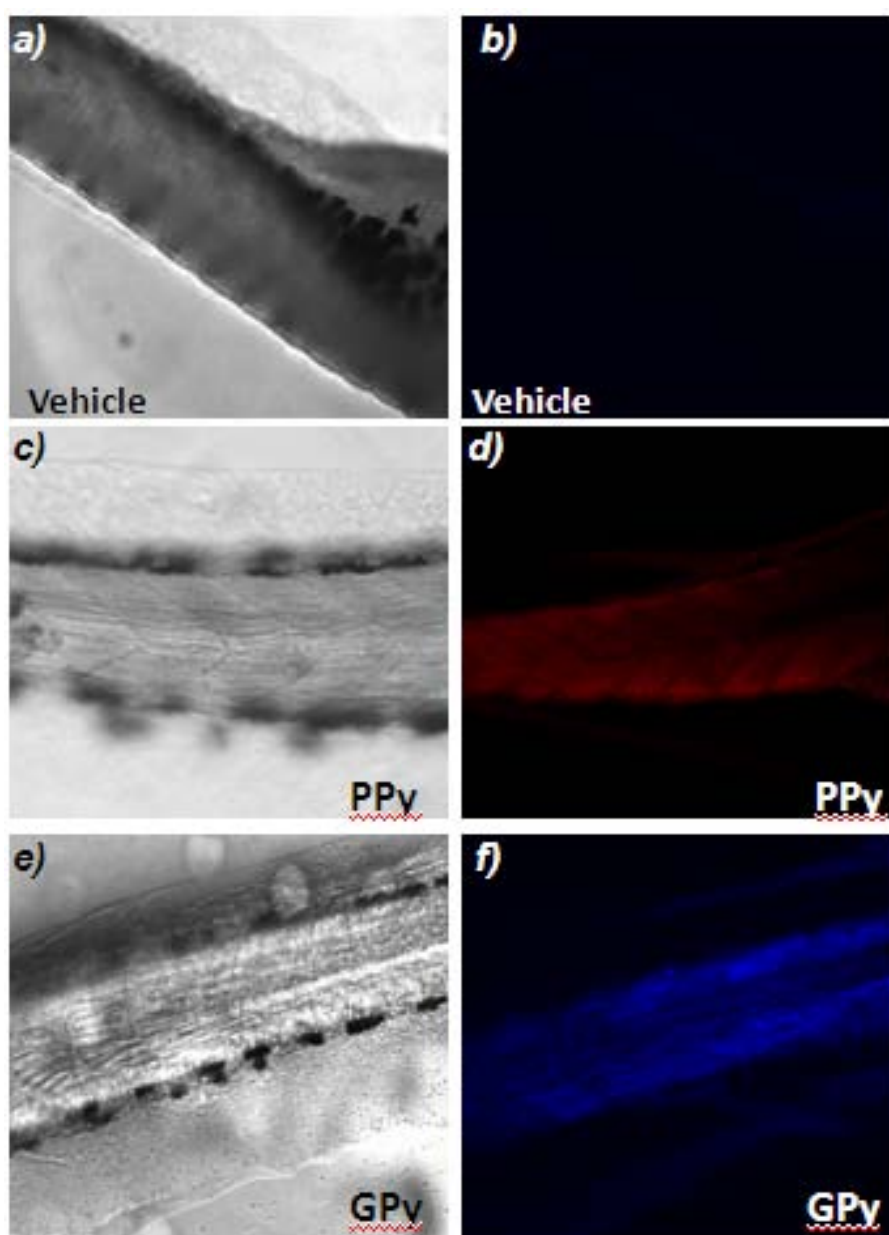


Figure A6: Confocal fluorescent microscopy images ($\lambda_{\text{ex}} = 350 \text{ nm}$) of zebrafish embryos exposed to vehicle (control) or **GPy**: a) bright field image of untreated embryos (vehicle); b) fluorescent image of embryos represented in (a); c) bright field images of embryos exposed to a solution containing **PPy** nanoparticles ($50 \mu\text{M}$); d) fluorescent images of (c) collected in the red, channel of the confocal system; e) bright field images of embryos exposed to a solution containing **GPy** nanoparticles ($50 \mu\text{M}$); f) fluorescent images of (c), collected in the blue channel of the confocal system.

2.14. NMR Spectra of Synthesized Compounds:

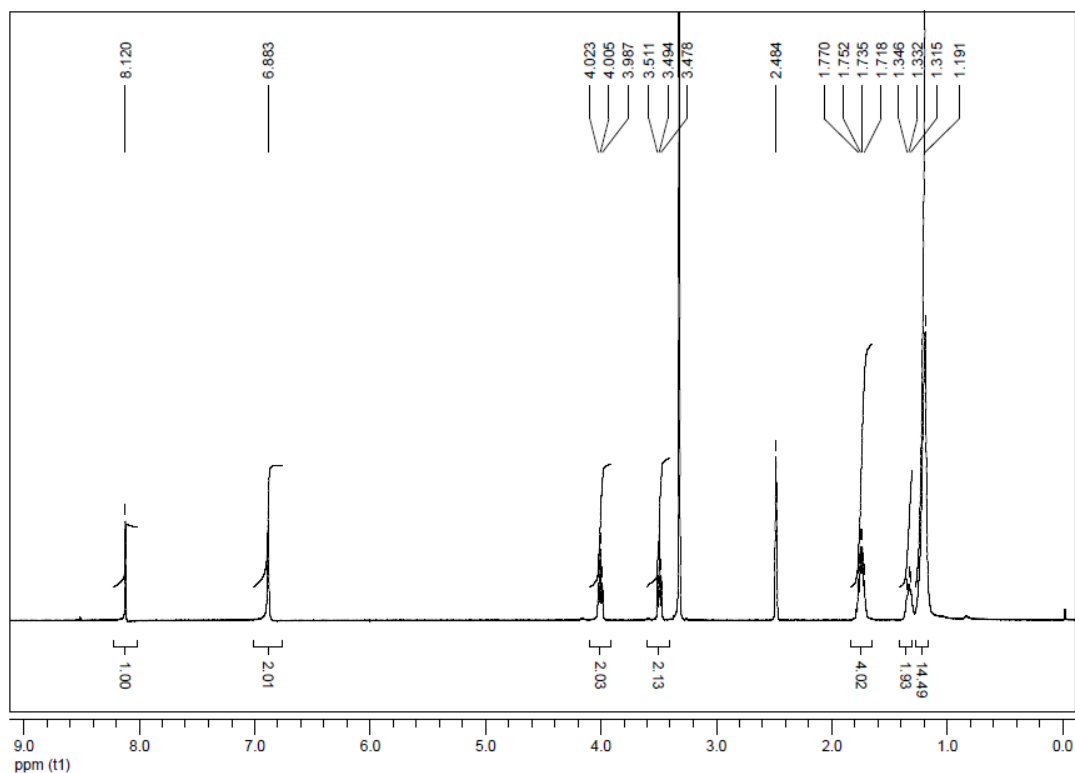


Figure A7: ¹H NMR (DMSO-*d*₆, 400 MHz) of compound **1.3**

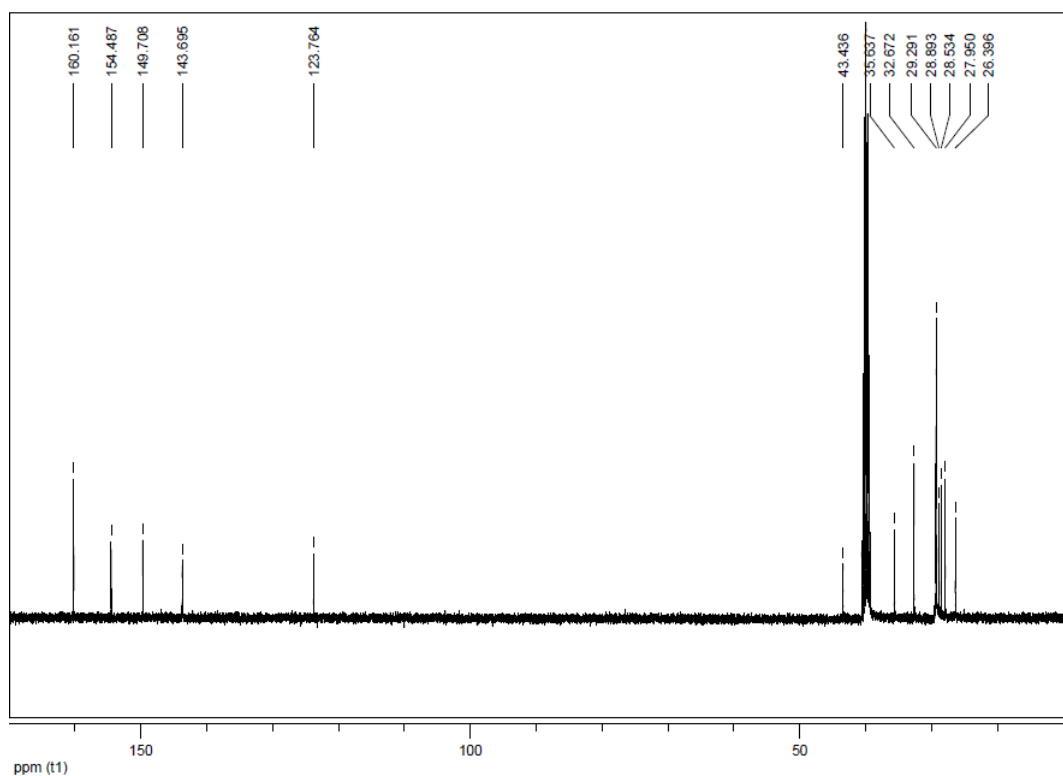


Figure A8: ¹³C NMR (DMSO-*d*₆, 100 MHz) of compound **1.3**

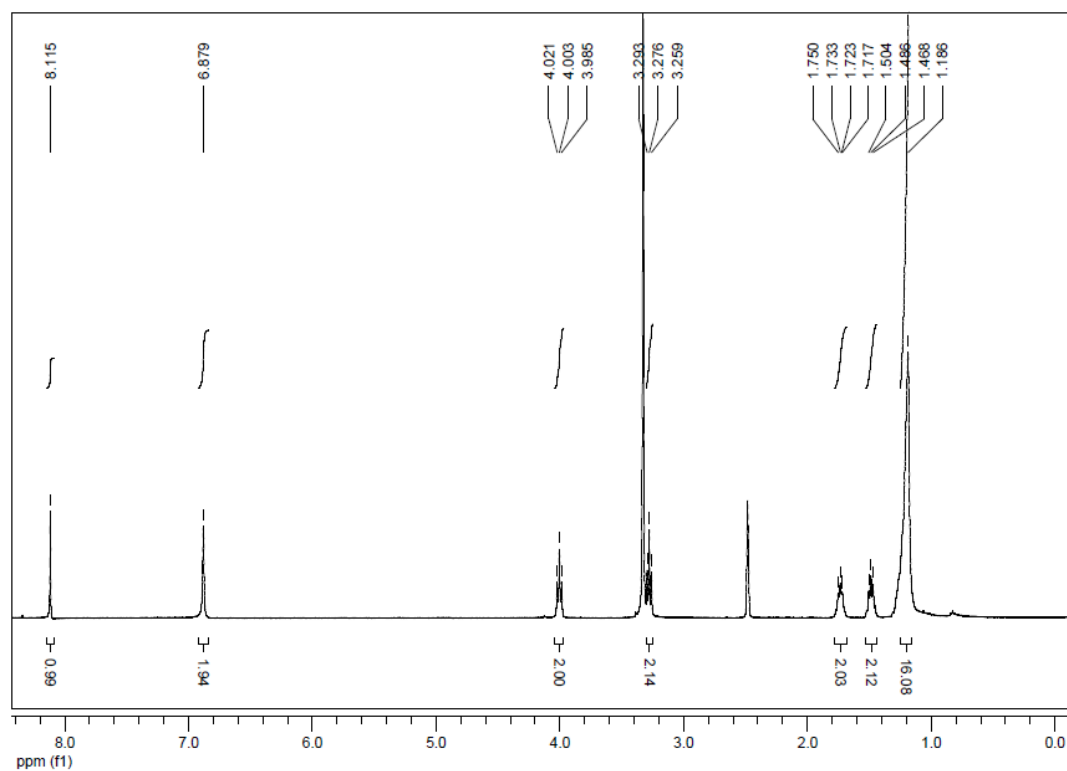


Figure A9: ¹H NMR (DMSO-*d*₆, 400 MHz) of compound **1.4**.

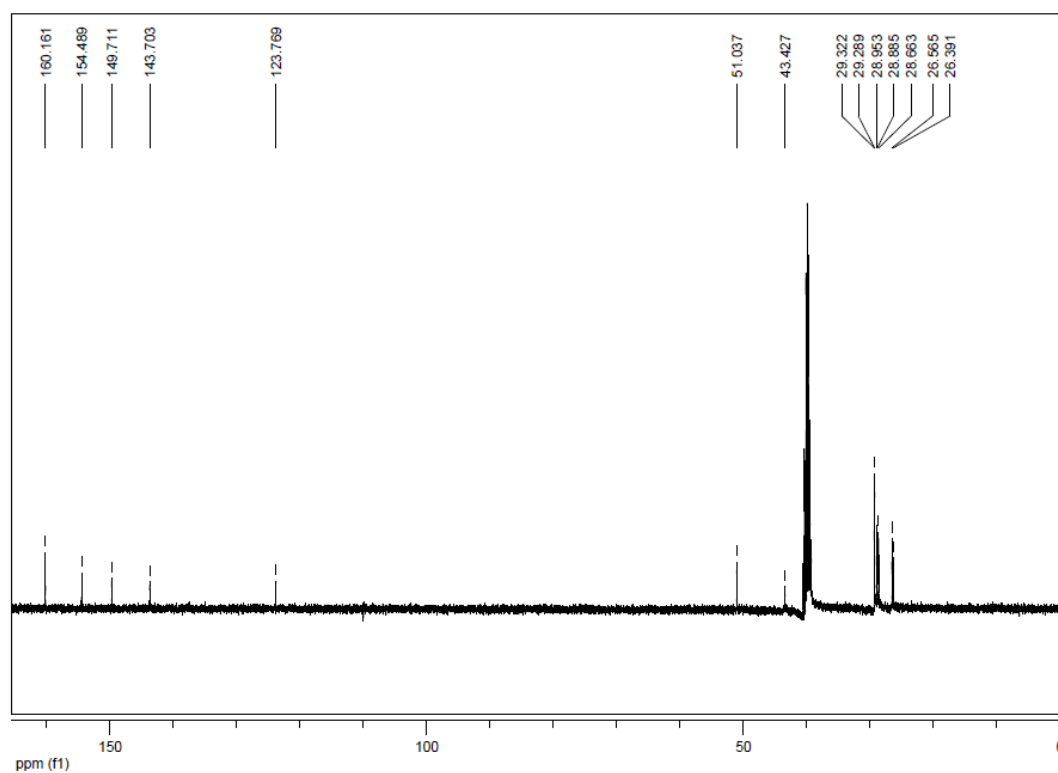


Figure A10: ¹³C NMR (DMSO-*d*₆, 100 MHz) of compound **1.4**

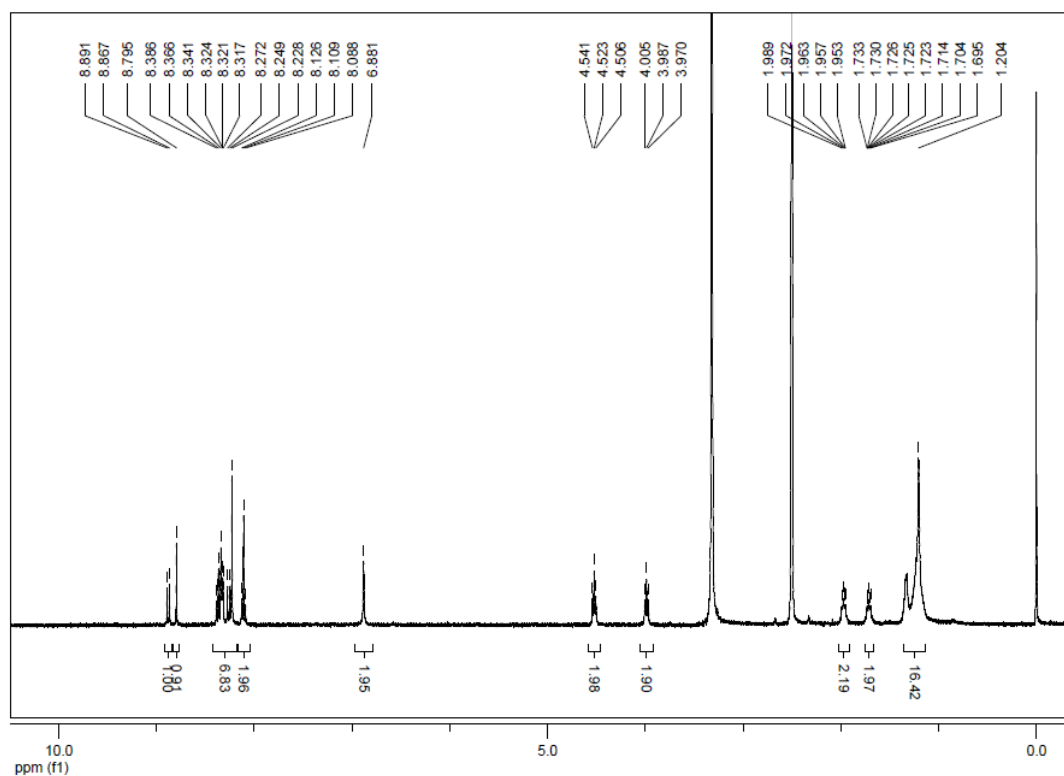


Figure A11: ¹H NMR (DMSO-*d*₆, 400 MHz) of compound PPy

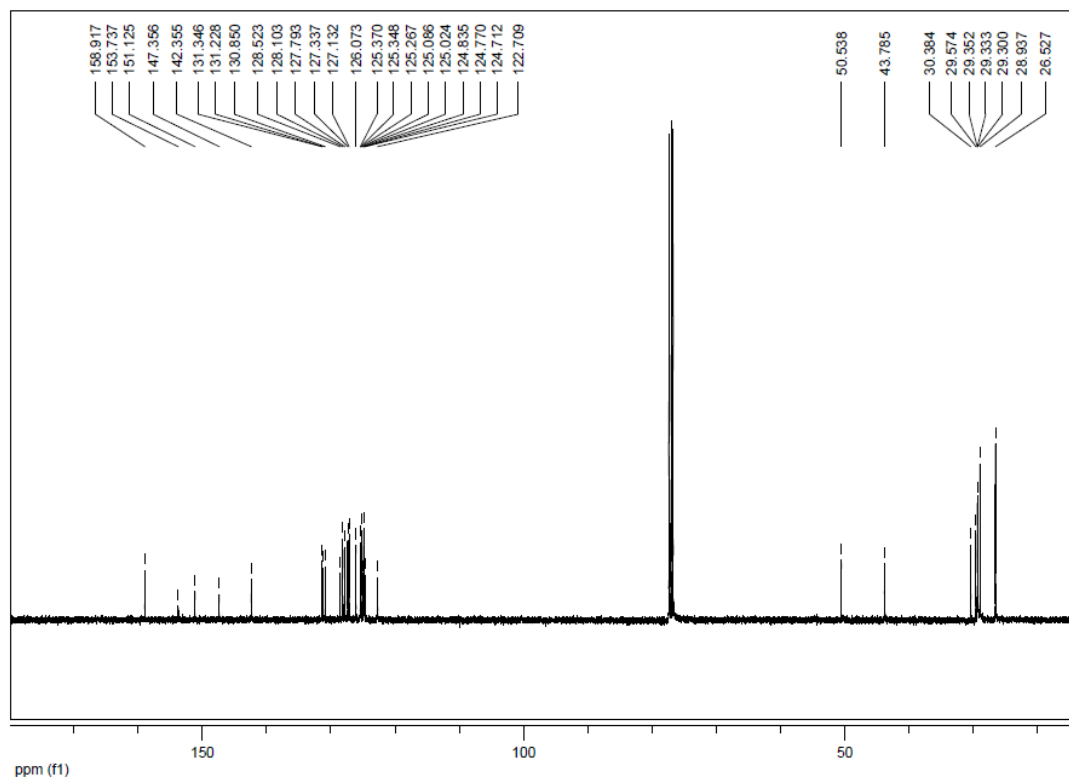


Figure A12: ¹³C NMR (CDCl₃, 100 MHz) of compound PPy

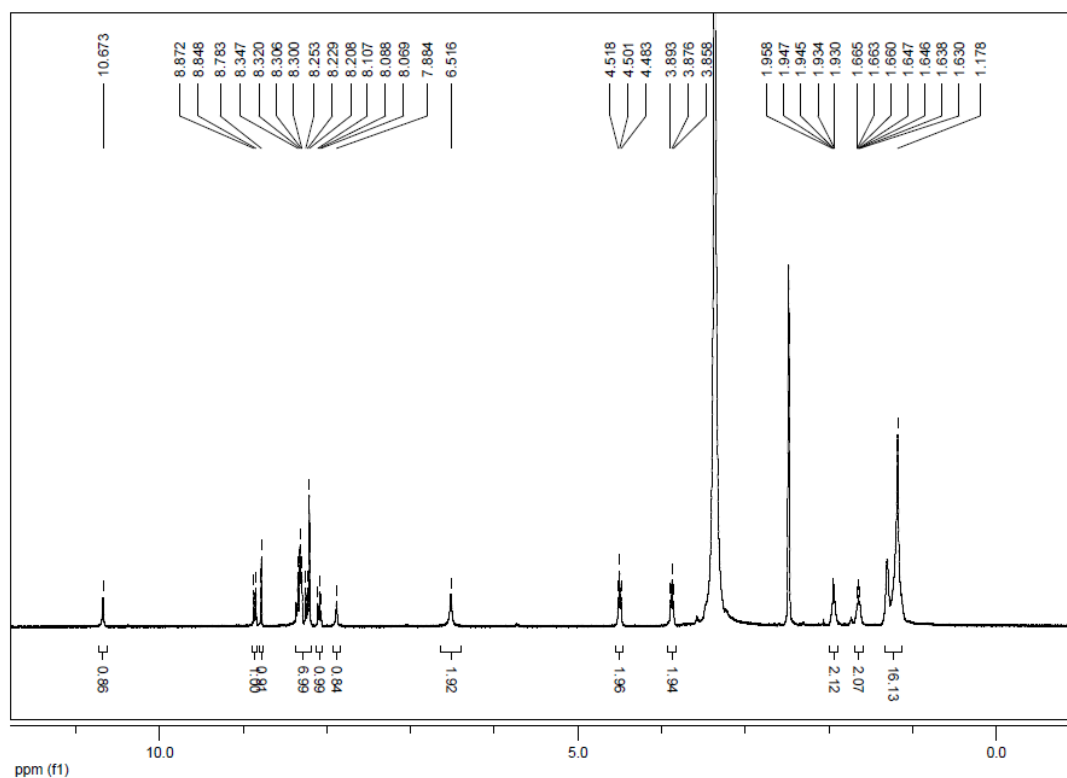


Figure A13: ¹H NMR (DMSO-*d*₆, 400 MHz) of compound GPy

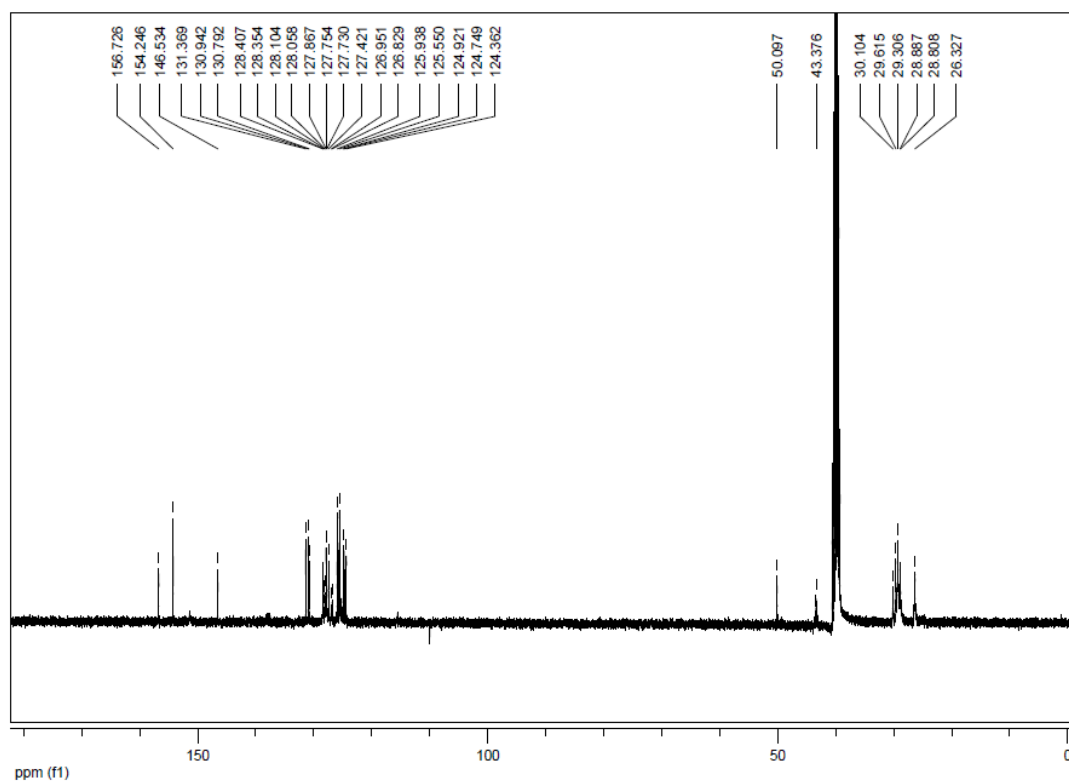


Figure A14: ¹³C NMR (DMSO-*d*₆, 100 MHz) of compound GPy

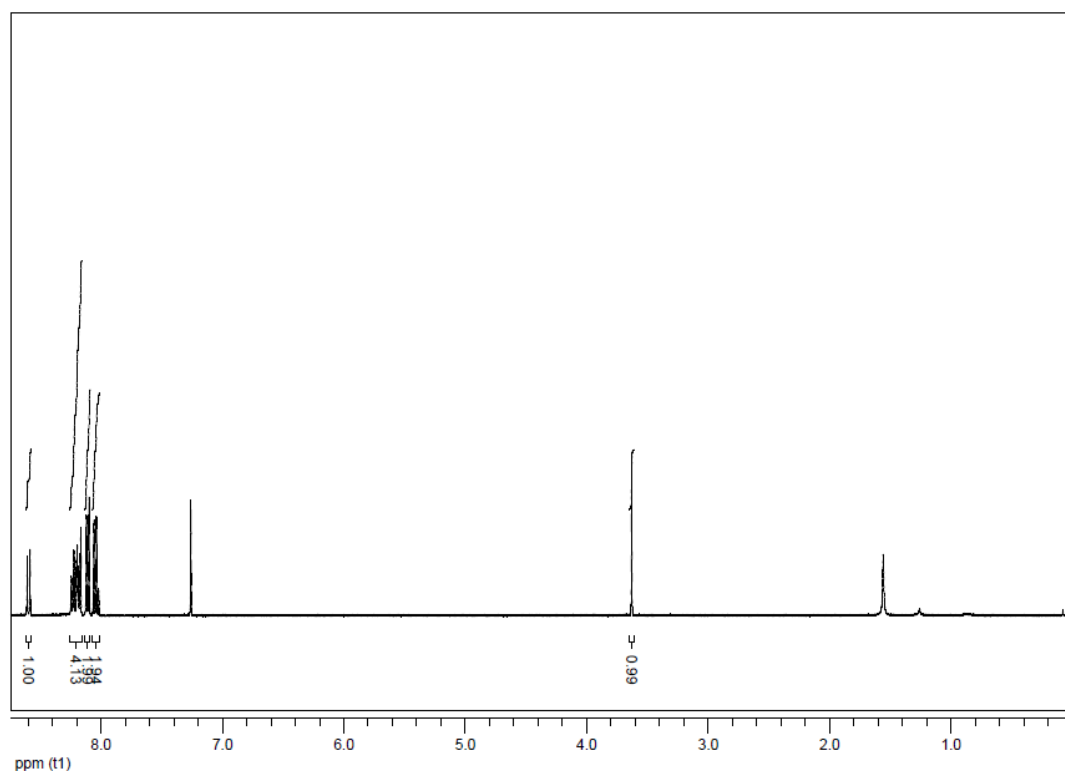


Figure A15: ¹H NMR (CDCl₃, 400 MHz) of compound **1.8**

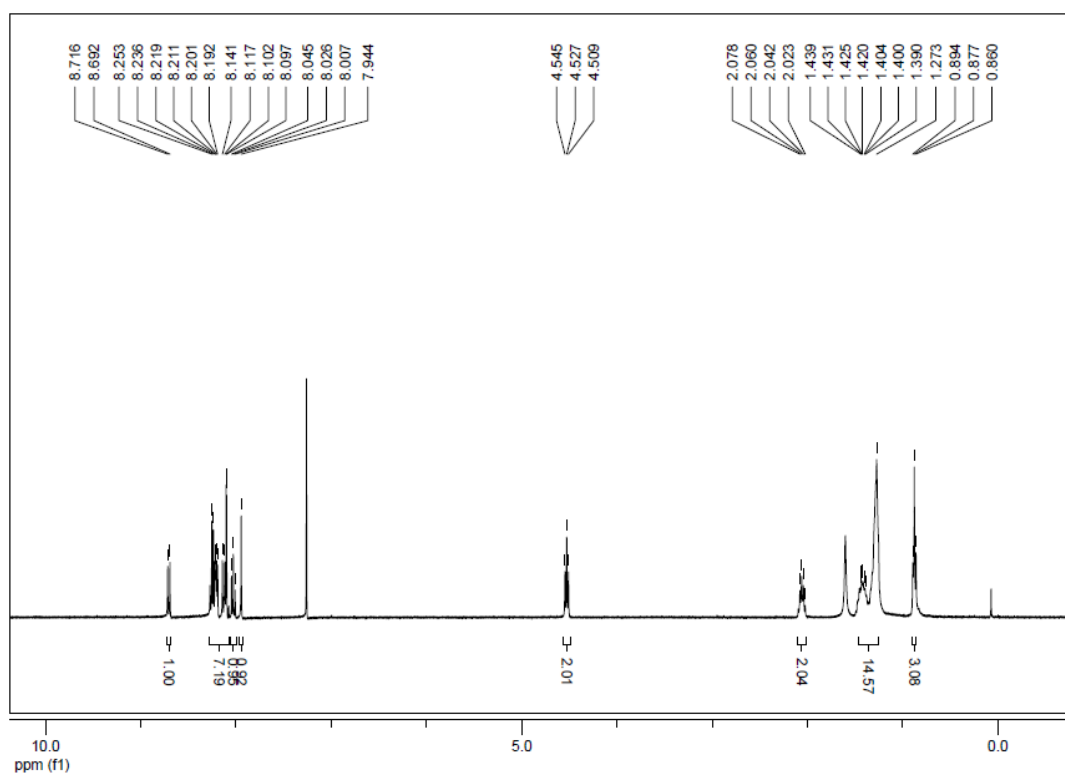


Figure A16: ¹H NMR (CDCl₃, 400 MHz) of compound **1.9**

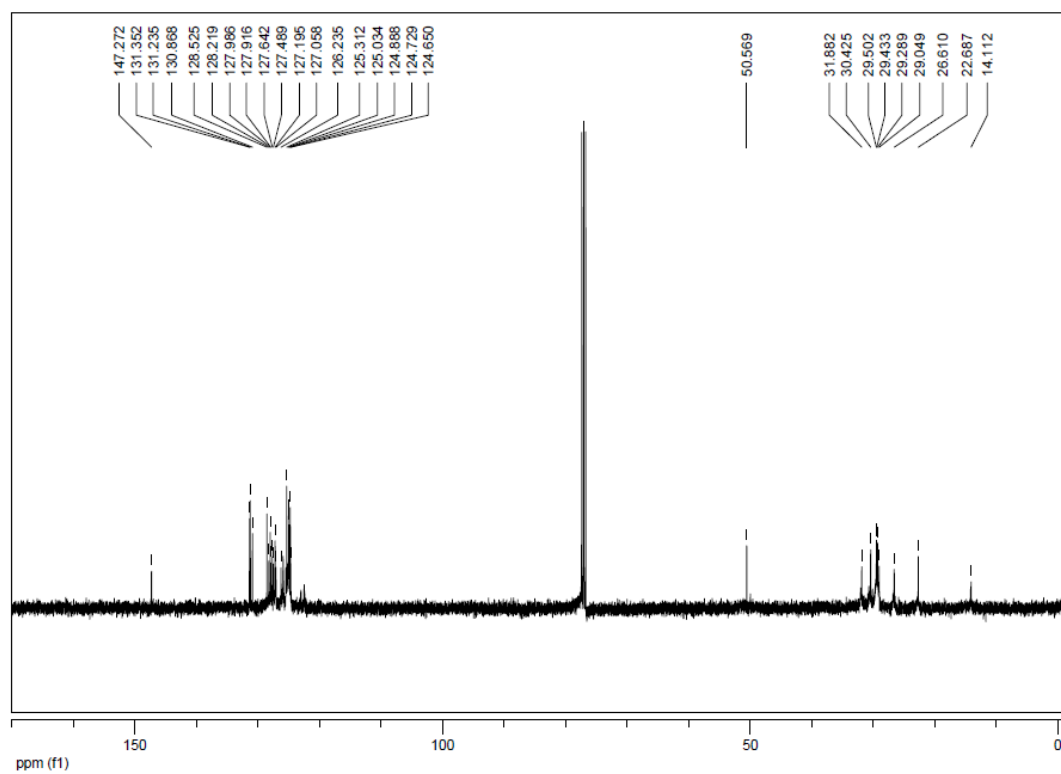
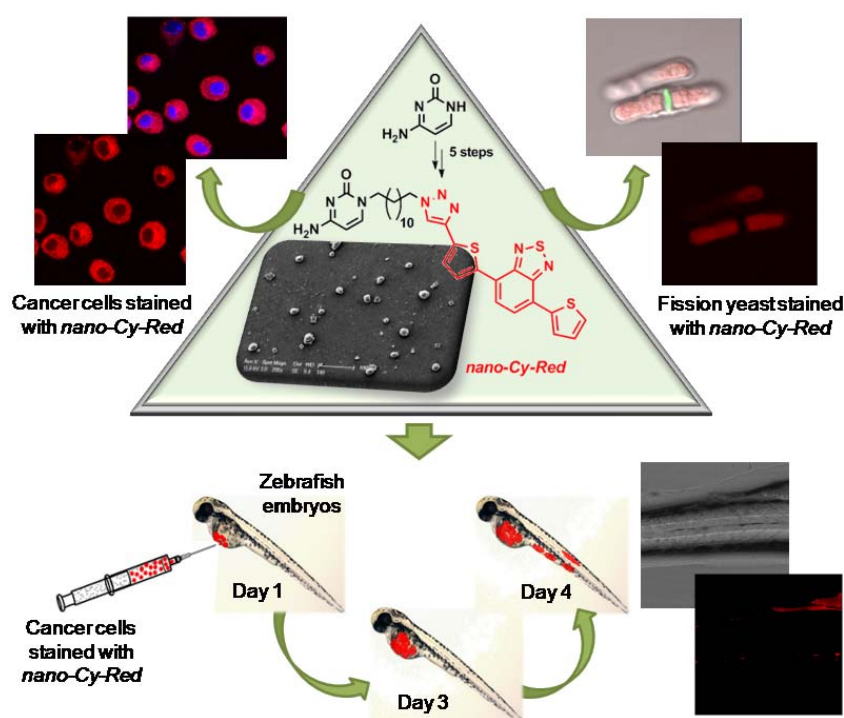


Figure A17: ¹³C NMR (CDCl₃, 100 MHz) of compound **1.9**

3

Red Fluorescent Organic Nanoparticles for Real Time *In Vitro* and *In Vivo* Bioimaging



*This chapter partly adapted from: **E. Ramanjaneya Reddy**, Swapna Yellanki, Raghavendra Medishetty, Lahiri Konada, Neeraja P Alamuru, Devyani Haldar, Kishore V.L. Parsa, Pushkar Kulkarni and Marina S. Rajadurai* *ChemNanoMat* **2015**, 1, 567-576. (Inside front cover)

3.1. Abstract:

Development of efficient FONs, for *in vitro* and *in vivo* bioimaging is one of the emerging areas of nano-biotechnology. This chapter reports the synthesis of novel FONs based on fluorescent chromophore (**Cy-Red**), composed of cytosine moiety connected to 4,7-di(thiophene-2-yl)benzo[c][1,2,5]thiadiazole by aliphatic chain using click chemistry approach.¹ Preparation of solution stable, red emissive nanoparticles (**nano-Cy-Red**) *via* bottom-up approach and their photophysical properties and morphology were fully investigated by UV-Vis and fluorescence spectroscopy, SEM, AFM, DLS, CFM and fluorescence microscopy studies. It was found that novel **nano-Cy-Red** are nontoxic, biocompatible and are able to penetrate into mouse macrophage cells, oral cancer cells and yeast and were retained in living cells for several generations serving as a cytoplasmic stain. The chapter also describes the utilization of **nano-Cy-Red** dye for direct *in vivo* visualization of cancer cell migration up to 72 h post transplantation in zebrafish embryos.²

3.2. Introduction:

For the last two decades, nanoparticles are attracting tremendous interest and being explored extensively because of their unique size dependent chemical and physical properties. They are especially interesting candidates for biomedical research since the size of nanoparticles is comparable to the most biological objects at the molecular level. FONs are particularly attractive members of nanoparticles family, because of its broad range of potential application in optoelectronic nano-devices, (bio-)chemical sensing, drug delivery and monitoring systems, diagnostics, immunofluorescent labeling and *in vitro/in vivo* imaging.³⁻⁷ FONs are very attractive candidates for fluorescent imaging, as they offer definite advantages over bulky organic chromophores, such as easy cellular uptake,⁸ size-dependent fluorescent properties⁹ and longer fluorescence life time.¹⁰ Red FONs are high in demand, because the red emitting FONs can be excited with a visible light source, which results in less harmful effects on the biological samples, such as cells and tissues, in comparison with ultraviolet light. Longer excitation and emission wavelength allows the light to penetrate through thicker samples which is beneficial for *in vivo* experiments.^{11a} Therefore, novel nontoxic, biocompatible red colour FONs would be a valuable addition to FONs family for *in vivo* and *in vitro* imaging.

The novel red fluorescent nanomaterials were designed according to following principle (**Figure 1**): biologically active molecule (nucleobase, nucleoside) is connected to the fluorescent tag through flexible and long aliphatic linker. Such compounds are expected to bind to genes and proteins and illuminate biological processes in the living cells across several cell cycles.

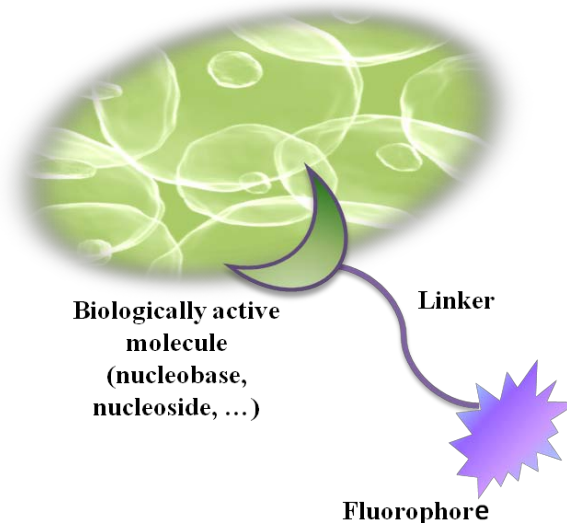


Figure 1: Design principle

Majority of commonly used for biological imaging and clinical screening fluorescent organic dyes, such as Fluorescein isothiocyanate (FITS) or Rhodamine derivatives aren't suitable for the long term imaging as they undergo rapid photobleaching.^{11b} Another drawback of some of these dyes is unwanted altering of the cells viability and proliferation.^{11c} Although FONs are an attractive alternative, some of them also suffer from above mentioned drawbacks, e.g. silica nanoparticles doped with fluorescent dyes.^{11d} Therefore, there is a need to develop nanoparticles with long term photo-stability and high biocompatibility. In continuation of the efforts to develop superior fluorescent nanoparticles as bio-probes,¹⁷ described in the previous chapter, this chapter is focused on design and synthesis of red biocompatible, stable and effective FONs. The FONs are prepared from the novel organic chromophore based on a biologically active molecule (nucleobase), which is connected to the fluorescent tag through a flexible and long aliphatic linker *via* “click”- chemistry. Such compounds may be expected to bind to biomolecules and illuminate biological processes in the living cells across several cycles.

The synthesis of a novel cytosine based red fluorescent chromophore (**Cy-Red**) followed by preparation of organic nanoparticles *via* “bottom-up” approach is reported for the first time. According to the design principle, cytosine was connected to the fluorescent tag 4,7-di(thiophene-2-yl)benzo[c][1,2,5]thiadiazole by 12-carbons

aliphatic chain. Self-assembly of the molecules in DMSO/H₂O solutions led to formation of solution-stable, red emissive, biocompatible, non-toxic FONs (**nano-Cy-Red**). This chapter also presents their photophysical properties and the results of SEM, AFM, DLS, CFM, and fluorescence microscopy studies. Finally the ability of **nano-Cy-Red** to penetrate into mouse macrophage, oral cancer cells and zebrafish embryos is also reported. One of the important advantages of this FONs is the ability to retain in living cells for several generations, serving as a cytoplasmic stain. This property allowed efficient long time tracking of transplanted cancer cells, stained with **nano-Cy-Red**, in live zebrafish embryo up to 72h. Apart from that, chapter 3 discloses an ability of **nano-Cy-Red** to easily penetrate through yeast cell wall, which is not a common property for many organic molecules, and demonstrate for the first time application of **Cy-Red** FONs for the yeast imaging.

3.3. Results and Discussion:

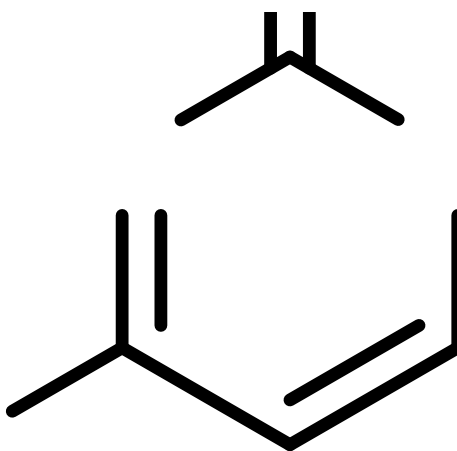
The synthesis of the novel chromophore **Cy-Red** was performed as outlined in **Scheme 1-3**. Overall synthesis of the target compound **Cy-Red** consists of ten steps and commence from simple and un-expensive starting materials: cytosine and thiophene. Fluorescent intermediate 4-(5-ethynylthiophen-2-yl)-7-(thiophene-2-yl)benzo[c][1,2,5]thiadiazole **1.7** was synthesized in 5 steps according to modified reported procedures. Namely 4,7-dibromobenzo[c][1,2,5]thiadiazole **1.2** was obtained with 92% yield after bromination of the commercially available 2,1,3-benzothiadiazole **1.1** with molecular bromine in hydrobromic acid.¹² Thiophene was lithiated using n-BuLi followed by treatment with tributylchlorostannane to afford tributyl(2-thienyl)stannane (**1.4**).¹³ Compound **1.4** was coupled to compound **1.2** in Stille coupling conditions in THF using palladium (II) catalyst to give 4,7-di-2-thienyl-2,1,3-benzothiadiazole **1.5** in good yield.¹⁴ Partial bromination of the compound **1.5** with N-bromosuccinimide in acetic acid-DCM gave mono-brominated compound **1.6** with improved yields (70%) in comparison with literature procedure.¹⁵ This could be associated with modification in presented here: The reaction started at 0 °C and then let it slowly reach room temperature, stirring reaction mixture overnight, while Jin-Liang *et al.* were running reaction at 0 °C for only 1 h. A similar procedure leading to improved result was also reported later from Jaejung Ko group.^{15b} Ethynyl derivative **1.7** was prepared using standard two-steps protection-deprotection procedure, where protection step was performed *via* Sonogashira coupling of **1.6** with

trimethylsilyl acetylene followed by conversion to terminal alkyne by deprotection with K_2CO_3 in methanol giving compound **1.7** in good yield¹⁶ (**Scheme 1**).

Scheme 1: Synthesis of red fluorescent tag

Biologically active chromophore **Cy-Red** was prepared as outlined in **Schemes 2** and **3**. At the first step, amine protection of commercially available cytosine **2.1** with acetic anhydride using DMAP/pyridine resulted in N4-acetyl cytosine **2.2** with 95% yield. Although acetylation is not a common protection strategy for amines, we incorporated N-4-acetyl in the cytosine scaffold because the acetoxy group might bring additional H-bond acceptor, improving binding ability and therefore potency of **Cy-Red**. Initially we did not have intention of amine deprotection and were planning to utilize **2.5** directly for bioimaging studies. N-alkylation of compound **2.2** with 3 equivalents of 1,12-dibromododecane in the presence of NaH gave compound **2.3** with decent 51% yield. According to literature, including published results described in the chapter **2**,¹⁷ low yields are typical for the selective alkylation reactions of nucleobases. Cytosine was not an exception and non-regiospecific alkylation resulted in unwanted side products. Reaction of bromo compound **2.3** with sodium azide was performed in DMSO at RT to afford azide derivative **2.4** in good yield. Subsequent 1,3-dipolar Huisgen cycloaddition reaction of compound **2.4** with compound **1.7** under “click reaction” conditions in presence of CuI led to formation of click product **2.5** with only 21% yield. This compound was

not soluble in any organic solvents including DMF and DMSO. Moreover, consequent N4-acetyl deprotection of compound **2.5** with aqueous ammonia in methanol was not successful. In order to avoid the problem, the sequence of the synthetic steps was corrected and deprotection of **2.4** was performed prior to “click-chemistry” step, In this case compound **2.6** was obtained effortlessly in decent yield. Subsequent 1,3-dipolar cyclo addition reaction of **2.6** with **1.7** gave cytosine connected to fluorescent 4,7-di(thiophene-2-yl)benzo[c][1,2,5]thiadiazole *via* triazole-alkyl linker (**Cy-Red**) in 43% yield. However, overall yield of this synthetic sequence was only 8%.



Scheme 2: Synthesis of fluorescent cytosine analogue **Cy-Red**

In order to improve yields, the protection group at N-4 position of cytosine was replaced with tert-butyloxycarbonyl (Boc) anhydride as it is better N-protecting agent. Treatment of cytosine in dry THF with an excess of Boc-anhydride in the presence of a catalytic amount of DMAP led to formation of tris-Boc-protected cytosine with an excellent yield. Tris-Boc cytosine was quantitatively converted into bis-Boc cytosine **3.1** by refluxing in MeOH with aq.NaHCO₃.^{18a} The structure of bis-

Boc cytosine **3.1** was confirmed by ^1H NMR spectroscopy and mass spectrometry. The next steps were performed following synthetic route similar to the one described above (**Scheme 2**). The alkylation of cytosine derivative **3.2** and sequential azide formation gave compound **3.3**, which in its turn was subjected to “click”-reaction with intermediate **1.7** to give Boc protected fluorescent precursor **3.4** with improved yield (62%). The formation of a five-membered triazole ring was confirmed by ^1H NMR spectroscopy. Clear evidence of the successful Huisgen cycloaddition was an appearance of a $\text{C}_{\text{triazole}}-\text{H}$ proton at 8.61 ppm and disappearance of the terminal acetylene proton at 3.48 ppm (see spectrum on page 117). At last step, deprotection of Boc-amino group in standard conditions using tri-flouro acetic acid in DCM resulted in the formation of final fluorophore **Cy-Red** with good yield. ^1H NMR spectrum showed a broad signal of N-H protons at 7.42 ppm belonged to free amino group and disappearance of $\text{C}_{\text{tert-butyl}}-\text{H}$ protons at 1.25 ppm (see spectrum on page 118). Apart from that, dramatic shift of $\text{C5}_{\text{cytosine}}-\text{H}$ proton from 6.72 ppm to 5.75 ppm was observed after deprotection, the position of this peak as well as peak of $\text{C5}_{\text{cytosine}}-\text{H}=5.58$ ppm are characteristic for free cytosine. Additionally, EI-MS showed predominant peak with m/z value of 645.2 corresponding to desired molecule. Thus, ^1H NMR and mass spectrometry confirmed the formation of final compound **Cy-Red**.

Scheme 3: Synthesis of fluorescent cytosine analogue Cy-Red

Unlike previous synthetic route (using acetyl-protected compounds (**2.1** → **Cy-Red**) there was no any problems related to solubility of intermediates and all reactions were going smoothly with good yields. The synthetic sequence *via* Boc-protected intermediates (**3.1** → **Cy-Red**) helped to improve overall yield to 18% (from 8% *via* previous synthetic route, **Scheme 2**).

3.4. Photophysical Properties of Cy-Red:

3.4.1. Overcoming the Solubility Issue:

Before describing studies performed with novel fluorescent compound **Cy-Red** it is worth to note that in its original form it is not soluble in any organic solvents apart from DMSO. Attempts to dissolve compound in water (since it is best non-toxic solvent for biological investigation) did not succeed at any conditions (shaking, heating and ultrasound). Therefore, an attempt has been made to overcome solubility issues by salt formation as it is the most common and effective method of increasing solubility and dissolution rates of pharmaceuticals.^{18b,c} Unfortunately, formation of **Cy-Red** salts with hydrochloric acid or hydrobromic acids did not improve its solubility. Moreover, **Cy-Red** salt of common organic acids (e.g. citric acid) resulted only in limited solubility (**Figure 2**) which was not enough for biological experiments. Subsequently nanonization using the nanoprecipitation method,^{18d,21b} similarly to the method developed for **PPy** and **GPy** chromophores (Chapter 2)^{17a}.

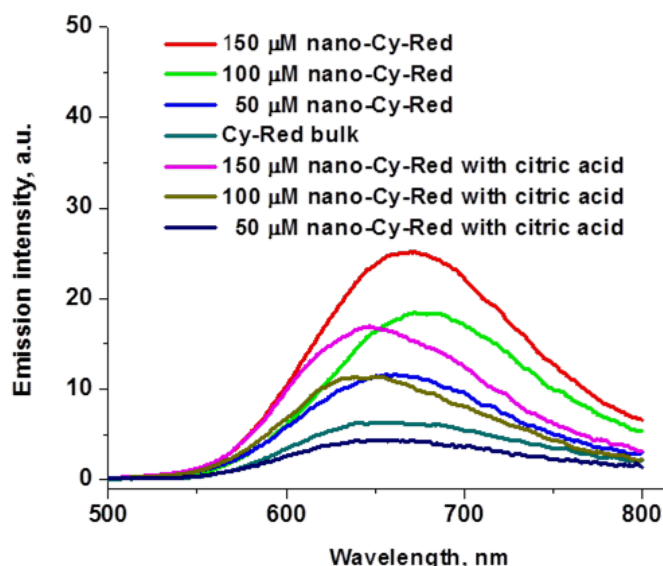


Figure 2: Emission spectra ($\lambda_{\text{ex}} = 473$ nm) of **Cy-Red** in DMSO/H₂O (2:98) solutions obtained after different methods of solubilization (none, salt formation with citric acid, and nanonization) at different concentrations

For that, DMSO solution of compound **Cy-Red** (60 μL , $c \sim 2.5 \text{ mM}$) was rapidly injected into water (3 mL) leading to the formation of nanoparticles (**nano-Cy-Red**) due to molecular aggregation.^{17a} Nanonization of the compound was very efficient: nanosized **Cy-Red** (**nano-Cy-Red**) become soluble in water up to 150 μM without precipitation and exhibited bright fluorescence emission. Prepared nanoparticles were used for characterization and biological studies immediately.

3.4.2. Optical Properties:

Having final pure fluorophore in hands, the photophysical properties of **Cy-Red** in DMSO as well as **nano-Cy-Red** in biocompatible solvent mixture-DMSO/H₂O (2:98) were investigated. In DMSO and DMSO/H₂O chromophore in both forms displayed nearly identical absorbance maxima at 471 nm and 473 nm (**Figure 3**). Fluorescent emission spectra ($\lambda_{\text{ex}}=473 \text{ nm}$) exhibited similar fluorescence bands, with a maximum at 634 nm for **Cy-Red** in DMSO and 647 nm for **nano-Cy-Red** in DMSO/H₂O solutions (**Figure 4**). Solid state spectrum of the bulk compound exhibited maximum emission at 709 nm (**Figure 5a**). Solid state and 2% DMSO/H₂O solution has decreased fluorescence intensity, probably due to aggregation induced fluorescence quenching (AIQ); however fluorescent microscopy studies demonstrated bright emission of **Cy-Red** upon excitation at 510-560 nm even in solid state (**Figure 5b** and **5c**). The solution state quantum yield of **Cy-Red** ($\Phi_{\text{f}}=0.58$) was quite high with respect to quinine sulphate as a reference compound.

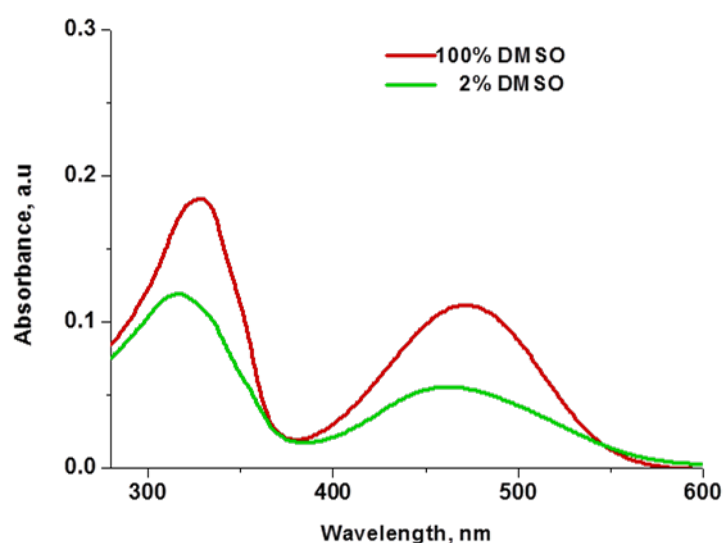


Figure 3: UV-Vis absorbance spectra of **Cy-Red** in DMSO and DMSO/H₂O at 10^{-5}M

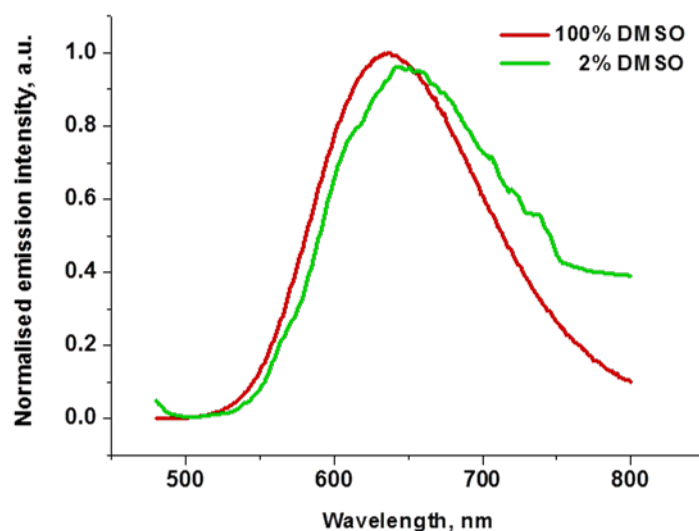


Figure 4: Fluorescence emission spectra of **Cy-Red** ($\lambda_{\text{ex}}=473$ nm) in DMSO and DMSO/H₂O at 10^{-5} M

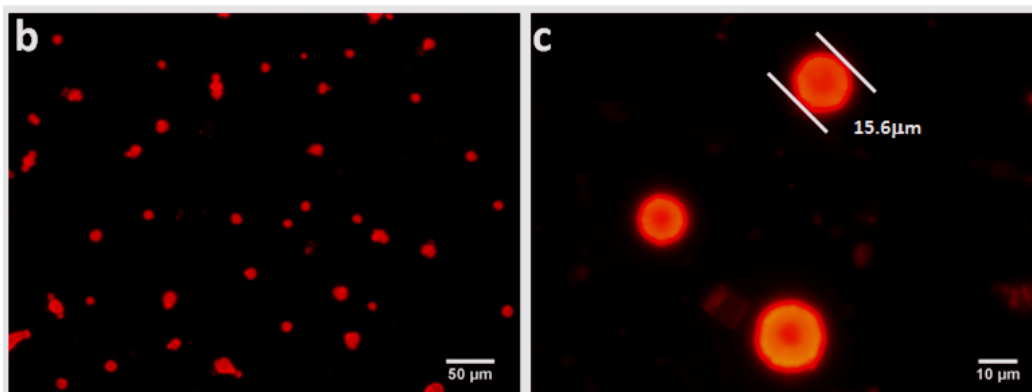
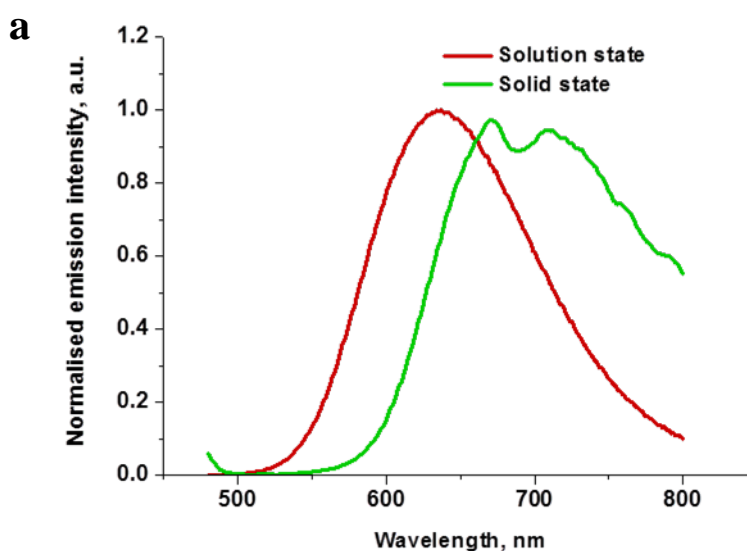


Figure 5: a) Comparative emission studies of **Cy-Red** ($\lambda_{\text{ex}}=473$ nm) in solution state and solid state: fluorescent microscopy images of **Cy-Red** microspheres in DMSO: b) magnification is 10x; c) magnification is 40x

3.4.3. Photostability Studies of Cy-Red Fluorophore:

Photobleaching is one of the main drawbacks for majority of organic fluorophores. In order to check the stability of the **Cy-Red**, **Cy-Red** in DMSO and DMSO/H₂O (2:98) solutions were treated with UV light (254 nm, 8W, 760 $\mu\text{W}/\text{cm}^2$) for 2h, 4h, 8h and 20h, measuring its emission at every time point (**Figure 6a** and **6b**). **Figure 6a** clearly shows no or negligible decrease of emission intensity upon UV-treatment for DMSO solution of **Cy-Red**, which indicates no photobleaching and fading throughout the photostability experiments. The emission intensity of **nano-Cy-Red** in DMSO/H₂O was slightly disordered and decreased by approximately 20% after overnight treatment. This fluorescence loss most probably is associated with nanoparticles aggregation resulting in AIQ effect, rather than with photobleaching.

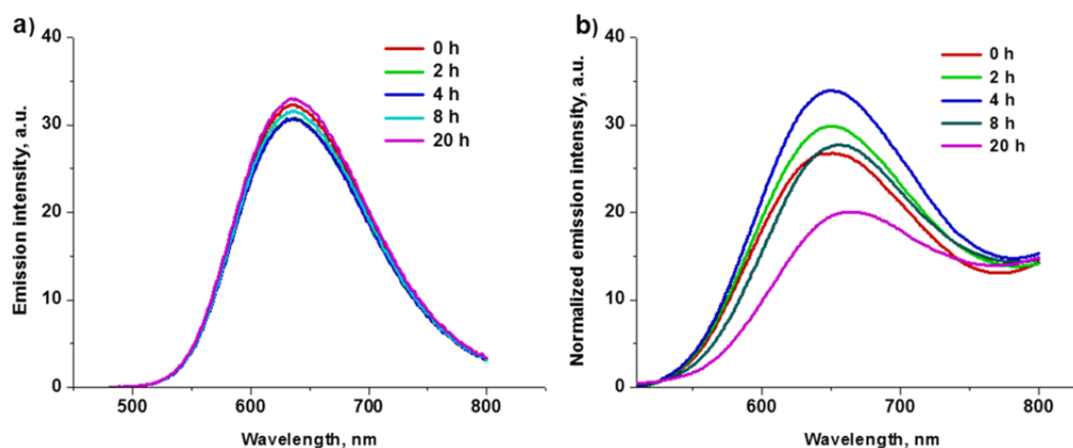


Figure 6: Fluorescence emission spectra of Cy-Red (10^{-5}M solutions) obtained in different time intervals before and after UV-treatment (254 nm, 8W, 760 $\mu\text{W}/\text{cm}^2$); a) in DMSO, b) in DMSO/H₂O (2:98)

These studies revealed that the characteristic features of **Cy-Red** fluorophore are as following:

1. It has longer absorption (at $\lambda_{\text{max}}=473$ nm) and longer emission (at $\lambda_{\text{max}}=634$ nm) wavelengths, which helps to overcome issue of autofluorescence in majority of biological objects, and decreased damage of cells/tissues by light beam.
2. The solution state quantum yield of **Cy-Red** is quite high $\Phi_f=0.58$ (measured with respect to quinine sulphate as reference $\Phi_f=0.577$).
3. **Cy-Red** fluorophore possesses high photobleaching thresholds.

4. Additional advantage of the new chromophore is large Stokes shift; **Cy-Red** has Stokes shift of 163 nm, while **nano-Cy-Red** has even larger Stokes shift of 174 nm, indicating the formation of J-type molecular aggregates.

Stokes shifts of most traditional dyes such as fluorescein, polymethinecyanine and rhodamine are about/less than 25 nm.^{19e} The chromophore *CellTracker Red* (by Molecular Probes™), with properties similar to **nano-Cy-Red**, has a Stokes shift of approximately 50 nm. A large Stokes shift such as that observed for **nano-Cy-Red** is advantageous for quantitative determination and bioimaging. This quality would also provide high resolution and low detection limits^{19a-d} in intracellular fluorescence imaging. All above facts indicate that **Cy-Red** fluorophore could be useful dye in any physical state (solution state or solid state, *e.g.* in form of **nano-Cy-Red**) for biological imaging applications.

3.5. Morphology and Stability Studies:

In order to investigate the morphology and size of **nano-Cy-Red** formed in DMSO/H₂O (2:98), SEM and AFM investigations were performed. For the SEM and AFM studies the sample was prepared using reprecipitation method, followed by drop-casting a solution containing **nano-Cy-Red** on silica substrate. SEM micrographs of **nano-Cy-Red** in DMSO/H₂O revealed their narrow distribution (**Figure 7a** and **b**), and size in range of 280-340 nm. AFM was also utilized to estimate the size of nanoparticles and their distribution. Topographical analysis of non-contact mode AFM images of the **nano-Cy-Red** nanoparticles showed the average diameter of ca. 500 nm and height in the range of approximately 50-80 nm (**Figure 7c** and **d**).

Investigation of potential aggregation of **nano-Cy-Red** in aqueous solution was performed using DLS. The study was done both in DMSO/H₂O (2:98) and in the solution DMSO/DMEM-FBS (2:98) which is used for biological studies: An average diameter of the nanoparticles (**Figure 8a**) in water solution immediately after precipitation is ca. 300 nm (average hydrodynamic radius is 164 nm), however after 3h larger population of particles with a larger size was observed as result of formation of the aggregates, an average diameter of nanoparticles in this case is ca. 500 nm (average hydrodynamic radius is 253 nm). At the same time, nanoparticles prepared directly in DMEM-FBS media used for our biological studies were slightly smaller

and no significant aggregation was observed even after 3 h of incubation at room temperature (**Figure 8b**). This might be due to presence of supplementation components (vitamins, glucose, amino acids and fetal bovine serum) in media, which are probably acting as capping agents thereby stabilizing nanoparticles and thus preventing aggregation for a longer time. The size of the described nanoparticles is small enough to penetrate into cells or whole organisms. Additionally, we performed Tyndal scattering experiment for solutions containing **Cy-Red** in both 100% DMSO and 2% DMSO solutions. Importantly, pronounced scattering was observed in 2% DMSO solution, whereas in 100% DMSO no scattering was displayed (**Figure 9**). This indicates formation of solution stable **nano-Cy-Red**. For farther investigation of solution stable **nano-Cy-Red**, we performed ^1H NMR titration studies of **Cy-Red** in DMSO- d_6 /D $_2$ O solutions (**Figure 10**), which showed an up-field chemical shift of the C_{triazole}-H aromatic protons (8.66, 8.53, 8.48 and 8.41 ppm for 0, 10, 20 and 30% addition of D $_2$ O to DMSO- d_6 solutions, respectively), as well as C6_{cytosine}-H and C5_{cytosine}-H. These observations support the theory of aggregation of **Cy-Red** molecules through supramolecular interactions and formation of solution-stable nanoparticles.

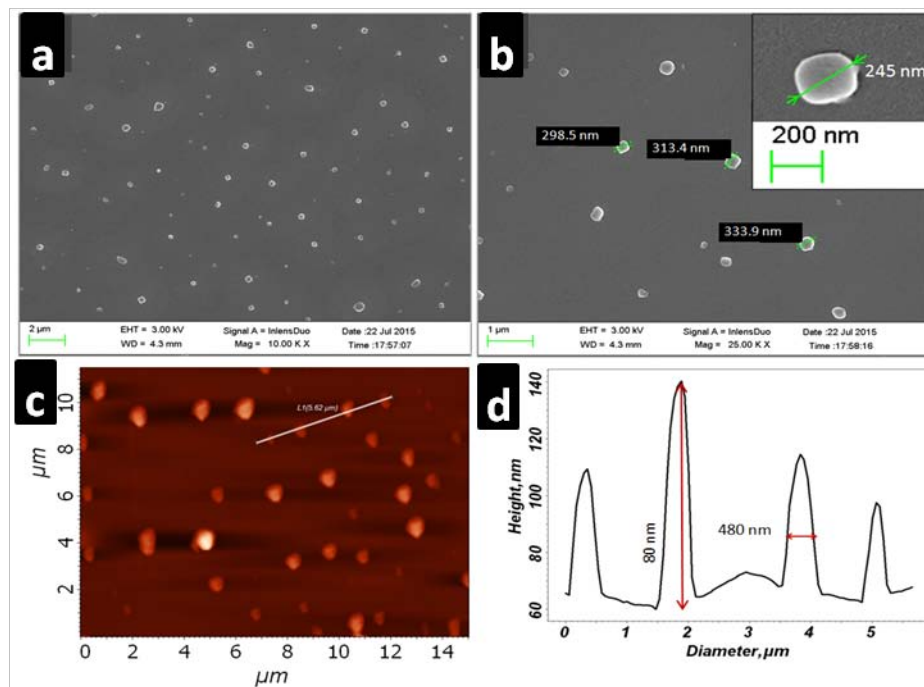


Figure 7: SEM micrographs of **Cy-Red** nanoparticles obtained from (a) DMSO and (b) DMSO/water (98%) (scale bar is 5 μm); (c) non-contact mode AFM image of **Cy-Red** nanoparticles; (d) height and length profile of selected nanoparticles shown in (C) as a white line

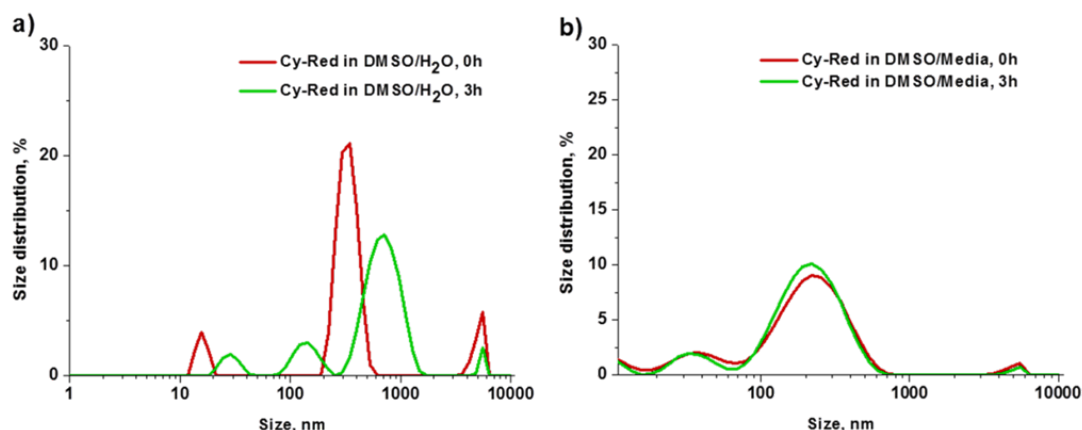


Figure 8: Size (hydrodynamic diameter) distribution of **nano-Cy-Red** in solutions of a) 2% DMSO/H₂O and b) 2% DMSO/DMEM-FBS media immediately and after 3 h obtained by DLS technique

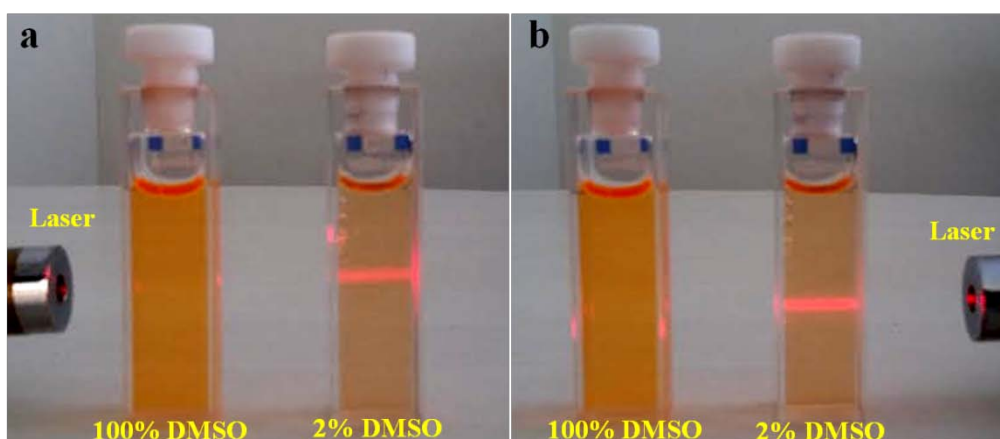


Figure 9: Tyndal effect observed as result of nanoparticles formation in 2% DMSO at 10⁻⁵ M, a) laser irradiation from left hand side and b) from right hand side

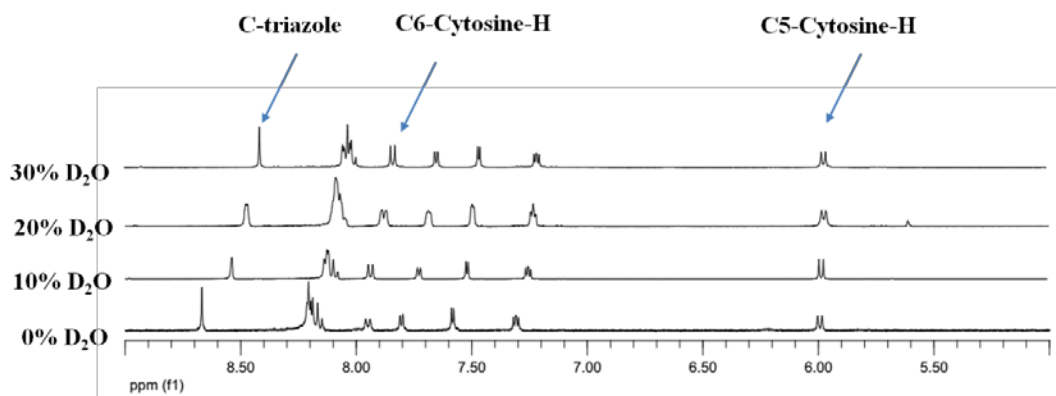


Figure 10: Stack ¹H NMR spectra of **Cy-Red** in DMSO-*d*₆ alone and upon gradual increase of D₂O (0, 10, 20 and 30% respectively)

3.6. Application of Cy-Red FONs for Bioimaging:

3.6.1. Toxicity Studies of Nano-Cy-Red and compound 3.4:

Before performing bioimaging experiments, the potential toxic effects of novel chromophores were investigated. Along with **nano-Cy-Red**, its well-soluble Boc-protected precursor **3.4** was also subjected to the study. Toxicity studies were performed using zebrafish embryos as model organism. Zebrafish are particularly attractive, because of their ease of maintenance, cost-effectiveness, low compound requirement and the advantage of being a whole organism, could well be utilized for evaluation of novel compounds toxicity in large scale.²⁰ Zebrafish embryos (24 hours post fertilization) treated with 10 μ M solution of **3.4** showed morphological abnormalities (edema, craniofacial defects and tail defects) after 24 - 48 h of exposure (**Figure 11**).

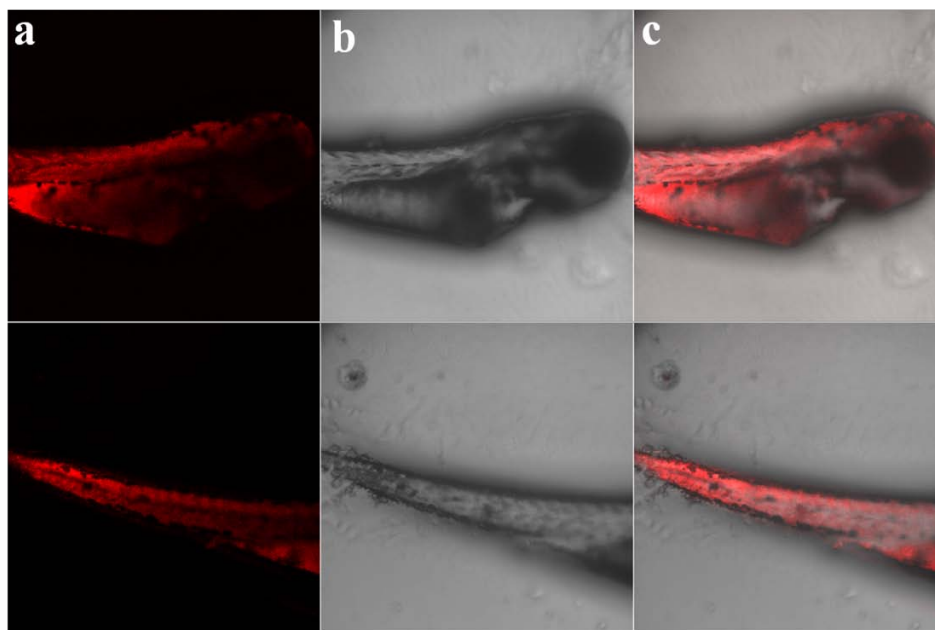


Figure 11: Confocal fluorescence microscopy images ($\lambda_{\text{ex}}=473$ nm) of zebrafish embryos (24 hpf) after treatment with compound **3.4** at 10 μ M for 24 h: a) fluorescence light image; b) transmitted light image; c) overlaid fluorescence and transmitted light images. The images were taken under Texas Red channel.

Unlike precursor compound **3.4**, **nano-Cy-Red** did not affect embryos development and vitality up to 96 h and was found to be non-toxic for live organisms and safe to be used for any biological experiments. Confocal fluorescent microscopy images were taken under Texas Red channel and show unaffected embryos exhibiting red fluorescence after treatment (**Figure 12**). **Nano-Cy-Red** displayed no specificity

towards any tissues and was distributed almost equally all over the body including zebrafish brain.

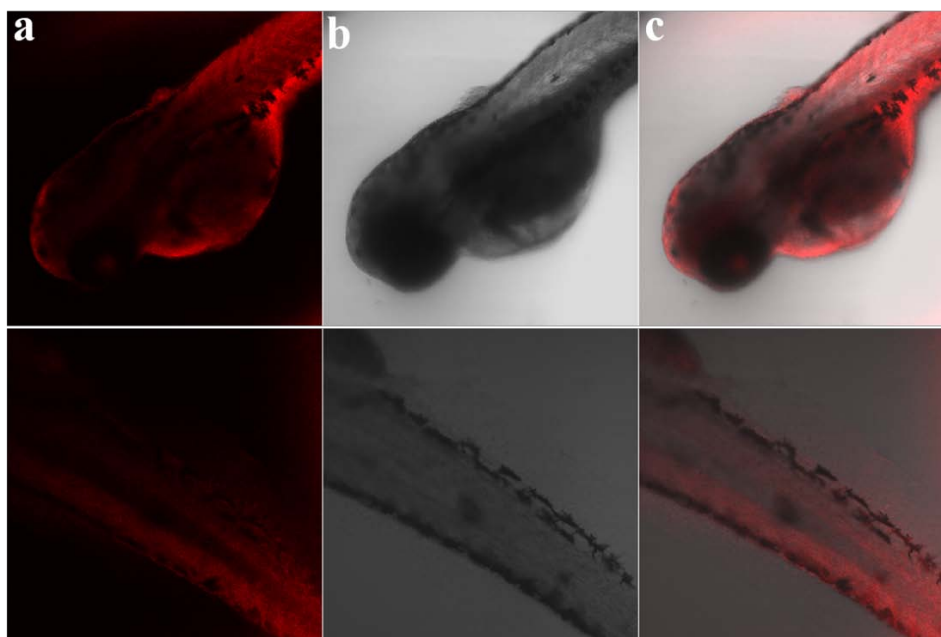


Figure 12: Confocal fluorescence microscopy images ($\lambda_{\text{ex}}=473$ nm) of zebrafish embryos (24 hpf) after treatment with compound **Cy-Red** at 50 μM for 72 h: a) fluorescence light image; b) transmitted light image; c) overlaid fluorescence and transmitted light images. The images were taken under Texas Red channel.

3.6.2. DNA Binding Study:

Keeping in mind that cytosine is one of the DNA and RNA bases, it was presumed that such non-specific distribution of **Cy-Red** in the organism may be the result of binding to DNA/RNA by cytosine unit. To test this theory DNA binding experiment was performed using Ethidium bromide as a reference fluorescent dye. **Figure 13** shows photographs of gel electrophoresis of plasmid and linear DNA stained with both Ethidium bromide and **nano-Cy-Red**. Although **nano-Cy-Red** imparted background colour, it is very clear that the compound do bind to both plasmid DNA and linear DNA as good as the reference compound.

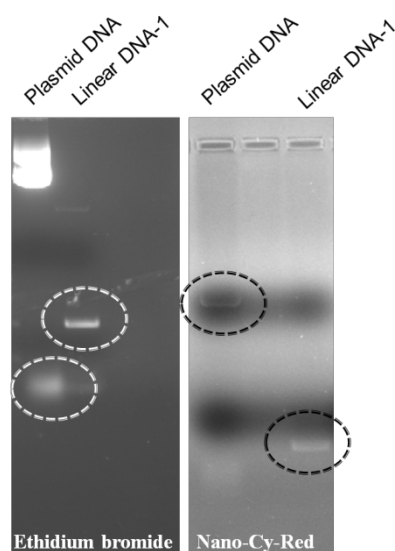


Figure 13: DNA binding study using Agarose gel electrophoresis

3.6.3. Mouse Macrophage (RAW264.7), Human Oral Cancer (Cal 27) and Metastatic Breast Cancer (MDAMB-231) Cells Staining:

Further, if **nano-Cy-Red** is able to bind to the DNA, it suppose to selectively stain only cell's nucleus but not cytoplasm. To test it, mouse macrophage cells (RAW 264.7) were incubated with **nano-Cy-Red** (10 μ M) for 30 min, 90 min and 3 h. Additionally cells were co-stained with 4',6-diamidino-2-phenylindole (DAPI) which is known to be a specific fluorescent DNA probe and exhibit enhanced fluorescence exclusively in nucleus. Surprisingly the majority of red fluorescence was observed only in cytoplasm instead of nucleus. **Figure 14** shows confocal fluorescence microscopy images of treated cells and control cells (treated only with DAPI). The difference between red illuminated cytoplasm and blue illuminated nucleus is particularly clear on merged images collected through DAPI and Texas-red channels. Likewise to zebrafish embryos, **nano-Cy-Red** did not cause major cytotoxicity in mouse macrophage cells (**Figure A1**, see page no 106).

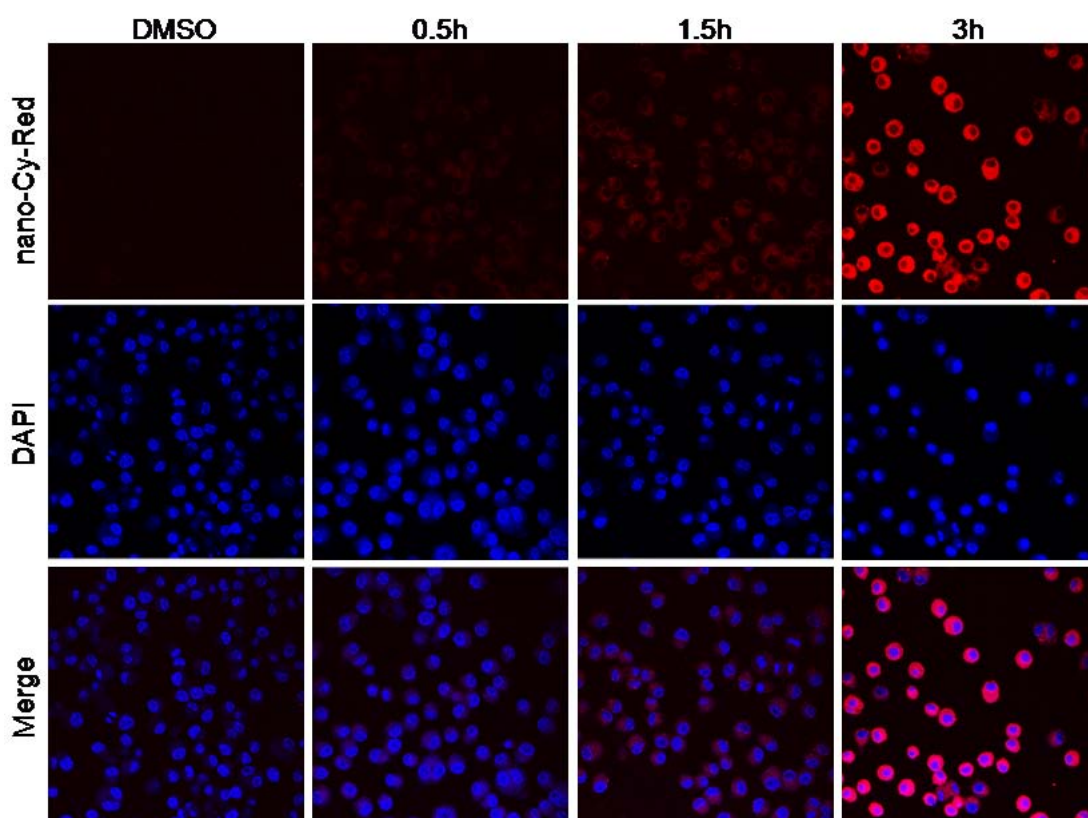


Figure 14: Confocal fluorescent microscopy images ($\lambda_{\text{ex}}=473$ nm) of mouse macrophage cells treated with: a) **nano-Cy-Red**, b) DAPI and c) co-stained with both **nano-Cy-Red** and DAPI at 10 μ M for 30 min, 90 min and 180 min

Similarly, treatment of human oral cancer cells (Cal 27 Human oral adenosquamous carcinoma cells) for 3h with **nano-Cy-Red** (10 μ M) resulted staining in only cytoplasm and no significant amount of red fluorescence was observed in nucleus (**Figure 15**). In order to check retention of **nano-Cy-Red** in cells after treatment, cells were treated with **nano-Cy-Red** with the final concentration of 10 μ M and 0.4% DMSO for 3 h at 37 $^{\circ}$ C. Cells were subsequently washed twice with 1X PBS. Retention of dye in cells was investigated after 6 h and 24 h post wash and found that **nano-Cy-Red** stayed in the cytoplasm of cells at both time points tested. Moreover fluorescence emission intensity remained largely unaltered (**Figure 15**).

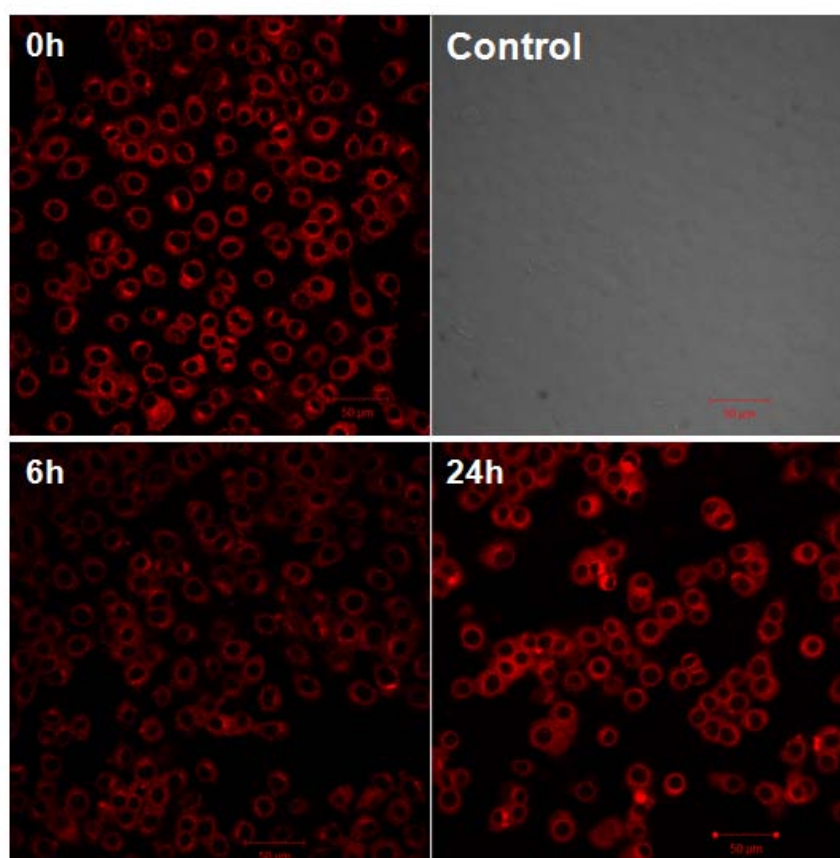


Figure 15: Confocal fluorescent microscope images of oral cancer cells treated with **nano-Cy-Red** for 3h, followed by wash and incubation in fresh medium without addition of **nano-Cy-Red** for 24h. The images were acquired under Texas Red channel ($\lambda_{\text{ex}} = 473\text{nm}$).

Similar effect was observed with MDAMB-231 (human metastatic breast cancer) cells loaded with **nano-Cy-Red** with the final concentration of 10 μ M and 0.4% DMSO for 3 h at 37 $^{\circ}$ C. Cells were subsequently washed twice with 1X PBS. Retention of dye in cells after 6 h, 24 h, 36 h, 48 h and 72 h post wash and it was

found that **nano-Cy-Red** was retained in cytoplasm of cells at all the time point tested. Moreover fluorescence emission intensity also remained largely unaltered (**Figure 16**). In addition, the **nano-Cy-Red** stained cells were analyzed by flow cytometry, which confirmed that majority of the cells were stained by the dye expanding its utility to study the cells by different methods (**Figure A2**, see page no **106**). Additional quality of this novel chromophore **nano-Cy-Red** is its retention in living cells through several generations and it is comparable with the Cell TrackerTM dye. However **nano-Cy-Red** has 3.5 times larger Stokes shift in comparison (174 nm vs 50 nm) with Cell TrackerTM. A large Stokes shift such as that observed for **nano-Cy-Red** is advantageous for quantitative determination and bioimaging. One of the proposed applications, arising from this property is tracking of transplanted cancer (or any other) stained cells in live animals (e.g. zebrafish or frog).

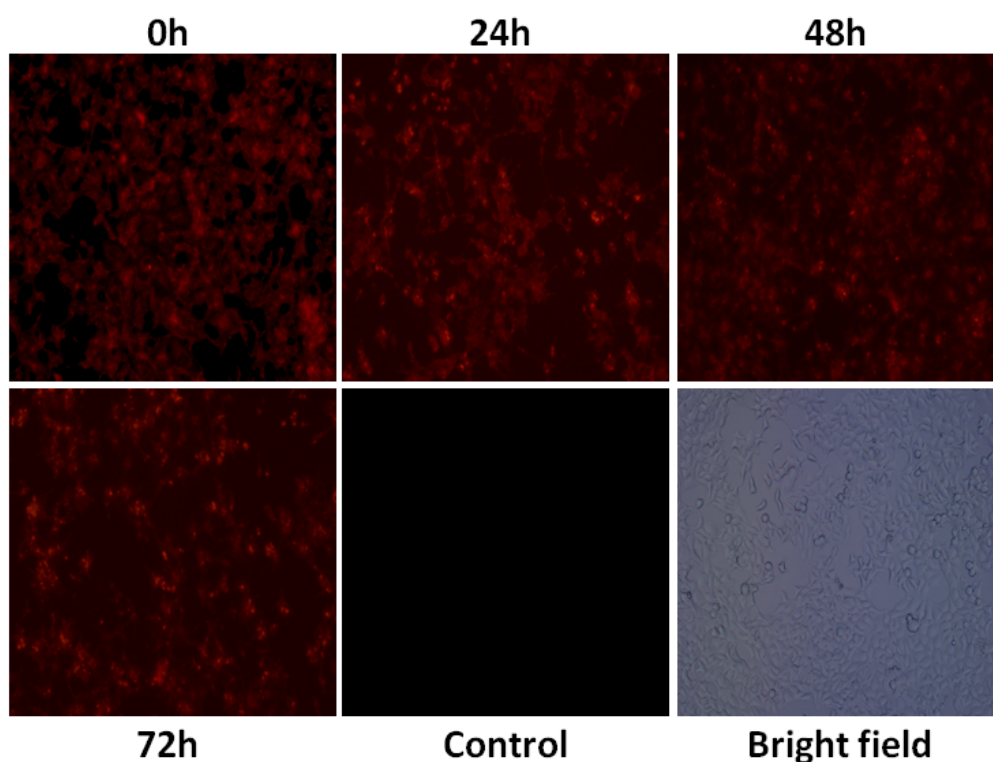


Figure 16: Fluorescent microscope images of MDAMB-231 cells treated with **nano-Cy-Red** for 3 h, followed by wash and incubation in fresh medium without addition of **nano-Cy-Red** for different time points.

3.6.4. Tracking Transplanted Cells in Live Animal:

Finally, an applicability of **nano-Cy-Red** treated cancer cells for tracking *in vivo* in real time was tested. For this, MDAMB-231 cancer cells were stained with **nano-Cy-Red** for 3 h as described above and injected into zebrafish embryos (3 dpf),

which were anesthetized with Tricaine and placed on an agarose mould. The cells were slowly injected into the yolk region of 3 dpf embryos by using electronically regulated microinjector. After injection, embryos were moved back into E3 medium and observed for microinjection positives. **Figure 17** shows fluorescent microscopy images of zebrafish embryos after injection of **nano-Cy-Red** stained cancer cells on the day of injection (day 1), day 2 and day 4. Up to day 3 stained cells were mostly observed in region of injection (yolk) and had bright fluorescence, migration of cells from yolk to tail region was observed on day 4, when stained cells moved from yolk to tail region.

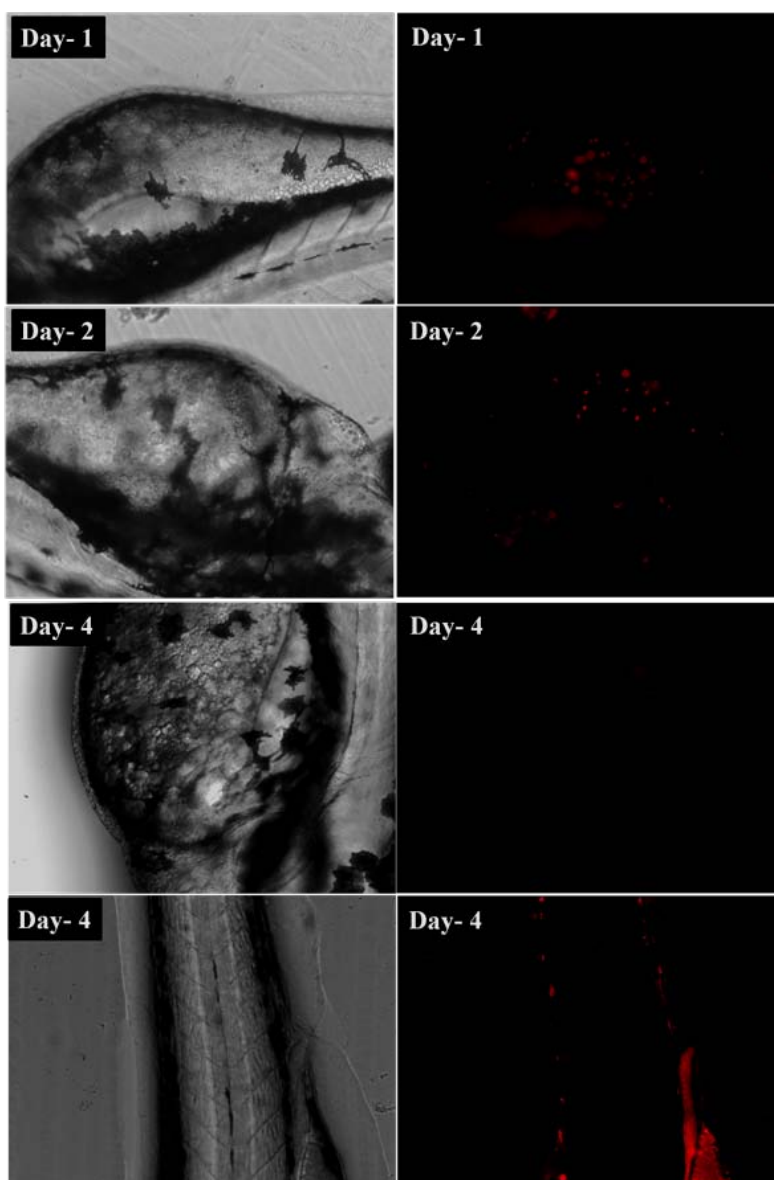


Figure 17: Fluorescent microscopy images of cancer cells stained with **nano-Cy-Red** and injected into zebrafish embryos. Observations were made on 0 hpi, 24 hpi and 72 hpi. The images were taken under Texas red channel

It is possible that a fraction of the dye may have leaked out of the cells diffusing through the embryo. However, since concentrated foci of **nano-Cy-Red** signal was observed anticipated in the tail region of zebrafish embryo^{21a} (when injected as stained cells) and considering that **nano-Cy-Red** displayed no specificity towards any tissues and was distributed almost equally all over the body including zebrafish brain when injected alone (**Figure 12**). Therefore a major portion of the signal is emanating from the **nano-Cy-Red** stained intact MDAMB-231 cells. However, further studies are needed to refine this application. Nevertheless, it is worth noting, that intracellular nanoparticles exhibited very bright red fluorescent emission, which was well detectable even with common fluorescent microscope. The possibility to perform imaging with help of common fluorescent microscopy, avoiding or minimizing usage of the confocal microscopy, which is not always available is one of the advantages of the novel **nano-Cy-Red** stain. As an example, **Figure A3** (see page no 107) display fluorescent microscope images of zebrafish embryos immediately (0 h) and after 24 h post injection of cancer cells treated with **nano-Cy-Red**.

3.6.5. Yeast Staining:

High degree of conservation in cellular processes between yeast and humans, combined with simple growth requirements, rapid cell division, ease of genetic manipulation of yeast, promoted its extensive use as a model organism in genetics and cell biology.²⁴ In order to examine an ability of **nano-Cy-Red** to penetrate and stain fission yeast, the unicellular, rod shaped fission yeast was utilized as a model. For that, fission yeast cells were grown overnight in the presence or absence of **nano-Cy-Red** (25 μ M) for 24 h. Additionally yeast cells were co-stained with DNA stain DAPI. The cells were then checked under confocal fluorescence microscope at excitation of 473 nm. Notably, although yeast is known to have cell wall which is not permeable to majority of organic compounds, **nano-Cy-Red** was able to cross it and stain whole cell (**Figure 18**), except for a fraction of cells where the middle part was not stained. Since **nano-Cy-Red** was exclusively absent in the center of cells, it was hypothesized that it binds all cellular components except septum. In fission yeast a medially placed septum or cell wall is usually formed towards the end of cell division. The septum separates the mother cell from daughter cell. Quantification of percentage of mitotic cells (septation index) is a very helpful application in yeast studies. Septation index is used for checking progression through cell cycle, testing efficiency

of cell synchronization as well as unveiling the functions of various genes and their role in cell division.²⁵ Traditionally, Calcofluor stain is used to stain chitin in the septum of live and fixed cells and is visualized under UV light. Therefore, to test whether **nano-Cy-Red** is excluded from septum, fission yeast cells were dually stained with Calcofluor and **nano-Cy-Red** and visualized under UV (355nm) light and 473 nm for Calcofluor and **nano-Cy-Red** respectively. Results, shown in **Figure 19**, demonstrate that **nano-Cy-Red** is excluded from the location stained by Calcofluor, indicating that it stains whole yeast cells including mitotic cells, but is specifically excluded from septum which is stained by Calcofluor. We propose staining with **nano-Cy-Red** as efficient and accurate method of quantification of mitotic cells which can be used in conjunction with or as an alternative to commonly used cell wall stains (e.g. Calcofluor White, Sigma). One of the advantages of the **nano-Cy-Red** is that it does not bleach as quickly as Calcofluor and the quantification is quite easy.

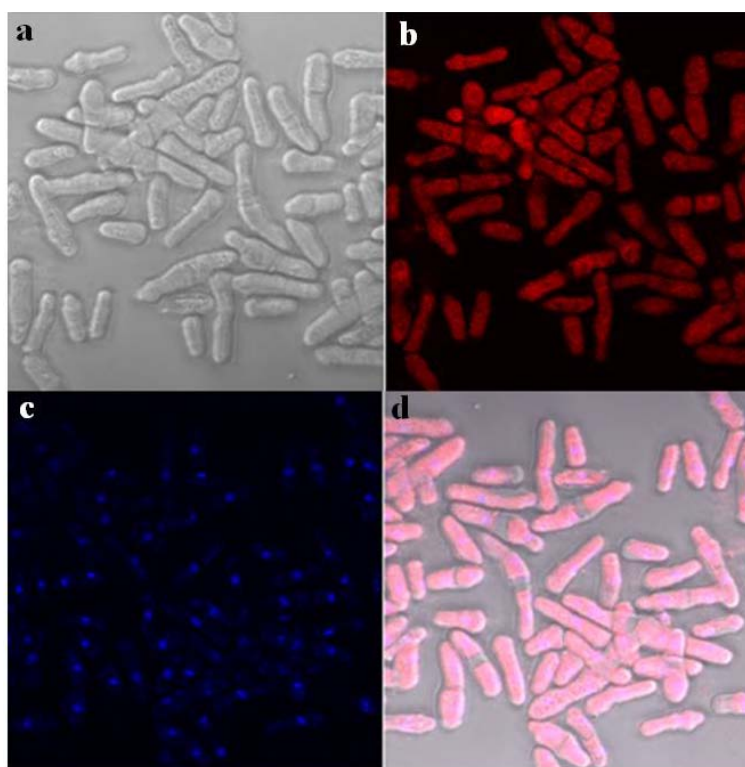


Figure 18: Confocal fluorescent microscopy images ($\lambda_{\text{ex}}=473$ nm) of yeast cells treated with **nano-Cy-Red** and DAPI (25 μM , 24 h treatment); a) transmitted light image, b) fluorescent image of **nano-Cy-Red** treated yeast cells, c) fluorescent image of DAPI treated yeast cells and d) overlaid fluorescence and transmitted light images of b and c. The images were taken under DAPI and Texas-red channel

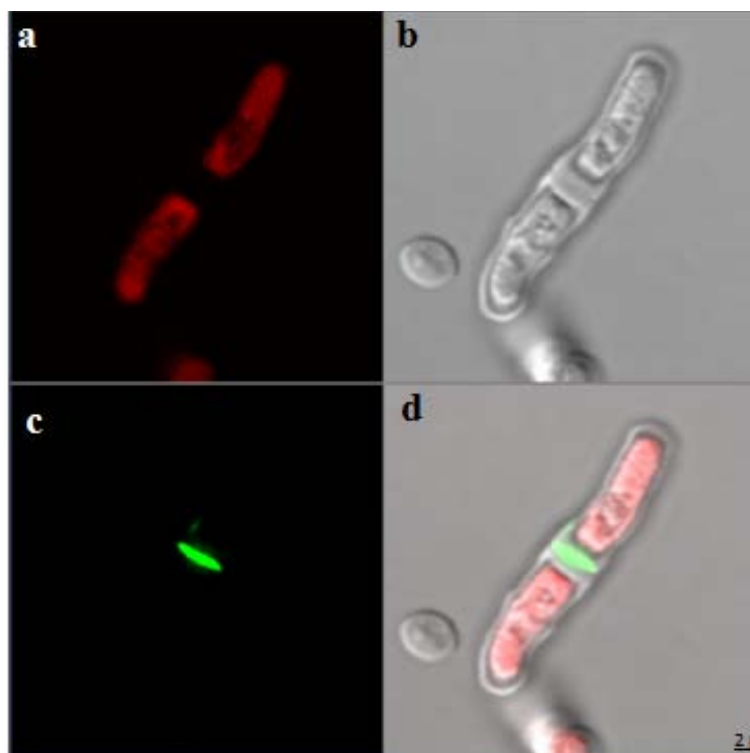


Figure 19: Confocal fluorescent microscopy images ($\lambda_{\text{ex}}=473$ nm) of yeast cells treated with; a) **nano-Cy-Red**, b) transmitted light image and c) Calcofluor White, Sigma and d) co-staining of both **nano-Cy-Red** and Calcofluor White, Sigma at 25 μM for 24 h. The images were taken under GFP and Texas-red filters

This novel dye may also be used to track pathogenic yeast strains to study mechanism of pathogenesis such as rate of clearance of pathogenic yeast cells by host immune system. This property can be utilised to develop a negative stain for yeast septum which can be replacement or complementary to currently used cell wall stain (e.g. Calcofluor White, Sigma).

3.7. Conclusions:

In conclusion, this chapter presents a novel biocompatible and non-toxic red FONs (**nano-Cy-Red**) and shows its utility for a broad range of applications, including real life, long-term *in vitro/in vivo* imaging. **Nano-Cy-Red** was prepared from the novel chromophore **Cy-Red**. **Cy-Red**, containing cytosine moiety connected to the fluorescent tag (4,7-di(thiophene-2-yl) benzo[c][1,2,5]thiadiazole) by 12-carbons aliphatic chain, was synthesized through simple and straight forward route, using click-chemistry approach. Nanonization of the almost insoluble chromophore (**Cy-Red**) helped to convert it into FONs (**nano-Cy-Red**), soluble in water up to 150

μM without precipitation and exhibiting bright fluorescence emission. Photophysical properties and surface morphology of **nano-Cy-Red** were investigated and also presented in this work. Exceptional photostability and particularly large Stokes shift are among certain advantages of this novel chromophore. The ability of **nano-Cy-Red** to penetrate into mouse macrophage cells, oral cancer cells and yeast was demonstrated in this chapter as well. **Nano-Cy-Red** FONs were exploited as cytoplasmic stain for cells, while in case of yeast **nano-Cy-Red** was acting as negative septum stain, ensuring better monitoring of yeast cells division with high quality clear images. An important property of the chromophore described here is its retention in living cells for several generations without significant loss of fluorescence. Taking advantage of this feature, **nano-Cy-Red** dye was exploited for direct *in vivo* visualization of cancer cell migration upto 72 h post transplantation in zebrafish embryos with help of confocal microscope. As illustrated in this work, cells stained with **nano-Cy-Red** were clearly observed using both GFP and Texas Red filters, which is definite advantage if the object of study exhibits auto fluorescence. Potential applications arising from the properties of **nano-Cy-Red** are xenotransplantation of human cancer cells and tracking them in real time, cytoplasmic stain for different types of cells, and negative septum stain for quantification of mitotic yeast cells. As this chapter demonstrates, novel chromophore **nano-Cy-Red** is a particularly useful addition to the family of organic fluorescent nanoparticles and may serve as a convenient tool helping to light up biological processes both *in vitro* and *in vivo*.

3.8. Experimental Section:

3.8.1. Materials and Methods:

The materials cytosine, 1,12-dibromododecane, 2,1,3-benzothiadiazole, thiophene, tributyltin chloride, bis(triphenylphosphine)palladium(II) dichloride, Calcofluor white and paraformaldehyde were purchased from Sigma Aldrich. Tertiary butyloxy carbonyl (Boc) anhydride, N,N-dimethyl-4-aminopyridine, copper(I) iodide, acetic anhydride were purchased from Spectro Chem. Commercial reagents (NaN_3 , ammonium bicarbonate, and HCl) were purchased from Merck and Rankem and were used as received. All solvents were distilled and dried before reactions and for extracting purposes. All reactions were carried out under an inert atmosphere with dry

solvents, unless otherwise stated. Syringes and needles for the transfer of reagents were dried at 100 °C and allowed to cool in a desiccator over P₂O₅ before use. Reactions were monitored by thin layer chromatography (TLC) on silica gel plates (60 F254), using UV light detection. Merck silica gel (particle size 100-200 mesh) was used for column chromatography. For UV-Vis and fluorescence measurements spectroscopic grade solvents were used.

3.8.2. Improvement of Cy-Red Solubility:

3.8.2.1. Salt Formation Using Hydrobromic Acid:

Cy-Red (0.04 g, 0.06 mmol) and 48% hydrobromic acid (3 mL) were heated at 110 °C for 12 h using seal tube. After 12 h, precipitate was filtered and solubility was analysed.

3.8.2.2. Complexation with Citric Acid:

Equal volumes of **Cy-Red** and citric acid from 2.5 mM stock solutions were mixed and stirred for 30 min at room temperature. From above mentioned mixture the solutions were prepared with final concentration of 50 µM, 100 µM, and 150 µM in 3 mL H₂O, fluorescence emission intensities were measured at $\lambda_{\text{ex}} = 473 \text{ nm}$

3.8.3. Nanoparticles Preparation for Biological Studies:

0.8 mg of compound **Cy-Red** was taken in a sample vial and dissolved in 0.5 mL of DMSO. Then 60 µL of the solution was rapidly injected to 2.94 mL of millipore water to obtain the final concentration of nanoparticles 50 µM in 2% DMSO. Prepared nanoparticles were used for the photo-physical and fluorescent imaging studies immediately.

3.8.4. Nanoparticles Preparation for SEM and AFM Studies:

0.8 mg of compound **Cy-Red** was dissolved in 0.5 mL of DMSO. Then 60 µL of the solution was rapidly injected to into 2.94 mL of millipore water to obtain the final concentration of nanoparticles 50 µM in 2% DMSO, and the sample vial was left for 0.5 h without disturbing. Prepared nanoparticles were dispersed on a clean glass slide by a capillary for SEM and AFM studies.

3.8.5. Nanoparticles Stability by Dynamic Light Scattering Studies:

The size of the aggregates was determined by dynamic light scattering technique using a Malvern Zeta size Instrument (NanoZS90, Malvern, U.K.). The laser light source (He–Ne) has a single wavelength of 633 nm and the detector was Avalanche photodiode. For the aggregation experiment, 0.8 mg of compound Cy-Red was taken in a sample vial and dissolved in 0.5 mL of DMSO. Then 60 μ L of the solution was rapidly injected to 3 mL of millipore water/DMEM medium to obtain the final concentration of nanoparticles 50 μ M in 2% DMSO. Before measurement, the scattered cell (DTS1060) was rinsed with biocompatible solution and equilibrated for 180 s in the system. The measurement was carried at 25 °C with a scattering angle of 90°.

3.8.6. Nanoparticles Exposure to Yeast Cells:

3.8.6.1. Nano-Cy-Red and Calcofluor Staining:

A wild type *S. pombe* strain LPY3279 (genotype: h-ade6-210 arg3-D4 his3-D1 leu1-32 ura4-D18) was grown in liquid YES media (yeast extract plus supplements) at 32 °C in the absence or presence of 25 μ M of **nano-Cy-Red** to an optical density OD₆₀₀=1. One mL of a culture of *S. pombe* cells was pelleted down and washed with 1mL PBS and resuspended in 20 μ L of PBS. Equal amount of Calcofluor white solution and 10% KOH is added and incubated for 1 min. The cells are washed with PBS and re-suspended in 20 μ L of PBS. Cells were then visualized under confocal microscope under UV light and at excitation wavelength 473 nm, respectively.

3.8.6.2. Nano-Cy-Red and DAPI Staining:

S. pombe strain ROP191 is grown in YES media at 32°C. 10 mL of culture in the absence or presence of 25 μ M of **nano-Cy-Red** is grown to an optical density OD₆₀₀=1. One mL of a culture of *S. pombe* cells was pelleted down and washed with 1mL PBS. Cells were fixed in 1 mL of 30% methanol/70% acetone for 20 min at -20°C. Cells were rehydrated with 5 min washes in 75, 50, and 25% methanol in PBS. Cells were then re-suspended in 20 μ L of PBS. Equal amount of 0.5 μ g/mL of DAPI was added to cells and incubated for 5 min, the cells were then washed with 100 μ L of PBS and resuspended in 20 μ L of PBS. 5 μ L of cells were taken and checked under confocal microscope at excitation wavelength 473 nm for **nano-Cy-Red** staining and UV range for DAPI staining.

3.8.7. Nanoparticles Exposure to Mouse Macrophage Cells:

The mouse macrophage cells (RAW 264.7) were seeded on cover slips in 6-well plates, in DMEM (Dulbecco's modified Eagle's medium) supplemented with 10% FBS (Fetal Bovine Serum) and 1% antibiotics (Penicillin-Streptomycin) and allowed to adhere overnight. Next day, cells were either treated with 0.4% DMSO (vehicle control) or 10 μ M **nano-Cy-Red**, and incubated at 37 °C, 5% CO₂ for different time points (30 min, 90 min and 180 min). Post incubation, cells were washed with 1X PBS (Phosphate-buffered Saline), fixed, stained with DAPI to visualize nuclei and mounted on a glass slide for confocal microscopy analysis.

3.8.8. Nanoparticles Exposure to Oral Cancer Cells:

The oral cancer cells (Cal-27) were cultured in DMEM supplemented with 10% FBS and antibiotics (Penicillin-Streptomycin) and allowed to adhere overnight. Next day, cells were both treated with 0.4% DMSO (vehicle control) or 10 μ M **nano-Cy-Red** and incubated at 37 °C, 5% CO₂ for 30 minutes. Post incubation the cells were washed with 1X PBS, fixed, stained with DAPI and mounted on to glass slide for confocal fluorescent microscopy analysis.

3.8.9. Nanoparticles Exposure to Metastatic Breast Cancer Cells:

The metastatic breast cancer cells (MDAMB-231) were cultured in DMEM supplemented with 10% FBS and antibiotics (Penicillin-Streptomycin) and were either treated with 0.4% DMSO (vehicle control) or 10 μ M **nano-Cy-Red** and, incubated at 37 °C, 5% CO₂ for 3 h. Post incubation the cells were washed with 1xPBS and bioavailability of the loaded **nano-Cy-Red** for different time points (24, 48 and 72 h) was monitored under microscope.

3.8.10. Nanoparticles Exposure to Zebrafish Embryos:

At 24 hours postfertilization (hpf), embryos were dechlorinated using 50 μ g/mL Proteinase-K (Sigma-Aldrich) for 5 minutes. All embryos were immersed (6 embryos/well) into 24 well culture plates containing 500 μ L of **3.4** or **nano-Cy-Red** at different concentrations (50 μ M, 5 μ M, 500 nM, 50 nM, 5 nM) for treatment. Control embryos were incubated in 2% DMSO. The complete study was carried out for 24, 48, 72, and 96 h. On the respective time points the embryos were washed with 1X PBS thrice for 5 min each and fixed in 4% paraformaldehyde in PBS, pH 7.0 for 4 h

at room temperature. Then embryos were used for fluorescent observations under confocal fluorescence or optical fluorescence microscope.

3.8.11. Nano-Cy-Red in Tracking Cancer Cells Using Zebrafish as a Model Organism:

The xenotransplantation of cancer cells was carried out as per a previously described protocol. The microinjections in zebrafish embryos were conducted by using Eppendorf FemtoJet[®]. MDAMB-231 cells, stained with **nano-Cy-Red** as described above, or cancer cells over-expressing GFP were micro-injected into 3 dpf (days post fertilization) zebrafish embryos. For that, cells were loaded into microinjection needle. The needle was inserted into micromanipulator and the position for injection was adjusted. The Eppendorf FemtoJet[®] express and the InjectMan parameters were calibrated by adjusting injection pressure (pi), time of injection (ti) and compression pressure (pc), injection pressure of 280 and injection time of 0.4 and compression pressure of 5 were set after calibration and found to inject a volume of 8 μ L of cells. One day post fertilized (24 hpf) embryos were transferred onto microinjection mould and were aligned in rows by using fine forceps and the excess medium was removed using pipette. The calibrated volume was injected into each embryo into the yolk and the volume of microinjection was maintained constant for all the larvae injected. After injection, embryos were transferred into E3 medium and observed for microinjection positives. Cells were tracked under fluorescent microscope at 24 hours post injection (hpi), 48 hpi and 72 hpi and their respective fluorescent images of zebrafish embryos injected with **nano-Cy-Red** stained cancer cells were captured and analyzed.

3.8.12. Differentiation of Cell Nature Using Flow Cytometry:

The metastatic breast cancer cells (MDAMB-231) were cultured in DMEM (Dulbecco's modified Eagle's medium) supplemented with 10% FBS (Fetal Bovine Serum) and antibiotics (Penicillin-Streptomycin) and were either treated with 0.4% DMSO (vehicle control) or 10 μ M **nano-Cy-Red** and incubated at 37 °C, 5% CO₂ for 1 h. The cells **nano-Cy-Red** loaded MDAMB-231 or **nano-Cy-Red** unloaded MDAMB-231 cells were prepared and analysed by flow cytometry analysis.

3.8.13. Preparation of Red Fluorescent Tag:

4,7-dibromobenzo[c][1,2,5]thiadiazole (1.2):¹²

To a 500 mL two-necked round-bottomed flask were added benzothiadiazole **1.1** (7.0 g, 51.4 mmol) and HBr (100 mL, 48%). A solution containing Br₂ (24.2 g, 154.2 mmol) in HBr (150 mL) was added dropwise very slowly. After the total addition of Br₂, the solution was heated at reflux for 6 h. Precipitation of a dark orange solid was noted. The mixture was cooled to room temperature and a sufficient amount of a saturated solution of NaHSO₃ was added to completely consume any excess Br₂. The mixture was filtered under vacuum and washed exhaustively with water. The solid was then washed once with cold Et₂O and dried under vacuum to afford dibrominated product **1.2** in 92% yield (13.85 g, 47.28 mmol). Spectroscopic data matches with the one from the reported procedure. ¹H NMR (CDCl₃, 400 MHz) δ : 7.73 (2H, s).

Tributyl(2-thienyl)stannane (1.4):¹³

To a stirred solution of thiophene **1.3** (1 mL, 12.2 mmol) in dry THF (30 mL) was added n-butyl lithium (1.6 M in hexane, 5.5 mL, 8.72 mmol) at -78 °C. After 2 h at -78 °C, tributyl tin chloride (2.15 mL, 7.90 mmol) was added drop wise to the above reaction mixture. After stirring over 6 h at room temperature, the mixture was quenched with 20 mL of saturated aqueous NaHCO₃. The organic phase was dried with anhydrous sodium sulphate, concentrated under reduced pressure, and the resulting residue was used without further purification (2.9 g, 8 mmol). Spectroscopic data matches with the one from the reported procedure. ¹H NMR (CDCl₃, 400 MHz) δ : 7.64 (1H, s), 7.25 (1H, m), 7.18 (1H, dd), 1.54 (6H, t), 1.32 (6H, m), 1.09 (6H, m), 0.89 (9H, t).

4,7-di(thiophen-2-yl)benzo[c][1,2,5]thiadiazole (1.5):¹⁴

To a solution of 4,7- dibromobenzo-2,1,3-thiadiazole **1.2** (2.00 g, 10.20 mmol) in 50 mL of THF were added compound **1.4** (6.00 g, 24.48 mmol) and PdCl₂(PPh₃)₂ (180.0 mg, 2.00 mol%) under nitrogen atmosphere. After 3 h at reflux, the solvent was removed under reduced pressure, and the crude residue was then purified by column chromatography on silica gel with hexane/CH₂Cl₂ (1:1) as eluent to yield **1.5** as a red solid (1.5 g, 88%). Spectroscopic data matches with the one from the reported procedure. ¹H NMR (CDCl₃, 400 MHz) δ : 8.14 (2H, dd), 7.89 (2H, s), 7.48 (2H, dd), 7.23 (2H, dd).

4-(5-bromothiophen-2-yl)-7-(thiophen-2-yl)benzo[c][1,2,5]thiadiazole (1.6):^{15a}

To a solution of compound **1.5** (3.12 g, 10.4 mmol) in 50 mL of dichloromethane was added 50 mL of acetic acid. The mixture was shielded from light and cooled in an ice bath and N-bromosuccinimide (1.48 g, 8.32 mmol) was added stepwise. After 12 h, then the mixture was poured into aqueous saturated Na₂CO₃ solution. The aqueous layers were extracted with ethyl acetate. The combined organic extracts were washed with brine and dried over anhydrous MgSO₄. After removal of solvents under reduced pressure, the crude residue was purified by column chromatography on silica gel with hexane/CH₂Cl₂ (1:1) as eluent to yield **1.6** as a red solid (2.75 g, 70%). Spectroscopic data match with the one from the reported procedure. ¹H NMR (CDCl₃, 400 MHz) δ : 8.12 (1H, dd), 7.85 (1H, m), 7.80 (2H, m), 7.47 (1H, dd), 7.21(1H, dd), 7.15 (1H, d).

4-(5-ethynylthiophen-2-yl)-7-(thiophen-2-yl)benzo[c][1,2,5]thiadiazole (1.7):^{16,22}

Step-I: A mixture of compound **1.6** (1g, 2.7 mmol), $\text{PdCl}_2(\text{PPh}_3)_2$ (80 mg, 0.1 mmol), copper(I) iodide (22 mg, 0.2 mmol) in distilled triethylamine (20 mL) was de-oxygenated using nitrogen. Trimethylsilylacetylene (0.6 g, 6 mmol) was then added to the reaction mixture and was stirred while being heated at reflux for 12 h. The mixture was filtered, and the solvent was evaporated under reduced pressure to give a solid residue and the crude residue was then purified by column chromatography on silica gel with hexane/ CH_2Cl_2 (1:1) as eluent to yield silyl protected alkyne as a red solid (0.7 g, 65%). Spectroscopic data matches with the one from the reported procedure. ^1H NMR (CDCl_3 , 400 MHz,) δ : 8.13 (1H, dd), 7.95 (1H, d), 7.86 (2H, m), 7.47 (1H, dd), 7.31 (1H, d), 7.21 (1H, m), 0.27 (9H, s).

Step-II: The above red solid (0.7 g, 1.76 mmol) was dissolved in MeOH (10 mL) was degassed by bubbling nitrogen for 2 minutes and then K_2CO_3 (0.732 g, 3 mmol) was added under nitrogen atmosphere. The mixture was stirred at room temperature for 2 hours. After completion of reaction, the solvent was evaporated at reduced pressure and the residue was purified through column chromatography using hexane/DCM (8:2) as eluent to yield compound **1.7** as a red-orange solid (0.23 g, 96%). Spectroscopic data matches with the one from reported procedure. TLC (20% DCM in hexane): $R_f = 0.26$. ^1H NMR (CDCl_3 , 400 MHz) δ : 8.14 (1H, dd), 7.97 (1H, d), 7.88 (2H, m), 7.47 (1H, dd), 7.36 (1H, d), 7.22 (1H, m), 3.47 (1H, s). ^{13}C NMR (100 MHz, CDCl_3) δ : 147.0, 135.4, 133.7, 128.5, 122.7, 122.4, 122.1, 121.7, 121.4, 121.2, 120.5, 120.3, 120.1, 119.5, 117.7, 77.5. MS (EI, 70 *ev*): m/z $[\text{M}]^+$ calcd for $\text{C}_{16}\text{H}_8\text{N}_2\text{S}_3$: 324.4, found 324.5 $[\text{M}]^+$.

3.8.14. Cy-Red Synthesis (Route I; Scheme 2):

N-(2-oxo-1,2-dihydropyrimidin-4-yl)acetamide (2.2):²³

To a suspension of cytosine **2.1** (2.00 g, 18.0 mmol) in toluene (6 mL) at room temperature, pyridine (2.2 mL, 27.3 mmol) and DMAP (10 mg) were added. Acetic anhydride (2.17 g, 21.3 mmol) was diluted with toluene (3.5 mL) and added to reaction mixture slowly. The mixture was heated to 50-55 °C and stirred for 6 h until the reaction was complete. The reaction mixture was then cooled to room

temperature, filtered and washed once with toluene and twice with water. The residue was dried at 60-65 °C under reduced pressure to give compound **2.2** as a white solid (2.58 g 93%). Spectroscopic data matches with the one from the reported procedure. ¹H NMR (DMSO-*d*₆, 400 MHz) δ : 11.48 (1H, brs), 10.8 (1H, brs), 7.80 (1H, d), 7.09 (1H, d), 2.08 (3H, s).

N-(1-(12-Bromododecyl)-2-oxo-1,2-dihydropyrimidin-4-yl)acetamide (2.3):

NaH (0.235 g, 9.79 mmol) was added portion wise to compound **2.2** (1 g, 6.53 mmol) suspended in 15 mL DMF. After stirring at room temperature for 0.5 h, 1, 12-dibromododecane (19.59 mmol, 6.4 g) was added drop wise to this clear solution. The mixture was stirred at 40-50 °C for 24 h. After addition of 1 mL methanol, the solvents were evaporated, the crude residue was then purified using column chromatography on silica gel with DCM/EtOAc (1:1) as eluent to yield compound **2.3** as a white solid (1.33 g, 51%). Mp: 79-81 °C. TLC (50% DCM in EtOAc): R_f = 0.257. IR (KBr): 3321, 3140, 3061, 2923, 2853, 2185, 1991, 1719, 1691, 1662, 1624, 1557, 1511, 1432, 1379, 1305, 1246, 1178, 1001, 755, 666 cm⁻¹. ¹H NMR (DMSO-*d*₆, 400 MHz) δ : 10.7 (1H, s), 8.02 (1H, d), 7.1 (1H, d), 3.74 (2H, t), 3.49 (2H, t), 2.06 (3H, s), 1.75 (2H, m), 1.57 (2H, m), 1.26 (16H, m). ¹³C NMR (DMSO-*d*₆, 100 MHz) δ : 171.2, 162.6, 155.6, 150.5, 95.2, 49.9, 35.6, 32.6, 29.33, 29.31, 28.5, 27.9, 26.2, 24.7. MS (EI, 70 *ev*): *m/z* [M]⁺ calcd for C₁₈H₃₀BrN₃O₂: 399.9, found 399.9 [M]⁺. Anal. Calcd for C₁₈H₃₀BrN₃O₂: C, 54.0; H, 7.55; Br, 19.96; N, 10.50; O, 7.99; found: C, 54.12; H, 7.58; N, 10.45.

N-(1-(12-azidododecyl)-2-oxo-1,2-dihydropyrimidin-4-yl)acetamide (2.4):

Compound **2.3** (1.336 g, 3.35 mmol) and sodium azide (0.653 g, 10.05 mmol) were dissolved in DMF (10 mL) and were stirred at room temperature for 12 h. DMF was

removed under reduced pressure, and the crude residue was then purified using column chromatography on silica gel with DCM/EtOAc (1:1) as eluent to yield compound **2.4** as a yellowish solid (0.78 g, 73%). Mp: 91-93 °C. TLC (50% DCM in EtOAc): R_f = 0.26. IR (KBr): 3321, 3141, 3062, 3016, 2924, 2854, 2508, 2096, 2002, 1725, 1692, 1661, 1557, 1514, 1458, 1380, 1299, 1249, 1177, 997, 899, 754, 666 cm^{-1} . ^1H NMR ($\text{DMSO-}d_6$, 400 MHz) δ : 10.7 (1H, S), 8.05 (1H, d), 7.13 (1H, d), 3.77 (2H, t), 3.3 (2H, t), 2.09 (3H, S), 1.62 (2H, m), 1.57 (2H, m), 1.24 (16H, m). ^{13}C NMR ($\text{DMSO-}d_6$, 100 MHz) δ : 171.2, 162.5, 155.5, 150.5, 95.2, 51.0, 49.9, 29.3, 29.0, 28.9, 28.6, 26.5, 26.2, 24.6. MS (EI, 70 *ev*): m/z $[\text{M}]^+$ calcd for $\text{C}_{18}\text{H}_{30}\text{N}_6\text{O}_2$: 362, found 363.2 $[\text{M}+\text{H}]^+$. Anal. Calcd for $\text{C}_{18}\text{H}_{30}\text{N}_6\text{O}_2$: C, 59.64; H, 8.34; N, 23.19; O, 8.83; found: C, 59.73; H, 8.45; N, 23.12.

4-amino-1-(12-azidododecyl) pyrimidin-2(1H)-one (2.6)

Compound **2.4** (0.5 g, 1.38 mmol) was dissolved in a methanol (15 mL) and 26% aqueous ammonia (60 mL). The turbid solution was stirred at 180 °C for 24 h in a sealed tube. The solvents were removed under reduced pressure, and the crude residue was then purified using column chromatography on silica gel with EtOAc/MeOH (97:3) as eluent to yield compound **2.6** as a white solid (0.22 g, 52%). Mp: 186-188 °C. TLC (10% MeOH in EtOAc): R_f = 0.46. IR (KBr): 3776, 3344, 3127, 2922, 2855, 2508, 2799, 2519, 2093, 1890, 1658, 1620, 1516, 1486, 1378, 1285, 1120, 924, 790, 711, 673, 622 cm^{-1} . ^1H NMR ($\text{DMSO-}d_6$, 400 MHz) δ : 7.52 (1H, d), 6.85 (2H, brs), 5.58 (1H, d), 3.57 (2H, t), 3.28 (2H, t), 1.47 (4H, m), 1.25 (16H, m). ^{13}C NMR ($\text{DMSO-}d_6$, 100 MHz) δ : 166.2, 156.1, 146.4, 93.3, 51.0, 49.0, 29.35, 29.33, 29.1, 28.9, 28.6, 26.5, 26.3. MS (EI, 70 *ev*): m/z $[\text{M}]^+$ calcd for $\text{C}_{16}\text{H}_{28}\text{N}_6\text{O}$: 320.43, found 321.1 $[\text{M}+\text{H}]^+$. Anal. Calcd for $\text{C}_{16}\text{H}_{28}\text{N}_6\text{O}$: C, 59.97; H, 8.81; N, 26.23; O, 4.99; found: C, 59.93; H, 8.79; N, 26.21.

4-amino-1-(12-(4-(5-(7-(thiophen-2-yl)benzo[c][1,2,5]thiadiazole-4-yl) thiophen-2-yl)-1H-1,2,3-triazol-1-yl)dodecyl)pyrimidin-2(1H)-one (Cy-Red):

A mixture of compound **2.6** (0.2 g, 0.62 mmol), compound **1.7** (0.241 g, 0.74 mmol), CuI (0.011 g, 0.74 mmol) was dissolved in 4 mL of DMF and stirred at 80 °C for 12 h. After cooling solvents were removed under vacuum the residue was dissolved in DCM and passed through celite plug, solvents were removed under reduced pressure to yield **Cy-Red** as a red solid (0.171 g, 43%) and was used without further purification. Mp: 243-245 °C. IR (KBr): 3770, 3336, 3120, 2920, 2852, 2503, 2791, 2515, 1741, 1697, 1664, 1621, 1512, 1457, 1425, 1389, 1312, 1261, 1158, 1072, 1028, 865, 794, 708, 632, 600 cm⁻¹. ¹H NMR (DMSO-*d*₆, 400 MHz) δ : 8.65 (1H, s), 8.16 (4H, m), 7.75 (1H, d), 7.69 (1H, d), 7.42 (brs, NH₂), 7.30 (1H, t), 5.75 (1H, d), 4.45 (2H, t), 3.64 (2H, t), 1.89 (2 H, m), 1.55 (2H, m), 1.23 (16H, m). ¹³C NMR (DMSO-*d*₆, 100 MHz) δ : 166.5, 152.0, 151.9, 147.3, 141.8, 138.8, 137.5, 135.4, 128.7, 128.5, 128.3, 127.8, 126.2, 125.9, 125.4, 125.1, 125.0, 121.4, 93.4, 50.1, 49.0, 29.9, 29.33, 29.24, 29.08, 28.9, 28.7, 26.29, 26.23. MS (EI, 70 *ev*): *m/z* [M]⁺ calcd for C₃₂H₃₆N₈OS₃: 644.17, found 644.9 [M+H]⁺. Anal. Calcd for C₃₂H₃₆N₈OS₃: C, 59.60; H, 5.63; N, 17.38; O, 2.48, S, 14.92; found: C, 59.72; H, 5.61; N, 17.26.

3.8.15. Cy-Red Synthesis (Route II; Scheme 3):

N,N-ditert-butyl (2-oxo-1,2-dihydropyrimidin-4-yl)carbamate (3.1):¹⁸

Cytosine **2.1** (0.5 g, 4.5 mmol) and DMAP (0.054 g, 0.45 mmol) were placed in a 100 mL flask flushed with nitrogen and equipped with a magnetic stir bar. Dry THF (25 mL) was added dropwise to this mixture. To the stirred suspension was added Boc₂O

(3.92 g, 18 mmol) under nitrogen atmosphere. The reaction mixture was stirred overnight at room temperature. Excess THF was removed by rota evaporator, and the crude residue was dissolved in ethyl acetate (150 mL), washed with 1M HCl and brine, dried with anhydrous Na₂SO₄ and concentrated in vacuum to give tri-Boc-cytosine. Later compound was dissolved in methanol (70 mL) and aq. saturated NaHCO₃ solution (25 mL) was added to the solution. The turbid solution was stirred at 50 °C for 1 h, at which point clean conversion to bis-Boc protected cytosine was observed by TLC. After evaporation of MeOH, water (40 mL) was added to the suspension, and the aqueous layer was extracted with DCM. The organic layer was dried with anhydrous sodium sulphate, filtered and evaporated to give compound **3.1** as a white solid. Spectroscopic data matches with the one from the reported procedure. ¹H NMR (CDCl₃, 400 MHz) δ : 12.8 (1H, brs), 7.64 (1H, d), 7.04 (1H, d), 1.49 (18H, s).

N,N-ditert-butyl(1-(12-bromododecyl)-2-oxo-1,2-dihydropyrimidin-4-yl) carbamate (3.2):

NaH (0.115 g, 4.81 mmol) was added portion wise to compound **3.1** (1 g, 3.21 mmol) suspended in 15 mL DMF. After stirring at room temperature for 0.5 h, 1, 12-dibromododecane (3.139 g, 9.63 mmol) was added drop wise to this clear solution. The mixture was stirred at 40-50 °C for 24 h. After addition of 1 mL methanol, the solvents were evaporated, the crude residue was then purified using column chromatography on silica gel with hexane/EtOAc (4:1) as eluent to yield compound **3.2** as a white solid (0.857 g, 48%). Mp: 82-85 °C. TLC (20% EtOAc in hexane): R_f = 0.20. IR (KBr): 3656, 3495, 3271, 3151, 3084, 2975, 2920, 2856, 2730, 2624, 2406, 2287, 2058, 1979, 1754, 1654, 1527, 1462, 1371, 1326, 1263, 1144, 1042, 963, 839, 805, 725, 624 cm⁻¹. ¹H NMR (DMSO-*d*₆, 400 MHz) δ : 8.16 (1H, d), 6.75 (1H, d), 3.79 (2H, t), 3.50 (2H, t), 1.77 (2H, m), 1.61 (2H, m), 1.48 (18H, s), 1.23 (16H, m). ¹³C NMR (DMSO-*d*₆, 100 MHz) δ : 156.6, 149.2, 145.7, 144.3, 90.6, 79.5, 55.8, 44.8, 30.3, 27.5, 27.3, 24.1, 24.07, 24.04, 23.97, 23.95, 23.6, 23.17, 23.13, 22.8, 22.5, 22.4, 22.3, 20.8, 20.5. MS (EI, 70 *ev*): *m/z* [M]⁺ calcd for C₂₆H₄₄BrN₃O₅: 557, found 558.2

$[M+H]^+$. Anal. Calcd for $C_{26}H_{44}BrN_3O_5$: C, 55.91; H, 7.94; Br, 14.31; N, 7.52; O, 14.32; found: C, 55.85; H, 7.92; N, 7.48.

N,N-ditert-butyl(1-(12-azidododecyl)-2-oxo-1,2-dihydropyrimidin-4-yl) carbamate (3.3):

Compound **3.2** (0.857 g, 1.54 mmol) and sodium azide (0.3 g, 4.62 mmol) were dissolved in DMF (10 mL) and were stirred at room temperature for 12 h. DMF was removed under reduced pressure, and the crude residue was then purified using column chromatography on silica gel with hexane/EtOAc (4:1) as eluent to yield compound **3.3** as a yellowish solid (0.58 g, 73%). Mp: 91-93 °C. TLC (20% EtOAc in hexane): R_f = 0.22. IR (KBr): 3902, 3649, 3482, 3309, 3191, 3092, 3030, 2978, 2922, 2856, 2727, 2622, 2499, 2409, 2283, 2100, 1985, 1916, 1883, 1754, 1657, 1528, 1462, 1372, 1321, 1260, 1153, 1041, 962, 845, 798, 727, 666, 596 cm^{-1} . 1H NMR (DMSO- d_6 , 400 MHz) δ : 8.17 (1H, d), 6.76 (1H, d), 3.79 (2H, t), 3.30 (2H, t), 1.61 (2H, m), 1.48 (18H, s), 1.23 (18H, m). ^{13}C NMR (DMSO- d_6 , 100 MHz) δ : 161.9, 154.5, 151.0, 149.6, 95.9, 84.7, 51.0, 50.1, 29.3, 28.9, 28.6, 28.4, 27.6, 26.5, 26.2. MS (EI, 70 ev): m/z $[M]^+$ calcd for $C_{26}H_{44}N_6O_5$: 520, found 521.3 $[M+H]^+$. Anal. Calcd for $C_{26}H_{44}N_6O_5$: C, 59.98; H, 8.52; N, 16.14; O, 15.36; found: C, 59.91; H, 8.59; N, 16.17.

N,N-ditert-butyl (2-oxo-1-(12-(3-(5-(7-(thiophen-2-yl)benzo[c][1,2,5]thiadiazol-4-yl)thiophen-2-yl)cyclopenta-2,4-dien-1-yl)dodecyl)-1,2-dihydropyrimidin-4-yl) carbamate (3.4):

A mixture of compound **3.3** (0.584 g, 1.12 mmol), compound **1.7** (0.434 g, 1.34 mmol) and CuI (0.021 g, 0.112 mmol) were dissolved in 5 mL DMF and stirred at 80

°C for 12 h. After cooling solvents were removed under vacuum and the residue was dissolved in DCM and passed through celite plug. Solvents were removed under reduced pressure using rota evaporator, the remaining solid was then purified using column chromatography on silica gel with hexane/EtOAc (1:1) as eluent to yield compound **3.4** as a red solid (0.586 g, 63%). Mp: 180-182 °C. IR (KBr): 3405, 2925, 2858, 2513, 2036, 1741, 1697, 1664, 1621, 1512, 1457, 1425, 1389, 1312, 1261, 1158, 1072, 1028, 865, 794, 708, 632, 600, 510, 481, 456, 409 cm⁻¹. ¹H NMR (DMSO-*d*₆, 400 MHz) δ : 8.61 (1H, s), 8.14 (5H, m), 7.75 (1H, d), 7.52 (1H, d), 7.26 (1H, t), 6.72 (1H, d), 4.38 (2H, t), 3.75 (2H, t), 1.84 (2H, m), 1.59 (2H, m), 1.45 (18H, s), 1.24 (16H, m). ¹³C NMR (DMSO-*d*₆, 100 MHz) δ : 161.9, 154.5, 150.9, 149.7, 141.8, 138.8, 137.6, 135.4, 128.6, 128.5, 128.4, 127.8, 126.2, 125.9, 125.4, 125.2, 125.0, 121.4, 95.9, 84.7, 60.1, 50.14, 50.11, 31.09, 31.03, 30.8, 29.9, 29.28, 29.20, 28.9, 28.7, 28.4, 27.6, 26.22, 26.20, 21.1, 14.5. MS (EI, 70ev): *m/z* [M]⁺ calcd for C₄₂H₅₂N₈O₅S₃: 845.0, found 844.8 [M]⁺. Anal. Calcd for C₄₂H₅₂N₈O₅S₃: C, 59.69; H, 6.20; N, 13.20; O, 9.47; S, 11.38; found: C, 59.58; H, 6.12; N, 13.14.

4-amino-1-(12-(4-(5-(7-(thiophen-2-yl)benzo[c][1,2,5]thiadiazole-4-yl) thiophen-2-yl)-1H-1,2,3-triazol-1-yl)dodecyl)pyrimidin-2(1H)-one (Cy-Red):

Compound **3.4** (0.293 g, 0.345 mmol) was dissolved in TFA: DCM (3 mL: 3 mL) and stirred at RT for 2 h. After 2 h solvents were removed and the reaction mixture was treated with sodium bicarbonate solution and extracted with DCM. DCM was removed using rota evaporator to obtain **Cy-Red** as a red solid which was used without further purification (0.189 g, 85%). Mp: 243-245 °C. IR (KBr): 3770, 3336, 3120, 2920, 2852, 2503, 2791, 2515, 1741, 1697, 1664, 1621, 1512, 1457, 1425, 1389, 1312, 1261, 1158, 1072, 1028, 865, 794, 708, 632, 600 cm⁻¹. ¹H NMR (DMSO-*d*₆, 400 MHz) δ : 8.65 (1H, s), 8.16 (4H, m), 7.75 (1H, d), 7.69 (1H, d), 7.42 (brs, NH₂), 7.30 (1H, t), 5.75 (1H, d), 4.45 (2H, t), 3.64 (2H, t), 1.89 (2H, m), 1.55 (2H, m), 1.23 (16H, m). ¹³C NMR (DMSO-*d*₆, 100 MHz) δ : 166.5, 152.0, 151.9, 147.3,

141.8, 138.8, 137.5, 135.4, 128.7, 128.5, 128.3, 127.8, 126.2, 125.9, 125.4, 125.1, 125.0, 121.4, 93.4, 50.1, 49.0, 29.9, 29.33, 29.24, 29.08, 28.9, 28.7, 26.29, 26.23. MS (EI, 70ev): m/z $[M]^+$ calcd for $C_{32}H_{36}N_8OS_3$: 644.17, found 644.9 $[M+H]^+$. Anal. Calcd for $C_{32}H_{36}N_8OS_3$: C, 59.60; H, 5.63; N, 17.38; O, 2.48, S, 14.92; found: C, 59.72; H, 5.61; N, 17.26.

3.9. References:

- (1) Kolb, H. C.; Finn, M. G.; Sharpless, K. B. *Angew. Chem. Int. Ed.* **2001**, *40*, 2004.
- (2) Konantz, M.; Balci, T. B.; Hartwig, U. F.; Dellaire, G.; André, M. C.; Berman, J. N.; Lengerke, C. *Ann. N. Y. Acad. Sci.* **2012**, *1266*, 124.
- (3) (a) An, B.-K.; Gierschner, J.; Park, S. Y. *Acc. Chem. Res.* **2012**, *45*, 544. (b) Martin, C. R.; Kohli, P. *Nat. Rev. Drug Disc.* **2003**, *2*, 29. (c) Choi, J. W., N.S. *Biomedical Engineering-From theory to applications* (Ed.: R. Fazel-Rezai) **2011**, 299. (d) Köstler, S.; Ribitsch, V. In *Nanotechnologies for the Life Sciences*; Wiley-VCH Verlag GmbH & Co. KGaA, **2007**. (e) Rajadurai, M. S. S., Z. B.; Kuchkina, N. V.; Rusanov, A. L.; Mullen, K. *Russ. Chem. Rev.* **2007**, *76*, 821. (f) An, B.-K.; Kwon, S.-K.; Jung, S.-D.; Park, S. Y. *J. Am. Chem. Soc.* **2002**, *124*, 14410.
- (4) (a) Wang, L. X., T.; Liu, J.; Wang, L.; Chen, H.; Dong, L.; Bain, G. *Spectrochim. Acta Part A* **2005**, *62*, 565. (b) Li, H.; Xu, J.; Yan, H. *Sens. Actuators B*:**2009**, *139*, 483. (c) Wang, L.; Dong, L.; Bian, G.; Xia, T.; Chen, H.; Wang, L.; Cao, Q.; Li, L. *Anal. Lett.* **2004**, *37*, 1811. (d) Shifrina, Z. B.; Rajadurai, M. S.; Firsova, N. V.; Bronstein, L. M.; Huang, X.; Rusanov, A. L.; Muellen, K. *Macromolecules* **2005**, *38*, 9920.
- (5) (a) Sreejith, S.; Carol, P.; Chithra, P.; Ajayaghosh, A. *J. Mater. Chem.* **2008**, *18*, 264. (b) Jana, A.; Devi, K. S. P.; Maiti, T. K.; Singh, N. D. P. *J. Am. Chem. Soc.* **2012**, *134*, 7656. (c) Cui, W.; Lu, X.; Cui, K.; Wu, J.; Wei, Y.; Lu, Q. *Langmuir* **2011**, *27*, 8384.
- (6) (a) Chandrasekhar, N.; Chandrasekar, R. *Angew. Chem. Int. Ed.* **2012**, *51*, 3556. (b) Chandrasekhar, N.; Chandrasekar, R. *Chem. Commun.* **2010**, *46*, 2915. (c) Narayana, Y. S. L. V.; Chandrasekar, R. *Chem. Phys. Chem* **2011**, *12*, 2391. (d) Basak, S.; Chandrasekar, R. *Adv. Funct. Mater.* **2011**, *21*, 667.

- (7) (a) Jiang, S.; Gnanasammandhan, M. K.; Zhang, Y. *J. R. Soc. Interface* **2010**, 7, 3. (b) Kim, H.-J.; Lee, J.; Kim, T.-H.; Lee, T. S.; Kim, J. *Adv. Mater.* **2008**, 20, 1117. (c) Kaeser, A.; Schenning, A. P. H. *J. Adv. Mater.* **2010**, 22, 2985. (d) Kumar, M.; George, S. J. *Nanoscale* **2011**, 3, 2130.
- (8) Dos Santos, T.; Varela, J.; Lynch, I.; Salvati, A.; Dawson, K. A. *Small* **2011**, 7, 3341.
- (9) Fu, H.-B.; Yao, J.-N. *J. Am. Chem. Soc.* **2001**, 123, 1434.
- (10) (a) Fujitsuka, M.; Cho, D. W.; Iwamoto, T.; Yamago, S.; Majima, T. *Phys. Chem. Chem. Phys.* **2012**, 14, 14585. (b) Wang, L.; Dong, L.; Bian, G.; Xia, T.; Chen, H.; Wang, L.; Cao, Q.; Li, L. *Anal. Lett.* **2004**, 37, 1811.
- (11) (a) Frangioni, J. V. *Curr. Opin. Chem. Biol.* **2003**, 7, 626. (b) Sitharaman, B. *Nanobiomaterials Handbook*, (Ed.: B. Sitharaman), CRC press, Boca Raton, Florida, **2011**, pp. 7-17. (c) Johansson, S.; Price, J.; Modo, M. *Stem Cells* **2008**, 26, 2444-2454. (d) Veiseh, O.; Sun, C.; Gunn, J.; Kohler, N.; Gabikian, P.; Lee, D.; Bhattarai, N.; Ellenbogen, R.; Sze, R.; Hallahan, A.; Olson, J.; Zhang, M. *Nano Lett.* **2005**, 5, 1003–1008.
- (12) Mancilha, F. S.; DaSilveira Neto, B. A.; Lopes, A. S.; Moreira, P. F.; Quina, F. H.; Gonçalves, R. S.; Dupont, J. *Eur. J. Org. Chem.* **2006**, 2006, 4924.
- (13) Zeng, T.-W.; Ho, C.-C.; Tu, Y.-C.; Tu, G.-Y.; Wang, L.-Y.; Su, W.-F. *Langmuir* **2011**, 27, 15255.
- (14) Kim, J.; Park, S. H.; Cho, S.; Jin, Y.; Kim, J.; Kim, I.; Lee, J. S.; Kim, J. H.; Woo, H. Y.; Lee, K.; Suh, H. *Polymer* **2010**, 51, 390.
- (15) (a) Wang, J.-L.; Tang, Z.-M.; Xiao, Q.; Ma, Y.; Pei, J. *Org. Lett.* **2009**, 11, 863. (b) Kim, J.-J.; Choi, H.; Lee, J.-W.; Kang, M.-S.; Song, K.; Kang, S. O.; Ko, J. *J. Mater. Chem.* **2008**, 18, 5223.
- (16) Kwok, E. C.-H.; Chan, M.-Y.; Wong, K. M.-C.; Lam, W. H.; Yam, V. W.-W. *Chem. Eur. J.* **2010**, 16, 12244.
- (17) Reddy, E. R.; Banote, R. K.; Chatti, K.; Kulkarni, P.; Rajadurai, M. S. *Chem. BioChem.* **2012**, 13, 1889.
- (18) (a) Porcheddu, A.; Giacomelli, G.; Piredda, I.; Carta, M.; Nieddu, G. *Eur. J. Org. Chem.* **2008**, 2008, 5786. (b) Serajuddin, A. *Advanced Drug Delivery Reviews* **2007**, 59, 603–616. (c) Savjani, K.T.; Gajjar, A.K.; Savjani K. *Drug Solubility: Importance and Enhancement Techniques*. Vol. **2012**, ISRN

- Pharmaceutics **2012**, pp. 195727. (d) Lepeltier, E. E.; Bourgaux, C.; Couvreur, P.; *Advanced Drug Delivery Reviews* **2014**, 71, 86–97.
- (19) (a) Rihn, S.; Retailliau, P.; De Nicola, A.; Ulrich, G.; Ziessel, R. *J. Org. Chem.* **2012**, 77, 8851. (b) Chen, Y.; Zhao, J.; Guo, H.; Xie, L. *J. Org. Chem.* **2012**, 77, 2192. (c) Xu, Z.; Liao, Q.; Wu, Y.; Ren, W.; Li, W.; Liu, L.; Wang, S.; Gu, Z.; Zhang, H.; Fu, H. *J. Mater. Chem.* **2012**, 22, 17737. (d) Shcherbakova, D. M.; Hink, M. A.; Joosen, L.; Gadella, T. W. J.; Verkhusha, V. V. *J. Am. Chem. Soc.* **2012**, 134, 7913. (e) Xue, L.; Liu, C.; Jiang, H. *Chem. Commun.* **2009**, 9, 1061–1063
- (20) (a) Hill, A. J.; Teraoka, H.; Heideman, W.; Peterson, R. E. *Toxicol. Sci.* **2005**, 86, 6. (b) Strähle, U.; Scholz, S.; Geisler, R.; Greiner, P.; Hollert, H.; Rastegar, S.; Schumacher, A.; Selderslaghs, I.; Weiss, C.; Witters, H.; Braunbeck, T. *Reprod. Toxicol.* **2012**, 33, 128.
- (21) (a) Teng, Y.; Xie, X.; Walker, S.; White, D. T.; Mumm, J. S.; Cowell, J. K. *BMC Cancer* **2013**, 13, 453. (b) Patra, A.; Chandaluri, C. G.; Radhakrishnan, T. P. *Nanoscale* **2012**, 4, 343.
- (22) Nisic, F.; Colombo, A.; Dragonetti, C.; Garoni, E.; Marinotto, D.; Righetto, S.; De Angelis, F.; Lobello, M. G.; Salvatori, P.; Biagini, P.; Melchiorre, F. *Organometallics* **2015**, 34, 94.
- (23) Vo, D. D.; Staedel, C.; Zehnacker, L.; Benhida, R.; Darfeuille, F.; Duca, M. *ACS Chem. Biol.* **2014**, 9, 711.
- (24) Botstein, D.; Fink, G. R.; *Genetics* **2011**, 189, 695-704
- (25) Oliva, A.; Rosebrock, A.; Ferrezuelo, F.; Pyne, S.; Chen, H.; Skiena, S.; Fitcher, B.; Leatherwood, J. *PLoS Biol* **2005**, 3, e225

3.10. Appendix:

3.10.1. Cytotoxicity evaluation Against Mouse Macrophage Cells:

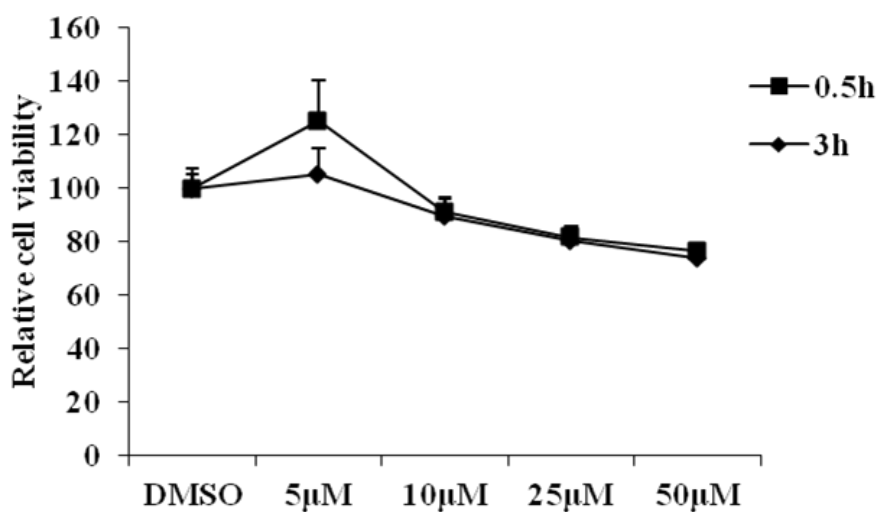
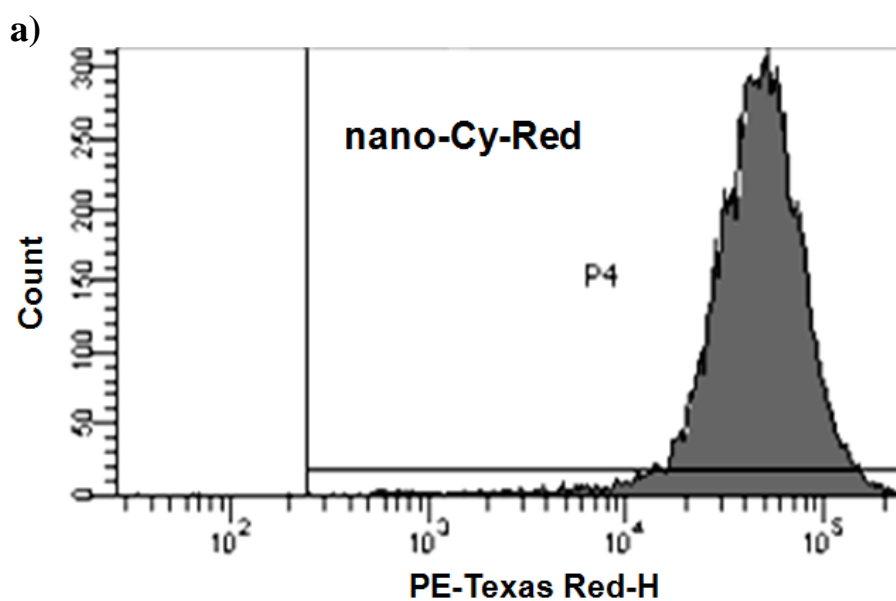


Figure A1: Dose dependent cytotoxicity of **nano-Cy-Red** in RAW 264.7 cells. Cells were incubated with different concentrations of the **nano-Cy-Red** for 30 min or 3 h, washed to remove excess dye and then incubated for 48 hours and cell viability was assessed by MTT assay.

3.10.2. Differentiation of Stained and Un-Stained Cells Using Flow Cytometry:



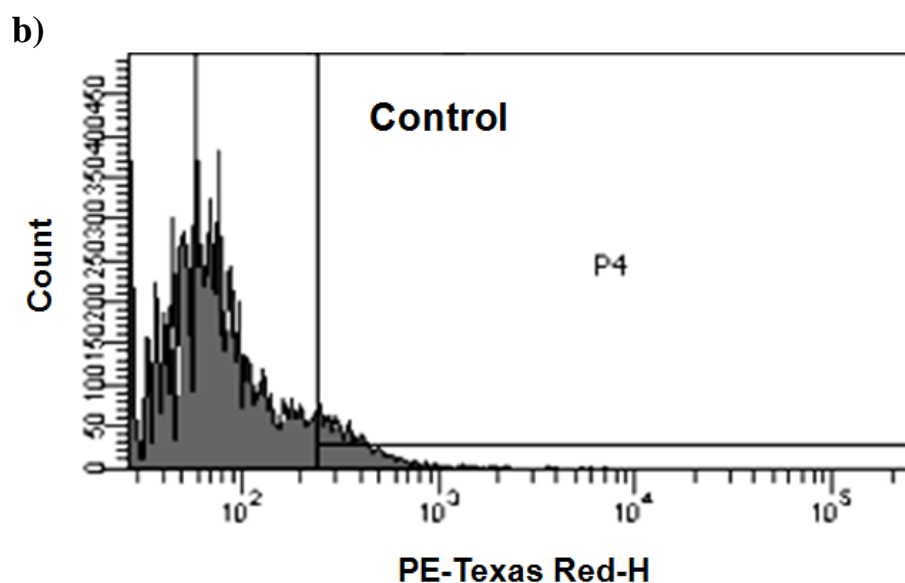


Figure A2: Analysis of **nano-Cy-Red** stained cells and control (unstained) by flow cytometry using phycoerythrin channel.

3.10.3. Transplantation of MDAMB-231 Cells in Zebrafish Embryos:

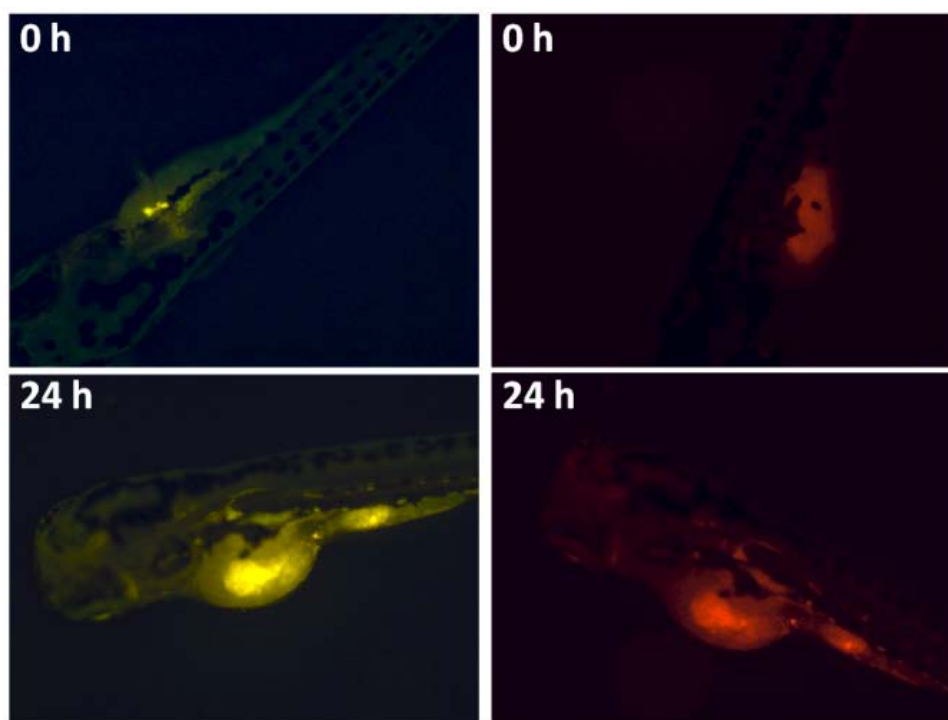


Figure A3: Fluorescent microscope images of zebrafish embryos immediately (0 h) and after 24 h post injection of MDAMB-231 cancer cells treated with **nano-Cy-Red**. The images were taken under GFP (left) and Texas Red (right) channels.

3.11. NMR Spectra of Synthesized Compounds:

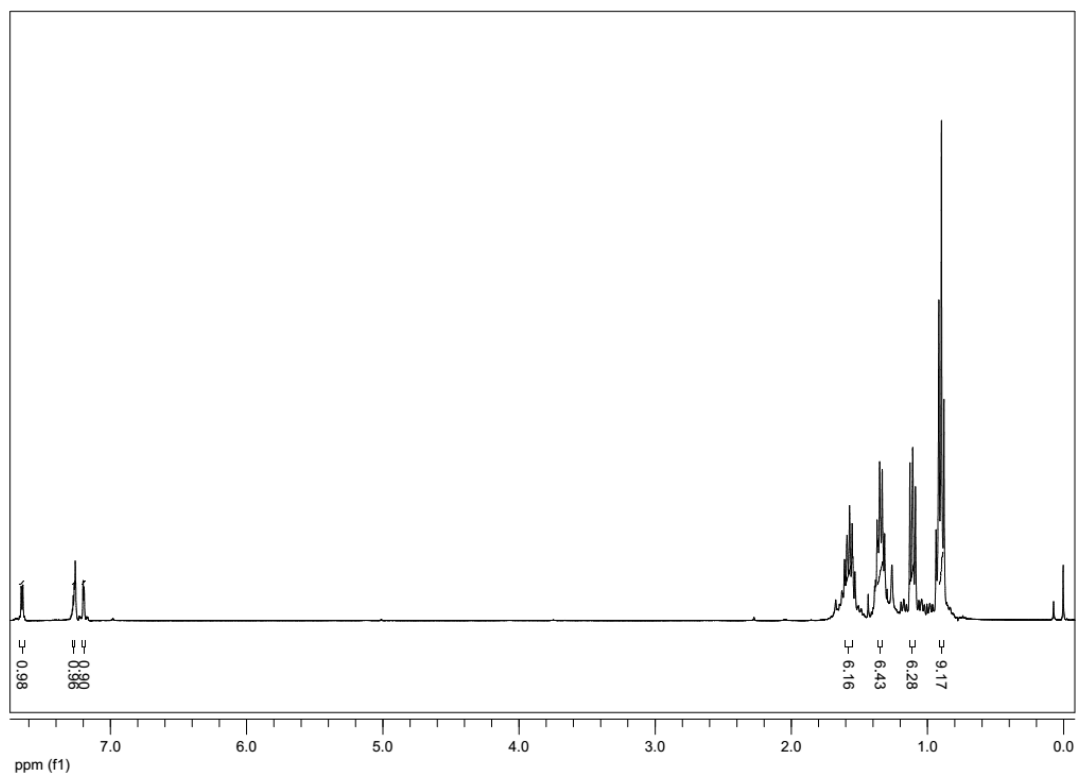


Figure A4: ^1H NMR (CDCl_3 , 400 MHz) of compound **1.4**

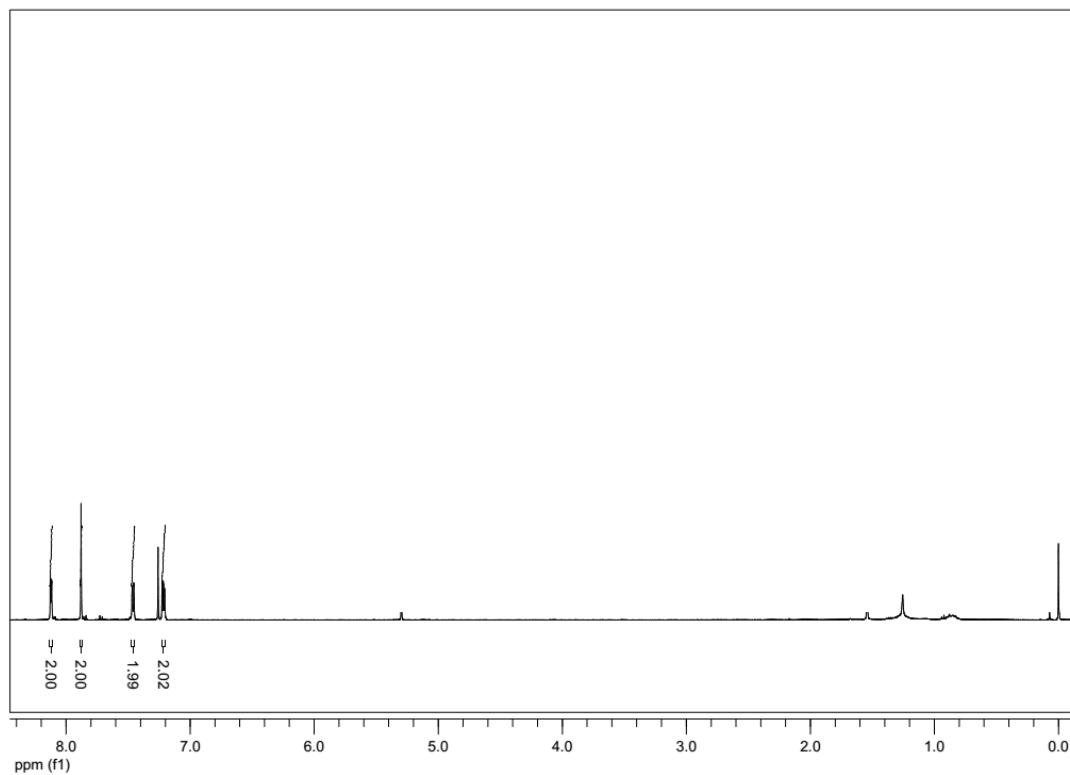


Figure A5: ^1H NMR (CDCl_3 , 400 MHz) of compound **1.5**

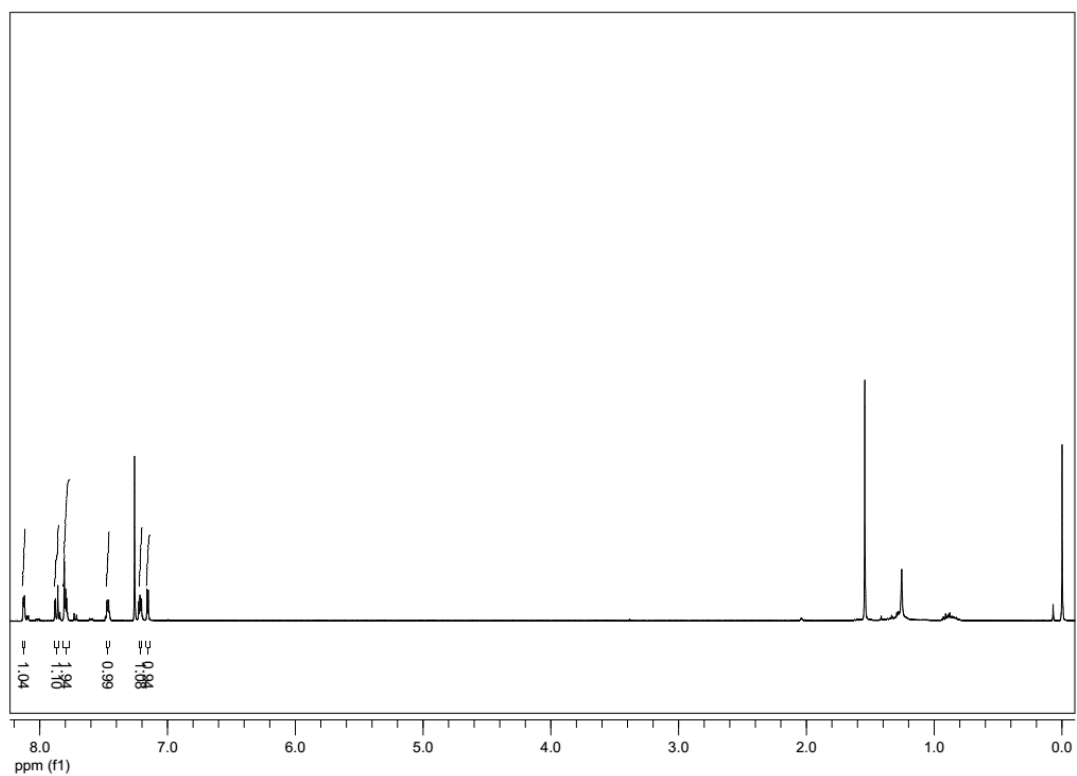


Figure A6: ¹H NMR (CDCl₃, 400 MHz) of compound **1.6**

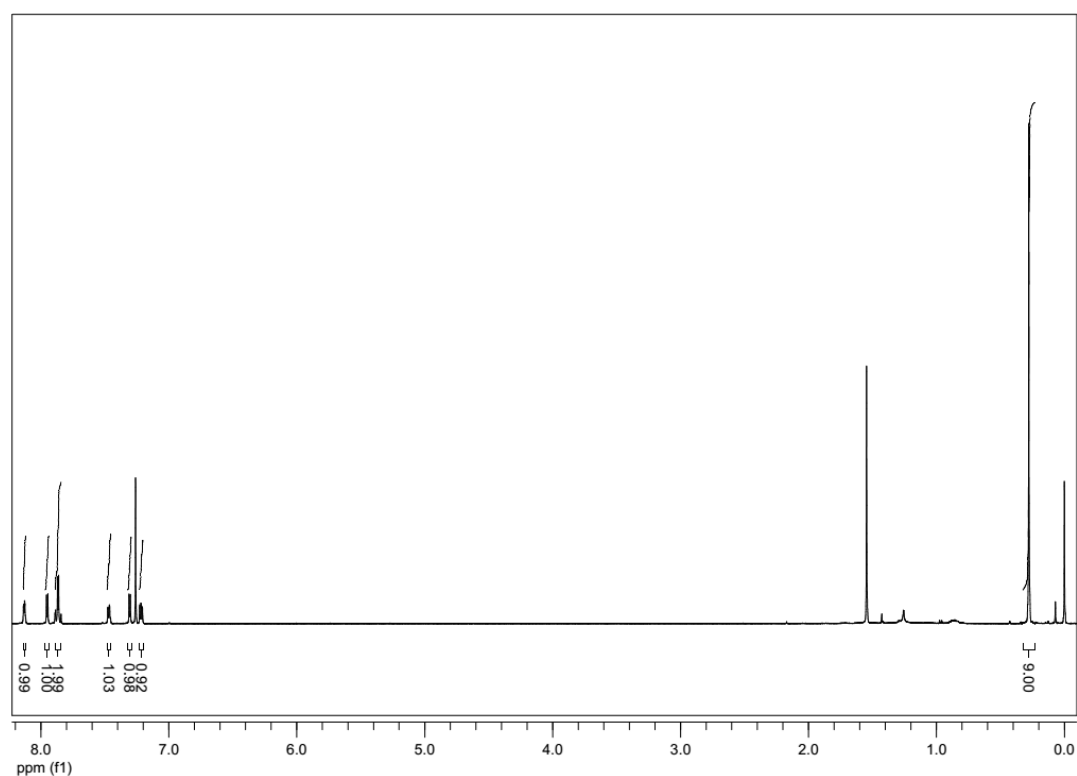


Figure A7: ¹H NMR (CDCl₃, 400 MHz) of intermediate **1.6** and **1.7**

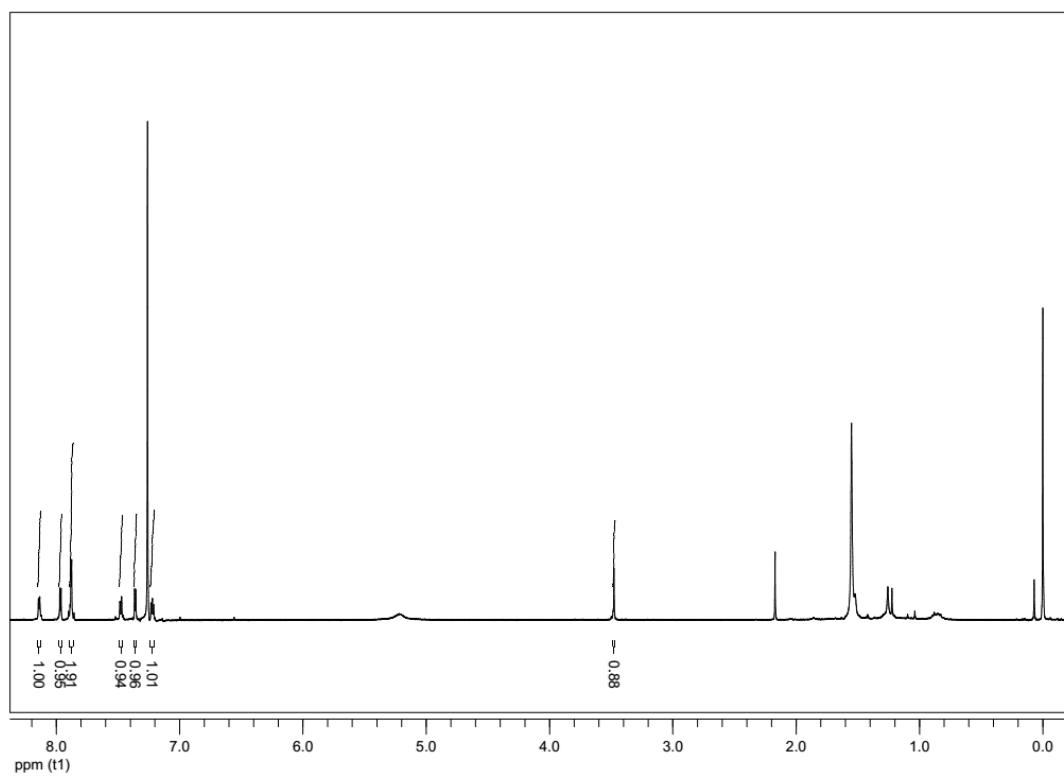


Figure A8: ¹H NMR (CDCl₃, 400 MHz) of compound **1.7**

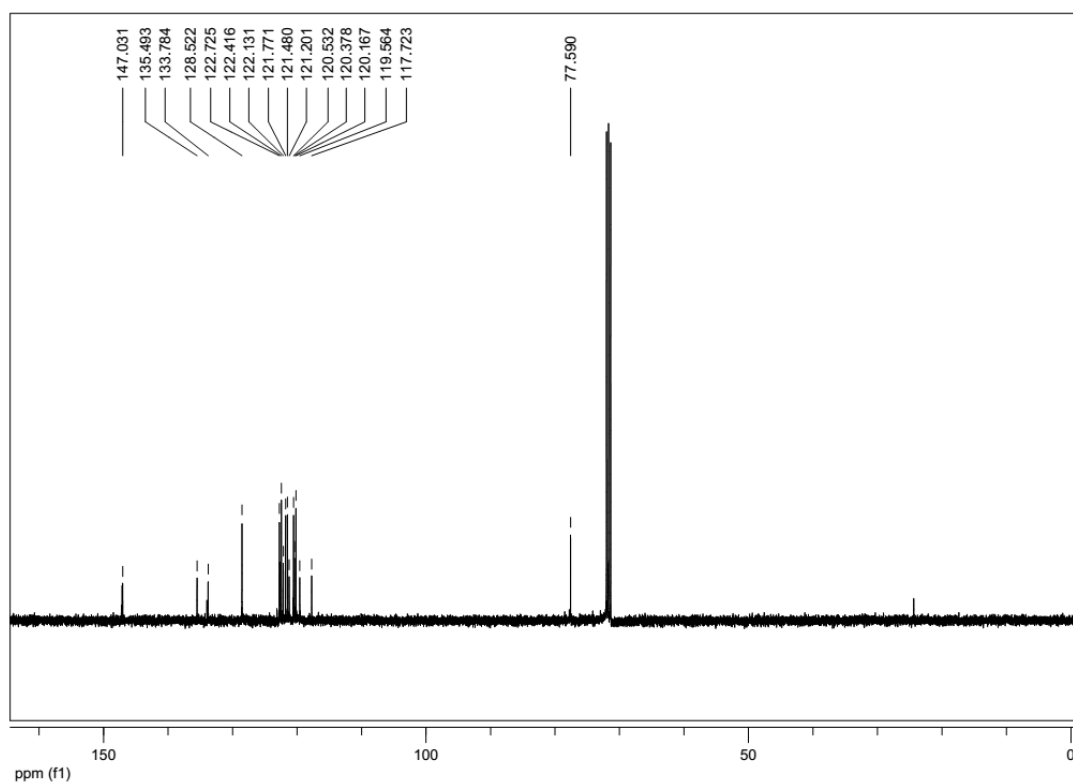


Figure A9: ¹³C NMR (CDCl₃, 100 MHz) of compound **1.7**

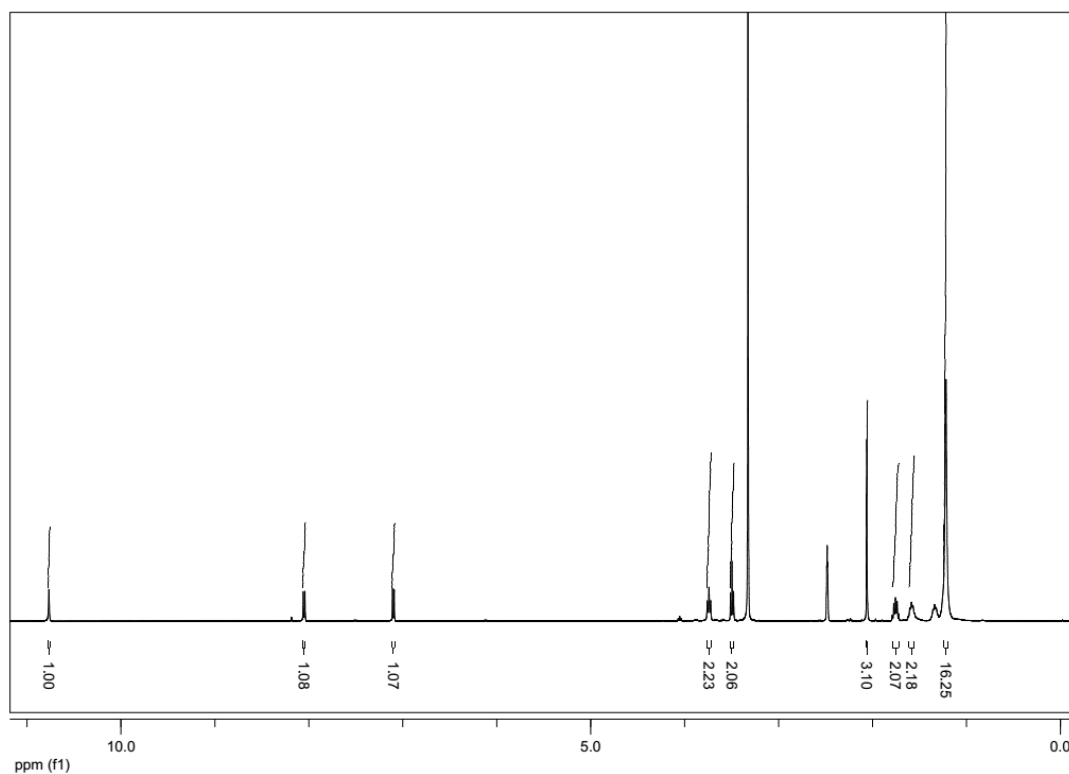


Figure A10: ¹H NMR (DMSO-*d*₆, 400 MHz) of compound **2.3**

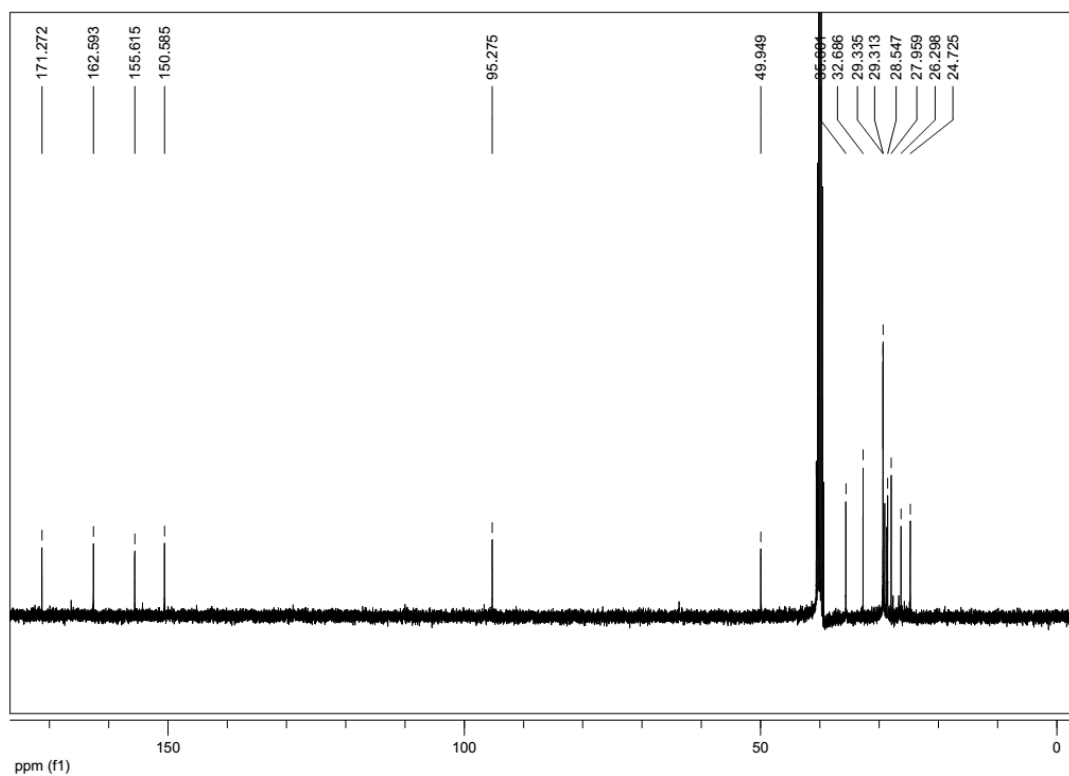


Figure A11: ¹³C NMR (DMSO-*d*₆, 100 MHz) of compound **2.3**

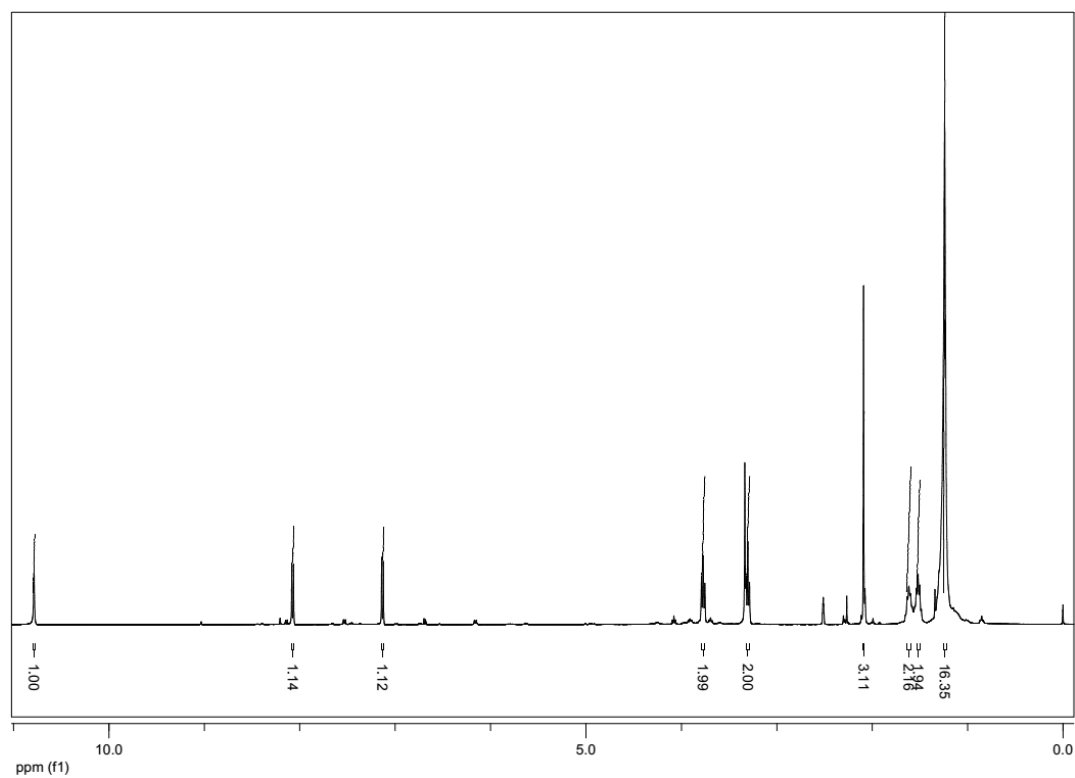


Figure A12: ¹H NMR (DMSO-*d*₆, 400 MHz) of compound **2.4**

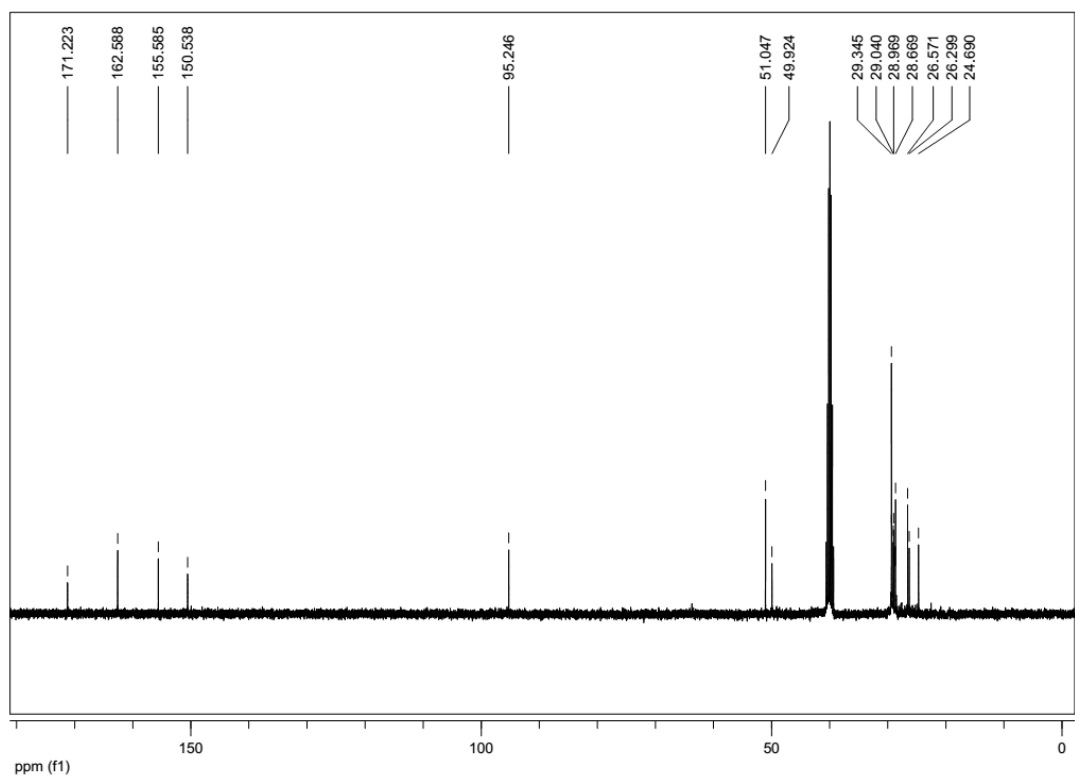


Figure A13: ¹³C NMR (DMSO-*d*₆, 100 MHz) of compound **2.4**

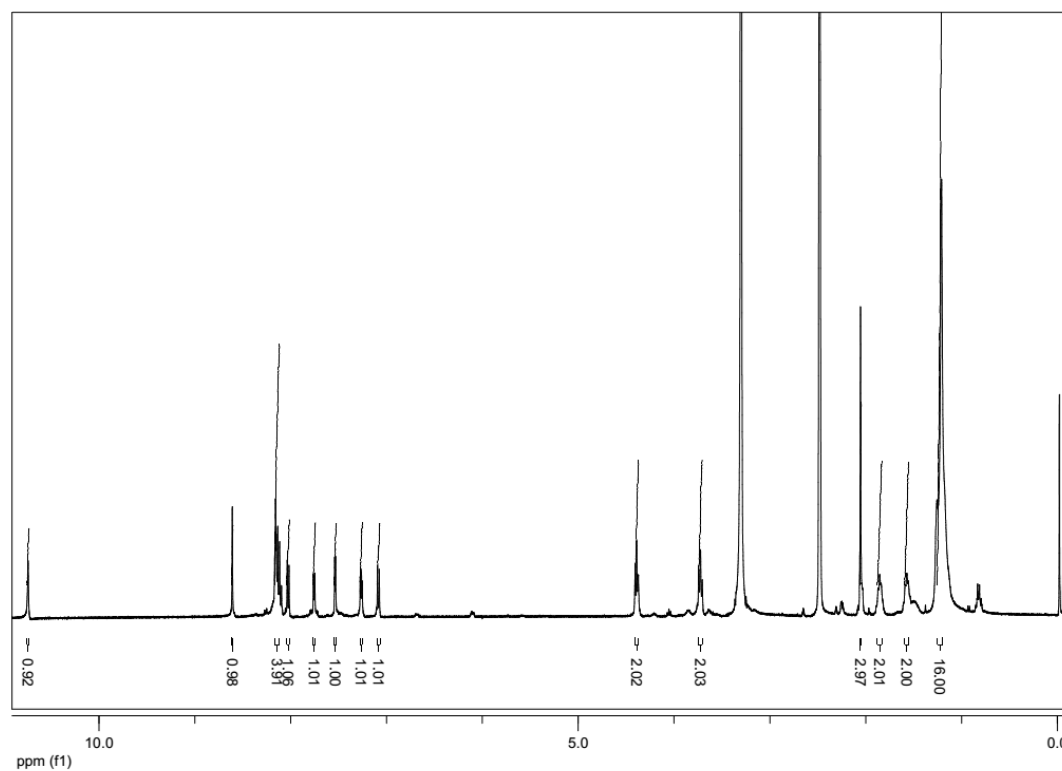


Figure A14: ¹H NMR (DMSO-*d*₆, 400 MHz) of compound **2.5**

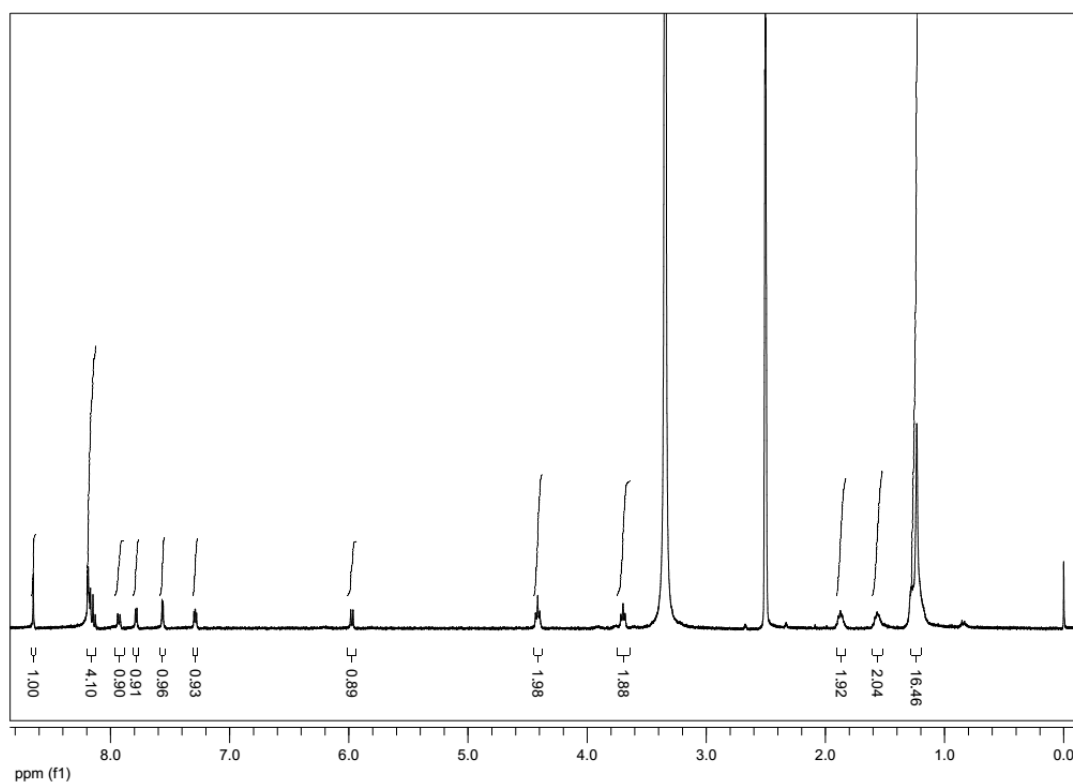


Figure A15: ¹H NMR (DMSO-*d*₆, 400 MHz) of **Cy-Red** (obtained through route I)

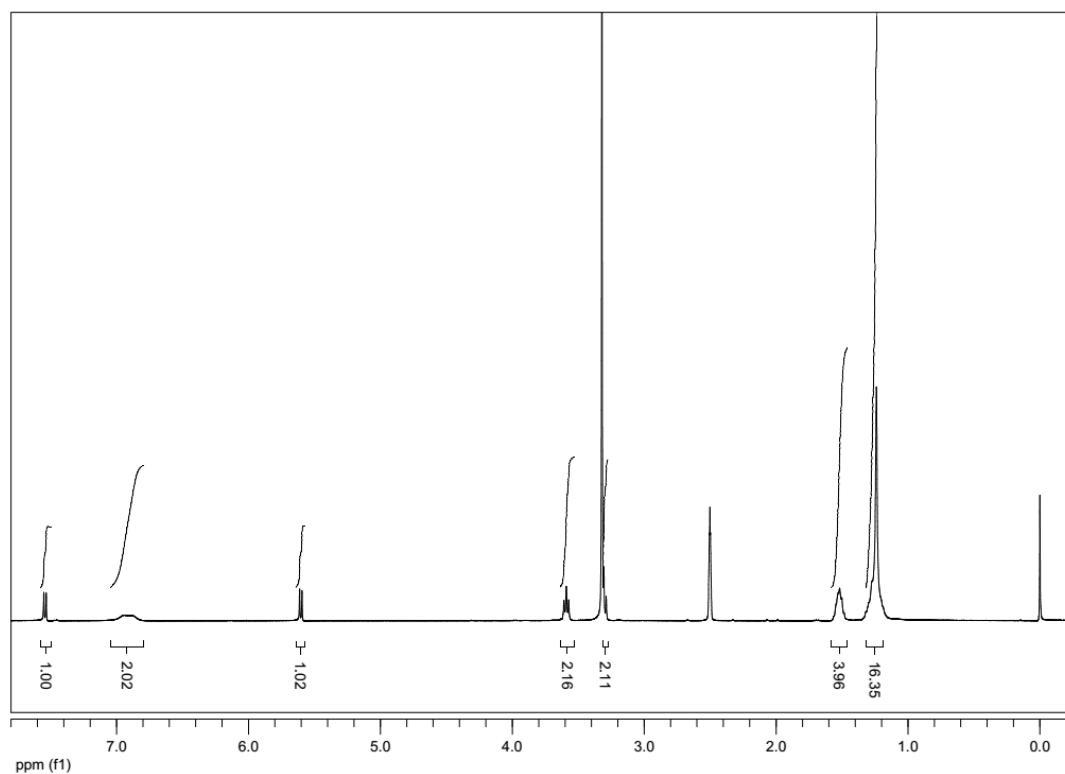


Figure A16: ^1H NMR (DMSO- d_6 , 400 MHz) of compound **2.6**

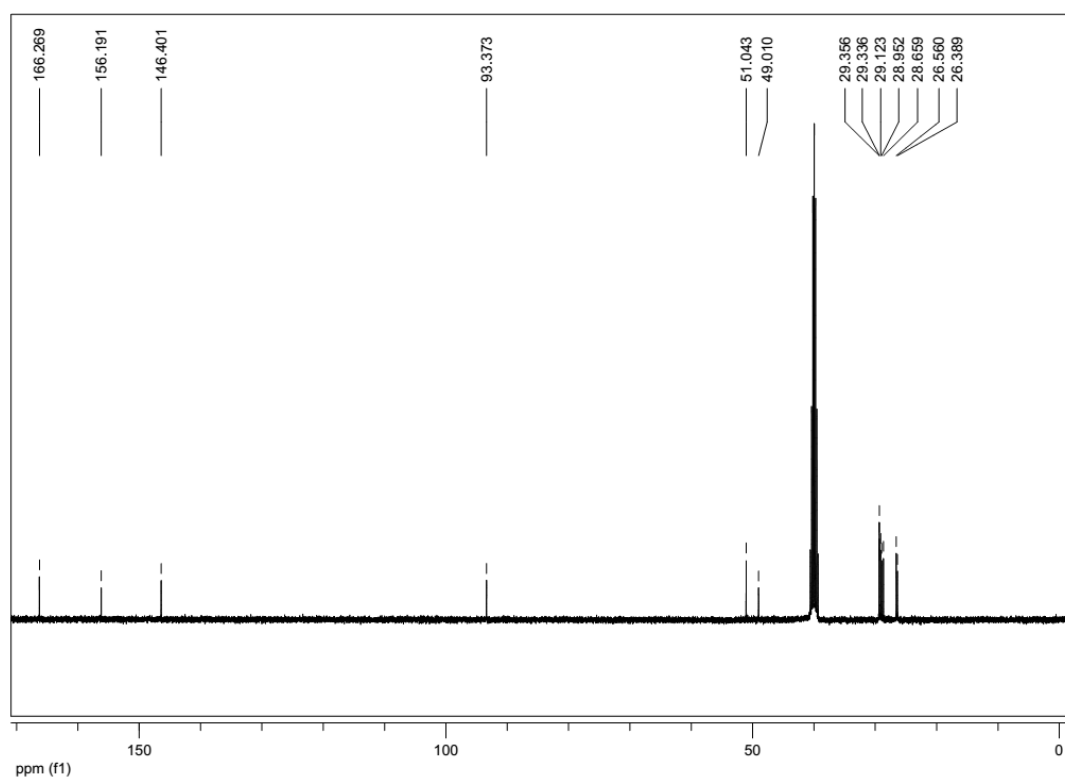


Figure A17: ^{13}C NMR (DMSO- d_6 , 100 MHz) of compound **2.6**

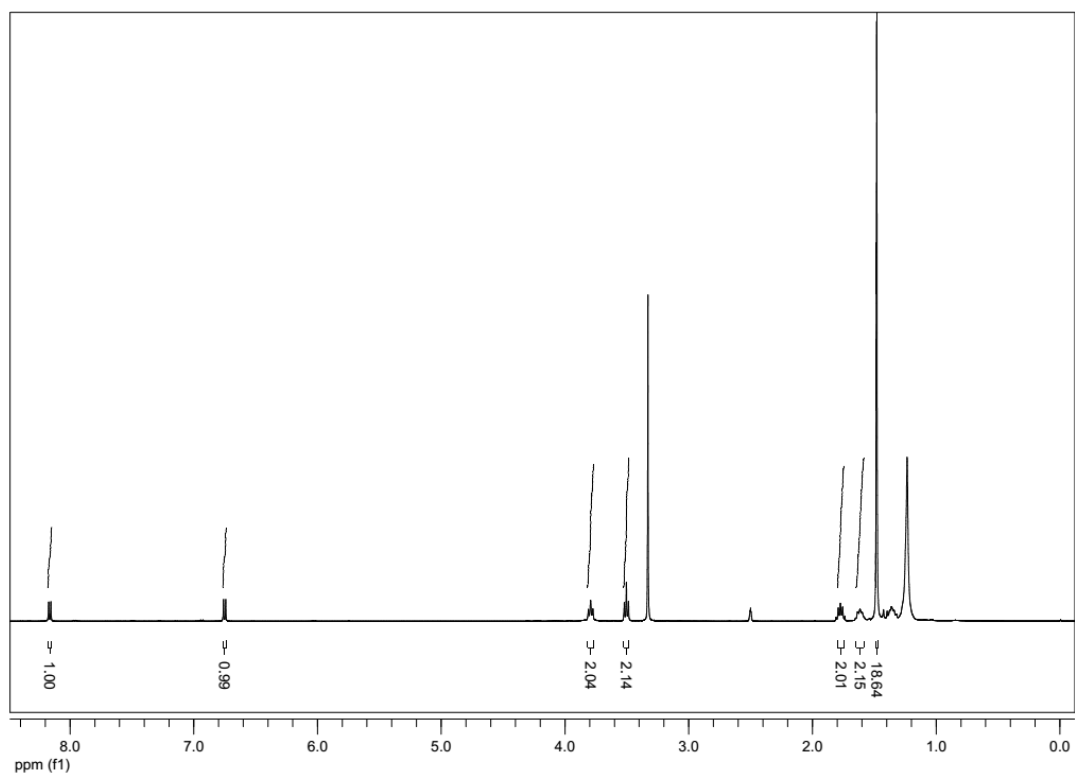


Figure A18: ¹H NMR (DMSO-*d*₆, 400 MHz) of compound **3.2**

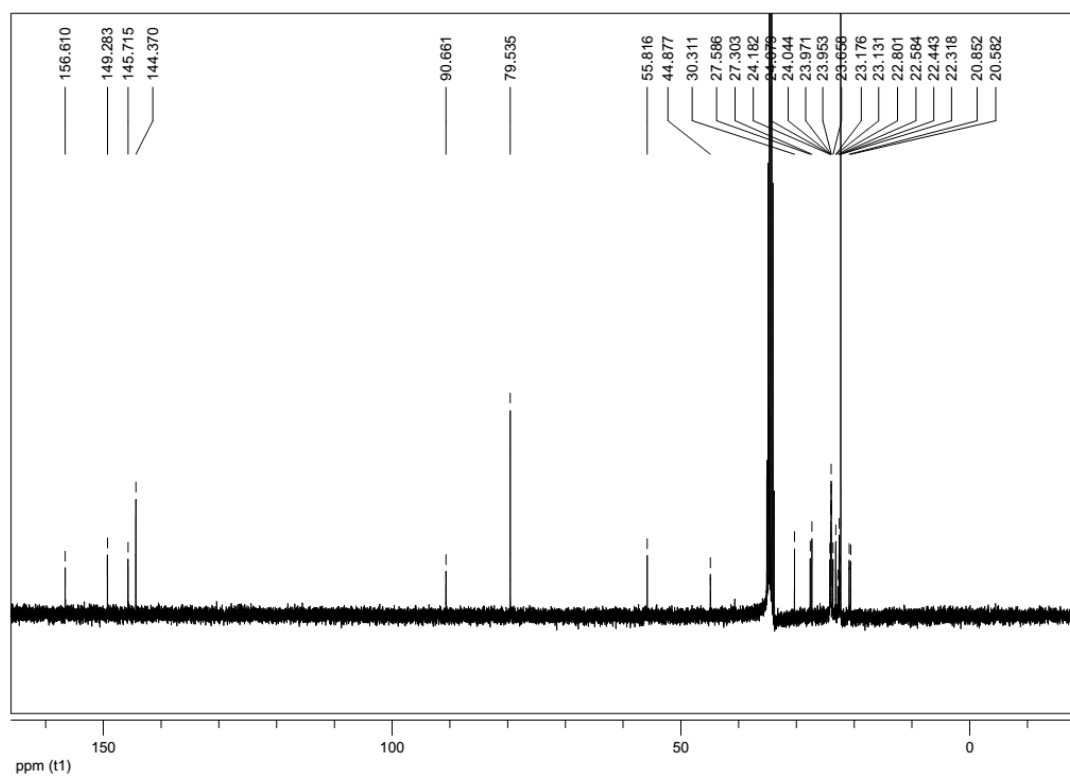


Figure A19: ¹³C NMR (DMSO-*d*₆, 100 MHz) of compound **3.2**

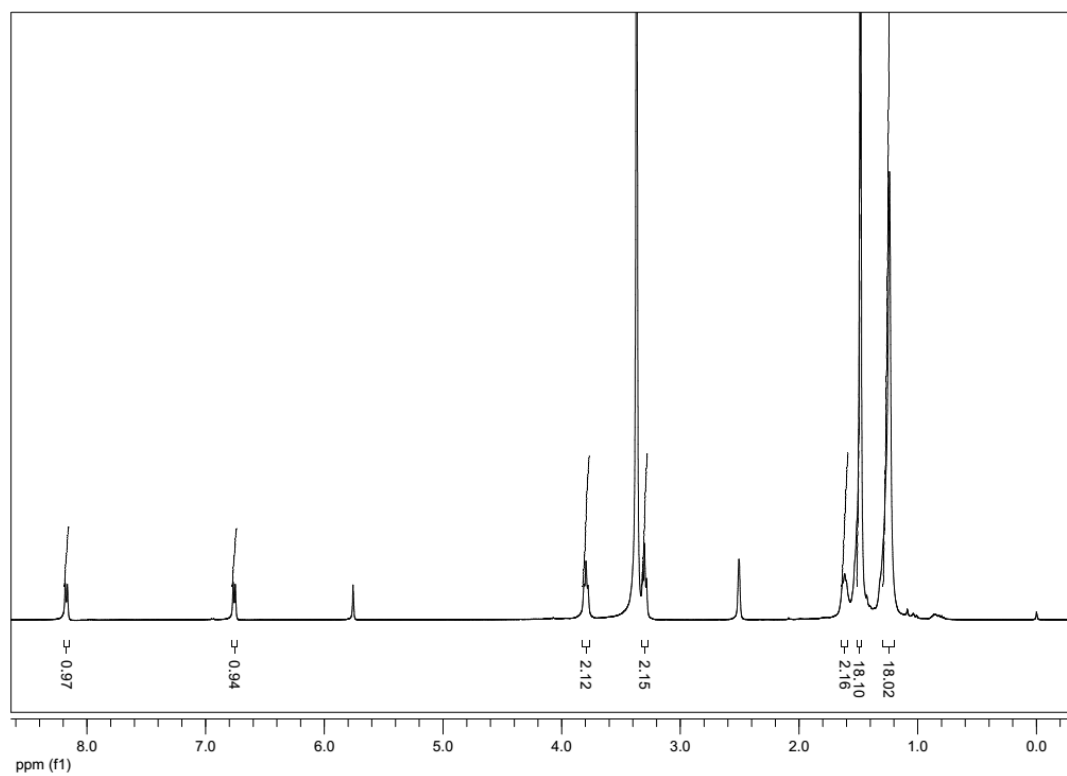


Figure A20: ¹H NMR (DMSO-*d*₆, 400 MHz) of compound **3.3**

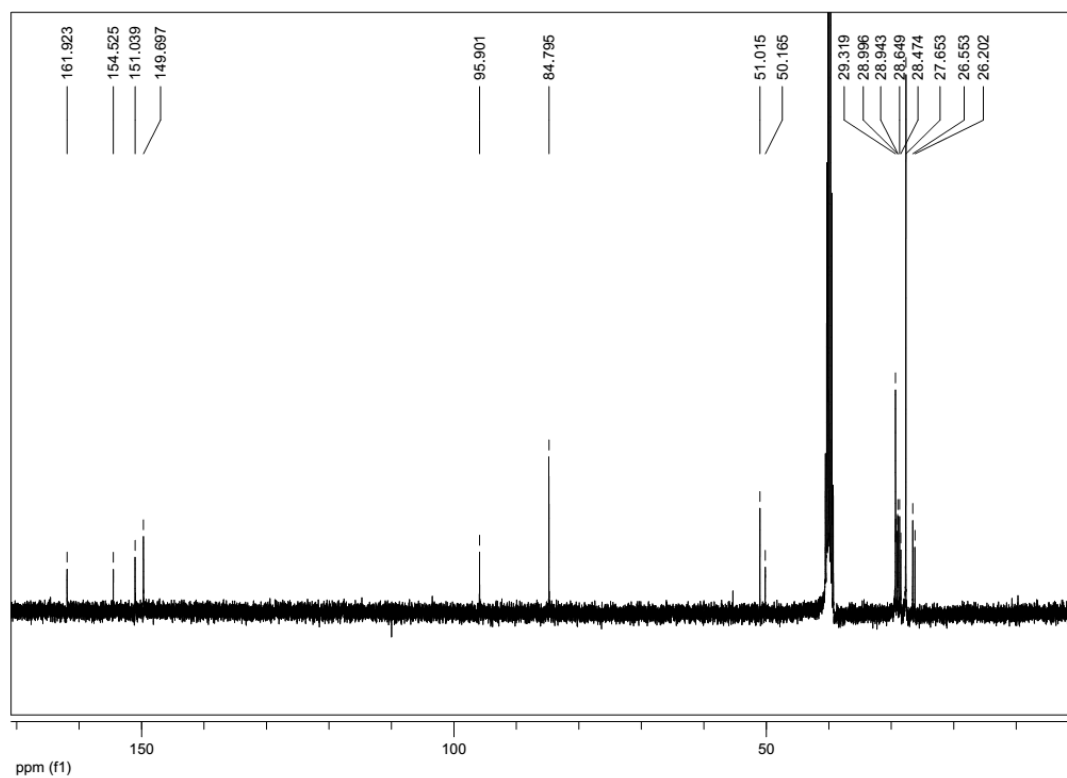


Figure A21: ¹³C NMR (DMSO-*d*₆, 100 MHz) of compound **3.3**

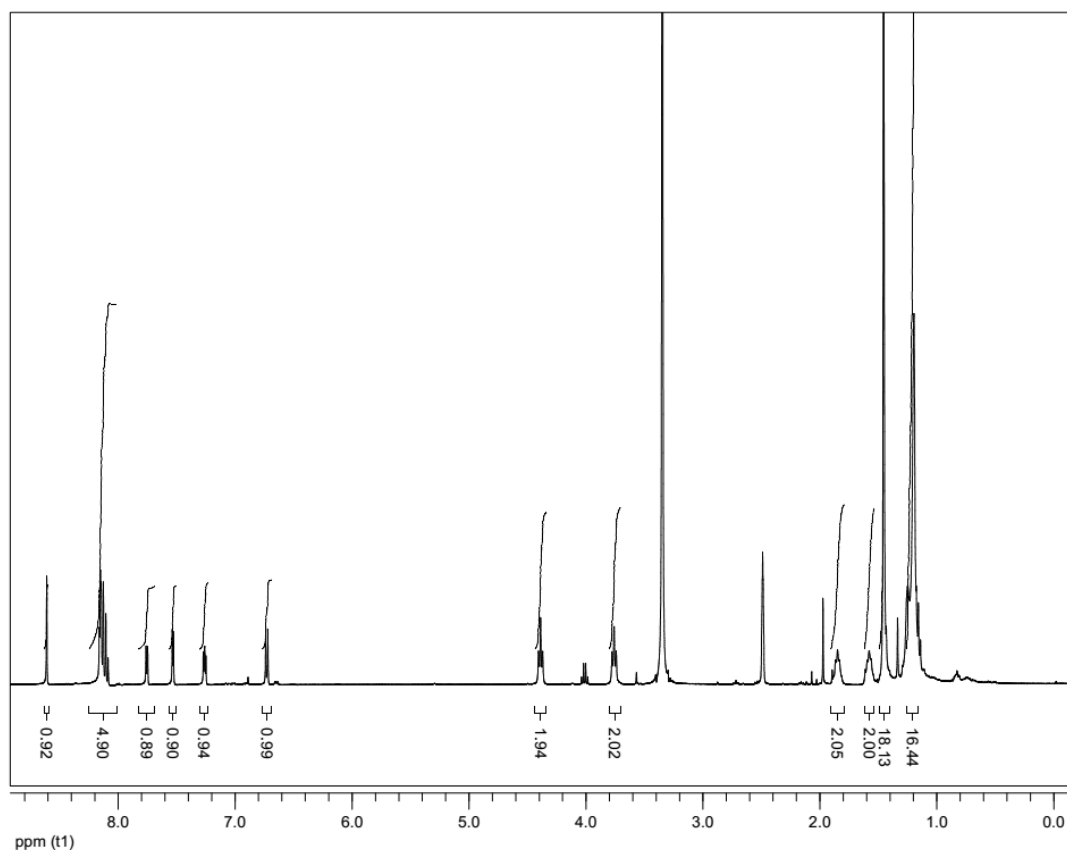


Figure A22: ¹H NMR (DMSO-*d*₆, 400 MHz) of compound 3.4

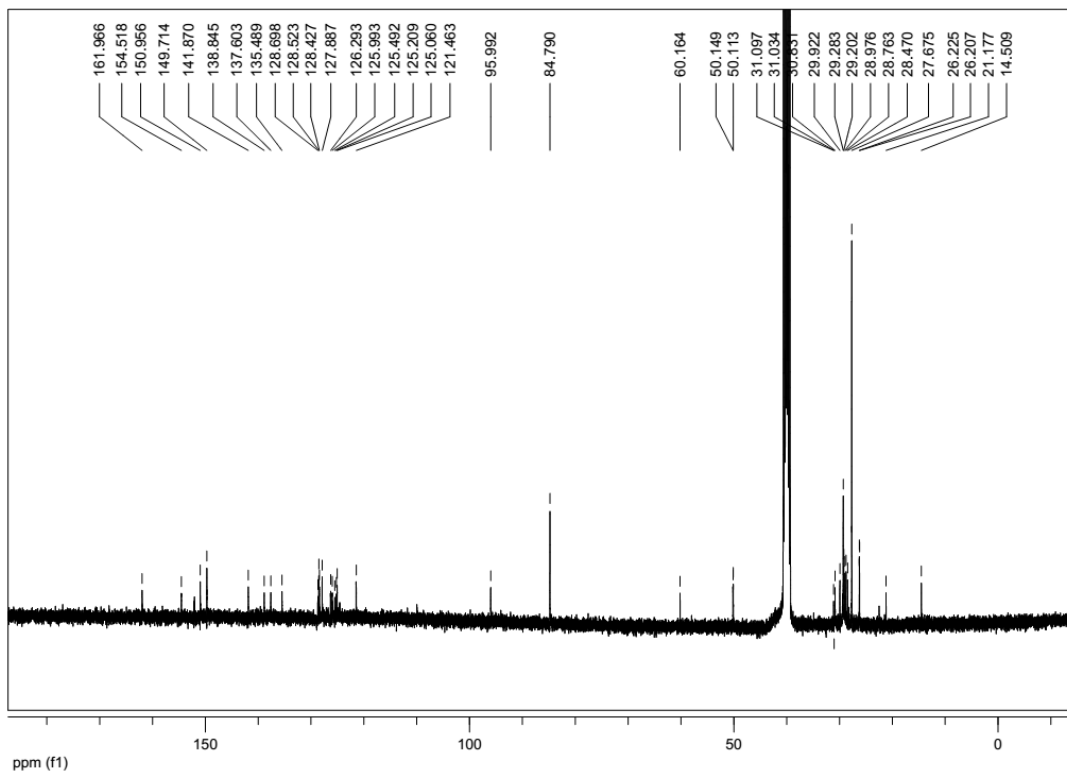


Figure A23: ¹³C NMR (DMSO-*d*₆, 100 MHz) of compound 3.4

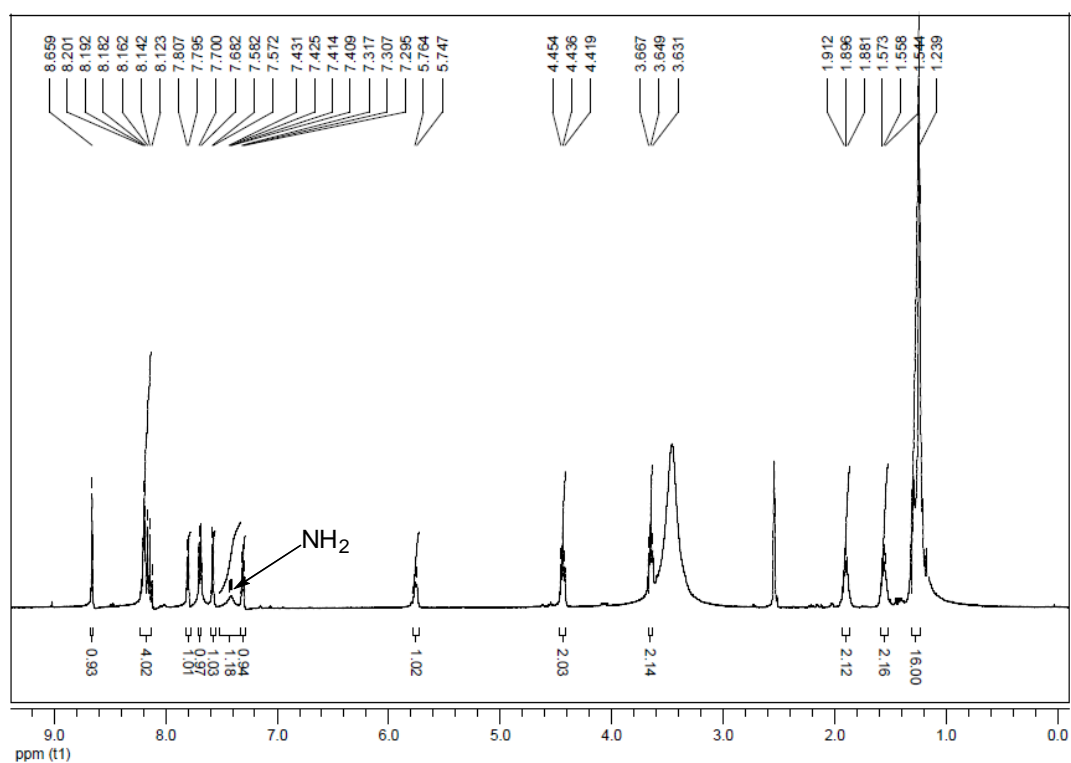


Figure A24: ¹H NMR (DMSO-*d*₆, 400 MHz) of compound **Cy-Red** (obtained through route II)

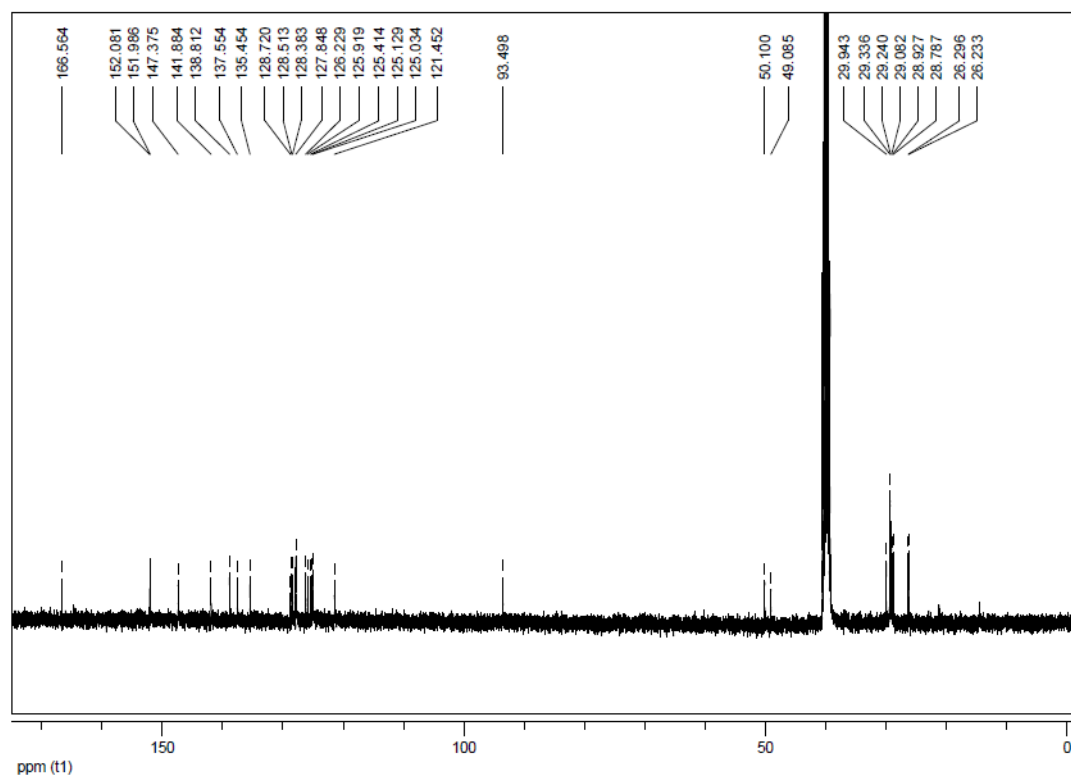
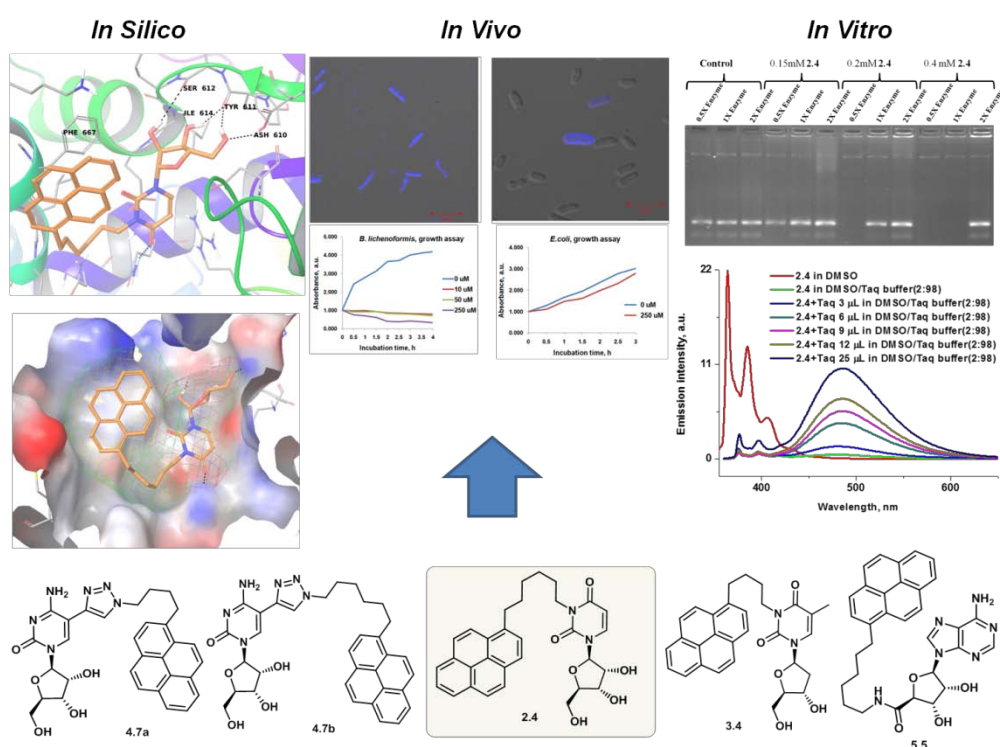


Figure A25: ¹³C NMR (DMSO-*d*₆, 100 MHz) of compound **Cy-Red** (obtained through route II)

4

Novel Fluorescent 3, 5 and 5'- Substituted Nucleosides Derivatives with Selective Antibacterial Activity



*This chapter partly adapted from: **E. Ramanjaneya Reddy**, Yaseen Abdul M, Arshad Rizvi, Giridhar S. Deora, Sharmista Banerjee, Aarti Sevilimedu, and Marina S. Rajadurai* *J. Med. Chem.* **2015**, submitted.

4.1. Abstract:

A small library of novel nucleoside derivatives have been prepared from various 3, 5 and 5' - substituted nucleosides *via* simple 3 to 5 steps synthesis in mild conditions. Their *in vitro* inhibitory activity was evaluated against *Mycobacterium tuberculosis* (Mtb, pathogenic H37Rv) using MTT assay. One of the tested compounds, 3-substituted pyrene alkyl uridine **2.4** showed mycobacterium inhibitory activity at MIC₅₀ = 62 μ M, without significant cytotoxic effect against host macrophages. Compound **2.4** also showed selective inhibitory activity against gram-positive bacteria, but was non-toxic to gram-negative bacteria at all concentrations tested. This work hypothesizes that bactericidal activity of active compound **2.4** stems from its ability to disrupt DNA replication. In support of this mechanism, a) it was demonstrated that active compound **2.4** inhibits polymerase chain reaction (PCR) *in vitro*; b) fluorescent properties of the compound **2.4** were utilized to perform microscopy studies in different bacteria, showing that selectivity of compound **2.4** is limited by cell permeability; c) *in vitro* binding studies and fluorescence measurements were used to establish direct binding of compound **2.4** to enzyme; and finally d) molecular modeling studies demonstrated a good fit of this compound within the active site of Taq DNA polymerase enzyme (Taq DNA Pol). SEM, AFM and Tyndal scattering of light revealed that compound **2.4** exist in the form of solution stable nanoparticles. The uniform shape and size of the nanoparticles was confirmed by SEM and the average diameter was ca. 250-300 nm, which was small enough to penetrate into micro organisms. Thus 3-substituted pyrene alkyl uridine **2.4** is a novel, potent, narrow spectrum antibacterial compound which can be used to target Mtb as well as gram-positive bacteria.

4.2. Introduction:

Bacteria are the most successful group of living organisms on earth. They owe their success to enormous phenotypic plasticity which allows them to survive in a wide range of environments by rapidly altering their physiology. Bacterial infections are treated using antibiotics. An antibiotic is a chemical produced by one species of bacteria that is toxic to several other species of bacteria. Evolution of antibiotics went hand in hand with the co-evolution of resistance mechanism in competitor species. In the past several decades, the wide spread and indiscriminate use of antibiotics,

combined with the immense adaptability of bacterial species has increased the selective pressure on the emergence of efficient resistance mechanisms to every known class of antibiotics. Constant exposure and horizontal gene transfer among bacterial species has resulted in a rapid spread of this resistance, making antibiotics increasingly ineffective and leaving us with very limited options for what used to be treatable infections. There is therefore, an urgent need for renewed discovery efforts to identify novel antibiotics, especially those that are difficult to evolve resistance to. One approach to slow down the emergence of resistance is to limit exposure by developing antibiotics that are selective.

Among the bacterial infections, tuberculosis is one of the leading diseases in humans.¹ According to World Health Organization (WHO), one third of population is infected with tuberculosis, killing approximately two million people annually.² The pathogen causing it, *Mycobacterium tuberculosis* has a unique cell wall structure. It contains mycolic acid,³ which possesses strong hydrophobic nature. It forms a lipid shell around the cell and provides impermeability to stains and resistance to antibiotics, osmotic lysis, etc.⁴ Therefore, it is a challenging task to develop novel drugs for *Mycobacterium tuberculosis*.⁵ Till now, the available drugs for *Mycobacterium tuberculosis* are designed based on nitrogen containing heterocycles.⁶ Among these heterocycles, nucleoside derivatives can act as effective antivirals,⁷ anti-malarials,⁸ anti-bacterials,⁹ anti-cancer agents¹⁰ and anti-mycobacterials.^{11,12} Appropriate combination of the hydrophilic and hydrophobic moieties in the nucleoside's scaffold would increase the permeability through bacterial cell wall and bring the required specificity, maintaining potency of the molecule. Particularly, introduction of a fluorescent unit ensures certain advantages, e.g. easy tracking of the molecule *in vitro* and *in vivo*. Also, it was reported earlier, that the introduction of the alkyl chain with ample length improves anti-microbial properties.¹³ Taking into account all above mentioned considerations, a series of novel nucleoside derivatives connected to the hydrophobic fluorescent unit through flexible and long aliphatic linkers were designed in this work. Such compounds are expected to have high permeability through the lipid shell surrounding the bacterial cell wall and either possess antibacterial property (for example, against Mtb) or act as a specific fluorescent tag. As per described above design principle, various novel 3-substituted uridine (**2.4**), 3-substituted thymidine (**3.4**), 5-substituted cytidine (**4.7**), 5'-substituted adenosine (**5.5**) and N9-substituted

guanine (**6.7**) derivatives were synthesized. This chapter presents biological evaluation of their antibacterial activity and reports their specific antibacterial activity towards gram-positive bacteria as well as proposed mechanism of action of compound **2.4**. Additionally, it discusses photophysical properties and the results of SEM, AFM, CFM, Tyndal scattering of light and fluorescence microscopy studies for the lead compound (**2.4**).

4.3. Results and Discussion:

Various nucleoside derivatives were synthesized in economic, efficient and ecology friendly manner, as the synthesis for each target compound was performed from in-expensive and readily available starting materials, mostly at room temperature (less energy consumption), and in short (not more than 5 steps) synthetic route (**Scheme 1-5**).

Fluorescent intermediate compound **1.5** was synthesized in four steps according to **Scheme 1**. At the first step, selective mono bromination of pyrene **1.1** with one equivalent of N-bromosuccinimide in the presence of anhydrous dimethylformamide gave compound **1.2** in 52% yield.¹⁴ At the next step, compound **1.2** was lithiated using n-BuLi followed by treatment with either C4 or C6 dibromo alkane to afford compound **1.3a, b** in 18 and 21% yields.¹⁵ Such low yield can be explained by the formation of dimeric form of compound **1.3**. Subsequently, compounds **1.3a, b** were treated with sodium azide to give compounds **1.4a, b** in 90 and 91% yield respectively. FTIR spectroscopy confirmed the formation of azide group by displaying a band at 2087 cm^{-1} , corresponding to **1.4**.

Scheme 1: Synthesis of fluorescent intermediates

Finally, compound **1.5b** was synthesized from compound **1.4b** by reduction of azide group to amine using 10% palladium on charcoal. Compound **1.5b** was obtained in good yield (65%) and structure was confirmed by FTIR spectroscopy. Additionally, the ^1H NMR spectrum showed the shifting of N-CH₂ peak from 3.26 ppm to 2.68 ppm, indicating formation of compound **1.5b**.

Fluorescent 3-substituted uridine analogue **2.4** was prepared in only three steps as outlined in **Scheme 2**. First, acetonide protection of commercially available uridine **2.1** with 2,2-dimethoxy propane in dry acetone as a solvent resulted in compound **2.2** in 90% yield.¹⁶ At the next step, N-alkylation of compound **2.2** with 1equivalent of compound **1.3b** in the presence of anhydrous potassium carbonate gave compound **2.3** in good yield. ^1H NMR spectroscopy showed the disappearance of N-H peak at 11.26 ppm and appearance of peak at N-CH₂ peak at 3.76 ppm, thus confirming successful N-alkylation. At the final step, deprotection of compound **2.3** with p-toluenesulfonic acid (PTSA) in methanol gave compound **2.4** in 85% yield. ^1H NMR spectroscopy confirmed the absence of methyl groups (from the acetonide protection) at 1.25 ppm and 1.46 ppm after formation of free hydroxyl group.

Scheme 2: Synthesis of fluorescent 3-substituted uridine analogue

3-Substituted thymidine analogue **3.4** was prepared in three steps as outlined in **Scheme 3**. Silyl protection of commercially available thymidine **3.1** with tertiary butyl dimethyl silyl chloride (TBDMS-Cl) gave di-hydroxyl protected compound **3.2** in 91% yield.¹⁷ At the next step, N-alkylation of compound **3.2** with 1equivalent of

1.3a in the presence of anhydrous potassium carbonate gave compound **3.3** in excellent yield. ^1H NMR spectroscopy showed the disappearance of N-H peak at 11.30 ppm and appearance of N-CH₂ peak at 3.89 ppm. Finally, deprotection of compound **3.3** with camphor sulphonic acid (CSA) gave compound **3.4** in 91% yield. ^1H NMR spectroscopy confirmed the absence of silyl attached methyl groups at 0.07 ppm and 0.86 ppm after the formation of free hydroxyl group, corresponding to compound **3.4**. Additionally, unambiguous conformation of the molecular structure of compound **3.4** was obtained by single crystal X-ray diffraction. Crystallization of compound **3.4** by slow evaporation technique in MeOH and DCM mixture at room temperature (4:6) led to formation of the pale yellow block crystals. Single crystal X-ray analysis of the crystals revealed the monoclinic P21 space group and the structure and corresponding data is presented in **Figure 1** and **Table I**.

Scheme 3: Synthesis of fluorescent 3-substituted thymidine analogue

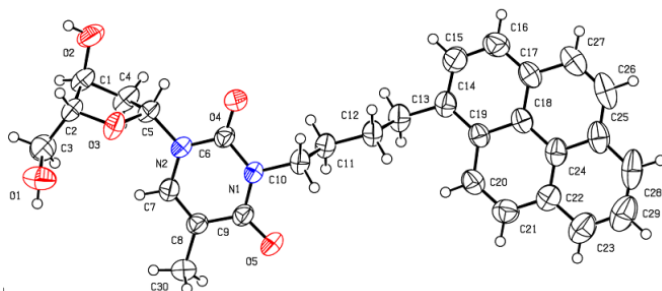


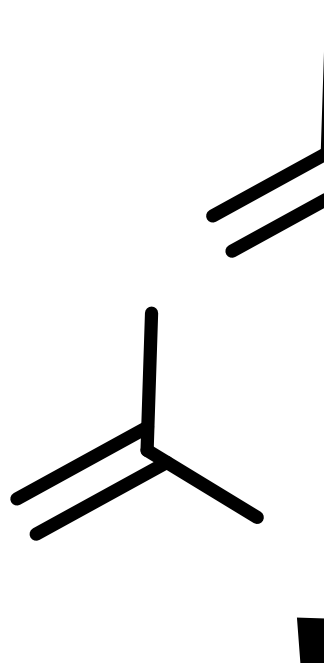
Figure 1: Crystal structure of the compound **3.4** (ORTEP diagram). Thermal ellipsoids are drawn at 50% probability level.

Table I: Crystal data of compound **3.4**

Empirical formula	C ₃₀ H ₃₀ N ₂ O ₅
Formula weight	498.56 g/mol
Temperature	298 K
Wavelength	1.54184 Å
Crystal system	Monoclinic
Space group	P21
Unit cell dimensions	$a = 10.4963(8)$ Å $\alpha = 90^\circ$. $b = 4.9461(4)$ Å $\beta = 95.320(7)^\circ$. $c = 24.1267(17)$ Å $\gamma = 90^\circ$.
Volume	1247.16(16) Å ³
Z	2
Density (calculated)	1.32754 g/cm ³
Absorption coefficient	0.735 mm ⁻¹
F(000)	528
Crystal size	0.38 x 0.36 x 0.04 mm
Theta range for data collection	3.6799 to 67.0586°.
Index ranges	-12 ≤ h ≤ 12, -5 ≤ k ≤ 5, -28 ≤ l ≤ 28
Reflections collected	2373
Independent reflections	3062 [R(int) = 0.1247]
Completeness to theta = 28.32	1.22/0.69
Absorption correction	Empirical
Refinement method	Full-matrix least-squares on F ²
Data/restraints/parameters	4869 / 0 / 270
Goodness-of-fit on F ²	1.047
Final R indices [I > 2σ(I)]	R1 = 0.1254, wR2 = 0.2486
R indices (all data)	R1 = 0.3022, wR2 = 0.3309
Largest diff. peak and hole	0.271 and -0.198 e.Å ⁻³

5-Substituted cytidine analogues (**4.7a** and **4.7b**) were prepared as outlined in **Scheme 4**. In the first step, O-acylation of cytidine **4.1** with acetyl chloride in acetic acid resulted in compound **4.2** in 78% yield.¹⁸ At the next step, iodination of compound **4.2** by iodic acid and iodine in carbon tetra chloride, acetic acid and water

at 40 °C gave compound **4.3** in 80% yield.¹⁸ Subsequently, C-C bond formation with TMS-acetylene in the presence of CuI and PdCl₂(PPh₃)₂ gave compound **4.4** in good yield. Selective deprotection of silyl group with tetrabutylammonium fluoride (TBAF) gave compound **4.5** containing terminal alkyne group in 95% yield.⁷ Coupling of **4.5** with compounds **1.4a** or **1.4b** in copper catalyzed click reaction conditions led to formation of coupled products **4.6a** and **4.6b** respectively, in good yields. ¹H NMR spectroscopy confirmed the formation of a five-member triazole ring by exhibiting a C_{triazole}-H proton at 8.66 ppm in DMSO-*d*₆ and disappearance of the terminal acetylene proton at 3.63 ppm. At the final stage, acetyl deprotection of compounds **4.6a** and **4.6b** under basic conditions (using potassium carbonate) gave compound **4.7a** and **4.7b** respectively, in good yields. ¹H NMR spectroscopy confirmed the absence of methyl groups (from the acetyl protection) at 1.99 ppm, 2.09 ppm and 2.11 ppm upon formation of free hydroxyl group.



Scheme 4: Synthesis of 5-substituted fluorescent cytidine analogues

5'-Substituted adenosine analogue was prepared in four steps according to **Scheme 5**. Acetonide protection of commercially available adenosine **5.1** with 2,2'-dimethoxy propane in the presence of catalytic amount of concentrated perchloric acid gave compound **5.2** in 83% yield.¹⁹ At the next step, 5'-OH group of compound **5.2** was oxidized using BIAB and TEMPO in acetonitrile/water medium to obtain compound **5.3** in 90% yield.²⁰ Coupling of compound **5.3** with **1.5b** using EDCI as a coupling agent gave compound **5.4** in 77% yield. ¹H NMR spectroscopy confirmed the formation of amide bond by exhibiting amide N-H proton at 9.04 ppm in DMSO-*d*₆. At final stage, deprotection of compound **5.4** with p-toluenesulfonic acid (PTSA) resulted in compound **5.5** in 85% yield. ¹H NMR spectroscopy displayed the absence of methyl groups (from the acetonide protection) at 1.37 ppm and 1.61 ppm upon formation of free hydroxyl group, corresponding to compound **5.5**.

Scheme 5: Synthesis of 5'-substituted fluorescent adenosine analogues

Additionally, N9-substituted guanine derivative was also prepared *via* five steps protocol as outlined in **Scheme 6**. For that, thiophene was lithiated using *n*-BuLi followed by treatment with tributyl tin chloride to afford tributyl(2-thienyl)stannane **6.2**.²¹ Then, compound **6.2** was coupled with compound **1.2** in Stille coupling conditions in THF using palladium (II) as a catalyst to give compound **6.3** in 82% yield.²¹ Partial bromination of the compound **6.3** with NBS in acetic acid-DCM gave mono-brominated compound **6.4** in 72% yield.²² Ethynyl derivative of compound **6.5** was prepared using standard two-steps protection-deprotection

procedure, where protection step was performed *via* Sonogashira coupling of **6.4** with trimethylsilyl acetylene, which was then converted to terminal alkyne by deprotection with potassium carbonate in methanol, giving compound **6.5** in overall 75% yield. ^1H NMR spectroscopy confirmed the formation of terminal acetylene group by displaying a signal at 4.74 ppm, corresponding to compound **6.5**. Coupling of **6.5** with compound **6.6** (reported earlier from our group²³) in copper catalyzed click reaction conditions led to formation of coupled product **6.7** in 50% yield. ^1H NMR spectroscopy confirmed the formation of a five-member triazole ring by exhibiting a $\text{C}_{\text{triazole}}\text{-H}$ proton at 8.60 ppm in $\text{DMSO-}d_6$ and disappearance of the terminal acetylene proton at 4.74 ppm, corresponding to compound **6.7**.

Scheme 6: Synthesis of fluorescent N9-substituted guanine derivative

4.4. Optical Studies:

Photophysical properties of synthesized compounds (**2.4**, **3.4**, **4.7a**, **4.7b**, **5.5** and **6.7**) were investigated and summarized in **Table II**. Absorbance and fluorescence emission of DMSO solutions of the tested compounds were measured at the concentration of 10^{-5} M. Compounds **2.4**, **3.4**, **4.7a**, **4.7b** and **5.5** displayed identical

absorbance maxima (at 329 nm and 346 nm, **Figure 2**) and emission maxima (at 363 and 384 nm, **Figure 3**), whereas compound **6.7** displayed absorbance maxima at 361 nm and emission maxima at 437 nm as shown in **Figures 2, 3** and **Table II**. The Stokes shift was 18 nm for compounds **2.4**, **3.4**, **4.7a**, **4.7b** and **5.5**, while compound **6.7** had larger Stokes shift of 76 nm. The solution state quantum yields of compounds **2.4**, **3.4**, **4.7a**, **4.7b**, **5.5** and **6.7** were in range of 0.19-0.24 (with respect to quinine sulphate, **Table III**)

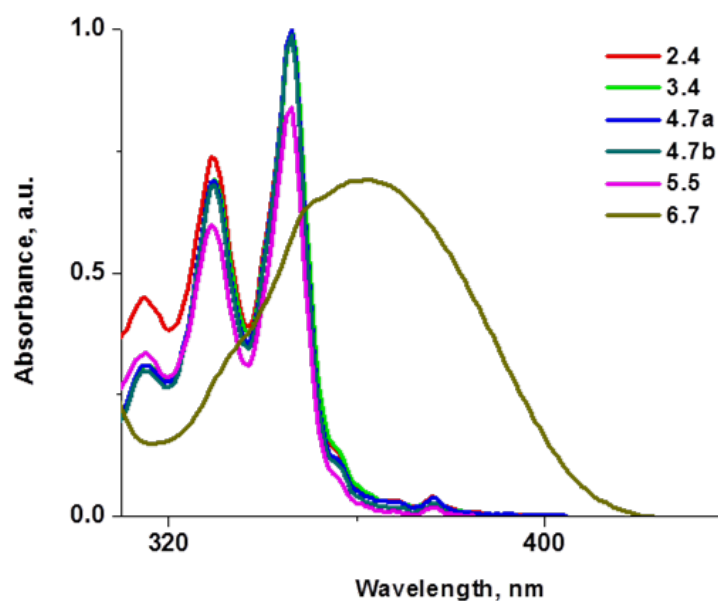


Figure 2: UV-Vis absorbance spectra of compound **2.4**, **3.4**, **4.7a**, **4.7b**, **5.5** and **6.7** in DMSO-*d*₆ at 10⁻⁵M

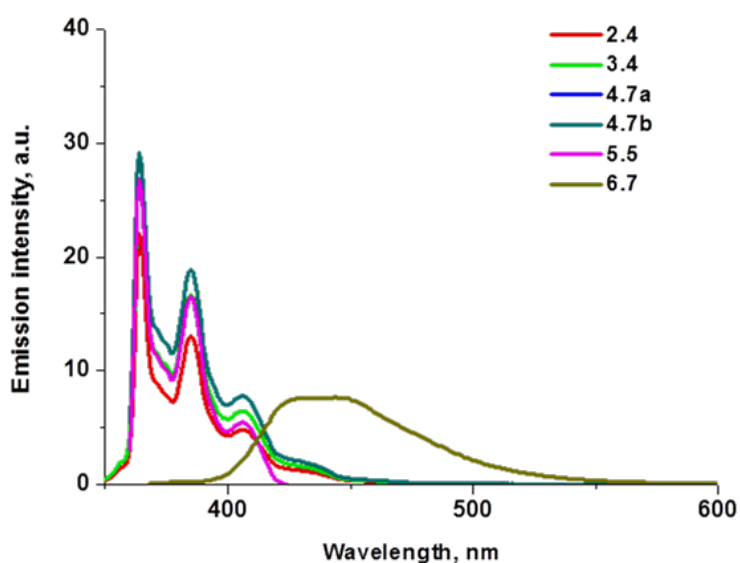


Figure 3: Fluorescence emission spectra of compound **2.4**, **3.4**, **4.7a**, **4.7b**, **5.5** and **6.7** in DMSO-*d*₆ at 10⁻⁵M

Table II: Summary of compounds

S. No	Compound Structure and code	Molecular weight	Solubility	λ_{abs} , nm	λ_{em} , nm
1		$\text{C}_{31}\text{H}_{32}\text{N}_2\text{O}_6$	Ethanol DMSO	329 and 346	363 and 384
2		$\text{C}_{30}\text{H}_{30}\text{N}_2\text{O}_5$	Ethanol DMSO	329 and 346	363 and 384
3		$\text{C}_{31}\text{H}_{30}\text{N}_6\text{O}_5$	Ethanol DMSO	329 and 346	363 and 384
4		$\text{C}_{33}\text{H}_{34}\text{N}_6\text{O}_5$	Ethanol DMSO	329 and 346	363 and 384
5		$\text{C}_{32}\text{H}_{32}\text{N}_6\text{O}_4$	Ethanol DMSO	329 and 346	363 and 384
6		$\text{C}_{39}\text{H}_{39}\text{ClN}_8\text{S}$	Ethanol DMSO	361	437

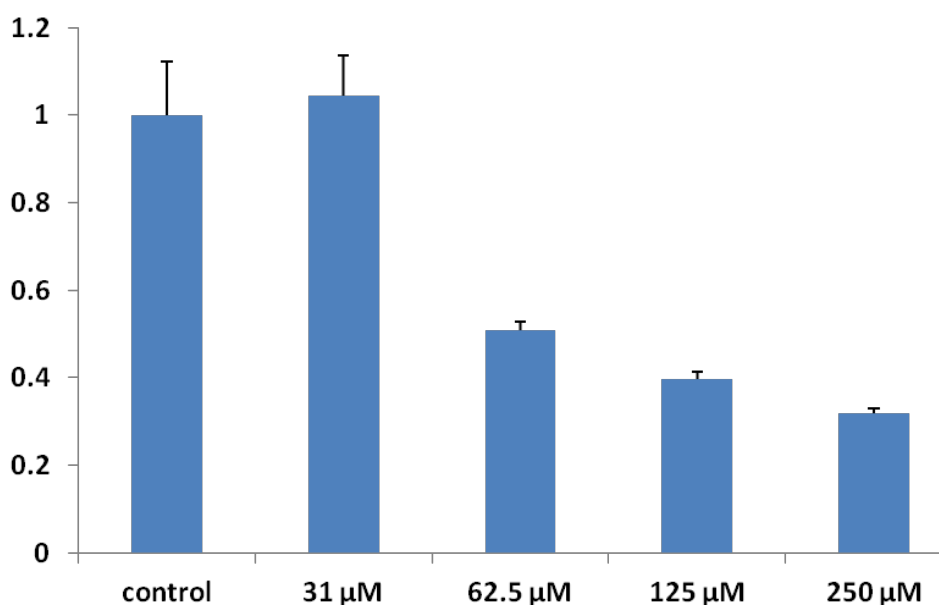
Table III: Relative quantum yields with respect to quinine sulphate

Compound	Relative Φ_f with respect to quinine sulphate
2.4	0.20
3.4	0.19
4.7 a	0.24
4.7b	0.24
5.5	0.18
6.7	0.19

4.5. Evaluation of Anti-Mycobacterial Properties:

(*Collaborative study with Dr. Sharmistha Banerjee group, Department of Biochemistry, School of Life Sciences, University of Hyderabad, India.)

The various synthesized nucleoside derivatives (**2.4**, **3.4**, **4.7a**, **4.7b**, **5.5** and **6.7**) were evaluated for their toxicity at various concentrations (31 μ M, 62.5 μ M, 125 μ M, 250 μ M) towards *Mycobacterium tuberculosis* (*Mtb*, pathogenic strain *H37Rv*) using a standard MTT assay. Among them, compound **2.4** displayed significant toxicity, with a MIC₅₀ of 62.5 μ M, as shown in **Figure 4**. The rest of the compounds did not display significant toxicity towards *H37Rv* even at 250 μ M, as shown in appendix (**Figure A1**, see page no **169**). Therefore, the MTT assay helped to identify hit compound **2.4**, and all further studies were performed only with it.

**Figure 4:** Toxicity studies on *mycobacterium tuberculosis* using compound **2.4**

4.6. Cytotoxicity Evaluation against Host Cells:

The active compound **2.4** was evaluated for the host cells cytotoxicity (human monocytic cell line THP1) at various concentrations (17.75 μ M, 35.5 μ M, 71 μ M, 142 μ M, 284 μ M) using MTT assay. Compound **2.4** showed negligible cytotoxicity at 71 μ M, whereas at higher concentrations (284 μ M) it shows 30% inhibition. This data indicates possibility of utilization of compound **2.4** as potential anti-mycobacterial drug. Although this compound is active in micro molar range, its potency could be improved *via* minor alteration of the structure and study of the structure-activity relationship. Although, this is not the major goal of the current work, our future plan includes such investigation.

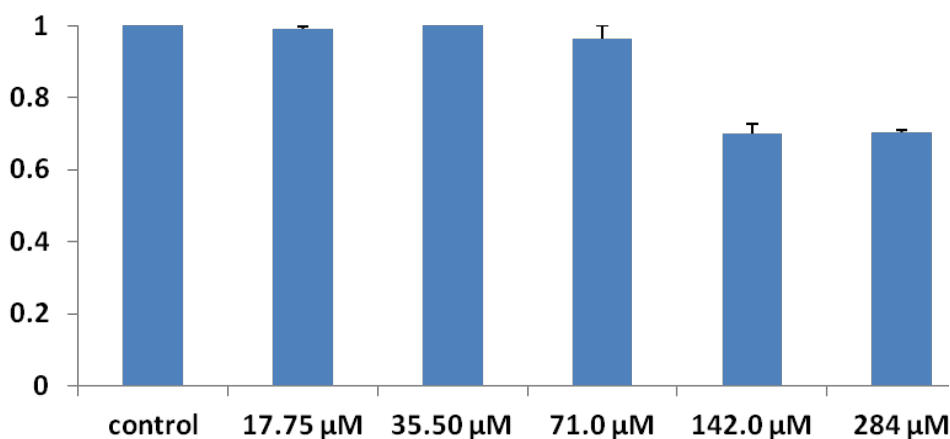


Figure 5: Toxicity studies on human monocytic cell line (THP1) using compound **2.4**

4.7. Antibacterial Studies:

Since compound **2.4** was toxic to *Mtb*, the antibacterial property of the lead compound **2.4** was evaluated against four additional bacterial species. Of these, one is gram-positive (*Bacillus licheniformis* (*B.l.*)), two are gram-negative (*Escherichia coli* (*E.c.*) and *Serratia marcescens* (*S.m.*)) and another is neither gram-positive nor gram-negative (*Paenibacillus elgii* (*P.e.*)). Compound **2.4** showed selective cytotoxicity towards gram-positive bacteria (*B.l.*) and non-toxic to *E.c.*, *P.e.* and *S.m.* as shown in **Figure A3**, see page no **170**. In order to determine minimum inhibitory concentration (MIC_{50}), gram-negative bacteria (*E.c.*) and gram-positive bacteria (*B.l.*) were treated with compound **2.4** at different concentrations in the range of 0-250 μ M. It was found to be non-toxic to *E.c.*, even at high concentration 250 μ M and while showing significant toxicity to *B.l.*, for which the MIC_{50} was determined to be 6 μ M (**Figure 6**).

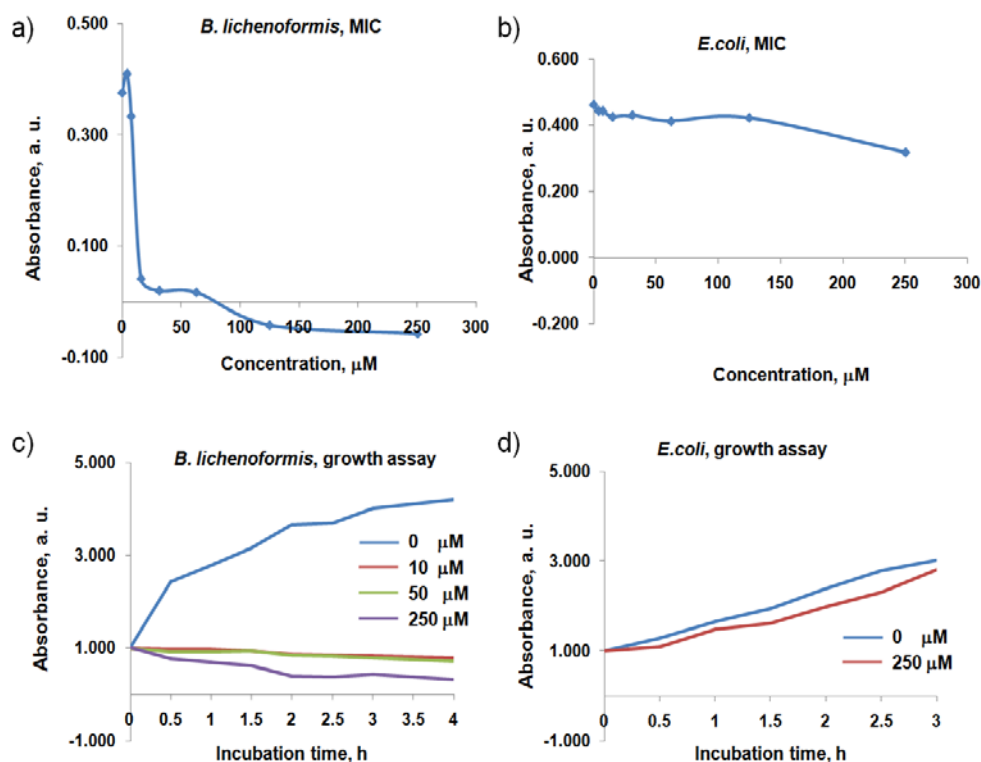


Figure 6: Toxicity studies on various bacterial cell lines using compound 2.4

4.8. Bacterial Staining and Microscopy Studies Using 2.4:

From our previous experiments were known that compound 2.4 is showing specific toxicity towards gram-positive bacteria, but does not show toxicity against gram-negative bacteria. Such specificity could be related to permeability of 2.4 through cell wall/bacterial membrane. In order to understand the mode of action of compound 2.4 and its mechanism, several experiments were performed. Specifically, *in vivo* bioimaging studies were done using the fluorescent compound 2.4 on each of these bacterial (*E.c.* and *B.l.*). For that, bacterial cultures in mid-log phase were treated with compound 2.4 at 250 μM concentration and incubated at 37 °C for 3 hours. The cells were washed with phosphate buffer solution (PBS) and were examined using confocal fluorescence microscopy. The experiment revealed, that in the case of *B.l.* majority of the bacterial cells were stained by compound 2.4, and that compound 2.4 was able to enter and stain the cytoplasm (**Figure 7**). On the other hand, in the case of *E.c.*, very few cells in each field were stained by compound 2.4 and among the stained cells, compound 2.4 appears to be localized on the cell membrane and shows no or very little cytoplasmic staining (**Figure 8**). The results support the hypothesis that the selectivity of compound 2.4 stems from its differential permeability in gram-positive and gram-negative bacteria.

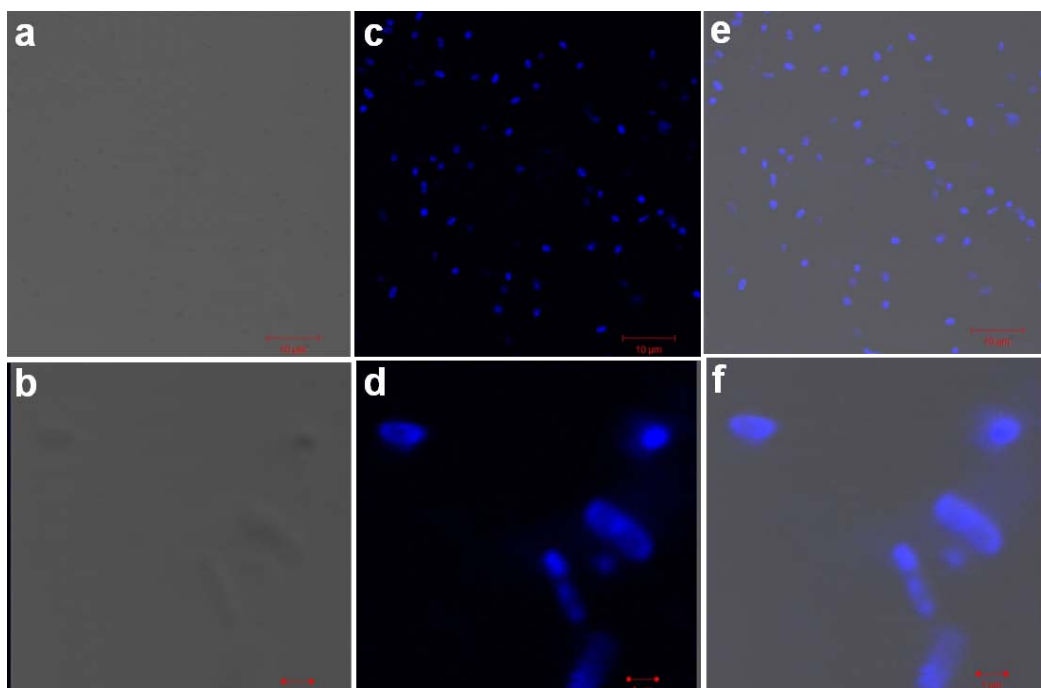


Figure 7: Confocal fluorescent microscopy images ($\lambda_{\text{ex}}=350$ nm) of *B.l.*; a, b) transmitted light image; c, d) fluorescence light image and e, f) overlaid fluorescence and transmitted light images. The images were taken under DAPI channel

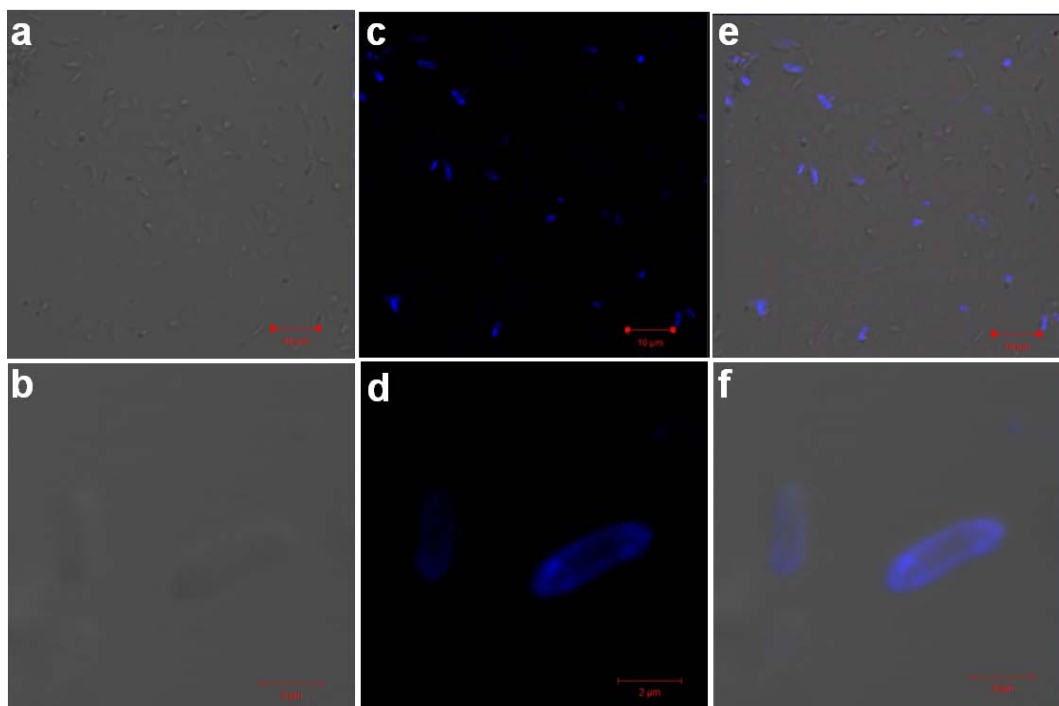


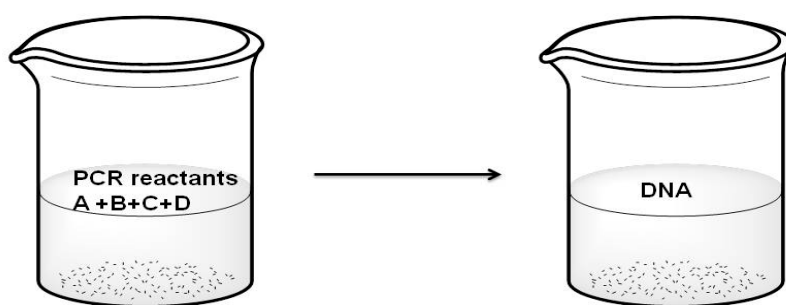
Figure 8: Confocal fluorescent microscopy images ($\lambda_{\text{ex}}=350$ nm) of *E.c.*; a, b) transmitted light image; c, d) fluorescence light image and e, f) overlaid fluorescence and transmitted light images. The images were taken under DAPI channel

4.9. Investigation of the Mechanism of Antibacterial Activity of 2.4

(*Collaborative study with Dr. Aarti's group, Department of Biology, Dr. Reddy's Institute of Life Sciences, University of Hyderabad Campus, India.)

Understanding of mechanism of action of the compound *in vivo* is extremely difficult task. Therefore all further experiments were performed *in vitro*, using PCR. As structurally compound **2.4** is a nucleoside derivative, there is a possibility that compound **2.4** mediates toxicity by interfering with cellular processes that used nucleosides or nucleotides, such as DNA or RNA synthesis and/or processing. Therefore, the first logical step is to check if compound **2.4** is able to bind single or double stranded DNA of various lengths and conformations and it was found that it is unable to do so. Next, the effect of compound **2.4** on DNA polymerization was investigated using the PCR experiment as a simple *in vitro* assay.

PCR is a standard method for amplification of DNA *in vitro* (**Scheme 7**) and the enzyme used in PCR is DNA Polymerase I from the thermophilic bacterium *Thermus aquaticus* (Taq DNA Pol). Once the DNA polymerase binds the primer-template complex, a dNTP (deoxyribonucleotide triphosphate) enters the active site, a conformational change occurs resulting in an open-closed transition in the complex, followed by phosphodiester bond formation. Because of the similarity in the core structure of compound **2.4** and dNTPs, it was expected that compound **2.4** could potentially alter the nucleotide pool or enter the active site of the DNA polymerase and thus interfere with this process.



Where, A=Deoxy-nucleotide triphosphate (dNTPs)

B=Taq DNA Pol

C=DNA template

D=Buffer (reaction medium)

Scheme 7: DNA synthesis by PCR technique

The PCR reaction was performed in the presence of compound **2.4** at various concentrations and PCR efficiency was analyzed by agarose gel electrophoresis of the DNA product. It was found that at 0.1 mM concentration, compound **2.4** shows slight inhibition of PCR (as evidenced by decreased DNA product on the gel). At higher concentrations (0.2 mM-1 mM) it showed complete PCR inhibition (**Figure 9**). One of the possibilities is that **2.4** may interact with one of the components of PCR reaction and thus inhibit DNA replication. For example, because of a similarity in the core structure of compound **2.4** and dNTPs (deoxyribonucleotide triphosphate) required for amplification of DNA, compound **2.4** could potentially alter availability or concentration of the nucleotide pool and thus inhibit DNA polymerase. To test this, the amount of dNTPs used in the PCR was varied, keeping in mind that an excess of dNTPs will compensate for and rescue inhibition caused by compound **2.4**. However, in every condition tested, excess of dNTPs did not rescue the inhibition caused by compound **2.4**, therefore there is no effect of compound **2.4** on dNTPs (**Figure 10**). Another possibility is that compound **2.4** could directly inhibit the DNA polymerase enzyme activity. To test this, the effect of compound **2.4** on PCR was measured in the presence of increasing enzyme concentration. It was found that excess Taq DNA Pol rescued the inhibition caused by compound **2.4** (**Figure 11**). This data suggests that compound **2.4** inhibits PCR by disrupting the polymerase activity of the enzyme Taq DNA Pol.

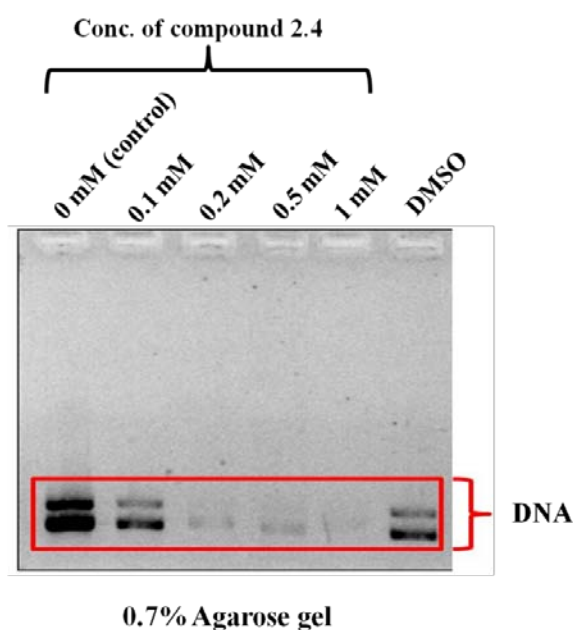


Figure 9: Agarose Gel electrophoresis of PCR amplified DNA: compound **2.4** inhibits PCR in a dose-dependent manner.

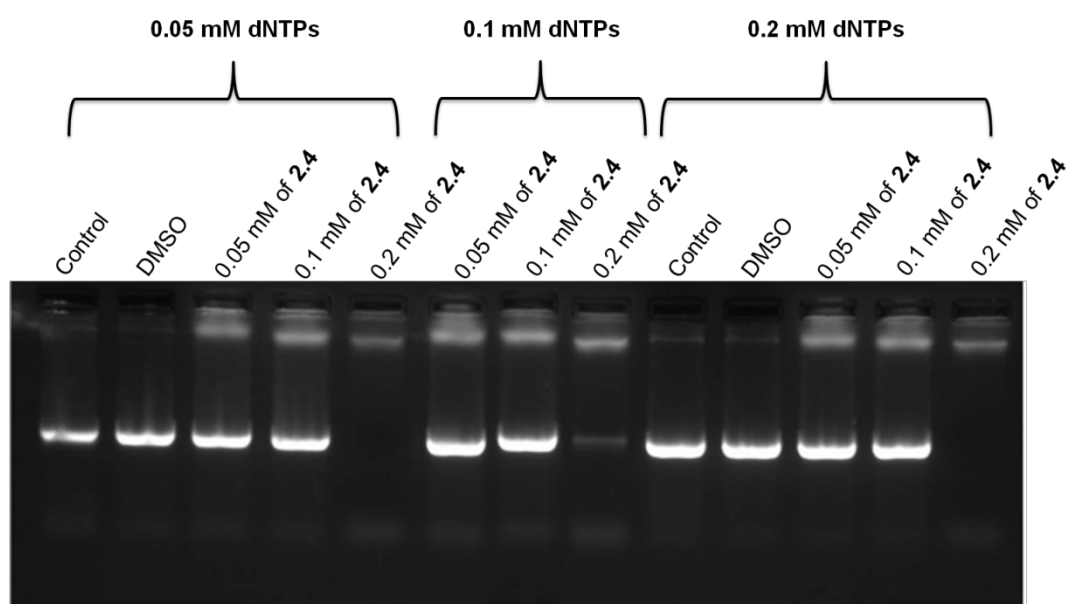


Figure 10: Agarose Gel electrophoresis of PCR amplified DNA: excess dNTPs do not rescue PCR inhibition by compound **2.4**

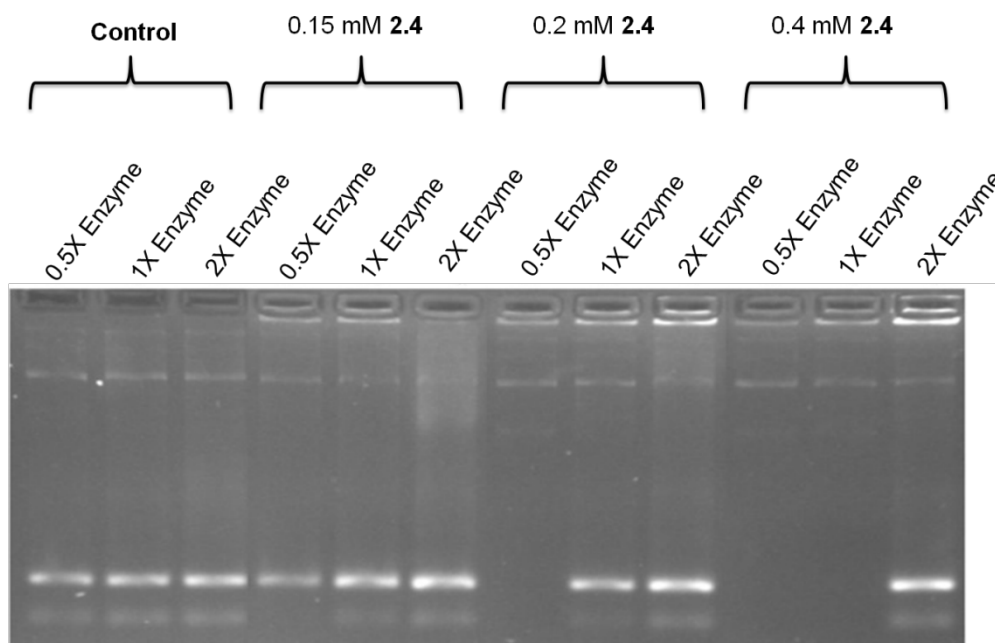


Figure 11: Agarose Gel electrophoresis of PCR amplified DNA: excess DNA polymerase enzyme is able to rescue PCR inhibition by compound **2.4**

Finally, the activity of the individual components of compound **2.4** (uridine, pyrene linker, pyrene and linker) was tested in PCR reaction. Unlike compound **2.4**, each individual component on its own was unable to inhibit PCR and DNA polymerase activity as shown in **Figure 12**.

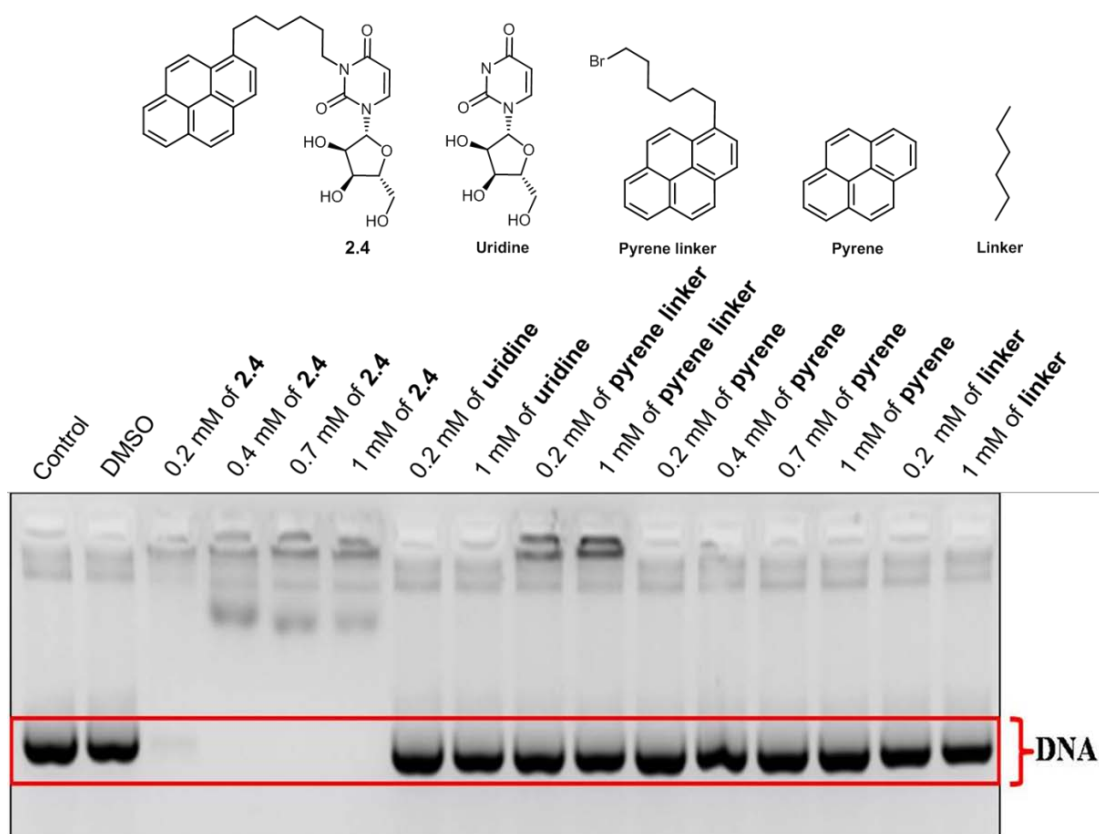


Figure 12: Agarose Gel electrophoresis of PCR amplified DNA: only compound **2.4**, and none of its individual components, are able to inhibit PCR.

4.10. Docking Study of **2.4** with Taq DNA Pol:

(*The docking studies were done by Giridhar Singh Deora, School of Pharmacy, The University of Queensland, Australia.)

In order to further confirm the mechanism of action *via* disruption of DNA polymerization by compound **2.4**, molecular docking studies were performed using Maestro (version 9.8), implemented from Schrödinger molecular modeling suite-2014. Docking of compound **2.4** into the active site of Taq DNA Pol reveals good binding interactions, which is in a good agreement with above *in vitro* results. The molecule is well occupied by the binding site of the enzyme. The aromatic part of compound **2.4** is oriented towards the hydrophobic surface, and sugar moiety is interacting with polar part of the enzyme surface (**Figure 13**). The molecule is interacting *via* hydrogen bonds with Asp610, Tyr611, Ser612, Ile614 and Gln754 residues of the enzyme. In addition, hydrophobic interactions between Phe667 and pyrene moiety of the molecule is observed and docking scores of these interactions are listed in **Table IV**. Hence, the possible basis of inhibition of DNA synthesis by

compound **2.4** observed *in vitro* and in PCR experiments might be the result of binding of compound **2.4** to Taq DNA Pol at a site that is usually bound by dNTPs. Both PCR and molecular docking investigations strongly supported the design principle and suggested that linking of the active biological molecule to the hydrophobic fragment *via* long enough linker can create a promising scaffold.

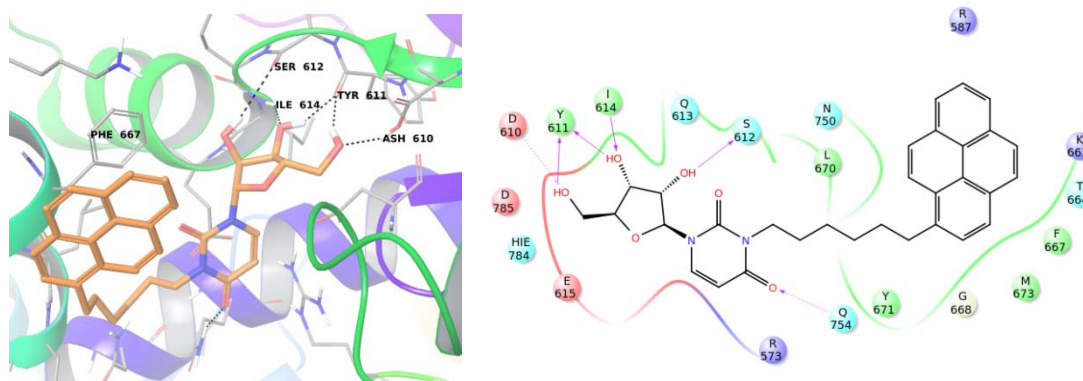


Figure 13: Docking of compound **2.4** with Taq DNA Polymerase-1. Hydrogen bonding with Asp 610, Tyr611, Ser612, Ile614 and Gln754. Hydrophobic interactions with Phe667

Table IV: Glide score and contributing XP parameters (docking with Taq DNA Pol).

Compound code	GScore	LipophilicEvdW	HBond	Electro	RotPenal
2.4	-6.8	-2.9	-3.1	-1.0	0.2

G. Score: glide score

LipophilicEvdW: Chemscore lipophilic pair term and fraction of the total protein-ligand vdw energy

HBond: Rewards for hydrogen bonding interaction between ligand and enzyme

Electro: Electrostatic reward

RotPenal: Rotatable bond penalty

4.11. Examination of Binding Ability of **2.4** to Taq DNA Pol:

In order to further prove the theory that compound **2.4** interacts with Taq DNA Pol, agarose gel electrophoresis was used to resolve reaction mixtures containing compound **2.4** alone, with Taq DNA Pol or with a control protein BSA. It was observed that compound **2.4** was able to enter the gel only in the presence of Taq DNA Pol, and displayed a dramatic increase in fluorescence under those conditions (**Figure 14**). Furthermore, fluorescent properties of the compound **2.4** were employed

for the additional conformation of the proposed mechanism. For that, fluorescent intensity changes of the compound **2.4** were recorded and analyzed along and upon its interaction with Taq DNA Pol enzyme at different concentrations in DMSO/water (2:98) solutions. In biologically compatible DMSO/water solution fluorescence intensity of compound **2.4** decreased significantly in comparison with pure DMSO solution (**Figure 15**). Although the emission maxima for both bands were still observed at the same positions at $\lambda_{em} = 363$ and 384 nm, new very broad red-shifted band appeared with maxima at $\lambda_{em} = \sim 480$ nm. Such changes might be associated with molecular aggregation resulted in aggregation-induced fluorescence quenching or excimer formation.²⁴ Such effect was already observed with structurally similar pyrene-based guanine analogues.²³ Moreover, intensity of the red-shifted fluorescent band increased upon addition of the Taq DNA Pol in concentration dependent manner (the concentration of compound **2.4** was maintained constant). The increase was about 3 folds in presence of the enzyme at 10.5 nM, and reached 25 folds increase at 87.5 nM of the enzyme, although enzyme alone does not exhibit significant fluorescence at the same wavelengths. The emission bands in all cases have broad and structureless features, characteristic for intermolecular exciplex emission, similar to exciplex fluorescence observed for pyrene–bipyridine complexes.²⁵ In this case, exciplex probably forms between pyrene moiety of compound **2.4** and phenylalanine unit in Taq DNA Pol active site (as suggested by molecular modeling study).

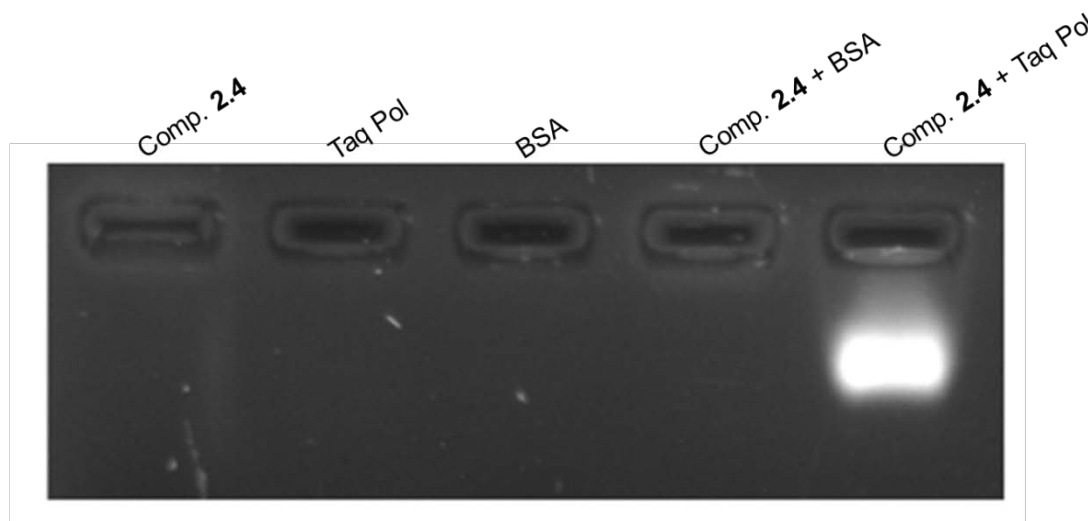


Figure 14: Agarose gel electrophoresis of compound **2.4** in the presence of Taq DNA Pol and BSA

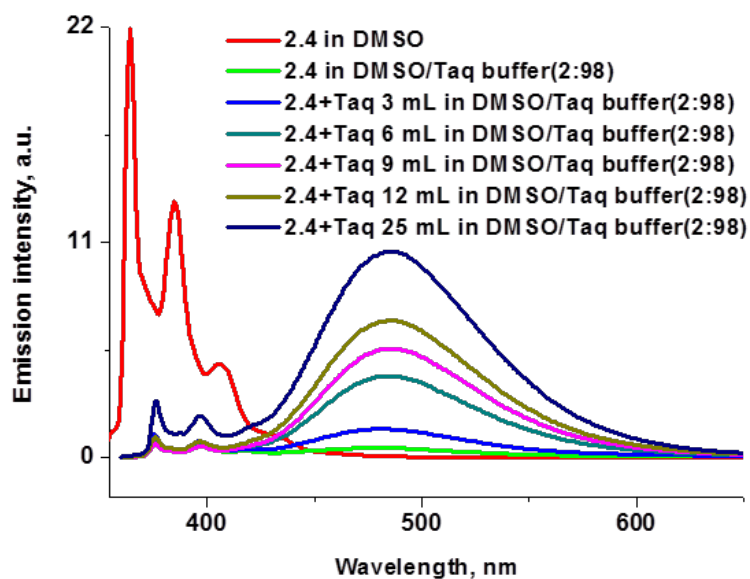


Figure 15: Emission spectra of compound **2.4** with Taq DNA Pol (at various concentrations)

DNA replication is a key cellular process and is a potential target for novel antimicrobials. Several classes of antibiotics that are in the clinic today, target enzymes involved in bacterial DNA replication, however none of these directly target the DNA polymerase domain of any of the bacterial polymerases. Prokaryotic DNA polymerases can be of five types- I to V,²⁶ and each performs a specific cellular function including replication, repair, and damage control. While Pol III (commonly referred to as Pol α) is responsible for most of the replication of the bacterial chromosome, Pol I is the most abundant Polymerase in the cell and is involved in the initiation of replication at the origin, processing of Okazaki fragments and excision repair.

Compound **2.4** appears to directly bind and inhibit the activity of Taq DNA Pol, which belongs to the Pol I family. The docking studies showed that compound **2.4** binds to the active site of the polymerase domain of Taq DNA Pol, occupying the same site that is bound by dNTPs. This binding may be stabilized by the hydrogen bonds formed by compound **2.4** with the residues in the active site, as well as by stacking interactions between the phenylalanine and the fluorescent moiety of compound **2.4**. Such a stable interaction may then prevent dNTP binding or alter the conformation of the enzyme and thus block polymerization.

Given the high degree of conservation of the polymerase domain of the Pol I family members among prokaryotes, compound **2.4** is expected to bind and inhibit the activity of the Pol I family members of other bacterial species as well.²⁷ In addition, all DNA polymerases whose crystal structures are known, share a common overall architecture.^{26,28} More specifically, the “palm” domain responsible for catalytic activity is homologous among the Pol I and Pol III polymerases, and the “finger” domain which interacts with the incoming dNTP shows strong structural similarities. This suggests the possibility that compound **2.4** may also bind and inhibit the activity of the main replicative polymerase Pol III observed in gram-positive bacteria. The elongated cell phenotype characteristic of disrupted cell division observed in *B.l.* cells treated with compound **2.4** lend additional support to this theory (**Figure 16**). It is to be noted that at concentrations where it is extremely toxic to *B.l.* cells, compound **2.4** does not appear to be significantly toxic to the mammalian cells. This may be due to the sterical differences in the placement of the “finger” domain, which prevents tight binding of compound **2.4** to the eukaryotic replicative polymerase Pol α , or due to lower sensitivity of mammalian cells to this compound, or a combination of these and other factors. The selective toxicity of compound **2.4** to gram-positive bacteria stems from the selective entry of compound **2.4** into these bacteria. As demonstrated, compound **2.4** is unable to penetrate the outer membrane in gram-negative cells and is therefore not toxic to them. This stringent selectivity combined with the potency of compound **2.4** against gram-positive bacteria make this a promising lead for development of other compounds with a similar scaffold and design principle.

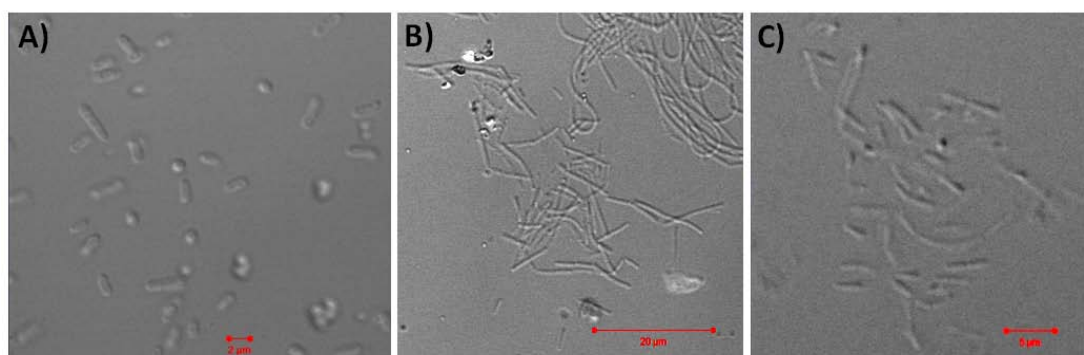


Figure 16: A) Untreated *B.l.* cells (scale 2 μ m); B) *B.l.* cells treated with compound **1** (250 μ M, scale 20 μ m); C) *B.l.* cells treated with compound **1** (250 μ M, scale 5 μ m).

4.12. Morphology Studies:

As compound **2.4** on its own is not soluble in water, the solutions for biological studies were prepared in biocompatible solvent mixture: DMSO/water = 2/98%. For this, compound **2.4** was dissolved in DMSO followed by rapid injection of the solution in water. Usually, such protocol leads to formation of compound's aggregates of micro, sub-micro or nanosize. In order to investigate the morphology and size of the aggregates of **2.4**, SEM and AFM investigations were performed in biocompatible solvent mixture DMSO/H₂O (2:98). For the SEM and AFM studies the sample was prepared as described above and a solution was drop-casted on silica substrate. As expected, both SEM and AFM analysis revealed that compound **2.4** exist in the form of nanoparticles. SEM micrographs revealed the uniform shape and size of nanoparticles (**Figure 17a** and **17b**). Image profile analysis of noncontact-mode AFM images of the nanoparticles showed the average width from 250 nm to 300 nm and height in the range of approximately 90 nm to 100 nm, as shown in **Figure 17c** and **17d**. The size of the nanoparticles is small enough to penetrate into micro organisms.

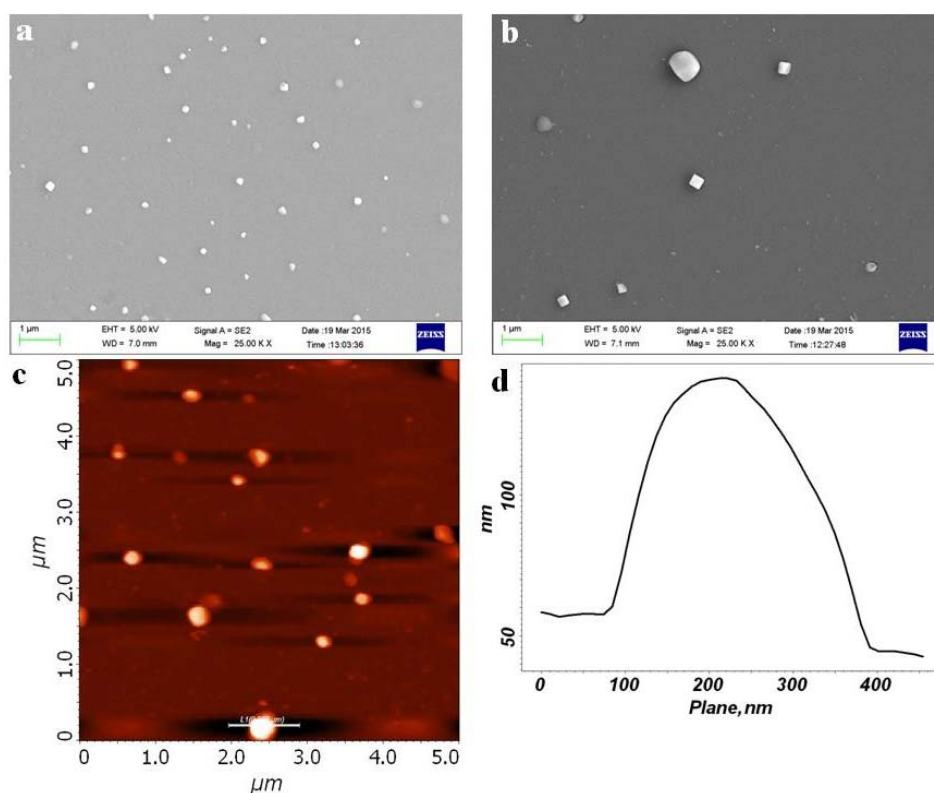


Figure 17: a, b) SEM micrographs of compound **2.4** obtained in DMSO/H₂O (2:98); c) non-contact mode AFM image of nanocrystals of compound **2.4**; d) height and length of selected nanocrystals shown in (c) as a white line

Additionally, we performed Tyndal scattering experiment for solutions containing compound **2.4** in both 100% DMSO and 2% DMSO solutions. Tyndal scattering is described as scattering of light either by particles in colloidal solution or particles in fine suspension.³¹ The Tyndal scattering is importantly used to determine whether it is true solution or colloidal one, If colloidal, it is possible to determine the approximate size and density of particles present in colloidal solution by Mie scattering theory.³² In our case, in 100% DMSO no scattering was displayed (**Figure 18**), whereas importantly pronounced scattering was observed at 2% DMSO solution, which indicates formation of solution stable nanoparticles.

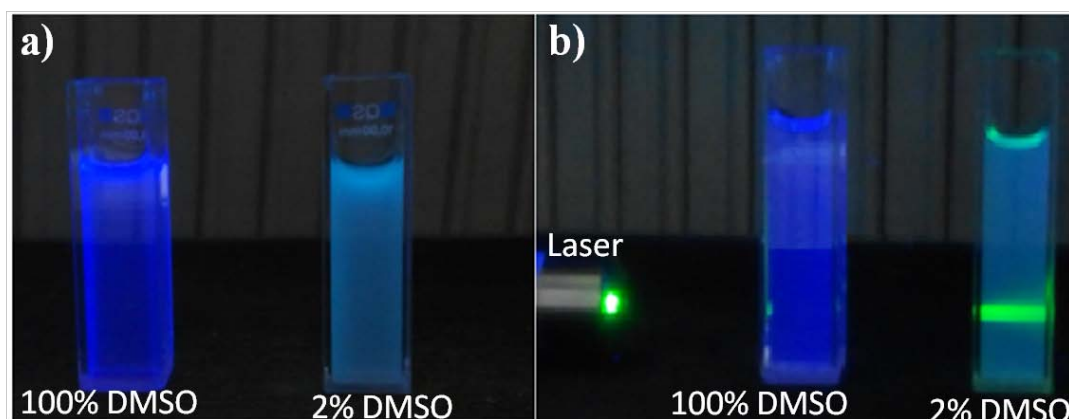


Figure 18: a) Fluorescence properties of **2.4** in 100% DMSO and in 2% DMSO at 10-5 M, b) Tyndal scattering of light observed in 2% DMSO solution, after formation of solution stable nanoparticles.

4.13. Conclusions:

This chapter presented the synthesis of six novel fluorescent nucleosides derivatives through simple and straightforward route using mild conditions. The synthesized nucleosides were tested against *Mtb* and set of other bacteria. Among them uridine based fluorescent organic compound **2.4** exhibited highest inhibition effect on bacterial growth. Compound **2.4** also showed selective inhibitory effect towards gram-positive bacteria without any effect on gram-negative bacteria. Mechanistic studies of inhibition by compound **2.4** were feasible due to fluorescent nature of the latter. Finally, this chapter also proposed the mechanism of inhibition and demonstrated the capability of **2.4** to selectively inhibit *Mtb* and gram-positive bacteria growth by binding to the Taq DNA polymerase enzyme and subsequently inhibiting the DNA replication machinery in those bacterial cells which it enters.

Tyndal scattering, SEM and AFM analysis showed that compound **2.4** exist in the form of nanoparticles, size with the below 300 nm, which probably allow them to penetrate into micro organisms. As the resistance to antibacterials is increasing dramatically every year while number of novel antibiotics is continuously declining, there is an unmet need to develop novel selective antibacterial compounds, such as **2.4**, to effectively combat resistance.

4.14. Experimental Section:

4.14.1. Materials and Methods:

The materials pyrene, n-butyl lithium, uridine, thymidine, cytidine, adenosine, 2,2,6,6-tetramethylpiperdine1-oxyl, trimethylsilyl acetylene, thiophene, tributyltin chloride, bis(triphenylphosphine)palladium(II) dichloride and paraformaldehyde were purchased from Sigma Aldrich. Copper(I) iodide, 1,4-dibromobutane, 1,6-dibromohexane, N-bromosuccinimide, tetrabutylammonium fluoride, iodic acid, iodine, acetyl chloride, imadazole, tert-butyldimethylsilyl chloride and camphorsulfonic acid, 10% palladium on charcoal, EDCI, perchloric acid, bis(acetoxy)iodobenzene were purchased from Spectro Chem. Commercial reagents (NaN_3 , sodium ascorbate, copper(II) sulfate pentahydrate, ammonium bicarbonate, and HCl) were purchased from Merck and Rankem and were used as received. The solvents THF, DMF and acetone were distilled and dried before reactions and for extracting purposes. All reactions were carried out under an inert atmosphere with dry solvents, unless otherwise stated. Syringes and needles for the transfer of reagents were dried at 100 °C and allowed to cool in a desiccator over P_2O_5 before use. Reactions were monitored by thin layer chromatography (TLC) on silica gel plates (60 F254), using UV light detection. Merck silica gel (particle size 100-200 mesh) was used for column chromatography. For UV-Vis and fluorescence measurements spectroscopic grade solvents were used.

4.14.2. Nanoparticles Preparation for Biological Studies:

1.42 mg of compound **2.4** was taken in a sample vial and dissolved in 0.5 mL of DMSO. Then 60 μL of the solution was rapidly injected to 2.94 mL of millipore water to obtain the final concentration of nanoparticles 50 μM in 2% DMSO. Prepared nanoparticles were used for the fluorescent imaging studies immediately.

4.14.3. Nanoparticles Preparation for SEM and AFM Studies:

1.42 mg of compound **2.4** was dissolved in 0.5 mL of DMSO. Then 60 μ L of the solution was rapidly injected into 2.94 mL of millipore water to obtain the final concentration of nanoparticles 50 μ M in 2% DMSO, and the sample vial was left for 4 h without disturbing. Prepared nanoparticles were dispersed on clean silica substrate by a capillary for SEM and AFM studies.

4.14.4. *In Vitro* Antimycobacterial Activity Assay (Mtb, Pathogenic Strain H37Rv):

The compounds (**2.4**, **3.4**, **4.7**, **5.5** and **6.7**) were dissolved in 2% DMSO. The compounds were screened for the antimycobacterial activity using *Mycobacterium tuberculosis*. *Mycobacterium tuberculosis* is grown in Middlebrook 7H9 media and seeded at 5×10^5 to 1×10^6 O.D600 along with the varying amounts (16.5 μ g/mL, 33 μ g/mL, 66 μ g/mL and 132 μ g/mL) of the compounds (**2.4**, **3.4**, **4.7**, **5.5** and **6.7**) and incubated at 37 °C for 7 days in triplicates. After incubation 20 μ L of MTT (3-(4, 5-dimethylthiazol-2-yl)-2, 5-diphenyltetrazolium bromide) was added and incubate at 37 °C for overnight. The formazan crystals were dissolved in DMSO and the absorbance was read at 350 nm.

4.14.5. Cytotoxicity Assay:

The compounds (**2.4**, **3.4**, **4.7**, **5.5** and **6.7**) were dissolved in DMSO. The compounds were screened for the cytotoxicity using (human monocytic cell line *ThP1*). *ThP1* were grown in DMEM and RPMI supplemented with 10% FBS respectively and seeded at 10000 cells and 20000 cells per well along with the varying amounts (16.5 μ g/mL, 33 μ g/mL, 66 μ g/mL and 132 μ g/mL) of the compounds (**2.4**, **3.4**, **4.7**, **5.5** and **6.7**) and incubated at 37°C for 24 h in triplicates. After incubation, 20 μ L of MTT (5mg/mL) (3-(4, 5-dimethylthiazol-2-yl)-2, 5-diphenyltetrazolium bromide) was added and incubated at 37°C for 4 h. The formazan crystals were dissolved in DMSO and the absorbance was read at 350 nm.

4.14.6. Bacterial MIC Assay:

Minimum inhibitory concentration (MICs) for bacterial strains *Escherichia coli* and *Bacillus licheniformis* was studied. Experiment was performed in a standard 96 well plate, compound **2.4** in 2% of DMSO was added to 200 μ L of LB media at different

concentrations (in μM) 250, 125, 62.5, 31.25, 15.625, 7.8125 and 4. DMSO/LB media (2:98) was used as the control. 5% of the secondary culture of $\text{OD}_{600\text{nm}} = 1.0$ was added to the LB media containing compound **2.4**. Another set with identical concentrations of compound **2.4** and LB was maintained as blank without the addition of bacterial culture. Plate was incubated at 37°C , 180 rpm shaking overnight. After overnight incubation absorbance was measured at 600 nm. Experiment was performed in triplicates.

4.14.7. Bacterial Growth Assay:

Overnight bacterial cultures were inoculated (5% inoculums) in 5mL fresh LB containing either 2% DMSO (control) or varied concentrations of compound **2.4** in 2% DMSO. Cultures were grown at 37°C , with shaking at 180 rpm for 4-6 h. OD at 600 nm was measured every 30 minutes and plotted to obtain growth curves.

4.14.8. Bacterial Staining Protocol:

5% inoculated secondary culture in 2 mL of LB media was incubated at 37°C , 180 rpm shaking, harvested at log phase (0.8 – 1.0 OD) and used for the experiment. Cells washed twice with 1X PBS and compound **2.4** was added in 2% DMSO at 250 μM concentration and 2% DMSO was used as control. Cells were incubated at 37°C , 180 rpm shaking for 1 h. After incubation cells were washed twice with 1X PBS and resuspended in 20 μL of 1X PBS. Bacteria were fixed on the slide with mounting media and covered with cover slip. Cells observed using a confocal microscope and images were captured.

4.14.9. Effect of 2.4 on Polymerase Chain Reaction (PCR):

A standard 50 μL PCR reaction was setup using a standard template and corresponding primers. Compound **2.4** in 4% DMSO of varying concentrations was added to the PCR reaction. 4% DMSO was used as the control. Reaction was setup in an Eppendorf thermocycler for 30 cycles (95° for 1', 60° for 30", 72° for 2'). Upon completion, PCR samples were loaded on a 0.7% agarose gel prepared with 1X TAE and prestained with EtBr. After electrophoresis at 100 V for 1h, the DNA was visualized in ultraviolet light and image was captured on a gel-doc.

4.14.10. Docking Study:

Molecular docking studies of compound **2.4** was performed using Maestro (version 9.8), implemented from Schrödinger molecular modeling suite-2014. Molecule was sketched in 3D format using build panel of maestro and energy minimized using OPLS-2005 force field to produce low-energy conformers. The 3D-structural coordinates of *Thermus aquaticus* DNA polymerase-I form complex with deoxyribonucleoside triphosphate were taken from protein data bank (PDB) with PDB id 5KTQ.²⁹ The above Raw PDB protein structure was prepared by giving preliminary treatment like adding hydrogen, refining the loop, and, finally minimized by using OPLS-2005 force field. The grid for docking analysis was generated using structural coordinates of deoxyribonucleoside triphosphate. Molecules were docked using Glide module in Extra-precision (XP) mode, with up to three poses saved per molecule. The ligands were kept flexible, whereas, the receptor was kept rigid throughout the docking studies. The lowest energy conformations were selected and, the ligand-protein interactions (H-Bond and Hydrophobic interactions) with target protein were determined.

4.14.11. Synthesis of Fluorescent Intermediates:

1-(4-bromobutyl)pyrene (1.3a):

To a stirred solution of 1-bromopyrene **1.2** (2g, 7.11 mmol) in anhydrous THF (15 mL) under nitrogen gas, n-BuLi (5.33 mL, 8.53 mmol) was slowly added at 0 °C followed by the addition of 1,4-dibromo butane (15.3 g, 71.1 mmol). The reaction mixture was then refluxed for 2 h. The resulting mixture was washed with water, and extracted with EtOAc and was dried over anhydrous Na₂SO₄. The crude product was purified by column chromatography using hexane as eluent to give compound **1.3a** as a white solid (0.42 g, 18% yield). Mp: 79-81°C. TLC (hexane): R_f = 0.23. IR (KBr): 3035, 2936, 2865, 1599, 1467, 1440, 1298, 1248, 1188, 843, 749, 711 cm⁻¹. ¹H NMR (CDCl₃, 400 MHz) δ : 2.03 (4H, m), 3.37 (2H, t), 3.47 (2H, t), 7.86 (1H, d), 7.99 (2H, t), 8.03 (1H, d), 8.11 (2H, d), 8.16 (1H, d), 8.18 (1H, d), 8.26 (1H, d). ¹³C NMR

(CDCl₃, 100 MHz) δ : 30.2, 32.5, 32.6, 33.6, 123.2, 124.7, 124.8, 124.9, 125.0, 125.1, 125.8, 126.9, 127.2, 127.3, 127.5, 128.6, 129.9, 130.8, 131.4, 136.0; MS (EI, 70ev): m/z [M]⁺ calcd for C₂₀H₁₇Br : 337, found 337.5 [M]⁺. Anal. Calcd for C₂₀H₁₇Br: C, 71.23; H, 5.08; Br, 23.69; found: C, 71.25; H, 5.02.

1-(6-bromohexyl)pyrene (1.3b):

To a stirred solution of 1-bromopyrene **1.2** (5g, 17.79 mmol) in anhydrous THF under nitrogen gas, n-BuLi (13.33 mL, 21.34 mmol) was slowly added at 0 °C followed by the addition of 1,6-dibromo hexane (27.35 mL, 177.9 mmol). The reaction mixture was then refluxed for 2 hours. The resulting mixture was washed with water, and was dried over Na₂SO₄. The crude product was purified by column chromatography (hexane) to give compound **1.3b** as a white solid (1.35 g, 21% yield). Mp: 76-78 °C. TLC (hexane): R_f = 0.30. IR (KBr): 3057, 2926, 2882, 2860, 1463, 1435, 1276, 1194, 843, 761, 706 cm⁻¹. ¹H NMR (CDCl₃, 400 MHz) δ : 1.53 (4H, m), 1.89 (4H, m), 3.3 (2H, t), 3.43 (2H, t), 7.87 (1H, d), 8.0 (2H, t), 8.04 (1H, d), 8.12 (3H, m), 8.17 (1H, d), 8.18 (1H, d), 8.29 (1H, d). ¹³C NMR (CDCl₃, 100 MHz) δ : 136.9, 131.4, 130.9, 129.7, 128.5, 127.5, 127.2, 127.1, 126.5, 125.8, 125.0, 124.8, 124.7, 124.6, 123.4, 34.0, 33.4, 32.7, 31.6, 28.8, 28.1. MS (EI, 70ev): m/z [M]⁺ calcd for C₂₂H₂₁Br: 365.3, found 366.1 [M+1]⁺. Anal. Calcd for C₂₂H₂₁Br: C, 72.33; H, 5.79; Br, 21.87; found: C, 72.37; H, 5.75; N, 23.12.

1-(4-azidobutyl)pyrene (1.4a):

Compound **1.3a** (0.42 g, 1.25 mmol) and sodium azide (0.24 g, 3.75 mmol) were dissolved in dry DMF (5 mL) and were stirred at room temperature for 12 h. DMF

was removed under reduced pressure, and the crude residue was then purified by column chromatography on silica gel with hexane as eluent to yield compound **1.4a** as a white solid (0.32 g, 90%). Mp: 86-88 °C. TLC (hexane): $R_f = 0.23$. IR (KBr): 3046, 2969, 2931, 2854, 2082, 1594, 1468, 1304, 1282, 1249, 1183, 893, 849, 761 cm^{-1} . ^1H NMR (CDCl_3 , 400 MHz) δ : 1.77 (2 H, m), 1.95 (2H, m), 3.33 (2H, t), 3.37 (2H, t), 7.85 (1H, d), 7.99 (2H, t), 8.03 (1H, d), 8.11 (2H, d), 8.15 (1H, d), 8.17 (1H, d), 8.25 (1H, d). ^{13}C NMR (CDCl_3 , 100 MHz) δ : 28.80, 28.89, 32.9, 31.3, 123.2, 124.7, 124.8, 124.9, 125.0, 125.1, 125.8, 126.6, 127.1, 127.3, 127.5, 128.5, 129.9, 130.8, 131.4, 136.0. MS (EI, 70ev): m/z $[\text{M}]^+$ calcd for $\text{C}_{20}\text{H}_{17}\text{N}_3$: 299.0, found 300.0 $[\text{M}+1]^+$. Anal. Calcd for $\text{C}_{20}\text{H}_{17}\text{N}_3$: C, 71.04; H, 4.08; N, 24.88; found: C, 71.03; H, 4.09; N, 24.90.

1-(6-azidohexyl)pyrene (1.4b):

Compound **1.3b** (0.7 g, 1.91 mmol) and sodium azide (0.49 g, 7.67 mmol) were dissolved in dry DMF (5 mL) and were stirred at room temperature for 12 h. DMF was removed under reduced pressure, and the crude residue was then purified by column chromatography on silica gel with hexane as eluent to yield compound **1.4b** as a white solid (0.56 g, 91%). Mp: 88-90 °C. TLC (hexane): $R_f = 0.30$; IR (KBr): 3046, 2931, 2859, 2087, 1599, 1478, 1287, 1254, 1182, 892, 843, 749, 711 cm^{-1} . ^1H NMR (CDCl_3 , 400 MHz) δ : 1.49 (4H, m), 1.62 (2H, m), 1.88 (2H, m), 3.26 (2H, t), 3.3 (2H, t), 7.86 (1H, d), 7.99 (2H, t), 8.02 (1H, d), 8.10 (2H, m), 8.15 (1H,d), 8.17 (1H, d), 8.27 (1H, d). ^{13}C NMR (CDCl_3 , 100 MHz) δ : 136.7, 131.2, 130.7, 129.5, 128.4, 127.3, 127.0, 126.3, 125.6, 124.93, 124.90, 124.6, 124.5, 123.2, 51.2, 33.2, 31.5, 29.0, 28.6, 26.4. MS (EI, 70ev): m/z $[\text{M}]^+$ calcd for $\text{C}_{22}\text{H}_{21}\text{N}_3$: 327.17, found 328.1 $[\text{M}+1]^+$. Anal. Calcd for $\text{C}_{22}\text{H}_{21}\text{N}_3$: C, 80.70; H, 6.46; N, 12.83; found: C, 80.73; H, 6.45; N, 12.85.

6-(pyren-1-yl)hexan-1-amine (1.5b):

To a solution of 1-(6-azido hexyl) pyrene **1.4b** (0.5 g, 1.52 mmol) in ethyl acetate (15 mL), 10% palladium on charcoal (50 mg, 10 wt %) was added and vigorously stirred under H₂ at 1 atm for 12 h or until reaction completion as determined by TLC. After filtration over celite the filtrate was evaporated and the crude residue was then purified by column chromatography using 5% MeOH in DCM yielding of **1.5b** as a yellowish solid (0.31 g, 65% yield). Mp: 118-120 °C. TLC (5% MeOH in DCM): R_f = 0.25. IR (KBr) 3035, 2920, 2854, 1468, 1183, 838, 745, 712 cm⁻¹. ¹H NMR (CDCl₃, 400 MHz) δ: 1.42 (4H, m), 1.50 (2H, m), 1.87 (2H, m), 2.68 (2H, t), 3.34 (2H, t), 7.86 (1H, d), 8.0 (3H, m), 8.12 (4H, m), 8.27 (1H, d). ¹³C NMR (DMSO-*d*₆, 100 MHz) δ: 26.7, 29.3, 31.9, 33.03, 33.08, 41.7, 123.8, 124.63, 124.67, 125.1, 125.2, 126.4, 126.8, 127.5, 127.7, 127.8, 128.4, 129.5, 130.8, 131.3, 137.4. MS (EI, 70eV): *m/z* [M]⁺ calcd for C₂₂H₂₃N: 301.4, found 302.1 [M]⁺. Anal. Calcd for C₂₂H₂₃N: C, 87.66; H, 7.69; N, 4.65; found: C, 87.53; H, 7.62; N, 4.71.

4.14.12. Synthesis of 3-Substituted Uridine Analogue:**2',3'-O-isopropylidene uridine (2.2):**¹⁶

To a suspension of uridine **2.1** (0.5 g, 2.04 mmol) in acetone para-toluenesulfonic acid monohydrate (0.015 g, 0.08 mmol) was added and cooled to 0°C then 2,2-dimethoxypropane (2 mL, 16.44 mmol) and leave it for 4 h at room temperature. The solvent was evaporated under reduced pressure and the residue was diluted with water and extracted with DCM, evaporated and the crude residue was then purified by column chromatography using 70% ethyl acetate in hexane as eluent to yield **2.2** as a

white solid (0.52 g, 90%). Spectroscopic data matches with the one from reported procedure. ^1H NMR ($\text{DMSO-}d_6$, 400 MHz) δ : 1.26 (3H, s), 1.46 (3H, s), 3.54 (2H, m), 4.03 (1H, m), 4.72 (1H, m), 4.86 (1H, m), 5.08 (1H, t), 5.61 (1H, d), 5.80 (1H, d), 7.77 (1H, d), 11.37 (1H, brs).

1-((3aR,4R,6R,6aR)-6-(hydroxymethyl)-2,2-dimethyltetrahydrofuro[3,4-d][1,3]dioxol-4-yl)-3-(6-(pyren-1-yl)hexyl)pyrimidine-2,4(1H,3H)-dione (2.3):

Anhydrous K_2CO_3 (0.246 g, 1.8 mmol) was added to a stirred solution of compound **2.2** (0.177 g, 0.60 mmol) in dry DMF (3 mL) under nitrogen at room temperature. After 30 min, a solution of compound **1.3b** (0.219 g, 0.60 mmol) in DMF (1 mL) was added, and the reaction mixture was stirred further 2h at room temperature. DMF was removed under reduced pressure, and the crude residue was then purified using column chromatography on silica gel with hexane/ethylacetate (1:1) as eluent to yield **2.3** as a white solid (0.315 g, 92%). Mp: 110-114 °C. TLC (50%EtOAc in hexane): R_f = 0.25. ^1H NMR ($\text{DMSO-}d_6$, 400 MHz) δ : 1.21 (2H, m), 1.25 (3H, s), 1.36 (2H, m), 1.46 (3H, s), 1.52 (2H, m), 1.77 (2H, m), 3.28 (2H, t), 3.55 (2H, m), 3.76 (2H, t), 4.09 (1H, m), 4.74 (1H, m), 4.87 (1H, m), 5.08 (1H, bs), 5.73 (1H, d), 5.8 (1H, d), 7.81 (1H, d), 7.93 (1H, d), 8.04 (1H, t), 8.10 (2H, m), 8.20 (2H, m), 8.25 (2H, m), 8.33 (1H, d). ^{13}C NMR ($\text{DMSO-}d_6$, 100 MHz) δ : 162.3, 150.9, 140.5, 137.0, 131.3, 130.8, 129.6, 128.5, 127.4, 127.1, 127.0, 126.3, 125.6, 125.0, 124.7, 124.6, 124.5, 123.4, 114.2, 102.1, 97.2, 86.8, 83.6, 80.2, 62.7, 41.1, 33.4, 31.7, 29.6, 29.4, 27.4, 27.2, 26.8, 25.2. MS (EI, 70eV): m/z $[\text{M}]^+$ calcd for $\text{C}_{34}\text{H}_{36}\text{N}_2\text{O}_6$: 568.6, found 569.2 $[\text{M}+1]^+$. Anal. Calcd for $\text{C}_{34}\text{H}_{36}\text{N}_2\text{O}_6$: C, 71.8; H, 6.38; N, 4.93; O, 16.88, found: C, 71.93; H, 6.48; N, 4.86.

1-((2R,3R,4S,5R)-3,4-dihydroxy-5-(hydroxymethyl)tetrahydrofuran-2-yl)-3-(6-(pyren-1-yl)hexyl)pyrimidine-2,4(1H,3H)-dione (2.4):

To a solution of compound **2.3** (0.15 g, 0.264 mmol) in methanol (5 mL), PTSA (0.15 g, 0.792 mmol) was added. The solution was stirred at room temperature for 12 h. After the completion of the reaction, MeOH was evaporated, and then the residue was placed in EtOAc (200 mL), washed with satd. NaHCO₃ and brine, dried with anhydrous Na₂SO₄ and concentrated. The crude residue was then purified by column chromatography using 5-10% MeOH in DCM yielding white solid **2.4** (0.118 g, 85% yield). Mp: 160-163 °C. TLC (10% MeOH in DCM): R_f = 0.32. ¹H NMR (DMSO-*d*₆, 400 MHz) δ: 1.35 (2H, m), 1.47 (4H, m), 1.76 (2H, m), 3.30 (2H, t), 3.53 (1H, m), 3.60 (1H, m), 3.77 (2H, t), 3.83 (1H, m), 3.94 (1H, m), 4.01 (1H, m), 5.08 (2H, m), 5.36 (1H, d), 5.73 (1H, d), 5.79 (1H, d), 7.91 (2H, dd), 8.03 (1H, t), 8.10 (2H, m), 8.19 (2H, m), 8.24 (2H, m), 8.32 (1H, d). ¹³C NMR (DMSO-*d*₆, 100 MHz) δ: 162.3, 151.1, 139.5, 137.4, 131.3, 130.8, 129.5, 128.4, 127.8, 127.7, 127.5, 126.8, 126.5, 125.3, 125.2, 125.1, 124.64, 124.60, 123.8, 101.3, 89.2, 85.2, 74.1, 70.1, 61.1, 32.9, 31.7, 29.1, 27.4, 26.6. MS (EI, 70ev): *m/z* [M]⁺ calcd for C₃₁H₃₂N₂O₆: 528.6, found 528.7 [M+1]⁺. Anal. Calcd for C₃₁H₃₂N₂O₆: C, 72.27; H, 6.06; N, 5.62; O, 16.05, found: C, 70.32; H, 6.05; N, 5.38.

4.14.13. Synthesis of 3-Substituted Thymidine Analogue:

1-((2R,4S,5R)-4-((tert-butyldimethylsilyl)oxy)-5-(((tert-butyldimethylsilyl)oxy)methyl)tetrahydrofuran-2-yl)-5-methylpyrimidine-2,4(1H,3H)-dione (3.2):¹⁷

To a solution of Thymidine **3.1** (0.2 g, 0.82 mmol) in dry DMF, imadazole (0.166 g, 2.46 mmol) was added and cooled to 0 °C, then add TBDMS-Cl (0.372 g, 2.46 mmol) portion wise and leave at room temperature for 3h. The reaction mixture was diluted with water and extracted with EtOAc (20 mL), dried with anhydrous sodium sulphate and concentrated. The crude residue was then purified by column chromatography using 10% EtOAc in hexane to give white solid **3.2** (0.35 g, 0.74 mmol, 91% yield). Spectroscopic data matches one from reported procedure. ¹H NMR (DMSO-*d*₆, 400 MHz) δ : 11.3 (1H, s), 7.4 (1H, s), 6.13 (1H, t), 4.34 (1H, m), 3.72 (3H, m), 2.17 (1H, m), 2.05 (1H, m), 1.75 (3H, s), 0.86 (9H, s), 0.85 (9H, s), 0.06 (6H, s), 0.05 (6H, s).

1-((2R,4S,5R)-4-((tert-butyldimethylsilyl)oxy)-5-(((tert-butyldimethylsilyl)oxy)methyl)tetrahydrofuran-2-yl)-5-methyl-3-(4-(pyren-1-yl)butyl)pyrimidine-2,4(1H,3H)-dione (3.3):

Anhydrous K₂CO₃ (0.088 g, 0.63 mmol) was added to a stirred solution of compound **3.2** (0.1 g, 0.21 mmol) in dry DMF (3 mL) under nitrogen at room temperature. After 30 min, a solution of compound **1.3a** (0.071 g, 0.21 mmol) in DMF (1 mL) was added, and the reaction mixture was stirred further 2h at room temperature. DMF was removed under reduced pressure, and the crude residue was then purified using column chromatography on silica gel with 10% EtOAc in hexane as eluent to yield **3.3** as a white solid (0.14 g, 92%). Mp 153-156 °C: TLC 10% EtOAc in hexane: R_f = 0.31. ¹H NMR (DMSO-*d*₆, 400 MHz) δ : 8.36 (1H, d), 8.27 (2H, d), 8.21 (2H, dd), 8.13 (2H, m), 8.06 (1H, t), 7.96 (1H, d), 7.46 (1H, s), 6.19 (1H, t), 4.35 (1H, m), 3.89 (2H, t), 3.74 (3H, m), 3.36 (2H, t), 2.15 (2H, m), 1.81 (3H, s), 1.73 (4H, m), 0.87 (9H, s), 0.86 (9H, s), 0.07 (6H, s), 0.05 (6H, s); ¹³C NMR (CDCl₃, 100 MHz) δ : 163.4, 150.8, 136.6, 133.3, 131.3, 130.9, 129.7, 128.5, 127.4, 127.2, 127.1, 126.4, 125.6, 125.0, 124.7, 124.6, 124.5, 123.4, 110.0, 87.7, 85.4, 72.2, 62.9, 41.3, 41.1, 33.1, 29.1, 27.7, 25.9, 25.7, 18.3, 17.9, 13.2, -4.6, -4.8, -5.3, -5.4. MS (EI, 70ev): *m/z* [M]⁺ calcd

for $C_{42}H_{58}N_2O_5Si_2$: 726.3, found 727.3 $[M+1]^+$. Anal. Calcd for $C_{42}H_{58}N_2O_5Si_2$: C, 69.38; H, 8.04; N, 3.85; O, 11.0, found: C, 69.45; H, 8.12; N, 3.81.

1-((2R,4S,5R)-4-hydroxy-5-(hydroxymethyl)tetrahydrofuran-2-yl)-5-methyl-3-(4-(pyren-1-yl)butyl)pyrimidine-2,4(1H,3H)-dione (3.4):

To a solution of compound **3.3** (0.14 g, 0.192 mmol) in methanol (5 mL), camphor sulphonic acid (0.044 g, 0.192 mmol) was added. The solution was maintained at room temperature for 12 h. After the completion of the reaction, MeOH was evaporated, and then the residue was placed in EtOAc (200 mL), washed with satd. aq. $NaHCO_3$ and brine, dried with anhydrous Na_2SO_4 and concentrated. The crude residue was then purified by column chromatography using 5-10% MeOH in DCM yielding of white yellowish solid **3.4** (0.087 g, 91%). Mp: 165-167 °C. TLC (10% MeOH in DCM): R_f = 0.34. 1H NMR ($DMSO-d_6$, 400 MHz) δ : 8.34 (1H, d), 8.24 (2H, m), 8.18 (2H, m), 8.10 (2H, m), 8.03 (1H, t), 7.94 (1H, d), 7.72 (1H, s), 6.19 (1H, t), 5.2 (1H, d), 5.0 (1H, t), 4.18 (1H, m), 3.87 (2H, t), 3.75 (1H, m), 3.55 (2H, m), 3.3 (2H, t), 2.06 (2H, m), 1.78 (3H, s), 1.70 (4H, m). ^{13}C NMR ($DMSO-d_6$, 100 MHz) δ : 163.0, 150.8, 137.1, 135.1, 131.2, 130.8, 129.6, 128.4, 127.9, 127.8, 127.5, 126.8, 126.4, 125.3, 125.2, 125.1, 124.6, 124.5, 123.8, 108.8, 87.7, 85.1, 70.6, 61.6, 32.6, 29.2, 27.5, 13.3. MS (EI, 70eV): m/z $[M]^+$ calcd for $C_{30}H_{30}N_2O_5$: 498.5, found 499.1 $[M]^+$. Anal. Calcd for $C_{30}H_{30}N_2O_5$: C, 72.27; H, 6.06; N, 5.62; O, 16.05, found: C, 72.15; H, 6.12; N, 5.71.

4.14.14. Synthesis of 5-Substituted Cytidine Analogues:

(2R,3R,4R,5R)-2-(acetoxymethyl)-5-(4-amino-2-oxopyrimidin-1(2H)-yl) tetrahydrofuran-3,4-diyl diacetate (4.2):¹⁸

To a stirred solution of cytidine (10 g, 41.1 mmol) in acetic acid (70 mL) was added acetyl chloride (17.6 mL, 246.7 mmol) dropwise at 0 °C, then leave to room temperature for 12 h. After 12 h, the solution was evaporated under reduced pressure and the crude residue was purified by column chromatography using 3% MeOH in DCM yielding of compound **4.2** as a white solid (12.99, 78%). Spectroscopic data matches one from reported procedure. ¹H NMR (DMSO-*d*₆, 400 MHz) δ : 10.19 (1H, brs), 9.01 (1H, s), 8.04 (1H, d), 6.3 (1H, d), 5.92 (1H, d), 5.5 (1H, dd), 5.34 (1H, m), 4.29 (3H, m), 2.07 (9H, s).

(2R,3R,4R,5R)-2-(acetoxymethyl)-5-(4-amino-5-iodo-2-oxopyrimidin-1(2H)-yl)tetrahydrofuran-3,4-diyl diacetate (4.3):¹⁸

To a solution of compound **4.2** (13.0 g, 35.2 mmol) in acetic acid-CCl₄-H₂O (100 mL, 1:1:0.5), iodine (5.32 g, 21.2 mmol) and iodic acid (5.32 g, 30.2 mmol) were added and stirred at 40 °C for 4h. Solvents were removed under reduced pressure, the crude residue was dissolved in DCM and washed with aq. sodium thiosulfate. DCM was evaporated and the crude residue was then purified by column chromatography using 3-5% MeOH in DCM yielding of compound **4.3** as a yellowish solid (13.9 g, 80%). Spectroscopic data matches one from reported procedure. ¹H NMR (CDCl₃, 400

MHz) δ : 8.39 (1H, brs), 7.87 (1H, s), 6.07 (1H, d), 5.68 (1H, brs), 5.36 (2H, m), 4.36 (3H, m), 2.23 (3H, s), 2.11 (3H, s), 2.09 (3H, s).

(2R,3R,4R,5R)-2-(acetoxymethyl)-5-(4-amino-2-oxo-5-((trimethylsilyl)ethynyl)pyrimidin-1(2H)-yl)tetrahydrofuran-3,4-diyl diacetate (4.4):¹⁸

To a solution of compound **4.3** (0.5 g, 1.01 mmol) in dry DCM-Et₃N (15 mL, 1:1), CuI (0.0038 g, 0.02 mmol), PdCl₂(PPh₃)₂ (0.021 g, 0.03 mmol) and TMS-acetylene (0.28 mL, 2.20 mmol) were added under nitrogen atmosphere. The reaction mixture stirred at room temperature for 24 h, solvents were removed under reduced pressure and the crude residue was dissolved in DCM and passed through celite plug. DCM was evaporated and crude residue was purified by column chromatography using 5% MeOH in DCM yielding of compound **4.4** as a yellow solid (0.32 g, 70%). Spectroscopic data matches one from reported procedure. ¹H NMR (CDCl₃, 400 MHz) δ : 9.6 (1H, brs), 7.92 (1H, s), 7.20 (1H, brs), 6.12 (1H, d), 5.32 (2H, m), 4.4 (3H, m), 2.20 (3H, s), 2.11 (3H, s), 2.10 (3H, s), 0.26 (9H, s).

(2R,3R,4R,5R)-2-(acetoxymethyl)-5-(4-amino-5-ethynyl-2-oxopyrimidin-1(2H)-yl)tetrahydrofuran-3,4-diyl diacetate (4.5):¹⁸

To a solution of compound **4.4** (2.0 g, 4.30 mmol) in dry THF (25 mL), 1M TBAF (8.61 mL, 8.60 mmol) was added dropwise and stirred at room temperature for 4 h. THF removed under reduced pressure and the crude yellow oil was purified by

column chromatography using 5% MeOH in DCM yielding of compound **4.5** as a white solid (1.33 g, 95%). Spectroscopic data matches one from reported procedure. ^1H NMR (CDCl_3 , 400 MHz) δ : 8.6 (1H, brs), 7.94 (1H, s), 6.04 (1H, brs), 6.03 (1H, d), 5.38 (1H, m), 5.29 (1H, m), 4.38 (3H, m), 3.38 (1H, s), 2.17 (3H, s), 2.10 (3H, s), 2.06 (3H, s).

(2R,3R,4R,5R)-2-(acetoxymethyl)-5-(4-amino-2-oxo-5-(1-(4-(pyren-1-yl)butyl)-1H-1,2,3-triazol-4-yl)pyrimidin-1(2H)-yl)tetrahydrofuran-3,4-diyl diacetate (4.6a):

To a stirred solution of compound **4.5a** (0.432 g, 1.1 mmol) in dry DMF, 1-(4-azido butyl) pyrene **1.4a** (0.36 g, 1.1 mmol), $\text{CuSO}_4 \cdot 5\text{H}_2\text{O}$ (0.038g, 0.154 mmol) and sodium ascorbate (0.060 g, 0.308 mmol). Stirring was continued for 8h at 80 °C. Solvent was then removed and the crude product was purified by flash column chromatography with DCM/MeOH (2-8%) as an eluent to give compound **4.6a** as a yellowish solid (0.54 g, 72%). Mp: 110-115 °C. TLC (10% MeOH in DCM): R_f = 0.43. IR (KBr): 3347, 3128, 3035, 2936, 2865, 1747, 1670, 1511, 1369, 1232, 1095, 1045, 843, 782 cm^{-1} . ^1H NMR (CDCl_3 , 400 MHz) δ : 1.87 (4H, m), 2.03 (3H, s), 2.08 (6H, s), 3.37 (2H, t), 4.20 (1H, d), 4.32 (1H, m), 4.39 (2H, t), 4.47 (1H, m), 5.23 (1H, m), 5.34 (1H, m), 6.18 (1H, s), 6.86 (1H, brs), 7.86 (1H, d), 7.91 (1H, brs), 7.99 (4H, m), 8.07 (2H, d), 8.15 (3H, m), 8.26 (1H, brs). ^{13}C NMR (CDCl_3 , 100 MHz) δ : 171.1, 170.6, 169.8, 162.6, 154.1, 142.1, 138.1, 135.4, 131.2, 130.7, 129.8, 128.4, 127.3, 127.1, 126.7, 125.8, 124.9, 124.78, 124.74, 123.0, 119.5, 98.6, 79.7, 73.5, 70.0, 63.0, 60.3, 50.4, 32.6, 29.8, 28.2, 21.0, 20.7, 14.1. MS (EI, 70ev): m/z $[\text{M}]^+$ calcd for $\text{C}_{37}\text{H}_{36}\text{N}_6\text{O}_8$: 692.7, found 693.0 $[\text{M}]^+$. Anal. Calcd for $\text{C}_{37}\text{H}_{36}\text{N}_6\text{O}_8$: C, 64.15; H, 5.24; N, 12.13; found: C, 64.13; H, 5.29; N, 12.15.

(2R,3R,4R,5R)-2-(acetoxymethyl)-5-(4-amino-2-oxo-5-(1-(6-(pyren-1-yl)hexyl)-1H-1,2,3-triazol-4-yl)pyrimidin-1(2H)-yl)tetrahydrofuran-3,4-diyl diacetate (4.6b):

To a stirred solution of compound **4.5** (0.432 g, 1.1 mmol) in dry DMF, 1-(6-azido hexyl) pyrene **1.4b** (0.36 g, 1.1 mmol), CuSO₄·5H₂O (0.038g, 0.154 mmol) and sodium ascorbate (0.060 g, 0.308 mmol). Stirring was continued for 8h at 80 °C. Solvent was then removed and the crude product was purified by flash column chromatography with DCM: MeOH (9:1), to yield compound **4.6b** as a yellow solid (0.625 g, 79%). Mp: 142-145 °C. TLC (10% MeOH in DCM): R_f = 0.47. IR (KBr): 3320, 2931, 2860, 1747, 1665, 1501, 1369, 1232, 1090, 1052, 843, 778, 712 cm⁻¹. ¹H NMR (CDCl₃, 400 MHz) δ: 1.44 (2H, m), 1.54 (2H, m), 1.87 (2H, m), 1.96 (2H, m), 1.99 (3H, s), 2.09 (3H, s), 2.11(3H, s), 3.3 (2H, t), 4.23 (1H, d), 4.34 (1H, m), 4.39 (2H, t), 4.55 (1H, m), 5.23 (1H, m), 5.27 (1H, m), 6.24 (1H, m), 6.44 (1H, brs), 7.82 (1H, d), 7.85 (1H, s), 7.99 (4H, m), 8.09 (1H, d), 8.10 (1H, m), 8.16 (2H, d), 8.24 (1H, d), 8.62 (1H, brs). ¹³C NMR (CDCl₃, 100 MHz) δ: 170.7, 169.6, 162.6, 155.3, 142.1, 136.6, 131.3, 130.7, 129.6, 128.4, 127.4, 127.14, 127.13, 126.5, 125.7, 124.9, 124.89, 124.81, 124.69, 124.62, 123.36, 98.4, 79.7, 73.6, 70.0, 63.0, 50.5, 33.2, 31.4, 30.2, 28.9, 26.3, 20.8, 20.5. MS (EI, 70ev): *m/z* [M]⁺ calcd for C₃₉H₄₀N₆O₈: 720.7, found 721.1 [M]⁺.

4-amino-1-((2R,3R,4S,5R)-3,4-dihydroxy-5-(hydroxymethyl)tetrahydrofuran-2-yl)-5-(1-(4-(pyren-1-yl)butyl)-1H-1,2,3-triazol-4-yl)pyrimidin-2(1H)-one (4.7a):

To a slurry of K_2CO_3 in MeOH (0.21 g, 1.55 mmol) in 10 mL was added compound **4.6a** (0.18 g, 0.258 mmol) and the mixture was stirred for 2h. After filtration over celite the filtrate was evaporated and the crude residue was then purified by column chromatography using 20% MeOH in DCM to give compound **4.7a** as a yellowish solid (0.079 g, 52%). Mp: 178-181 °C. TLC (20% MeOH in DCM/MeOH): R_f = 0.27. IR (KBr): 3424, 2926, 2860, 1649, 1567, 1419, 1106, 854 cm^{-1} . 1H NMR (DMSO- d_6 , 400 MHz) δ : 1.77 (2H, m), 2.03 (2H, m), 3.29 (2H, t), 3.65 (1H, dd), 3.81 (1H, dd), 4.01 (2H, m), 4.49 (2H, t), 5.77 (1H, m), 7.8 (1H, brs), 7.94 (1H, d), 7.97 (1H, brs), 8.04 (1H, t), 8.12 (2H, m), 8.24 (5H, m), 8.34 (1H, d), 8.66 (1H, s). ^{13}C NMR (DMSO- d_6 , 100 MHz) δ : 28.6, 30.0, 32.3, 50.0, 59.9, 60.2, 68.6, 74.8, 84.0, 90.2, 96.8, 120.7, 123.8, 124.5, 124.6, 125.2, 125.3, 126.5, 126.9, 127.6, 127.8, 128.4, 129.7, 130.7, 131.2, 136.8, 140.4, 142.6, 154.3, 162.7. MS (EI, 70eV): m/z $[M]^+$ calcd for $C_{31}H_{30}N_6O_5$: 566.0, found 567.0 $[M+1]^+$. Anal. Calcd for $C_{31}H_{30}N_6O_5$: C, 65.71; H, 5.34; N, 14.83, O, 14.12; found: C, 65.59; H, 5.42; N, 14.72.

4-amino-1-((2R,3R,4S,5R)-3,4-dihydroxy-5-(hydroxymethyl)tetrahydrofuran-2-yl)-5-(1-(6-(pyren-1-yl)hexyl)-1H-1,2,3-triazol-4-yl)pyrimidin-2(1H)-one (4.7b):

To a slurry of K_2CO_3 in MeOH (0.18 g, 0.258 mmol) in 15 mL was added compound **4.6b** and the mixture was stirred for 2h. After filtration over celite the filtrate was evaporated and the crude residue was then purified by column chromatography using (DCM: MeOH, 8:2) as eluent to yield compound **4.7b** as a pale yellow solid (0.22 g, 60%). Mp: 120-122 °C. TLC (20% MeOH in DCM): R_f = 0.28. IR (KBr) 3358, 2920, 2843, 1654, 1600, 1512, 1112, 1057, 843, 789 cm^{-1} . 1H NMR (DMSO- d_6 , 400 MHz) δ : 1.33 (2H, m), 1.45 (2H, m), 1.82 (2H, m), 1.84 (2H, m), 3.29 (2H, t), 3.60 (1H, d), 3.78 (1H, d), 3.87 (1H, m), 3.98 (2H, m), 4.37 (2H, t), 5.01 (1H, m), 5.46 (2H, m), 5.76 (1H, m), 7.79 (1H, brs), 7.90 (1H, d), 7.97 (1H, brs), 8.03 (1H, t), 8.10 (2H, m), 8.24 (5H, m), 8.31 (1H, d), 8.62 (1H, s). ^{13}C NMR (DMSO- d_6 , 100 MHz) δ : 164.1, 155.8, 144.0, 141.7, 138.7, 132.7, 132.2, 131.0, 129.8, 129.2, 129.0, 128.2, 127.9,

126.7, 126.5, 126.0, 125.9, 125.2, 122.1, 96.7, 91.7, 85.5, 76.2, 70.1, 61.4, 51.6, 34.3, 33.1, 31.4, 30.2, 27.5. MS (EI, 70eV): m/z $[M]^+$ calcd for $C_{33}H_{34}N_6O_5$: 594.6, found 565.1 $[M]^+$. Anal. Calcd for $C_{33}H_{34}N_6O_5$: C, 66.75; H, 5.76; N, 14.13, O, 13.45; found: C, 66.48; H, 5.71; N, 14.25.

4.14.15. Synthesis of 5'-Substituted Adenosine Analogue:

((3aR,4R,6R,6aR)-6-(6-amino-9H-purin-9-yl)-2,2-dimethyltetrahydrofuro[3,4-d][1,3]dioxol-4-yl)methanol (5.2):²⁰

To a solution of compound **5.1** (0.5 g, 1.87 mmol) in acetone (60 mL) was added 70% perchloric acid (0.21 mL, 2.50 mmol). After completion of reaction, the reaction mixture was cooled to 0 °C and neutralized with aq. ammonium hydroxide. The solid was filtered out and dried under reduced pressure to give **5.2** as a white solid. Spectroscopic data matches one from reported procedure. ¹H NMR (DMSO-*d*₆, 400 MHz) δ : 8.35 (1H, s), 8.17 (1H, s), 7.36 (2H, s), 6.13 (1H, d), 5.35 (1H, dd), 4.97 (1H, dd), 4.22 (1H, d), 3.56 (2H, m), 1.56 (3H, s), 1.34 (3H, s).

(3aS,4S,6R,6aR)-6-(6-amino-9H-purin-9-yl)-2,2-dimethyltetrahydrofuro[3,4-d][1,3]dioxole-4-carboxylic acid (5.3):²⁰

BAIB (1.150 g, 3.58 mmol), TEMPO (50 mg, 0.324 mmol), and a 2',3'-isopropylidene-protected nucleoside **5.2** (0.5 g, 1.62 mmol) were combined in a reaction vessel, and to this mixture was added 2 mL of a 1:1 acetonitrile-water solution. The reaction mixtures were stirred for 4 h. The resulting precipitate was

filtered, triturated sequentially with diethyl ether and acetone, and dried in vacuo to yield compound **5.3** as a white solid. Yield: 90%. Mp: 246-249 °C. Spectroscopic data matches the one from reported procedure. ¹H NMR (DMSO-*d*₆, 400 MHz) δ : 1.53 (3H, s), 1.63 (3H, s), 4.67 (1H, d), 5.48 (1H, d), 5.52 (1H, dd), 6.32 (1H, s), 7.15 (2H, brs), 8.10 (1H, s), 8.23 (1H, s).

(3aS,4S,6R,6aR)-6-(6-amino-9H-purin-9-yl)-2,2-dimethyl-N-(6-(pyren-1-yl)hexyl)tetrahydrofuro[3,4-d][1,3]dioxole-4-carboxamide (5.4):

Compounds **5.3** (0.24 g, 0.747 mmol) and compound **1.5b** (0.22 g, 0.747 mmol) were dissolved in dry DMF (3 mL) and cooled to 0 °C, followed by addition of EDCI and stirred at room temperature for 4h. The reaction mixture was diluted with water and extracted with DCM, solvent was evaporated and the crude residue was purified by column chromatography using 5% MeOH in DCM yielding of compound **5.4** as a yellowish solid (0.35 g, 77%). Mp: 123-126 °C. ¹H NMR (DMSO-*d*₆, 400 MHz) δ : 1.19 (4H, m), 1.37 (3H, s), 1.61 (3H, s), 1.78 (4H, m), 3.01 (1H, m), 3.06 (1H, m), 3.29 (2H, t), 4.69 (1H, d), 5.37 (2H, m), 5.50 (2H, bs), 6.02 (1H, d), 6.89 (1H, t), 7.83 (2H, m), 7.9 (1H, m), 8.01 (2H, d), 8.08 (1H, d), 8.11 (1H, s), 8.16 (2H, m), 8.24 (1H, d), 8.28 (1H, s). ¹³C NMR (DMSO-*d*₆, 100 MHz) δ : 25.4, 27.1, 28.9, 29.1, 31.9, 33.0, 36.2, 38.7, 83.53, 83.56, 86.2, 89.9, 113.3, 119.36, 123.93, 124.58, 124.63, 125.16, 125.31, 125.35, 126.5, 126.8, 127.6, 127.9, 128.4, 129.5, 130.8, 131.3, 137.5, 140.6, 149.2, 152.9, 156.5, 168.7. MS (EI, 70ev): *m/z* [M]⁺ calcd for C₃₅H₃₆N₆O₄: 604.7, found 605.1 [M]⁺. Anal. Calcd for C₃₅H₃₆N₆O₄: C, 69.52; H, 6.0; N, 13.90; O, 10.58, found: C, 69.53; H, 6.05; N, 13.92.

(2S,3S,4R,5R)-5-(6-amino-9H-purin-9-yl)-3,4-dihydroxy-N-(6-(pyren-1-yl)hexyl)tetrahydrofuran-2-carboxamide (5.5):

To a solution of compound **5.4** (0.35 g, 0.579 mmol) in methanol (8 mL) PTSA (0.22 g, 1.15 mmol) added. The solution was stirred for 12 h at RT. After the completion of the reaction, MeOH was evaporated, and the residue was placed in EtOAc (200 mL), washed with satd. aqNaHCO₃ and brine, dried with anhydrous Na₂SO₄ and concentrated. The crude residue was then purified by column chromatography using 20% MeOH in DCM yielding compound **5.5** as a creamy solid (0.28 g, 85% yield). Mp: 180-183 °C. TLC (20% MeOH in DCM): R_f = 0.25. ¹H NMR (DMSO-*d*₆, 400 MHz) δ: 9.04 (1H, t), 8.36 (1H, s), 8.27 (1H, d), 8.23 (2H, d), 8.20 (1H, s), 8.16 (2H, m), 8.09 (2H, m), 8.02 (1H, m), 7.88 (1H, d), 7.47 (1H, bs), 5.94 (1H, d), 5.77 (1H, d), 5.56 (1H, d), 4.60 (1H, m), 4.30 (1H, d), 4.11(1H, m), 3.25 (2H, t), 3.20 (2H, t), 1.72 (2H, m), 1.40 (6H, m). ¹³C NMR (DMSO-*d*₆, 100 MHz) δ: 168.7, 156.5, 149.2, 140.6, 137.5, 131.3, 130.8, 129.5, 128.4, 127.9, 127.6, 126.8, 126.5, 125.35, 125.31, 125.1, 124.6, 124.5, 123.9, 119.3, 113.3, 89.9, 86.2, 83.56, 83.53, 38.7, 36.2, 33.0, 31.9, 29.1, 28.9, 27.1, 25.4. MS (EI, 70eV): *m/z* [M]⁺ calcd for C₃₂H₃₂N₆O₄: 564.6, found 565.2 [M]⁺. Anal. Calcd for C₃₂H₃₂N₆O₄: C, 68.07; H, 5.71; N, 14.88; O, 11.33, found: C, 68.21; H, 5.63; N, 14.78.

4.14.16. Synthesis of Fluorescent N9-Substituted Guanine Analogue:**2-(pyren-1-yl)thiophene (6.3):**²¹

To a solution of compound **6.2** (2.0 g, 7.1 mmol) in dry THF (50 mL) were added bromo pyrene (3.2 g, 8.5 mmol) and $\text{PdCl}_2(\text{PPh}_3)_2$ (0.099 g, 0.014 mmol) under nitrogen atmosphere. After 3 h at reflux, the solvent was removed under reduced pressure, and the residue was purified by column chromatography using hexane as eluent to yield compound **6.3** as a yellowish solid (1.65 g, 82%). Spectroscopic data matches with the one from reported procedure. ^1H NMR (CDCl_3 , 400 MHz) δ : 8.49 (1H, d), 8.20 (3H, m), 8.09 (5H, m), 7.52 (1H, m), 7.38 (1H, m), 7.27 (1H, d).

2-bromo-5-(pyren-1-yl)thiophene (6.4):³⁰

A solution of compound **6.3** (1.1 g, 3.85 mmol) in acetic acid (25 mL) and CH_2Cl_2 (25 mL) was cooled to 0 °C temperature, and then NBS (0.547 g, 3.08 mmol) was added in small portions over 30 min. The solution was stirred at 0 °C for 2h. The mixture was poured into water (100 mL) and the separated organic layer was dried over anhydrous sodium sulphate, and the solvent was evaporated. The crude residue was purified by column chromatography using hexane as an eluent to yield compound **6.4** as a yellowish solid (1.0 g, 72%). Spectroscopic data matches with the one from reported procedure. ^1H NMR (CDCl_3 , 400 MHz) δ : 8.45 (1H, d), 8.19 (3H, m), 8.06 (5H, m), 7.21 (1H, d), 7.12 (1H, d).

2-ethynyl-5-(pyren-1-yl)thiophene (6.5):

Under nitrogen atmosphere, compound **6.4** (1.0 g, 2.75 mmol), TMS-Acetylene (0.540 g, 5.5 mmol), $\text{PdCl}_2(\text{PPh}_3)_2$ (0.058 g, 0.082 mmol), and CuI (0.032 mg, 0.165

mmol) were dissolved in Et₃N (30 mL). The flask was bubbled with nitrogen several times and mixture was heated to 90 °C for 12 h. The reaction mixture was filtered through celite and Et₃N was evaporated. The crude residue was dissolved in methanol (25 mL) add K₂CO₃ (0.87 g, 6.31 mmol) and stirred at room temperature for 2 h. The mixture was poured into water (100 mL) and the separated organic layer was dried over anhydrous sodium sulphate, and the solvent was evaporated. The crude residue was purified by column chromatography using hexane to give yellow solid **6.5** (0.64 g, overall 75%). Mp: 115-116 °C. TLC (hexane): R_f = 0.22. ¹H NMR (CDCl₃, 400 MHz) δ: 8.43 (1H, d), 8.35 (3H, m), 8.25 (3H, m), 8.15 (2H, m), 7.58 (1H, d), 7.45 (1H, d), 4.74 (1H, s). ¹³C NMR (CDCl₃, 100 MHz) δ: 143.6, 134.3, 131.2, 130.6, 128.89, 128.82, 128.5, 128.46, 128.43, 128.0, 127.5, 127.0, 126.1, 125.7, 125.2, 124.4, 124.2, 124.0, 122.5, 86.5, 77.0. MS (EI, 70ev): *m/z* [M]⁺ calcd for C₂₂H₁₂S: 308.4, found 308.6 [M]⁺. Anal. Calcd for C₂₂H₁₂S: C, 85.68; H, 3.92; S, 10.40; found: C, 85.73; H, 3.95.

A mixture of compound **6.5** (0.2 g, 0.64 mmol), compound **6.6** (0.245 g, 0.64 mmol) and CuI (0.012 g, 0.064 mmol) in DMF (3 mL) was stirred at 80 °C for 12 h. The reaction mixture was filtered through celite and filtrate was washed with water and extracted with DCM. After evaporation of DCM, the crude residue was purified by column chromatography using 70% EtOAc in hexane as eluent to yield **6.7** as a yellowish solid (0.22 g, 50%). Mp: 150-153 °C. TLC (EtOAc): R_f = 0.47. ¹H NMR (DMSO-*d*₆, 400 MHz) δ: 8.60 (1H, s), 8.53 (1H, d), 8.34 (3H, m), 8.24 (3H, m), 8.13 (3H, m), 7.60 (1H, d), 7.48 (1H, d), 6.91 (2H, s), 4.41 (2H, t), 3.99 (2H, t), 1.86 (2H, m), 1.72 (2H, m), 1.18 (16H, m). ¹³C NMR (CDCl₃, 100 MHz) δ: 160.1, 154.4, 149.6, 143.6, 141.8, 140.6, 134.6, 131.3, 131.0, 130.7, 129.6, 129.3, 129.1, 128.7, 128.5, 128.38, 128.33, 127.7, 127.0, 126.1, 125.7, 125.4, 125.1, 124.6, 124.5, 124.2, 123.7, 121.2, 50.1, 43.3, 29.9, 29.2, 28.8, 28.7, 26.3, 26.2. MS (EI, 70ev): *m/z* [M]⁺ calcd for

C₃₉H₃₉ClN₈S: 687.3, found 687.2 [M]⁺. Anal. Calcd for C₃₉H₃₉ClN₈S: C, 68.15; H, 5.72; Cl, 5.16; N, 16.30; S, 4.67, found: C, 68.26; H, 5.78; N, 16.18.

4.15. References:

- (1) Spigelman, M. K. *J. Infect. Dis.* **2007**, *196*, S28.
- (2) Dye, C.; Scheele, S.; Dolin, P.; Pathania, V.; Raviglione, M. C.; for the, W. H. O. G. S.; Monitoring, P. *J. Am. Med. Assoc.* **1999**, *282*, 677.
- (3) Daffe, M.; Draper, P. *Adv. Microb. Physiol.* **1998**, *39*, 131.
- (4) Wivagg, C. N.; Bhattacharyya, R. P.; Hung, D. T. *J. Antibiot.* **2014**, *67*, 645.
- (5) Zumla, A.; Nahid, P.; Cole, S. T. *Nat. Rev. Drug Disc.* **2013**, *12*, 388.
- (6) (a) Koch, M. A.; Schuffenhauer, A.; Scheck, M.; Wetzel, S.; Casaulta, M.; Odermatt, A.; Ertl, P.; Waldmann, H. *Proc. Nat. Acad. Sc. U. S.* **2005**, *102*, 17272. (b) Stark, L. M.; Lin, X.-F.; Flippin, L. A. *J. Org. Chem.* **2000**, *65*, 3227. (c) Phillips, S. D.; Castle, R. N. *J. Heterocycl. Chem.* **1981**, *18*, 223.
- (7) Bobek, M.; Kawai, I.; Sharma, R. A.; Grill, S.; Dutschman, G.; Cheng, Y. C. *J. Med. Chem.* **1987**, *30*, 2154.
- (8) Crandall, I. E.; Wasilewski, E.; Bello, A. M.; Mohammed, A.; Malhotra, P.; Pai, E. F.; Kain, K. C.; Kotra, L. P. *J. Med. Chem.* **2013**, *56*, 2348.
- (9) Sriharsha, S. N.; Satish, S.; Shashikanth, S.; Raveesha, K. A. *Bioorg. Med. Chem.* **2006**, *14*, 7476.
- (10) Van Rompay, A. R.; Johansson, M.; Karlsson, A. *Pharmacol. Ther.* **2003**, *100*, 119.
- (11) (a) Srivastav, N. C.; Shakya, N.; Bhavanam, S.; Agrawal, A.; Tse, C.; Desroches, N.; Kunimoto, D. Y.; Kumar, R. *Bioorg. Med. Chem.* **2012**, *22*, 1091. (b) Rai, D.; Johar, M.; Manning, T.; Agrawal, B.; Kunimoto, D. Y.; Kumar, R. *J. Med. Chem.* **2005**, *48*, 7012.
- (12) Johar, M.; Manning, T.; Kunimoto, D. Y.; Kumar, R. *Bioorg. Med. Chem.* **2005**, *13*, 6663.
- (13) Beres, J.; Bentrude, W. G.; Balzarini, J.; De Clercq, E.; Otvos, L. *J. Med. Chem.* **1986**, *29*, 494.
- (14) Hu, J.-Y.; Feng, X.; Seto, N.; Do, J.-H.; Zeng, X.; Tao, Z.; Yamato, T. *J. Mol. Struct.* **2013**, *1035*, 19.
- (15) Kurteva, V. B.; Santos, A. G.; Afonso, C. A. M. *Org. Biomol. Chem.* **2004**, *2*, 514.

- (16) Shen, X.-M.; Zheng, B.-Y.; Huang, X.-R.; Wang, L.; Huang, J.-D. *Dalton Trans.* **2013**, 42, 10398.
- (17) Lin, G.; Chen, C.-H.; Pink, M.; Pu, J.; Li, L. *Chem. Eur. J.* **2011**, 17, 9658.
- (18) Piton, N.; Mu, Y.; Stock, G.; Prisner, T. F.; Schiemann, O.; Engels, J. W. *Nucleic Acids Res.* **2007**, 35, 3128.
- (19) Zhang, B.; Cui, Z.; Sun, L. *Org. Lett.* **2000**, 3, 275.
- (20) Epp, J. B.; Widlanski, T. S. *J. Org. Chem.* **1998**, 64, 293.
- (21) Kim, J.; Park, S. H.; Cho, S.; Jin, Y.; Kim, J.; Kim, I.; Lee, J. S.; Kim, J. H.; Woo, H. Y.; Lee, K.; Suh, H. *Polymer* **2010**, 51, 390.
- (22) Kim, J.-J.; Choi, H.; Lee, J.-W.; Kang, M.-S.; Song, K.; Kang, S. O.; Ko, J. J. *Mater. Chem.* **2008**, 18, 5223.
- (23) Reddy, E. R.; Banote, R. K.; Chatti, K.; Kulkarni, P.; Rajadurai, M. S. *Chem. Bio. Chem.* **2012**, 13, 1889.
- (24) (a) Duhamel, J. *Polymers* **2012**, 4, 211. (b) Winnik, F. M. *Chem. Rev.* **1993**, 93, 587. (c) Dabrowski, M. J.; Schrag, M. L.; Wienkers, L. C.; Atkins, W. M. *J. Am. Chem. Soc.* **2002**, 124, 11866.
- (25) (a) McManus, G. J.; Perry; PerryPerry, M.; Wagner, B. D.; Zaworotko, M. J. *J. Am. Chem. Soc.* **2007**, 129, 9094. (b) Wagner, B. D.; McManus, G. J.; Moulton, B.; Zaworotko, M. J. *Chem. Commun.* **2002**, 2176.
- (26) Steitz, T. A. *J. Biol. Chem.* **1999**, 274, 17395.
- (27) (a) Kim, Y.; Eom, S. H.; Wang, J.; Lee, D.-S.; Suh, S. W.; Steitz, T. A. *Nature* **1995**, 376, 612. (b) Ollis, D. L.; Brick, P.; Hamlin, R.; Xuong, N. G.; Steitz, T. A. *Nature* **1985**, 313, 762. (c) Kiefer, J. R.; Mao, C.; Braman, J. C.; Beese, L. S. *Nature* **1998**, 391, 304.
- (28) Brautigam, C. A.; Steitz, T. A. *Curr. Opin. Struct. Biol.* **1998**, 8, 54.
- (29) Li, Y.; Kong, Y.; Korolev, S.; Waksman, G. *Protein Sci.* **1998**, 7, 1116.
- (30) Wang, J.-L.; Tang, Z.-M.; Xiao, Q.; Ma, Y.; Pei, J. *Org. Lett.* **2009**, 11, 863.
- (31) Tyndall, J. *New Fragments* **1896**, 386.
- (32) Lindner, H.; Fritz, G.; Glatter, O. *J. Colloid Interface Sci.* **2001**, 242, 239.

4.16. Appendix:

4.16.1. *In Vitro* Anti-Mycobacterial Studies of Various Nucleosides:

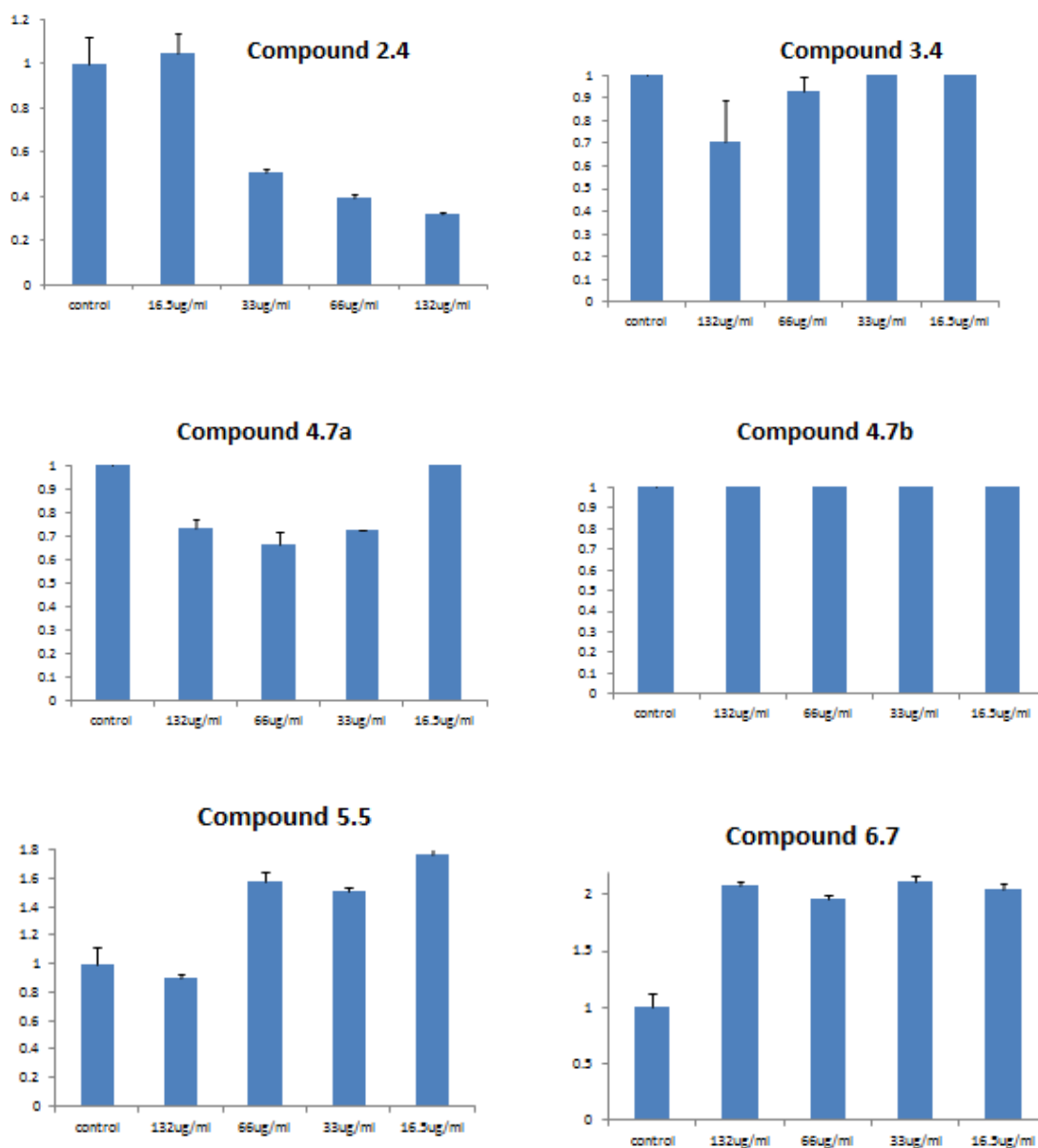


Figure A1: Toxicity studies on *Mycobacterium tuberculosis* using various nucleosides analogues

4.16.2. *In Vitro* Cytotoxicity Assay of Human Monocytic Cell Lines:

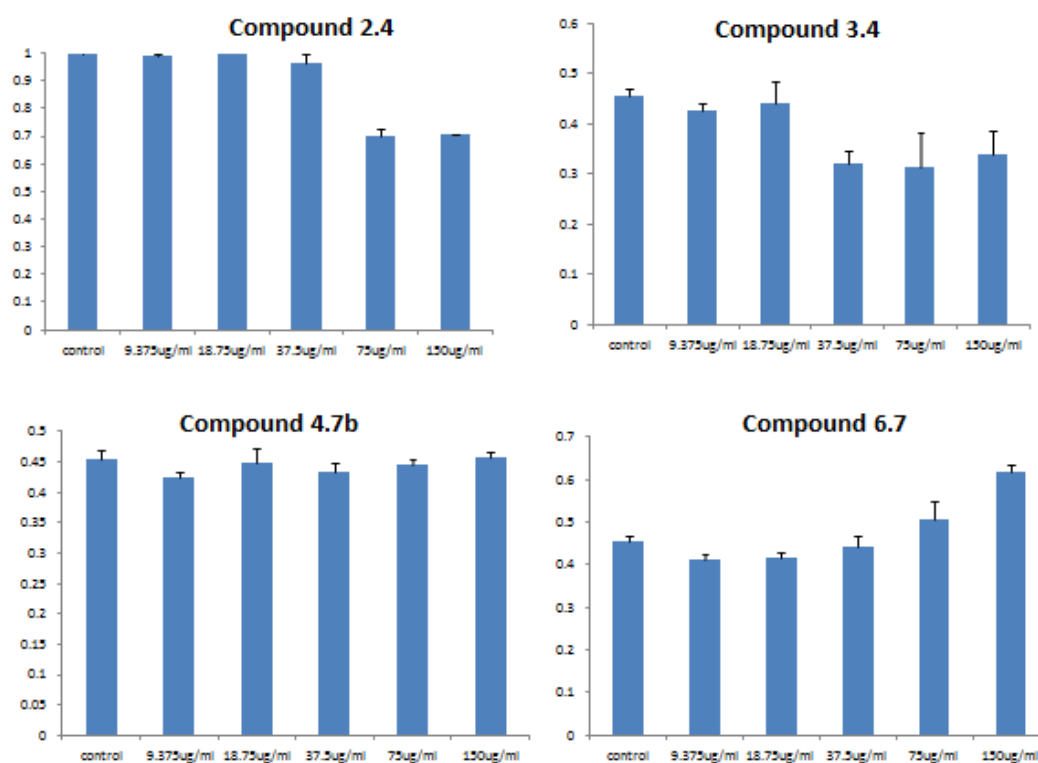


Figure A2: Toxicity studies on human monocytic cell lines (THP 1) using various nucleosides analogues

4.16.3. Toxicity Study on Various Bacterial Cell Lines:

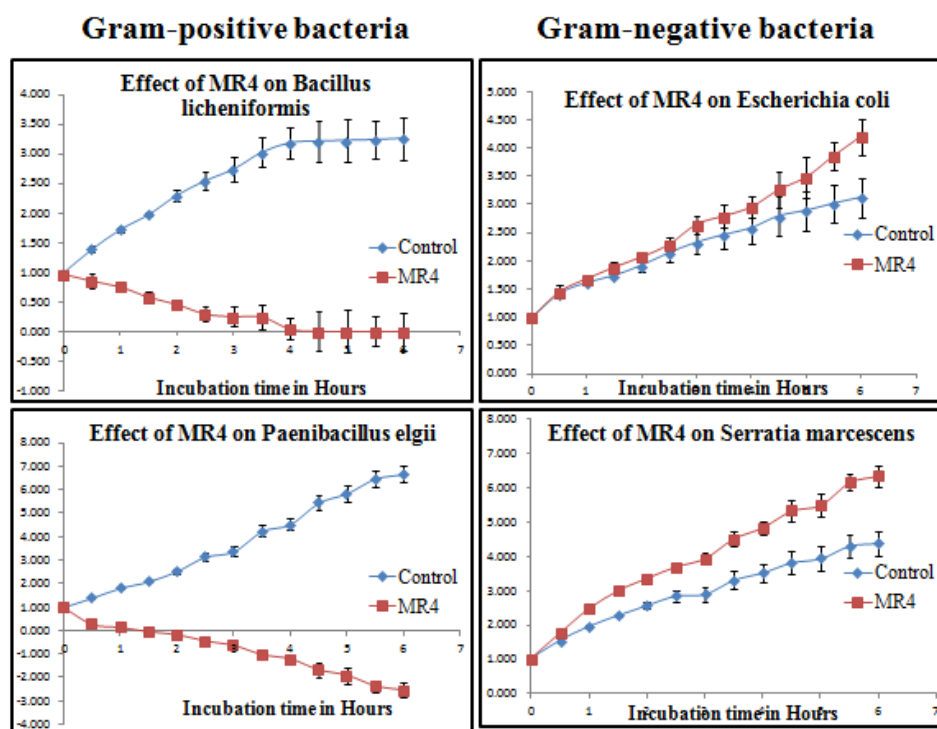
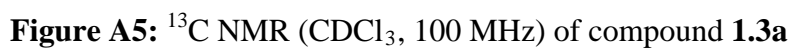
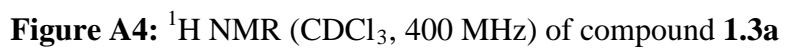


Figure A3: Toxicity studies on various bacterial cell lines using compound 2.4



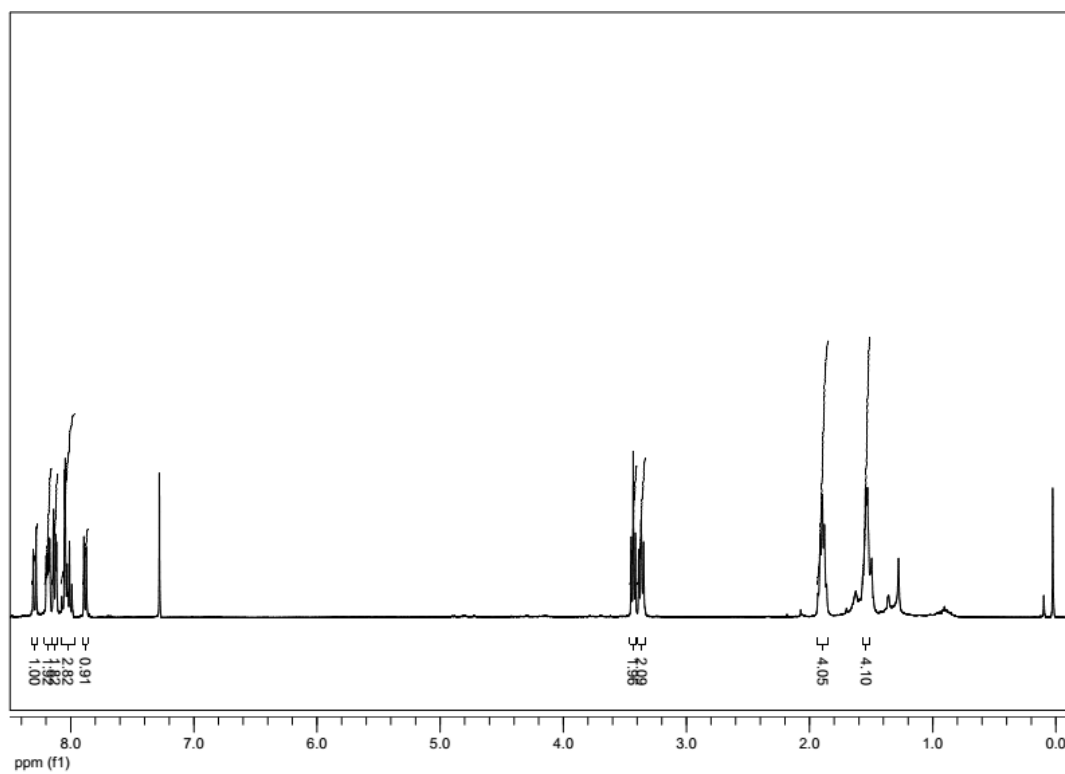


Figure A6: ^1H NMR (CDCl_3 , 400 MHz) of compound **1.3b**

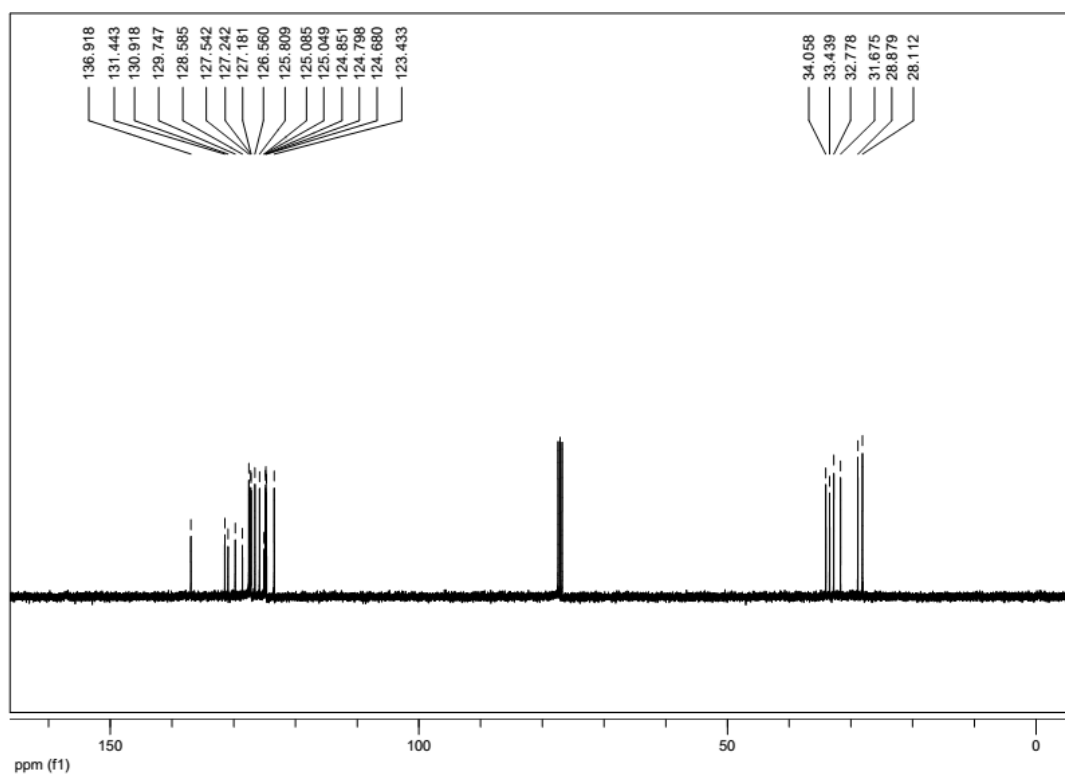


Figure A7: ^{13}C NMR (CDCl_3 , 100 MHz) of compound **1.3b**

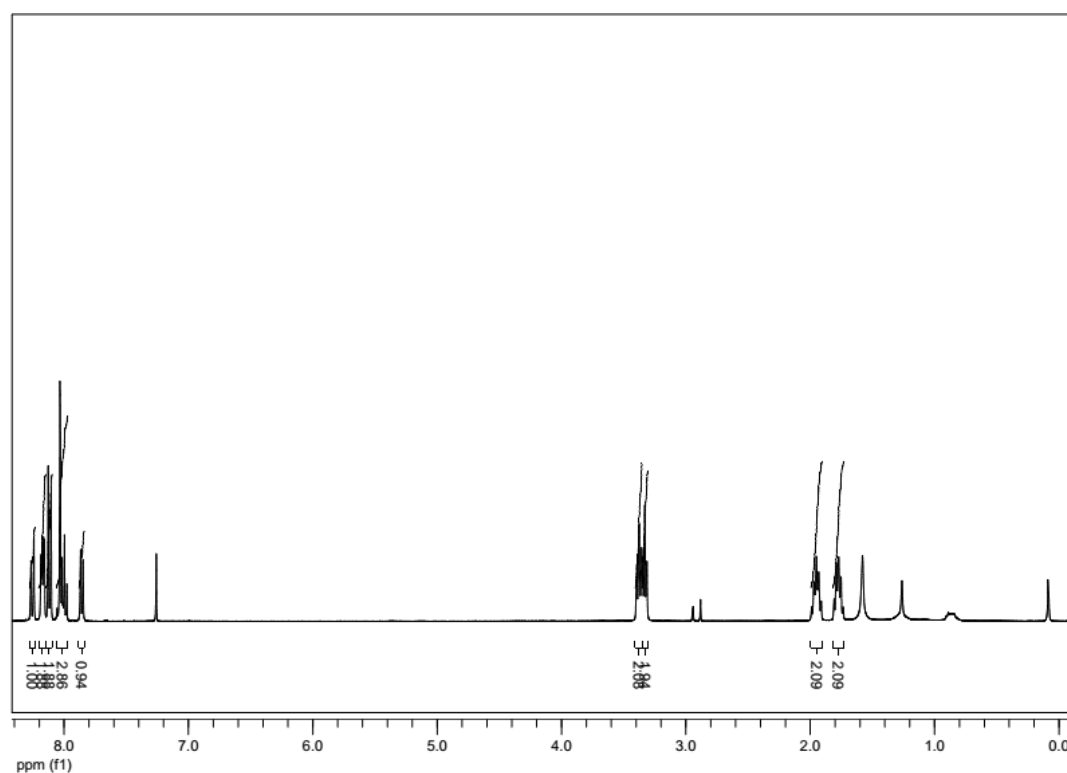


Figure A8: ^1H NMR (CDCl_3 , 400 MHz) of compound **1.4a**

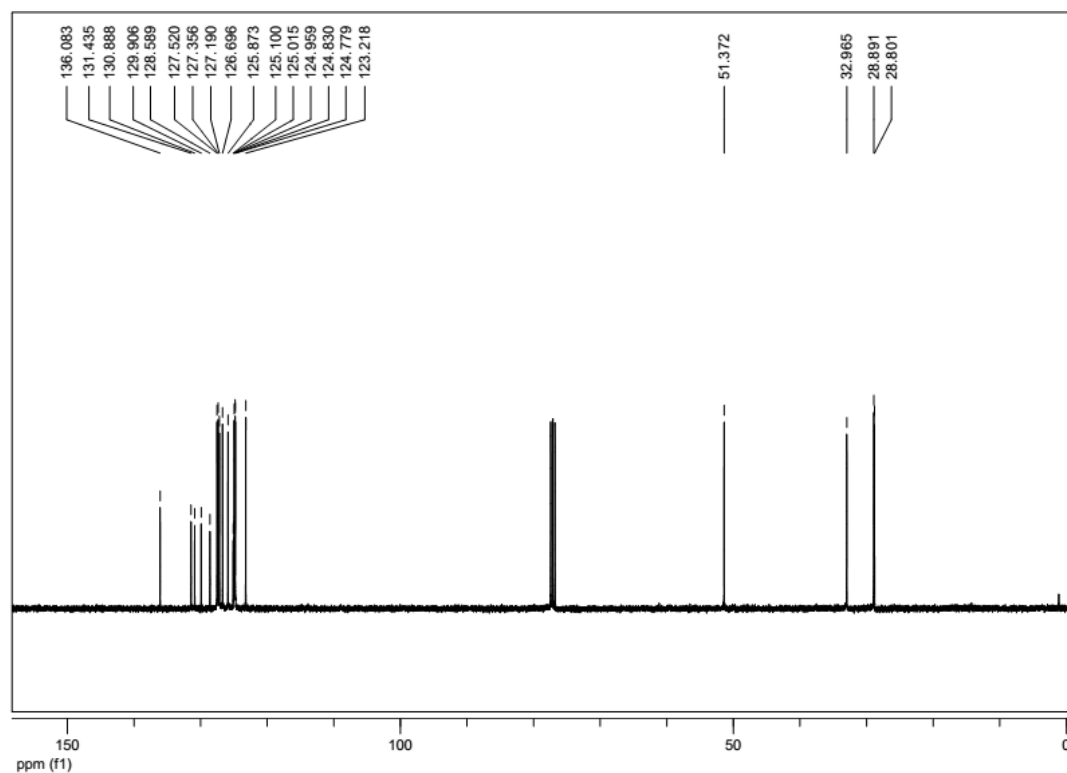


Figure A9: ^{13}C NMR (CDCl_3 , 100 MHz) of compound **1.4a**

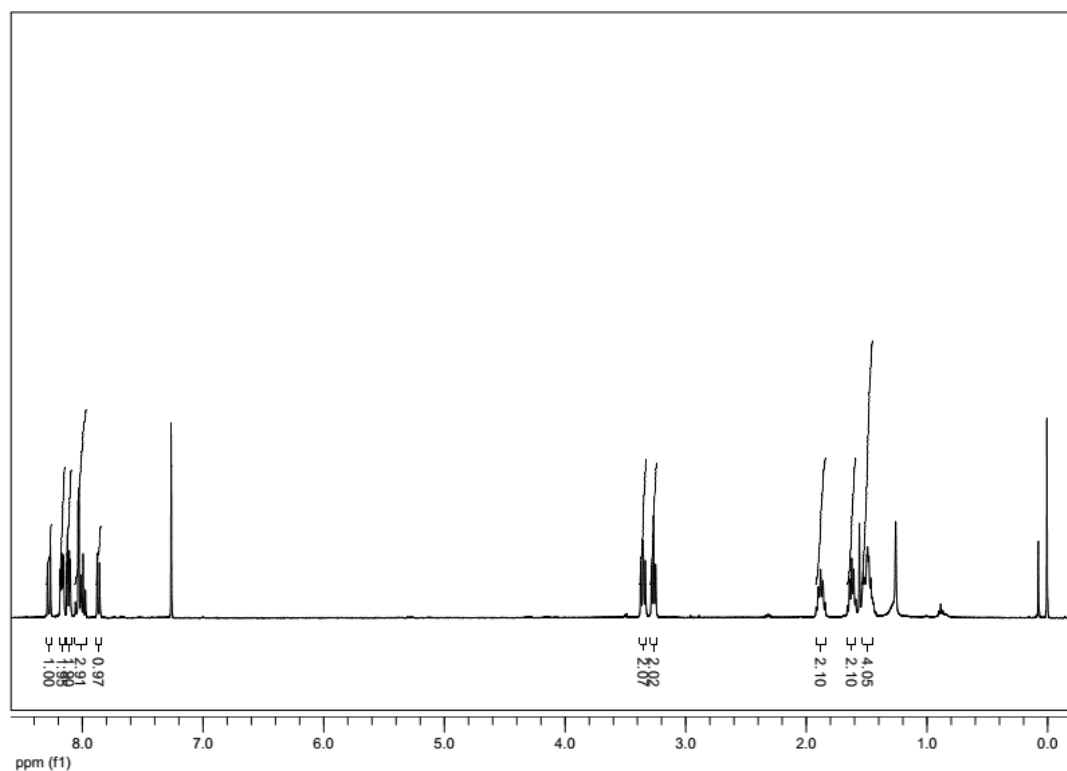


Figure A10: ¹H NMR (CDCl₃, 400 MHz) of compound **1.4b**

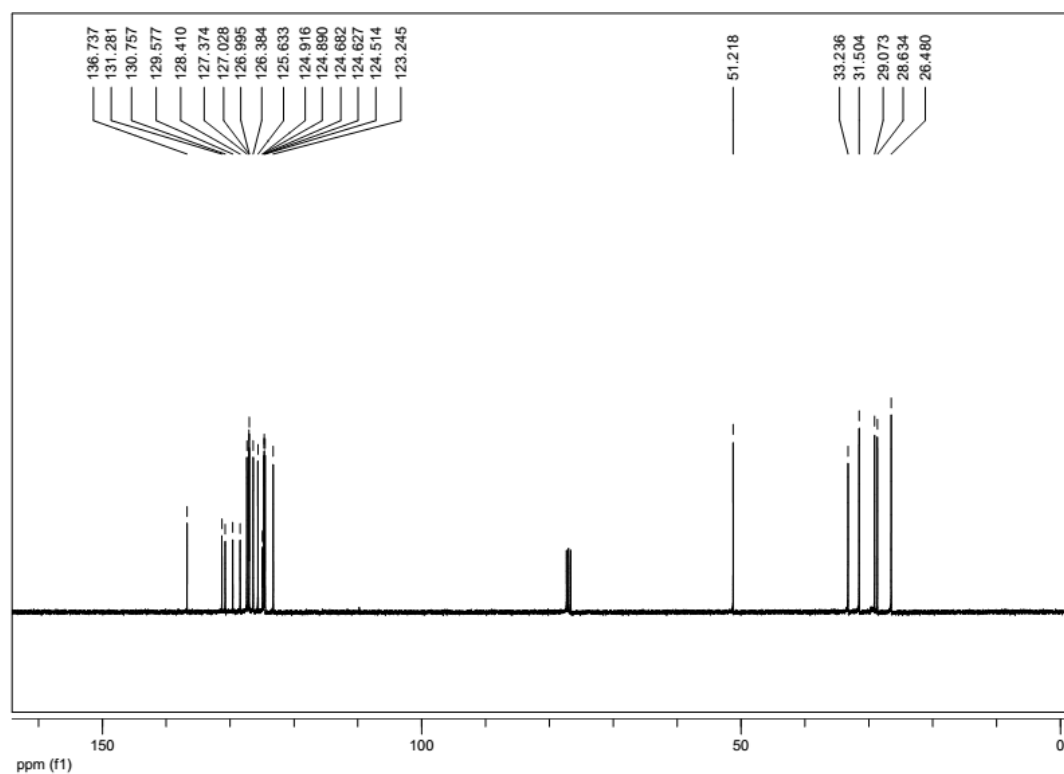


Figure A11: ¹³C NMR (CDCl₃, 100 MHz) of compound **1.4b**

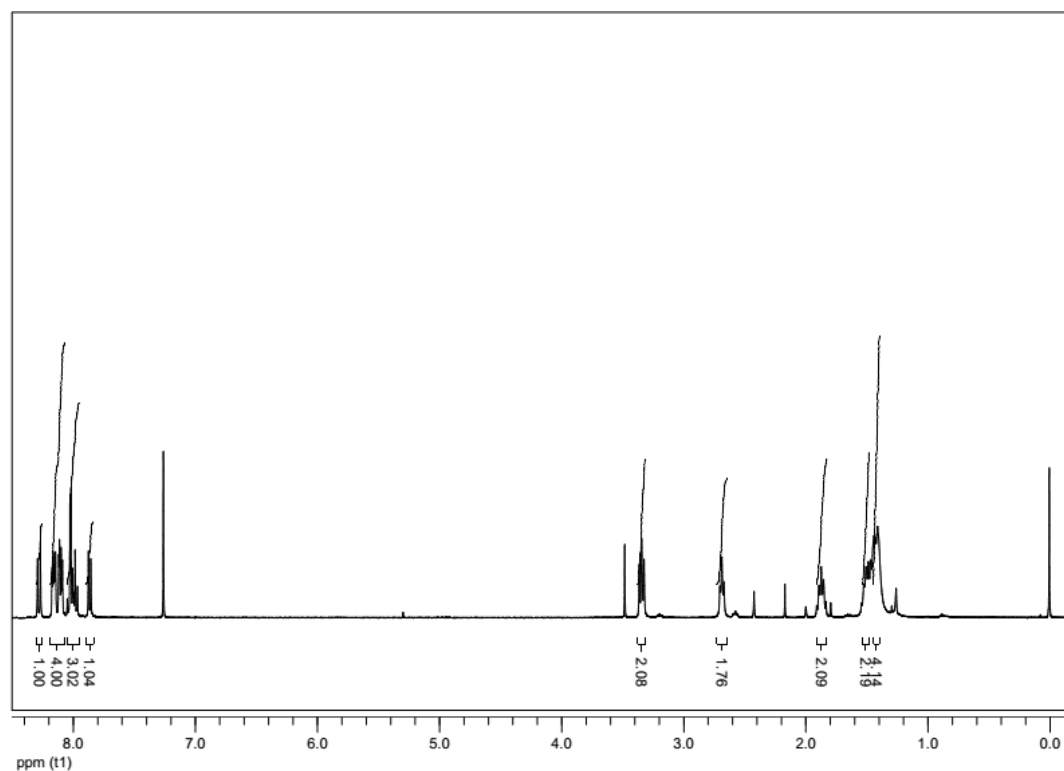


Figure A12: ¹H NMR (CDCl₃, 400 MHz) of compound **1.5b**

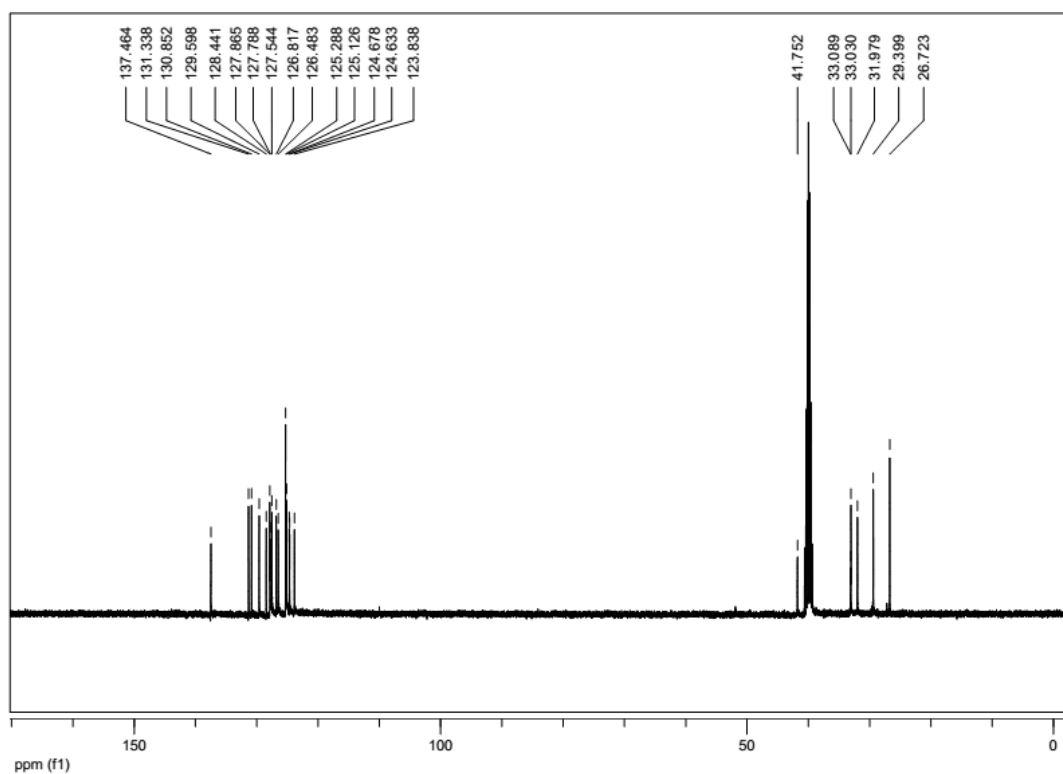


Figure A13: ¹³C NMR (CDCl₃, 100 MHz) of compound **1.5b**

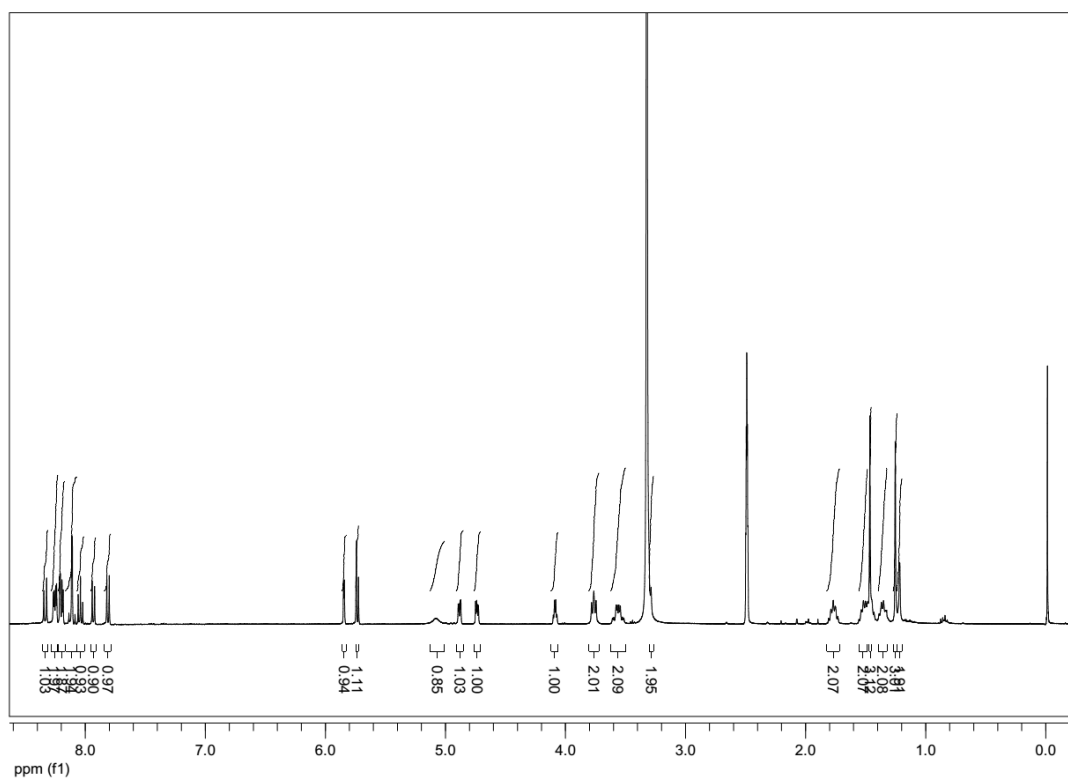


Figure A14: ¹H NMR (DMSO-*d*₆, 400 MHz) of compound **2.3**

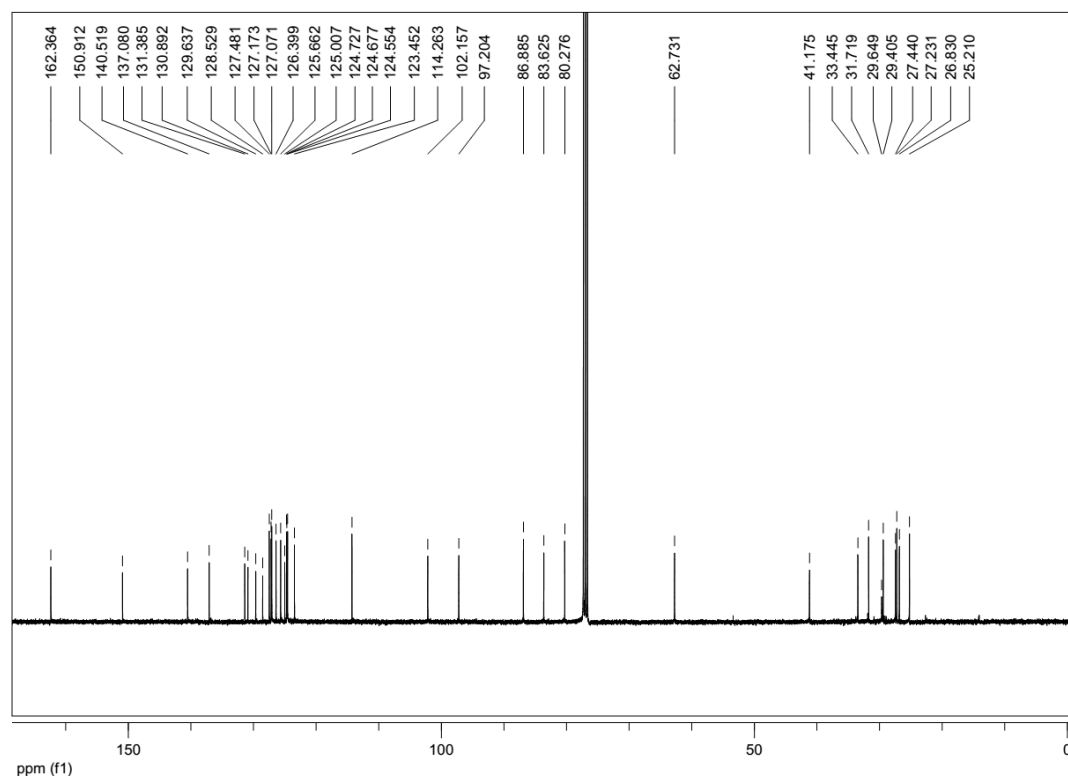


Figure A15: ¹³C NMR (CDCl₃, 100 MHz) of compound **2.3**

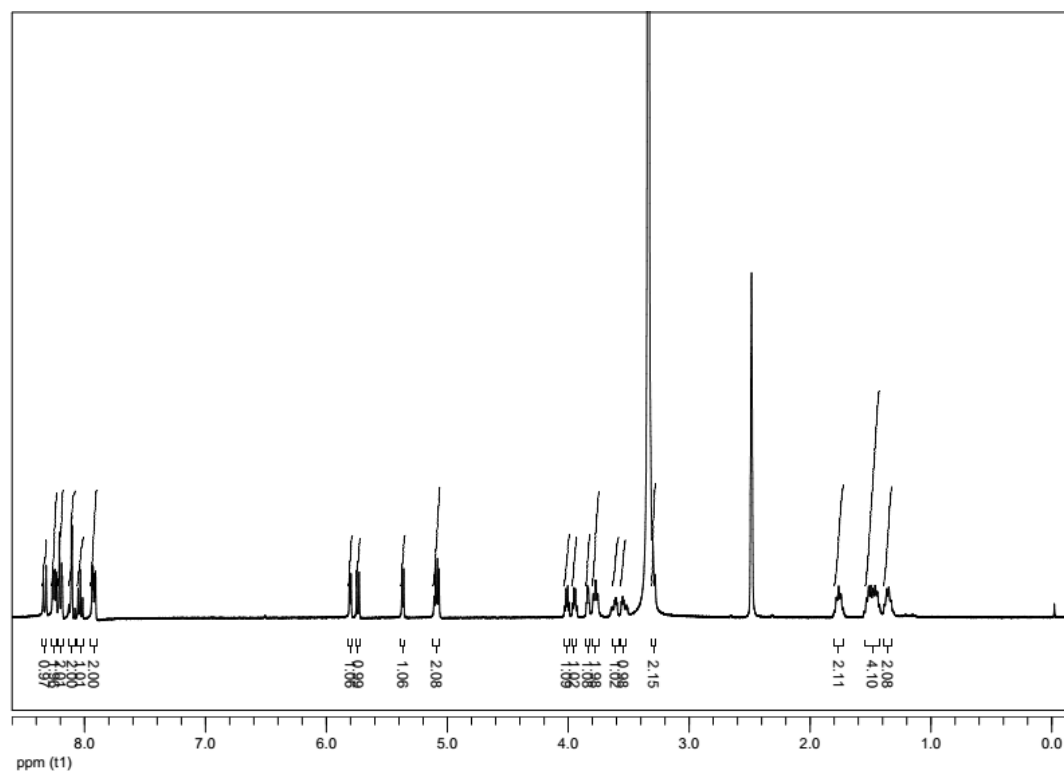


Figure A16: ¹H NMR (DMSO-*d*₆, 400 MHz) of compound **2.4**

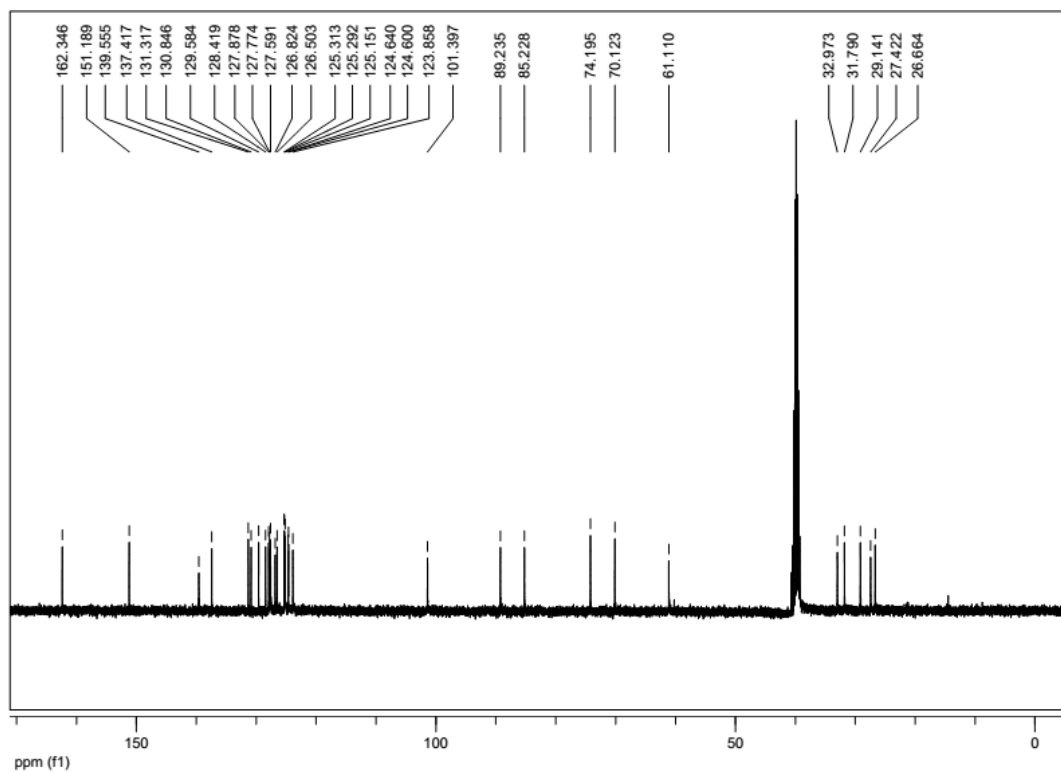
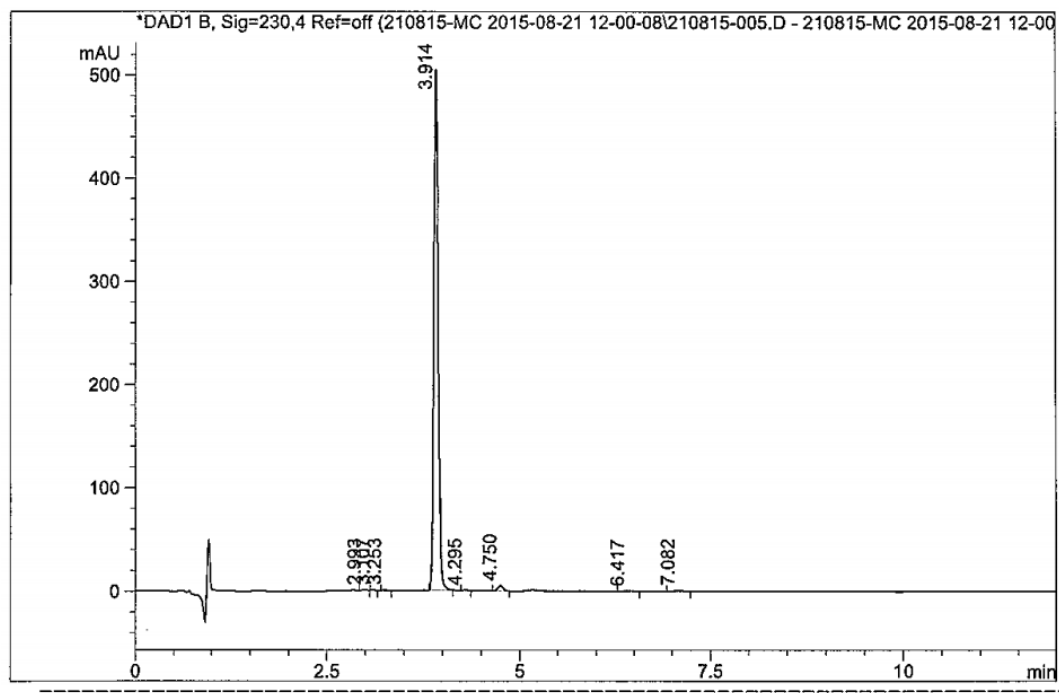


Figure A17: ¹³C NMR (DMSO-*d*₆, 100 MHz) of compound **2.4**

CPRI @ DRILS
HPLC ANALYSIS REPORT

Inj Date : Fri, 21. Aug. 2015 Acq Operator: RADHA
Sample Name : ILS-MR-C36-R-hp-281 Vial 6
A R Number : CM15H024 ->Inj. Vol. : 1.000p
Acq. Method : D:\chem32\1\DATA\210815-MC 2015-08-21 12-00-08\MC.M
Analysis Method : D:\CHEM32_002\1\METHODS\MC.M
Method Info : Column: Symmetry C-18 75*4.6mm 3.5µm
Mobile phase: A) 0.1% TFA in water ,B) ACN
T/%B:0/20,0.5/20,2/95,10/95,10.5/20,12/20
Flow:1.0mL/min Diluent: MEOH:Water(80:20)



Signal 1: DAD1 B, Sig=230,4 Ref=off

Peak #	RT [min]	Area	Area %
1	2.993	2.572	0.128
2	3.107	2.743	0.137
3	3.253	3.414	0.171
4	3.914	1955.791	97.718
5	4.295	2.846	0.142
6	4.750	25.144	1.256
7	6.417	2.477	0.124
8	7.082	6.487	0.324

Analysed by :

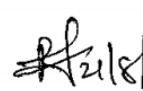
Checked by : 

Figure A18: HPLC data of compound 2.4

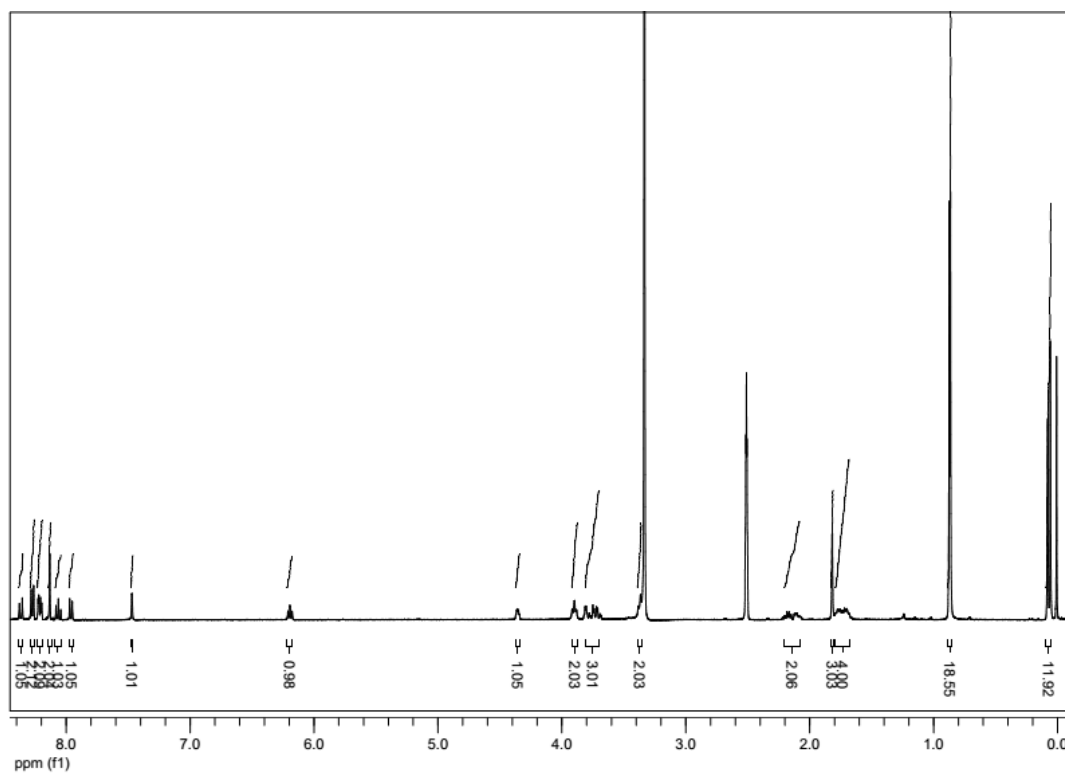


Figure A19: ^1H NMR ($\text{DMSO}-d_6$, 400 MHz) of compound **3.3**

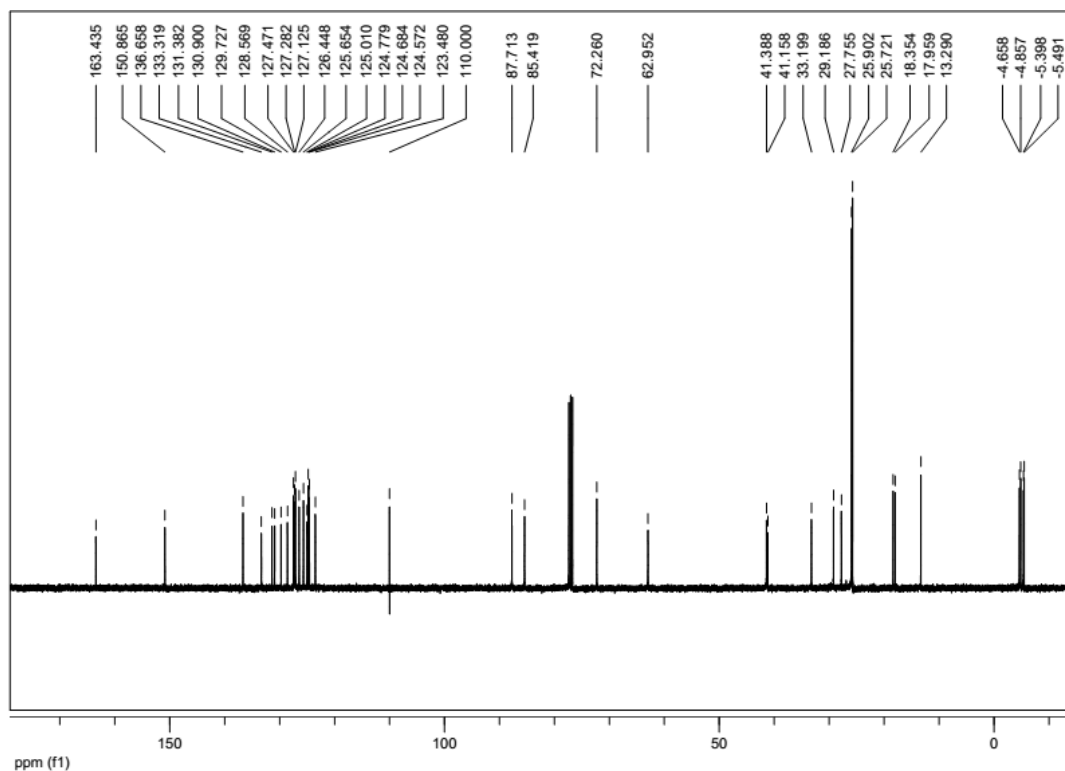


Figure A20: ^{13}C NMR (CDCl_3 , 100 MHz) of compound **3.3**

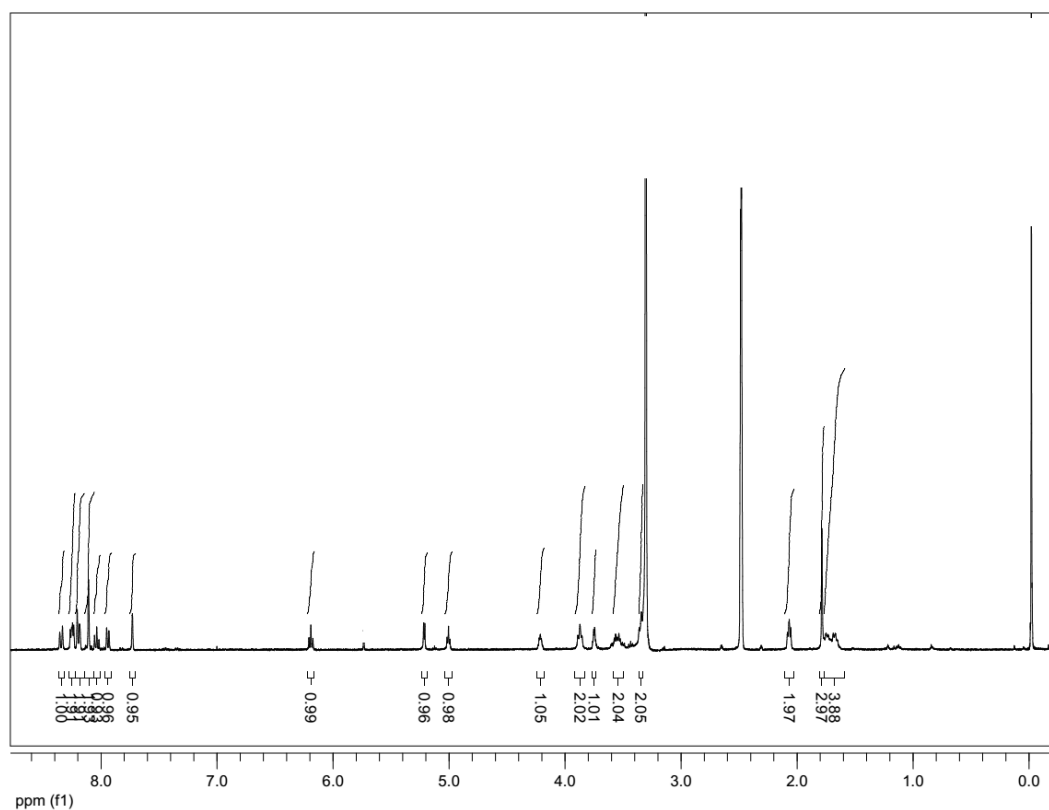


Figure A21: ¹H NMR (DMSO-*d*₆, 400 MHz) of compound **3.4**

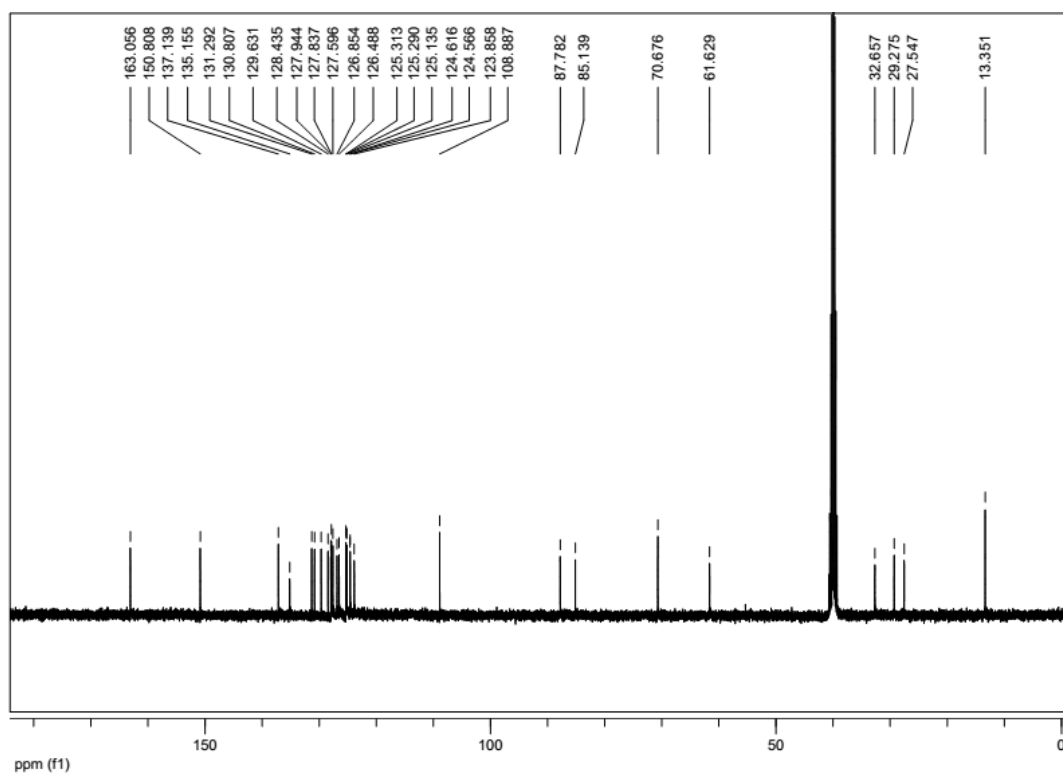
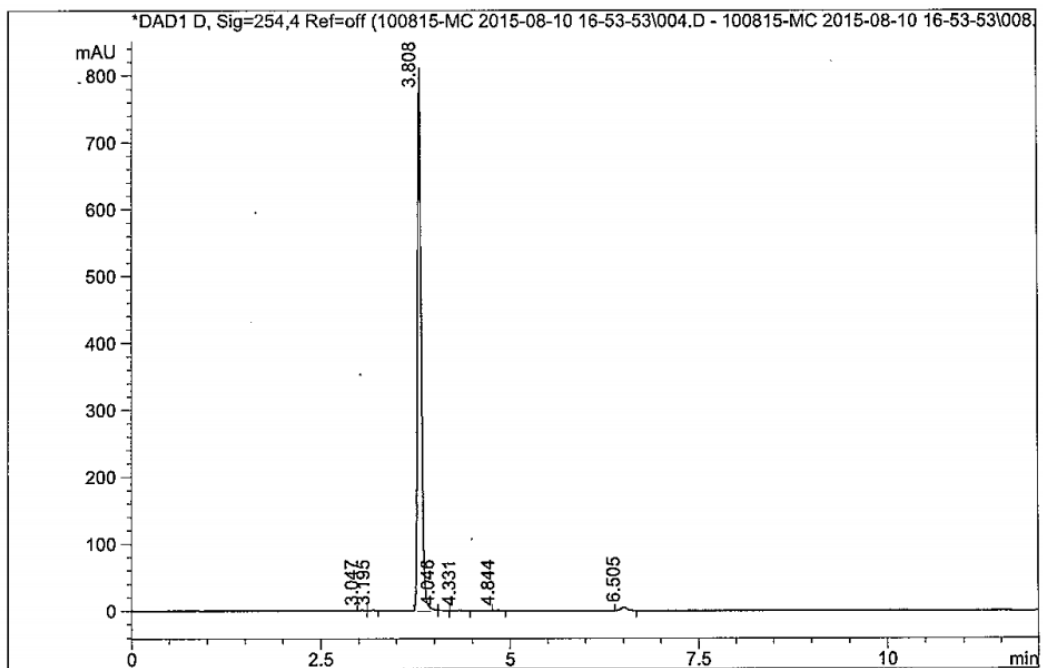


Figure A22: ¹³C NMR (DMSO-*d*₆, 100 MHz) of compound **3.4**

CPRI @ DRILS
HPLC ANALYSIS REPORT

Inj Date : Mon, 10. Aug. 2015 Acq Operator: RADHA
Sample Name : ILS-MR-C36-hp-420 Vial 29
A R Number : CM15H011 ->Inj. Vol. : 1.000µL
Acq. Method : D:\chem32\1\DATA\100815-MC 2015-08-10 16-53-53\MC.M
Analysis Method : D:\CHEM32_002\1\METHODS\MC.M
Method Info : Column: Symmetry C-18 75*4.6mm 3.5µm
Mobile phase: A) 0.1% TFA in water ,B) ACN
T/%B:0/20,0.5/20,2/95,10/95,10.5/20,12/20
Flow:1.0mL/min Diluent: ACN:Water(80:20)



Signal 1: DAD1 D, Sig=254,4 Ref=off

Peak #	RT [min]	Area	Area %
1	3.047	1.259	0.044
2	3.195	1.519	0.053
3	3.808	2811.064	98.555
4	4.046	2.986	0.105
5	4.331	3.235	0.113
6	4.844	1.836	0.064
7	6.505	30.369	1.065

Analysed by :

M
21/8/15

Checked by :

Figure A23: HPLC data of compound 3.4

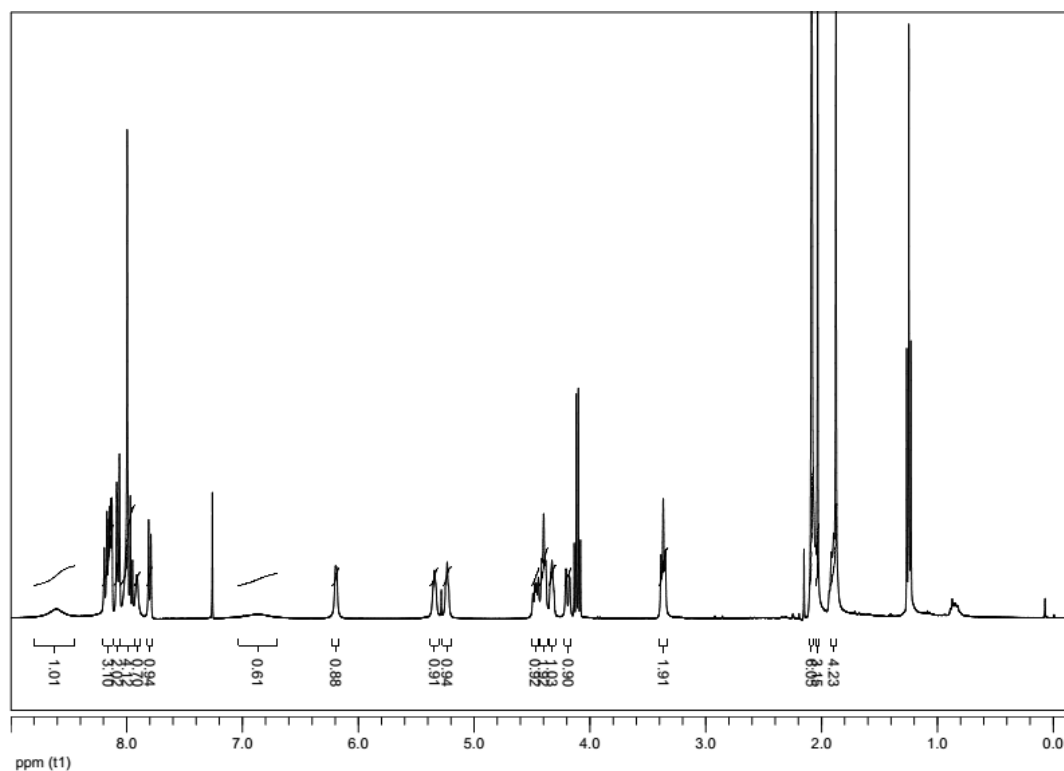


Figure A24: ¹H NMR (CDCl₃, 400 MHz) of compound **4.6a**

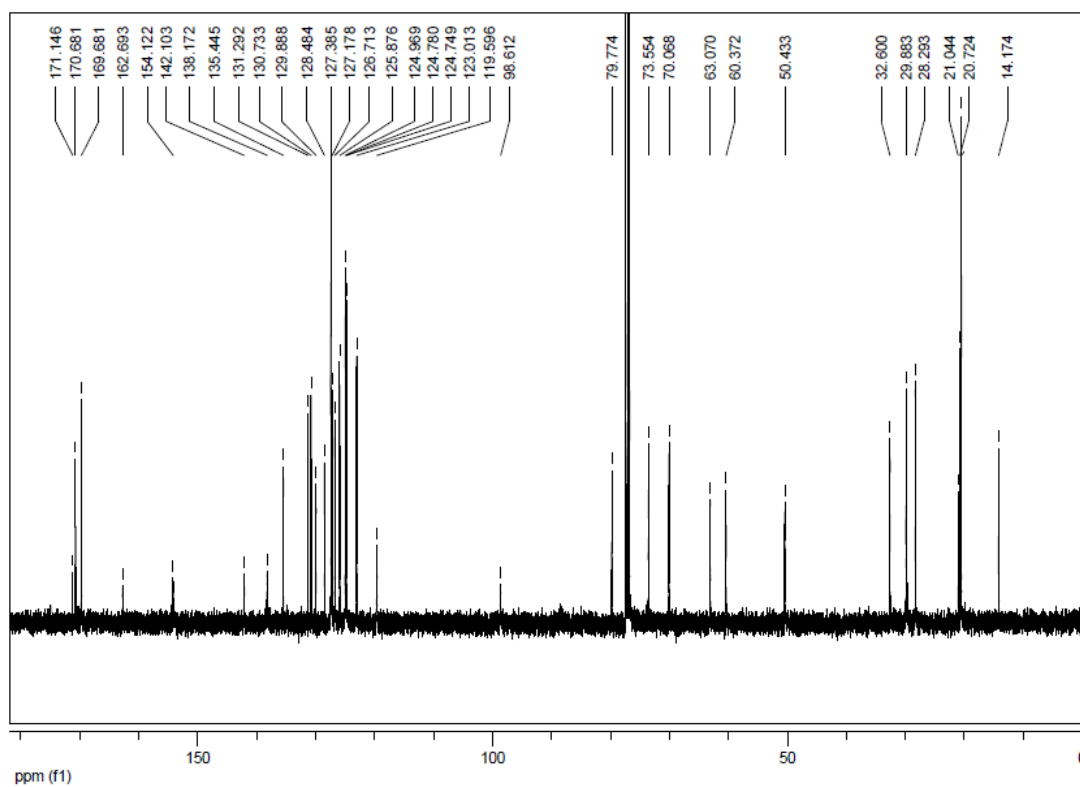


Figure A25: ¹³C NMR (CDCl₃, 100 MHz) of compound **4.6a**

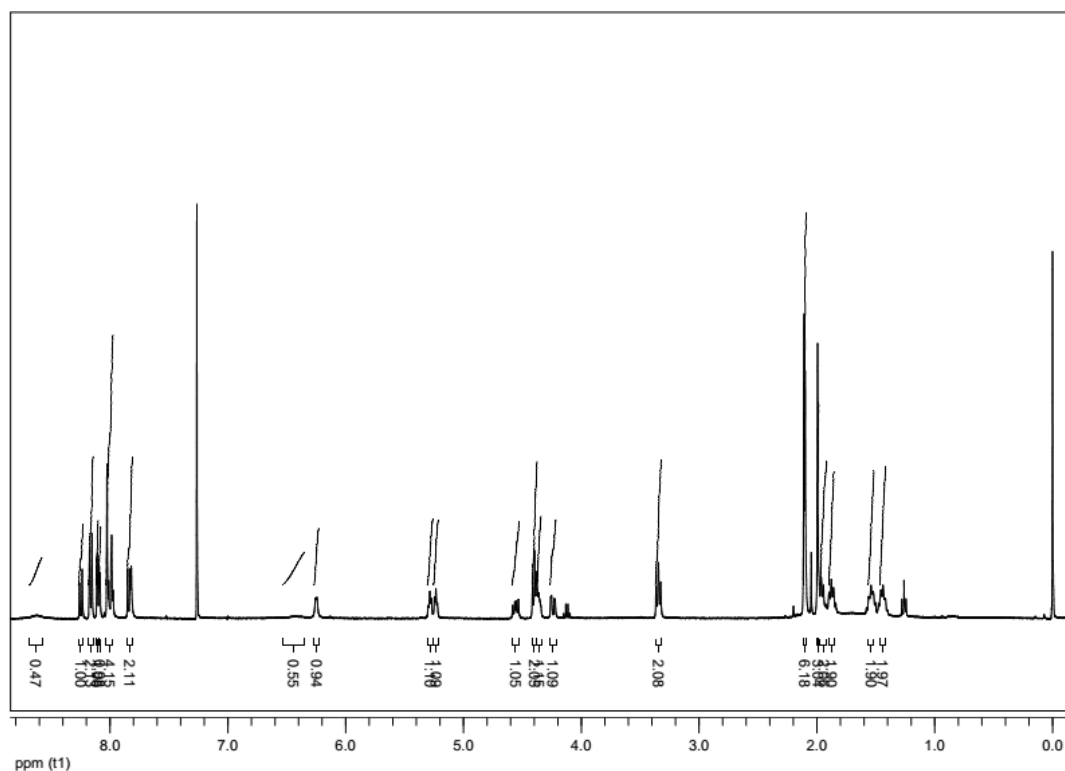


Figure A26: ¹H NMR (CDCl₃, 400 MHz) of compound **4.6b**

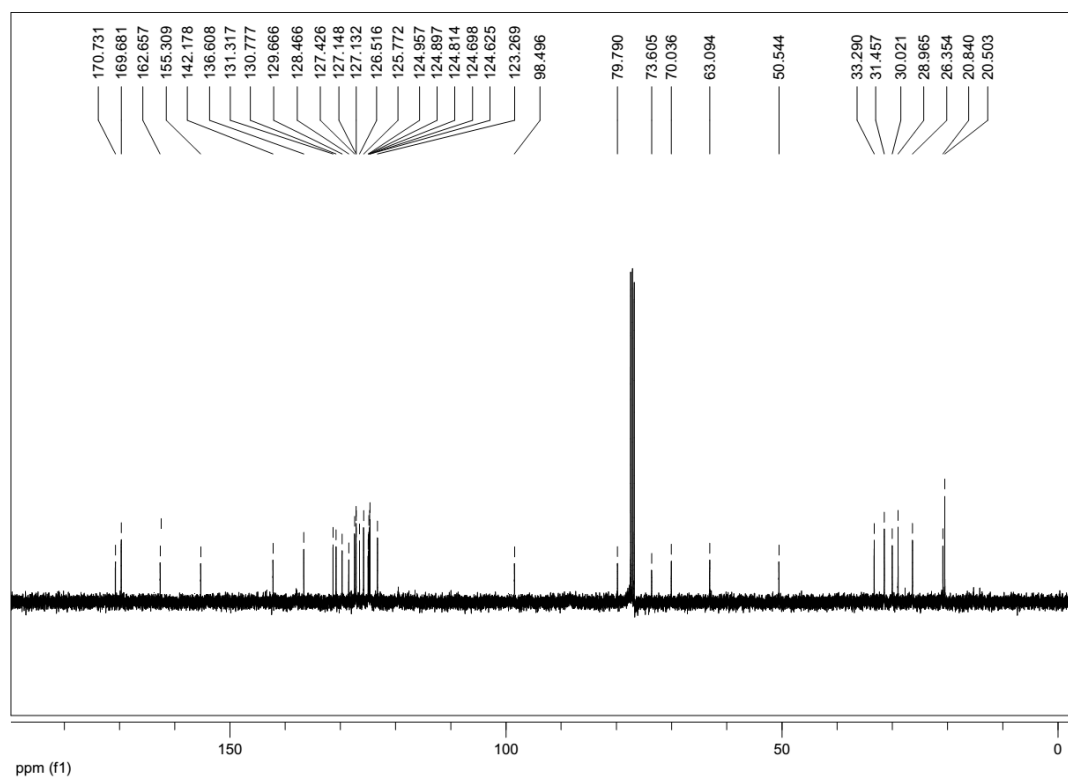


Figure A27: ¹³C NMR (CDCl₃, 100 MHz) of compound **4.6b**

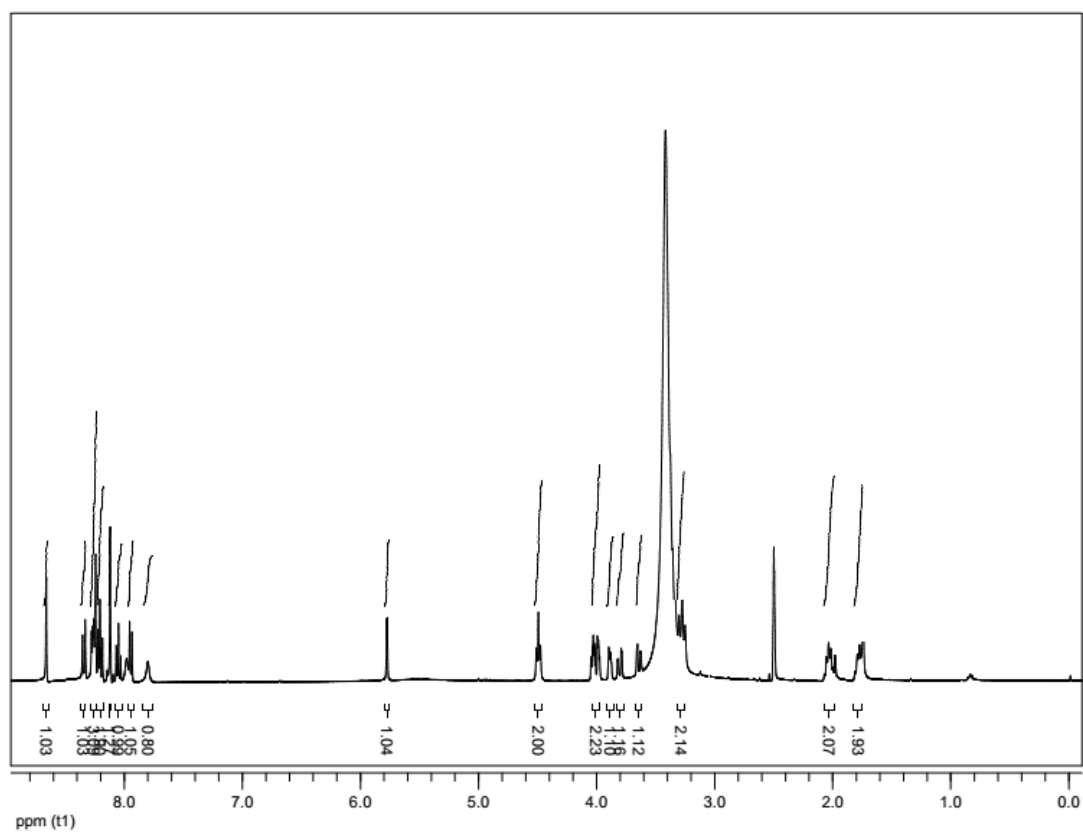


Figure A28: ¹H NMR (DMSO-*d*₆, 400 MHz) of compound **4.7a**

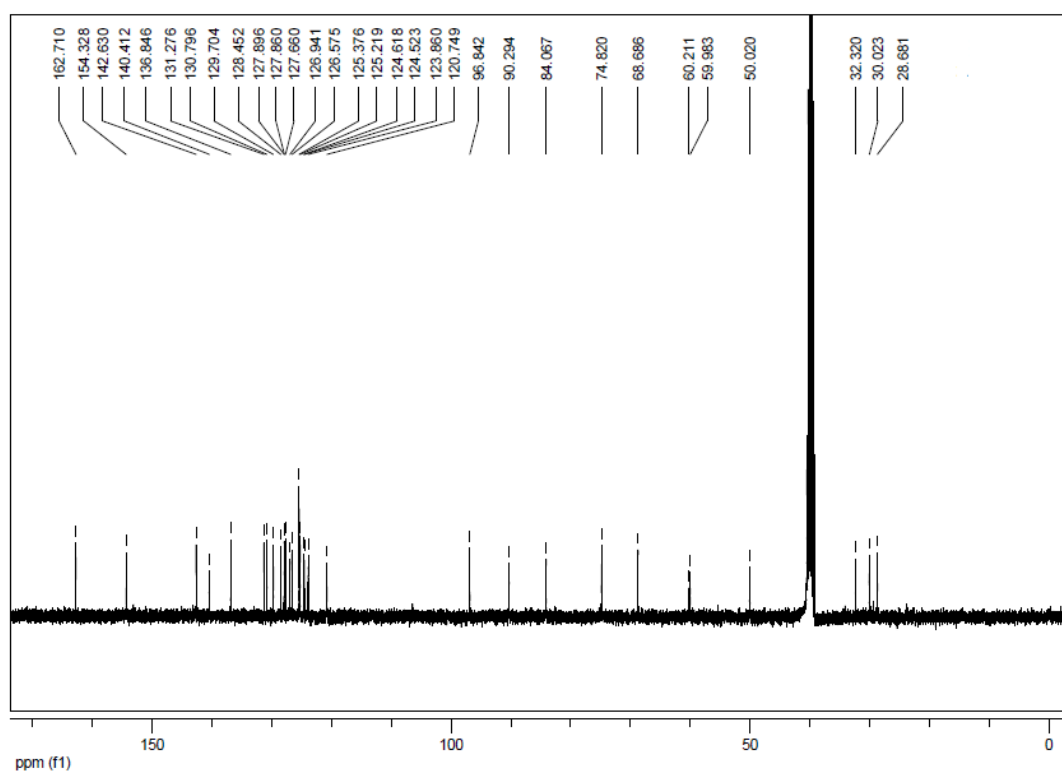
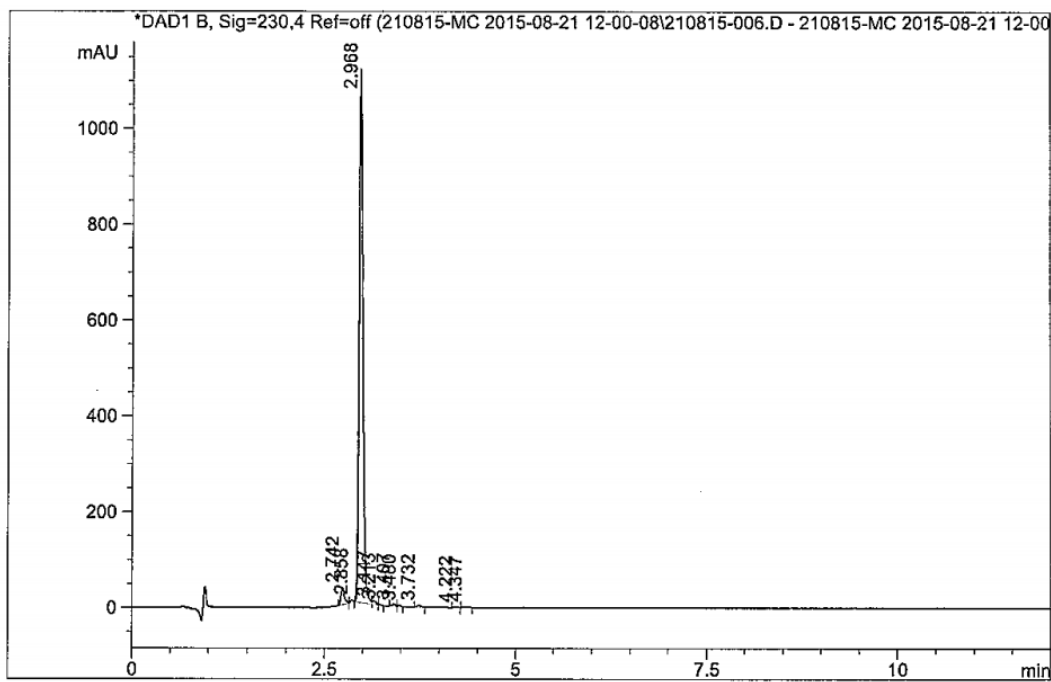


Figure A29: ¹³C NMR (DMSO-*d*₆, 100 MHz) of compound **4.7a**

CPRI @ DRILS
HPLC ANALYSIS REPORT

Inj Date : Fri, 21. Aug. 2015 Acq Operator: RADHA
Sample Name : ILS-MR-C36-hp-267 Vial 7
A R Number : CM15H023 ->Inj. Vol. : 1.000µL
Acq. Method : D:\chem32\1\DATA\210815-MC 2015-08-21 12-00-08\MC.M
Analysis Method : D:\CHEM32_002\1\METHODS\MC.M
Method Info : Column: Symmetry C-18 75*4.6mm 3.5µm
Mobile phase: A) 0.1% TFA in water ,B) ACN
T/%B:0/20,0.5/20,2/95,10/95,10.5/20,12/20
Flow:1.0mL/min Diluent: MEOH:Water(80:20)



Signal 1: DAD1 B, Sig=230,4 Ref=off

Peak #	RT [min]	Area	Area %
1	2.742	110.548	2.772
2	2.858	11.882	0.298
3	2.968	3791.107	95.074
4	3.147	22.337	0.560
5	3.213	2.738	0.069
6	3.407	16.957	0.425
7	3.480	7.342	0.184
8	3.732	15.159	0.380
9	4.222	2.464	0.062
10	4.347	7.017	0.176

Analysed by :

Checked by : *BP 21/8/15*

Figure A30: HPLC data of compound 4.7a

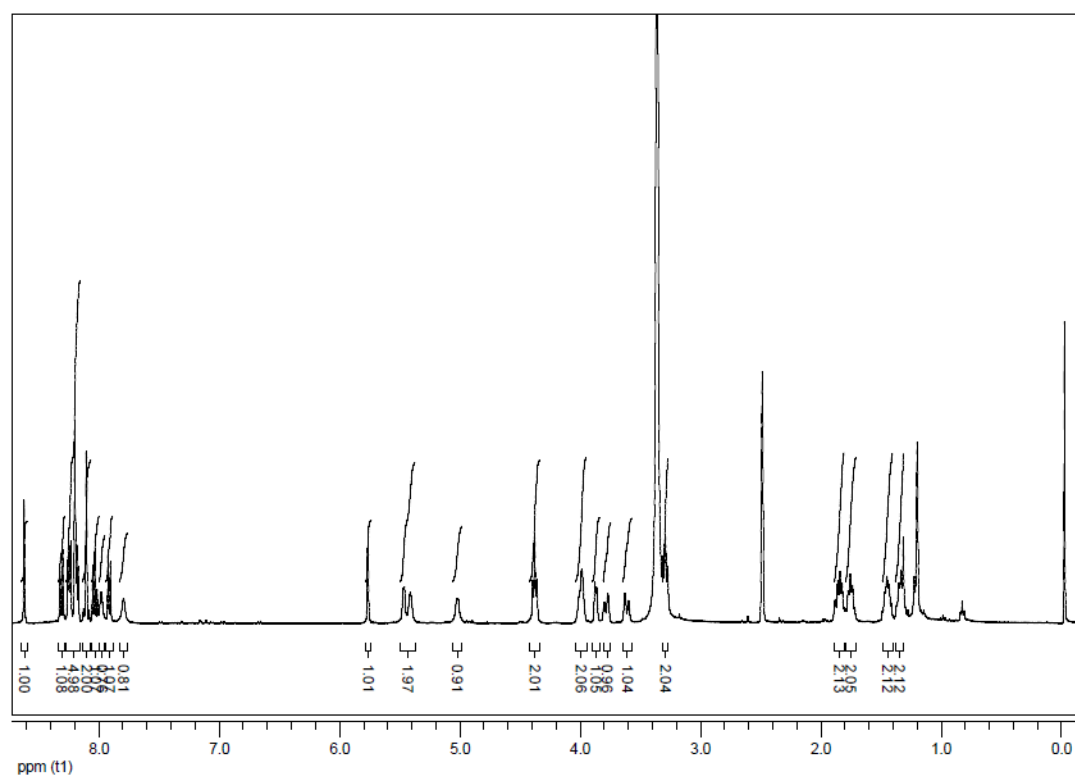


Figure A31: ^{13}C NMR (DMSO- d_6 , 400 MHz) of compound **4.7b**

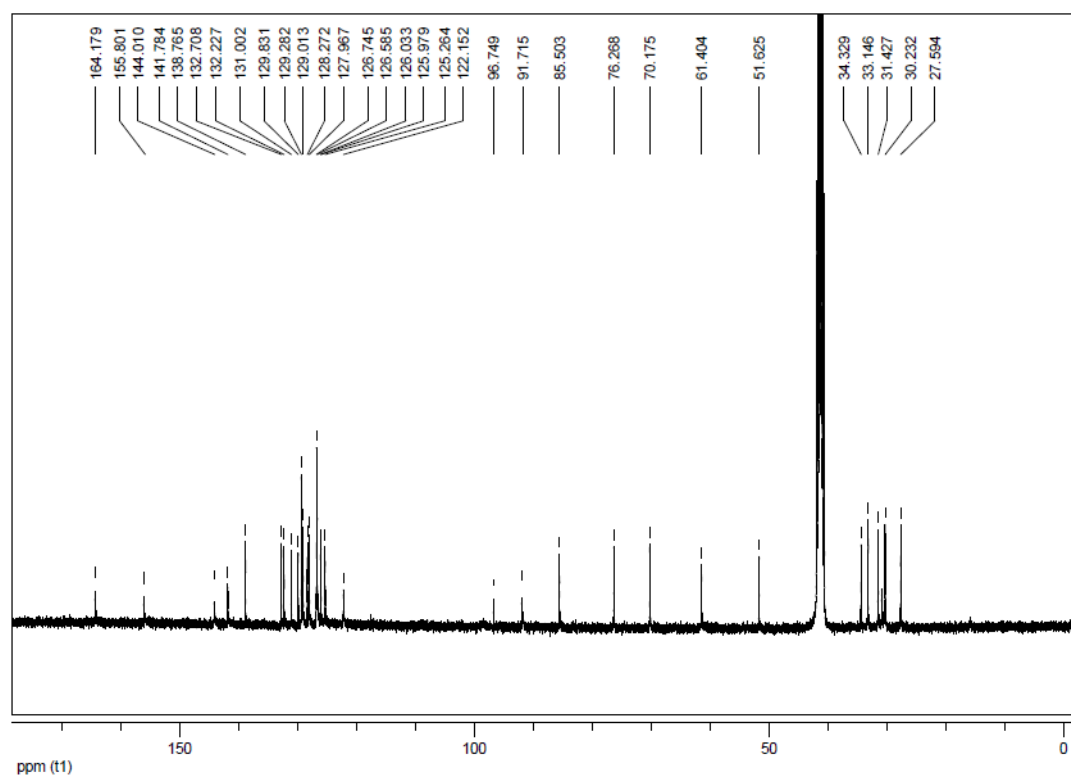
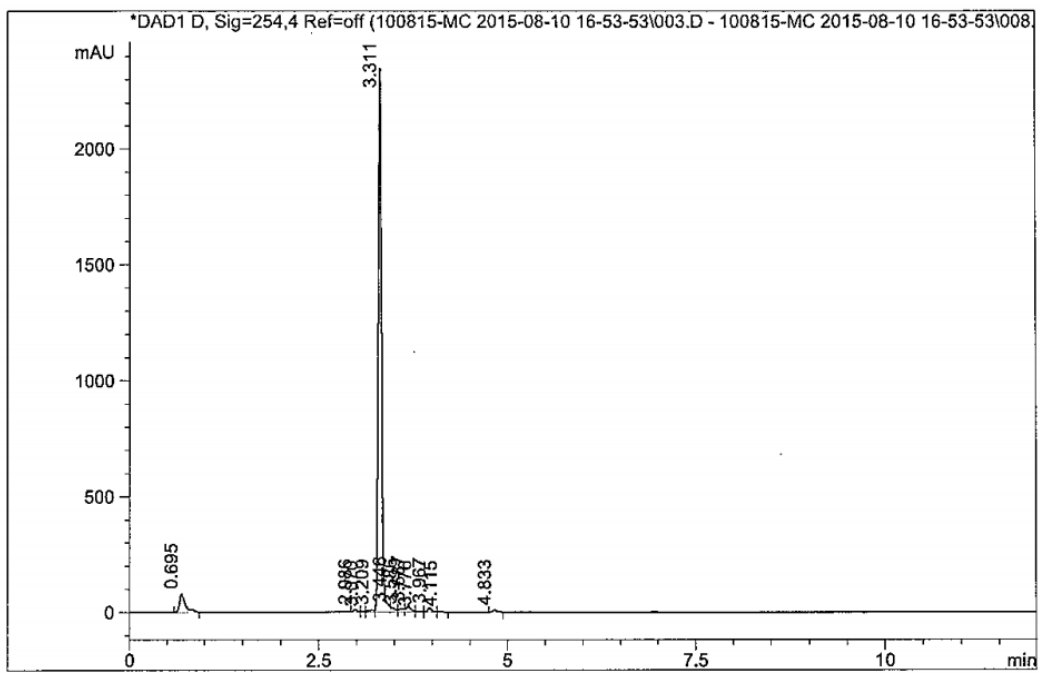


Figure A32: ^{13}C NMR (DMSO- d_6 , 100 MHz) of compound **4.7b**

CPRI @ DRILS
HPLC ANALYSIS REPORT

Inj Date : Mon, 10. Aug. 2015 Acq Operator: RADHA
Sample Name : ILS-MR-C36-HP-296 Vial 28
A R Number : CM15H010 ->Inj. Vol. : 1.000µL
Acq. Method : D:\chem32\1\DATA\100815-MC 2015-08-10 16-53-53\MC.M
Analysis Method : D:\CHEM32_002\1\METHODS\MC.M
Method Info : Column: Symmetry C-18 75*4.6mm 3.5µm
Mobile phase: A) 0.1% TFA in water ,B) ACN
T/%B:0/20,0.5/20,2/95,10/95,10.5/20,12/20
Flow:1.0mL/min Diluent: ACN:Water(80:20)



Signal 1: DAD1 D, Sig=254,4 Ref=off

Peak #	RT [min]	Area	Area %
1	0.695	435.327	5.286
2	2.986	31.236	0.379
3	3.070	6.035	0.073
4	3.209	41.214	0.500
5	3.311	7334.035	89.048
6	3.446	81.174	0.986
7	3.586	64.279	0.780
8	3.687	107.708	1.308
9	3.776	17.059	0.207
10	3.967	66.040	0.802
11	4.115	12.146	0.147
12	4.833	39.774	0.483

Analysed by :

Handwritten signature
11/8/15

Checked by :

Figure A32: HPLC data of compound 4.7b

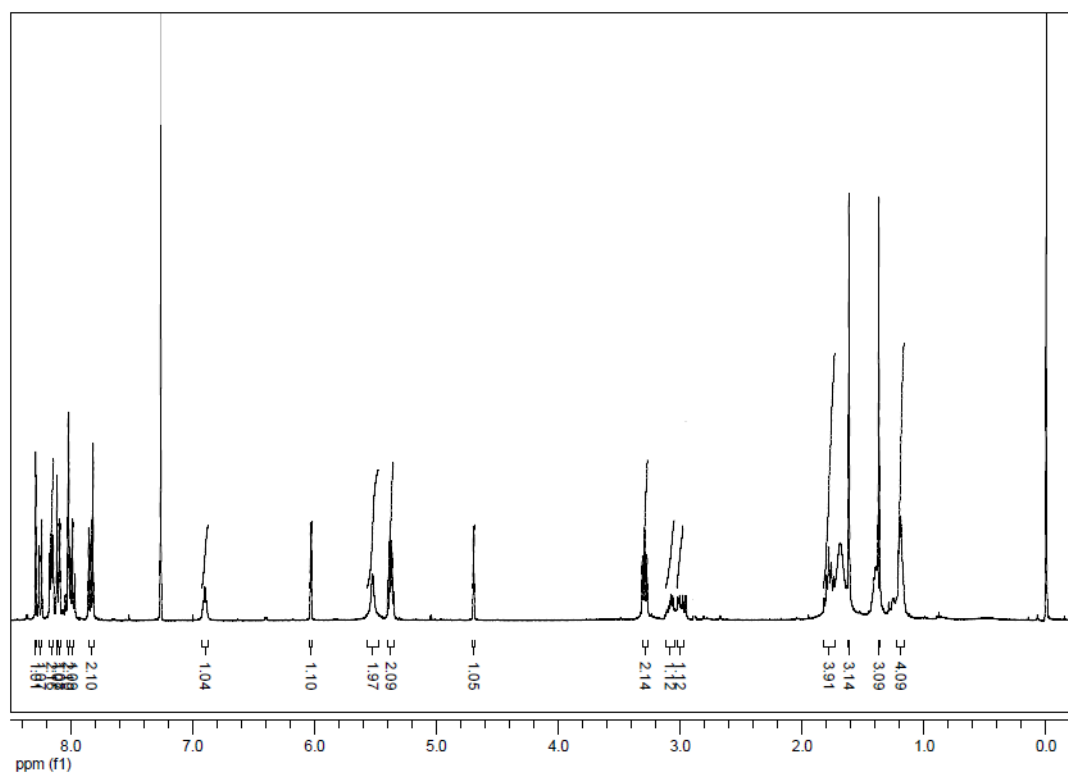


Figure A33: ¹H NMR (CDCl₃, 400 MHz) of compound **5.4**

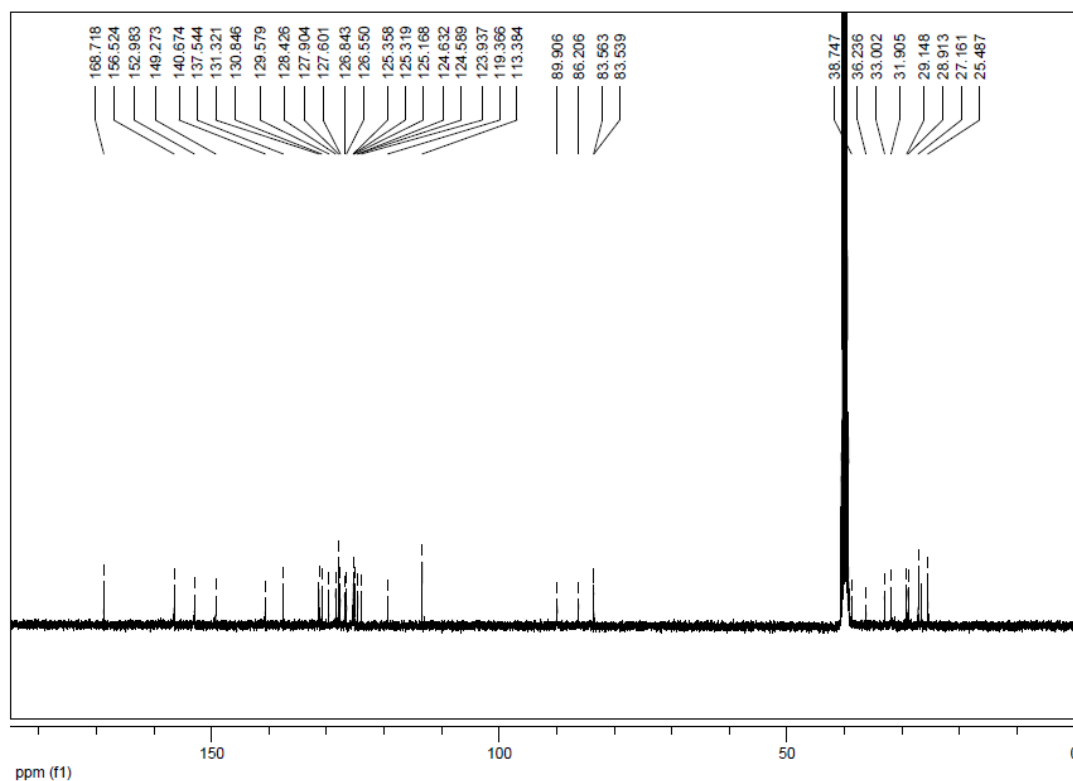


Figure A34: ¹³C NMR (DMSO-*d*₆, 100 MHz) of compound **5.4**

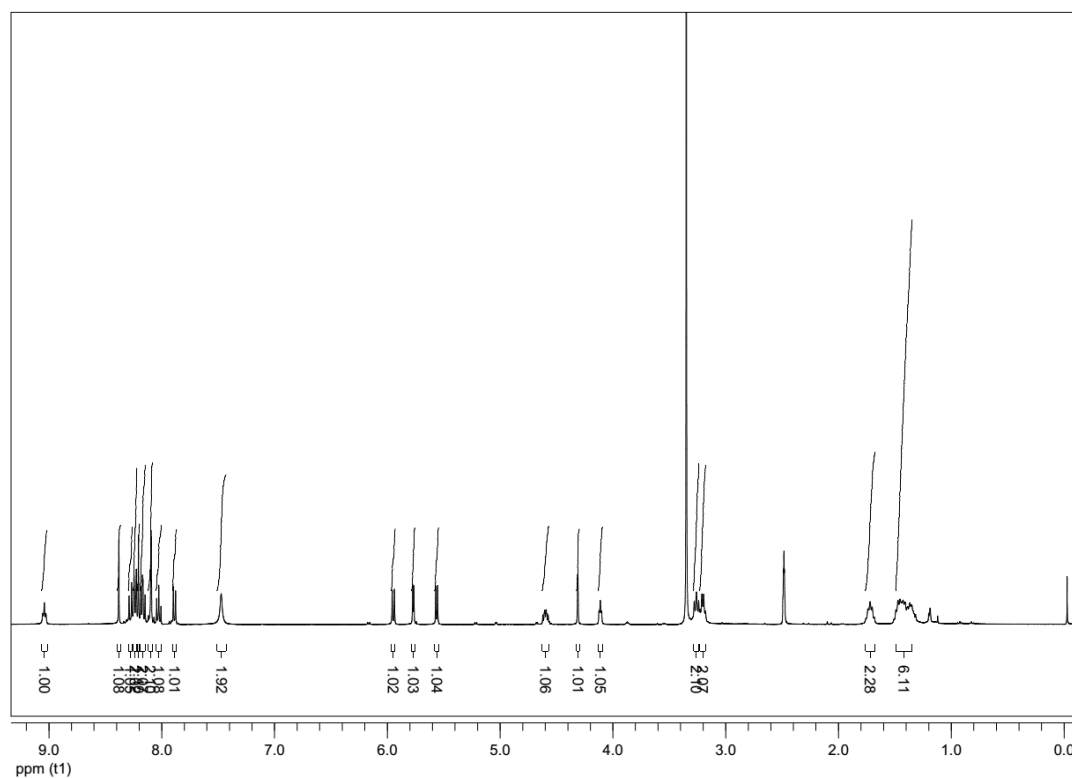


Figure A35: ^1H NMR (DMSO- d_6 , 400 MHz) of compound **5.5**

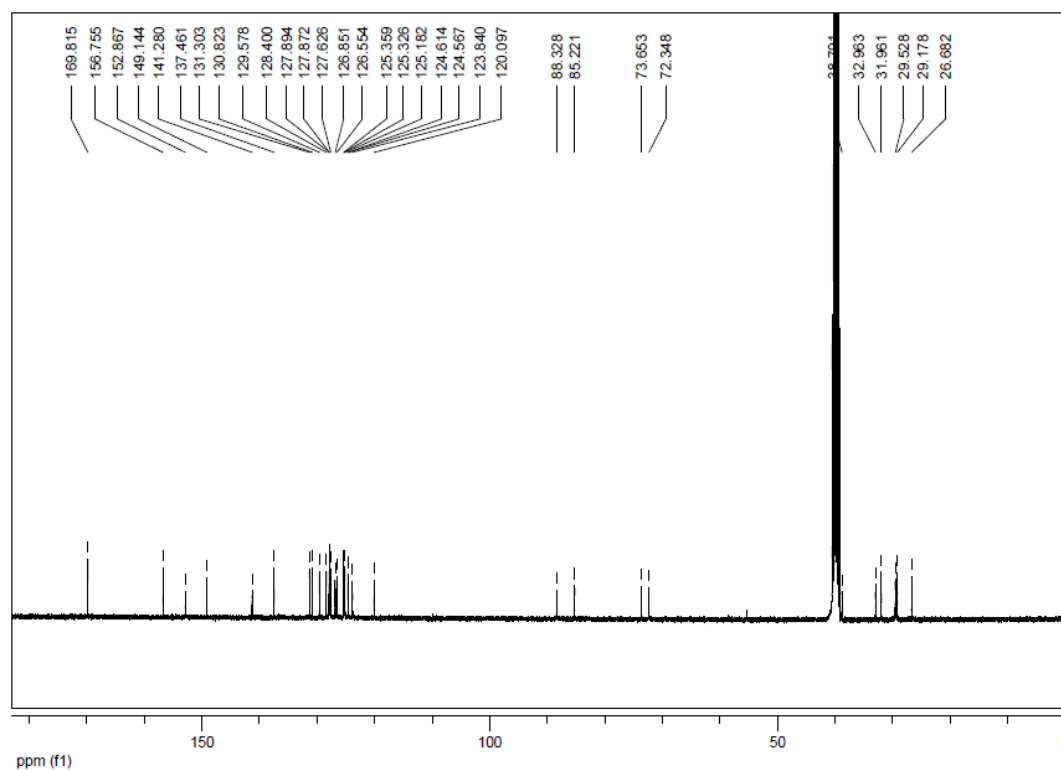
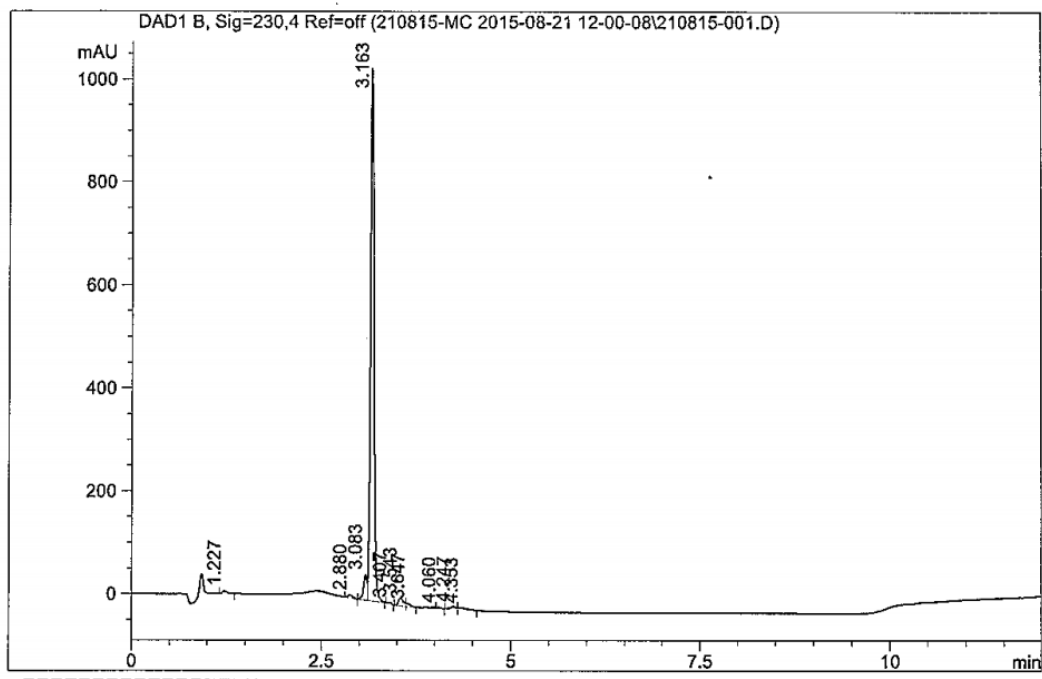


Figure A36: ^{13}C NMR (DMSO- d_6 , 100 MHz) of compound **5.5**

CPRI @ DRILS
HPLC ANALYSIS REPORT

Inj Date : Fri, 21. Aug. 2015 Acq Operator: RADHA
Sample Name : ILS-MR-C36-R-HP-349 Vial 3
A R Number : CM15H025 ->Inj. Vol. : 1.000µL
Acq. Method : D:\chem32\1\DATA\210815-MC 2015-08-21 12-00-08\MC.M
Analysis Method : D:\CHEM32_002\1\METHODS\MC.M
Method Info : Column: Symmetry C-18 75*4.6mm 3.5µm
Mobile phase: A) 0.1% TFA in water ,B) ACN
T/%B:0/20,0.5/20,2/95,10/95,10.5/20,12/20
Flow:1.0mL/min Diluent: MEOH:Water(80:20)



Signal 1: DAD1 B, Sig=230,4 Ref=off

Peak #	RT [min]	Area	Area %
1	1.227	22.123	0.593
2	2.880	29.840	0.800
3	3.083	164.152	4.401
4	3.163	3352.597	89.876
5	3.407	7.563	0.203
6	3.543	70.128	1.880
7	3.647	18.527	0.497
8	4.060	3.762	0.101
9	4.247	28.809	0.772
10	4.353	32.730	0.877

Analysed by :

Checked by : *21/8/15*

Figure A36: HPLC data of compound 5.5

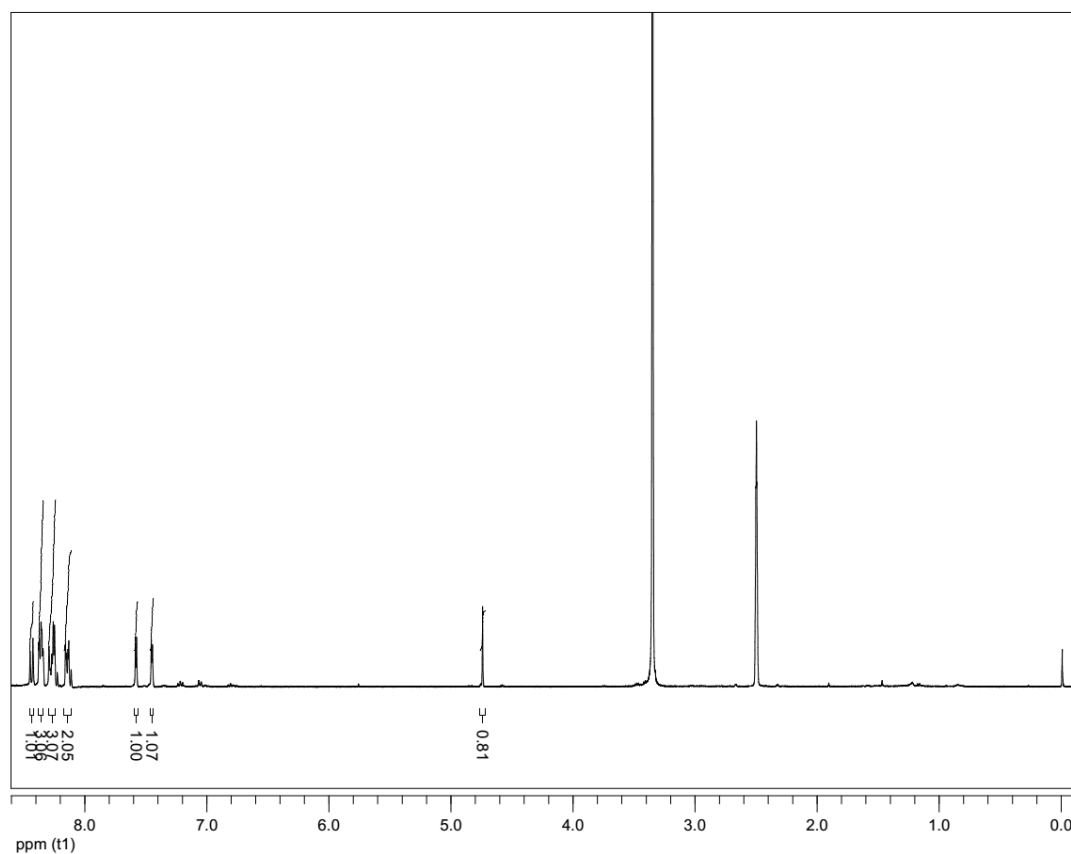


Figure A37: ¹H NMR (DMSO-*d*₆, 400 MHz) of compound **6.5**

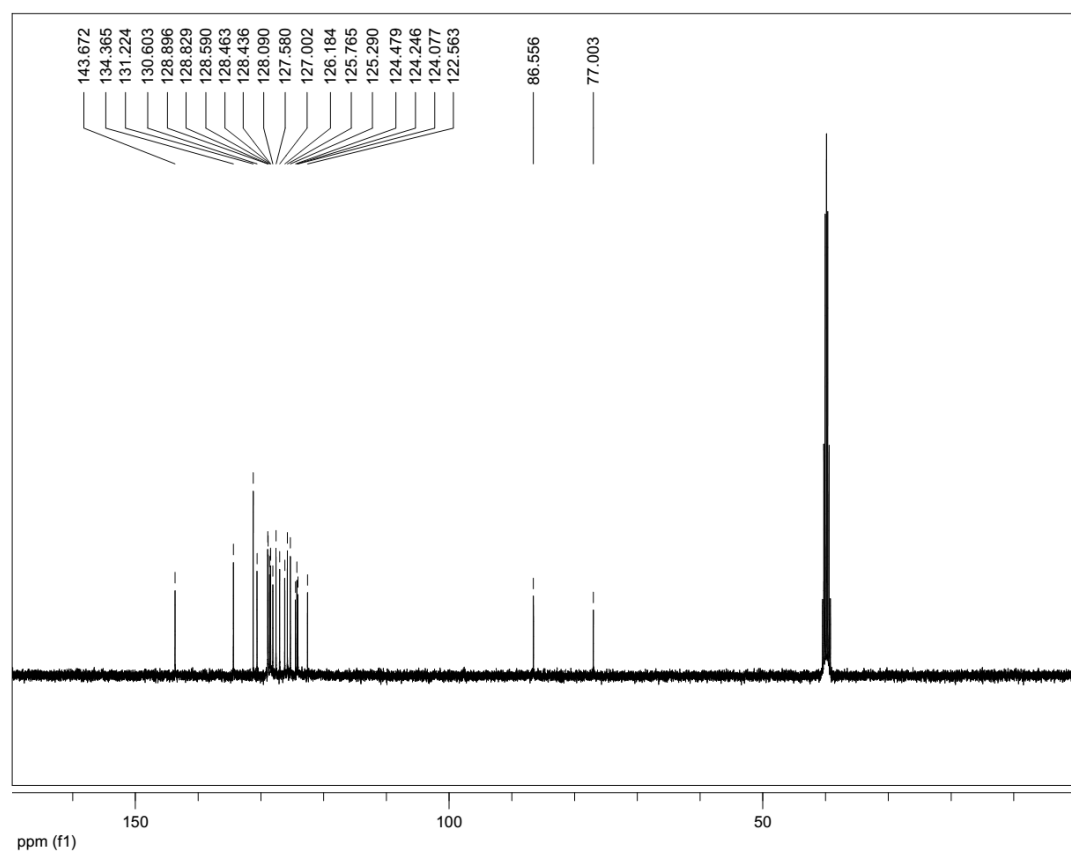


Figure A38: ¹³C NMR (DMSO-*d*₆, 100 MHz) of compound **6.5**

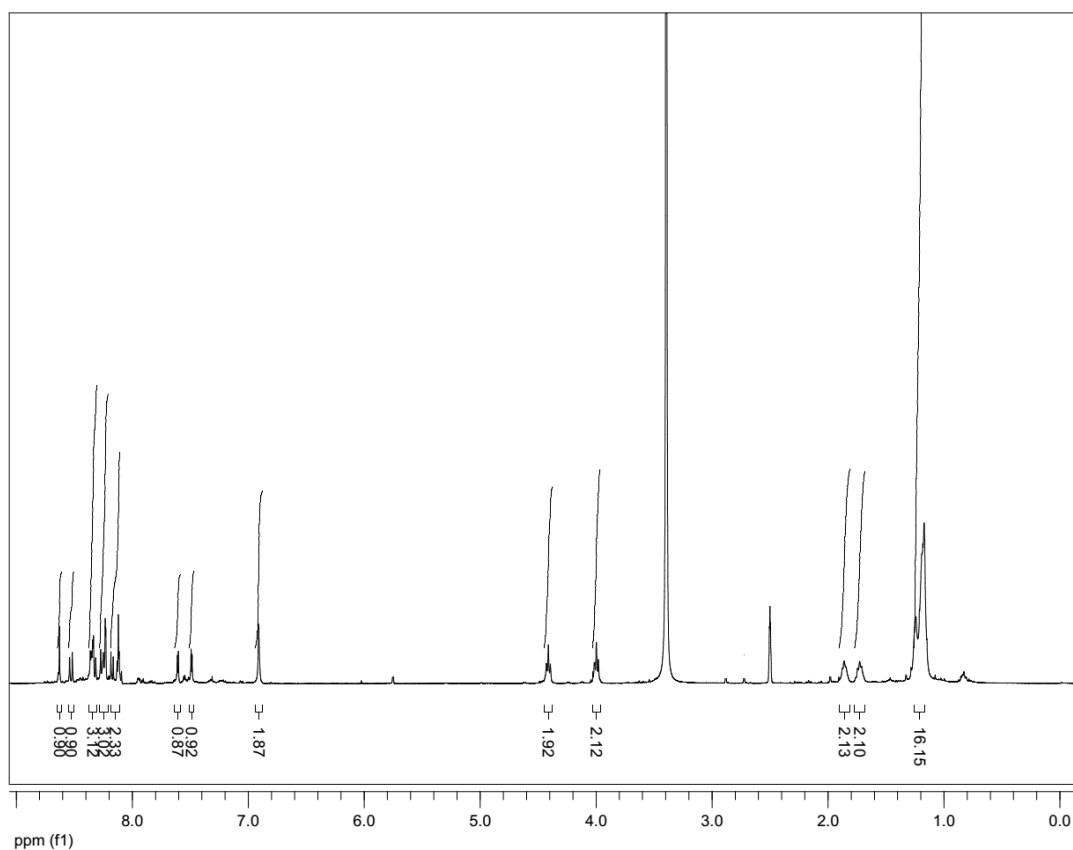


Figure A39: ¹H NMR (DMSO-*d*₆, 400 MHz) of compound **6.7**

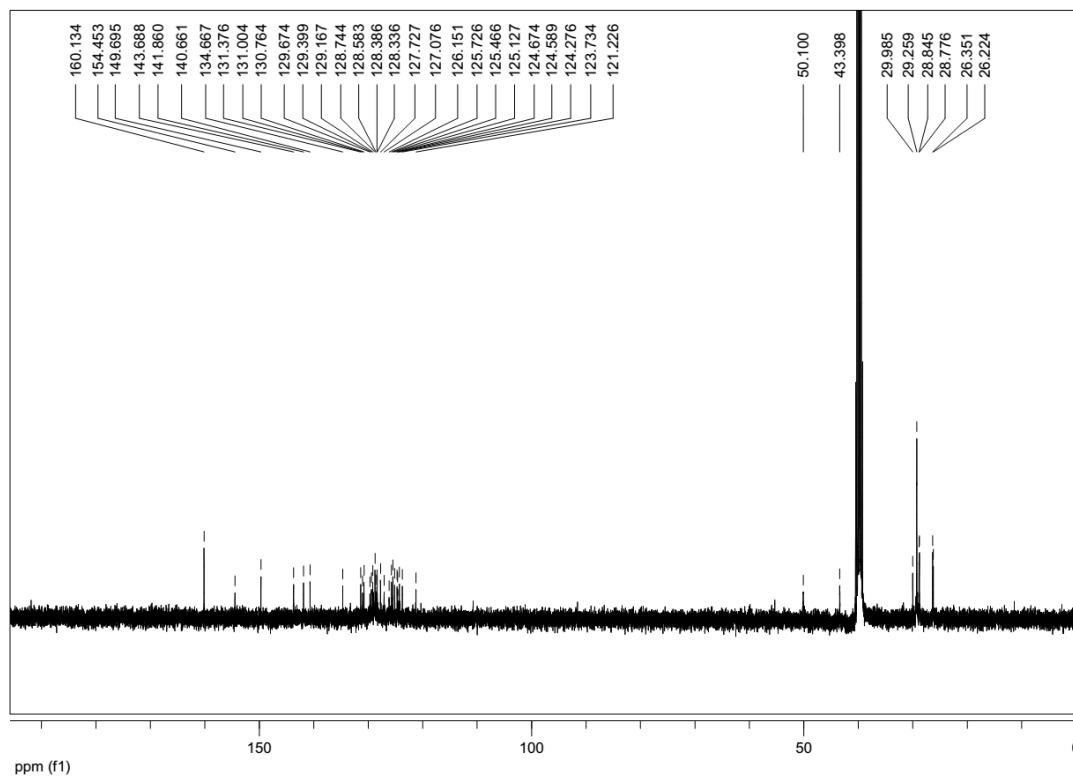
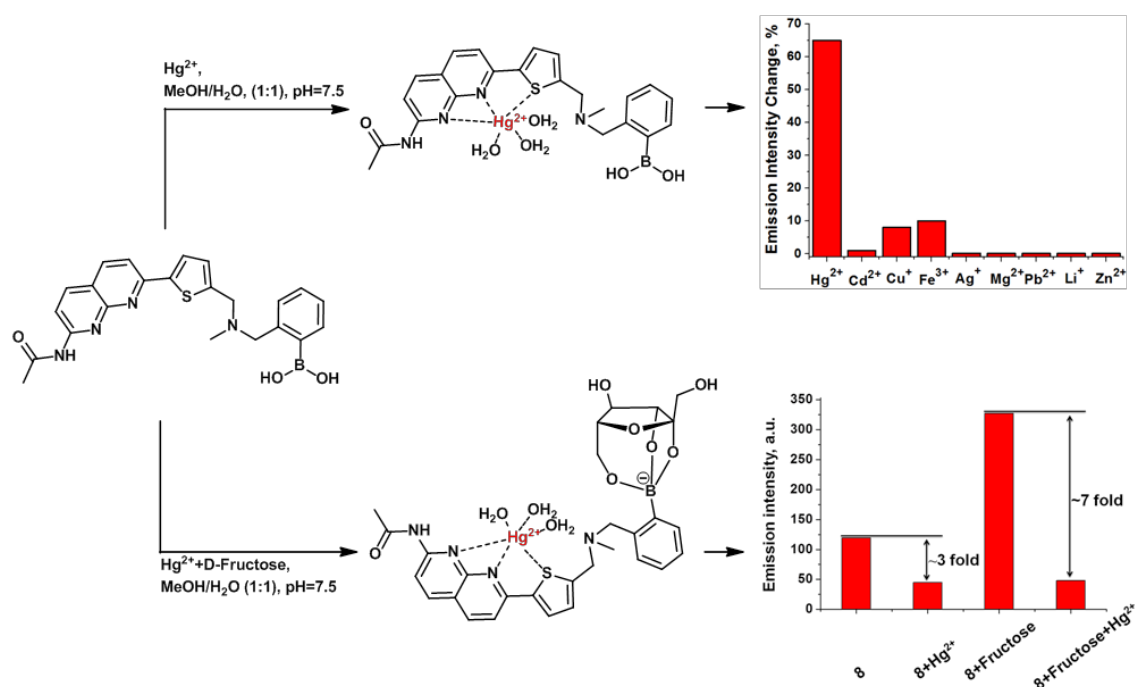


Figure A40: ¹³C NMR (DMSO-*d*₆, 100 MHz) of compound **6.7**

5

1,8-Naphthyridine-Based Boronic Acid as Fluorescent Chemosensor for Hg^{2+} and D-Fructose



*This chapter partly adapted from: **E. Ramanjaneya Reddy** and Marina S. Rajadurai* 2016, to be submitted.

5.1. Abstract:

A novel fluorescent chemosensor naphthyridine-boronic acid derivative (**1.1**) was synthesized and its ability to act as a selective chemosensor was examined for various metal ions. Compound **1.1** displayed highly selective fluorescence quenching upon interaction with Hg²⁺, possibly by means of photo induced electron transfer (PET) mechanism. The binding stoichiometry of the naphthyridine-boronic acid-Hg²⁺ complex and the association constant was determined. It was found that in the presence of D-fructose at physiological concentration, the sensitivity of chemosensor **1.1** towards Hg²⁺ improved by at least 7 folds, perhaps as result of the cooperative binding of both D-fructose and mercury ion to the sensor. Till date, presented in this chapter dual D-fructose-mercury chemosensor is the first example of utilizing boronic acid–diol complexation for enhancement of the sensor's sensitivity towards toxic metal ion. The utility of compound **1.1** lays in applications in food industry, e.g. for detection of mercury contamination of high fructose corn syrup, or in estimation of mercury in polluted biological samples and underground water.

5.2. Introduction:

Mercury and mercuric salts are extensively circulated in atmospheric air, water and soil and considered to be highly toxic and hazardous to humans and environment.¹ For humans, mercury contamination may cause a wide variety of symptoms, including neuro-disorders, neuromuscular changes, memory loss and carcinogenic diseases.² Despite of danger mercury poses, especially to unborn children, it is still used in industry. Its contaminants are often detected in various products, including food industry products, for example in high fructose corn syrup, which is cheaper and sweeter than regular sugar. Traces of mercury were found in high fructose corn syrup containing beverages/ confectioneries, and the alarming amounts upto 0.570 micrograms mercury per gram of high fructose corn syrup were found.³ Various methods have been employed for the detection of Hg²⁺, including cold vapor atomic absorption spectroscopy,⁴ high performance liquid chromatography⁵ and inductively coupled plasma atomic emission spectrometry.⁶ The above methods are extremely sensitive and able to detect Hg²⁺ in nanomolar range. However, their drawbacks are costly equipment, time-consuming and laborious procedures, and need for the trained professionals in order to perform the analysis. At

the same time, mercury detection based on fluorescence changes allow rapid, convenient and inexpensive detection. Fluorescence chemosensors offer definite advantages, such as high selectivity, high sensitivity, accuracy and possibility to investigate molecule-molecule recognition in both environmental and biological samples.⁷ Till date, numerous fluorescent chemosensors for Hg^{2+} are developed based on Rhodamine,⁸ BODIPY,⁹ and modified naphthalimide derivatives, which are low aqueous solubility and interference with some other metal ions. However, they often suffer from such drawbacks, as laborious, complex or expensive synthesis, low aqueous solubility or limited selectivity as result of interference with other metal ions.

1,8-Naphthyridine and its derivatives are extensively studied for molecular recognitions events, including nucleosides sensing (*e.g.* for guanine, cytosine and thymidine),¹⁰ monosaccharide sensing¹¹ and heavy transition metal ions sensing¹² (*e.g.* for Zn^{2+} , Hg^{2+} , Cd^{2+}). In order to improve fluorescent properties, affinity, aqueous solubility and stability of 1,8-naphthyridine based chemosensors, this chapter reports design and synthesis of novel fluorescent chemosensor **1.1** [(2-(((5-(7-acetamido-1,8-naphthyridin-2-yl)thiophen-2-yl)methyl)(methyl)amino)methyl)phenyl)boronic acid]. In order to strengthen an interaction of mercury ion with the chemosensor, 1, 8-naphthyridine was conjugated to thiophene moiety, keeping in mind high affinity of mercury to sulfur. At the same time, boronic acid group, which is known to easily form cyclic ester with monosaccharides, was additionally introduced in the same scaffold aiming cooperative action of boronic acid and metal chelate, which could possibly enhance sensitivity and selectivity either to metal ion or sugar. There are very few examples are known for using boronic acid containing compounds for direct detection of metal ions.¹³

This chapter reports for the first time the synthesis of naphthyridine-boronic acid based fluorescent chemosensor **1.1**, its fluorescence properties and investigation of interaction with various metal ions and monosaccharides (D-glucose, D-fructose, D-mannose and D-galactose). Compound **1.1** showed much higher selectivity and affinity towards Hg^{2+} compared to various metal ions tested. At the same it had high selectivity to D-fructose among various monosaccharides. In this work the ability of chemosensor **1.1** to form reversible covalent bonds with D-fructose was employed for the first time to significantly enhance selectivity towards metal ion, namely Hg^{2+} .

5.3. Results and Discussion:

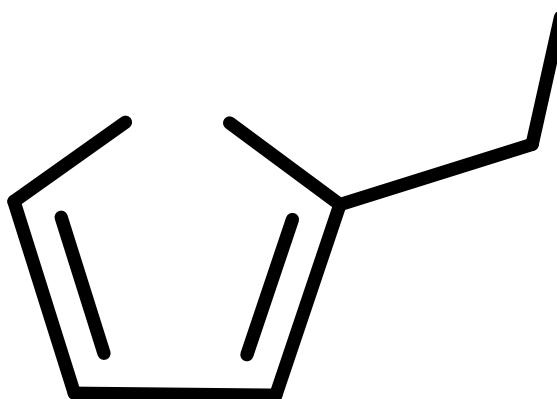
5.3.1. Synthesis of Naphthyridine-Boronic Acid (1.1):

This chapter provides a detailed account of the preparation of naphthyridine-boronic acid (**1.1**), evaluation of its photophysical properties and sensitivity towards heavy metals and sugars. The key intermediate in synthesis of the chemosensor **1.1** is compound **1.2**, which in its turn could be synthesized through four different routes (**Scheme 1**).

Scheme 1: Plausible retrosynthesis of key intermediate **1.2** and target molecule **1.1**

The route **I** allowed to successfully synthesize key intermediate **1.2** and target compound **1.1** as described in **Scheme 2**. Thiophene methyl amine, which was protected with Boc-anhydride to give compound **2.1** served as the starting material for this synthetic route.¹⁴ Compound **2.1** was subjected to lithiation using n-BuLi followed by treatment with tributyl tin chloride resulting in compound **2.2** in excellent yield.¹⁴ Further, compound **2.2** was methylated using methyl iodide and potassium hexamethyldisilazane as a base, to give compound **1.3** in 96% yield. In order to build naphthyridine moiety, 2,6-diamino pyridine **2.3**, was cyclised using DL-malic acid in the presence of conc. H₂SO₄, according to standard procedure,¹⁵ to give 7-amino-1,8-naphthyridin-2-ol (**2.4**) in 86% yield. Amino group of 7-amino-1,8-naphthyridin-2-ol was protected using acetic anhydride to obtain acetamide protected compound **2.5** in

89% yield.¹⁶ This step allowed subsequent selective conversion of hydroxyl group to the halogen via chlorination with phosphorus oxychloride to obtained **1.4** in 60% yield.¹⁶ In the next step, coupling of compound **1.3** with **1.4** in Stille coupling conditions in 1,4-dioxane using palladium (II) catalyst resulted in compound **2.6** in 67% yield. In order to introduce phenyl-boronic acid moiety in this scaffold, Boc-protection of the compound **2.6** was removed using trifluoroacetic acid to give key intermediate **1.2** in 82% yield, followed by N-alkylation with commercially available 2-bromomethylphenylboronic acid, using potassium carbonate as a base. Final compound **1.1** was obtained in 70% yield and its structure was confirmed by different methods, including NMR spectroscopy and mass-spectrometry. Particularly, ¹H NMR spectrum showed an appearance of characteristic N-CH₂ peak at 3.72 ppm and B-(OH)₂ peak at 9.03 ppm, additionally EI-MS spectrum showed predominant peak with *m/z* value of 447.1 corresponding to target molecule **1.1**.



Scheme 2: Route **I** towards key intermediate **1.2** and target compound **1.1**

Apart from the successful route described above, other attempts to synthesize target compound **1.1** were made as sketched in Scheme 1, including:

- imine formation followed by reduction using intermediate **1.5**, as presented in route **II**;

- b) conversion of bromine to amine, via azide formation followed by N-alkylation using intermediate **1.6**, as presented in route **III**;
- c) N-alkylation using intermediate **1.7**, as presented in route **IV**.

Our attempt to synthesize key intermediate **1.2** following route **II** is outlined in **Scheme 3a**. Commercially available starting material thiophene-2-carbaldehyde **3.1** was protected with ethylene glycol to give compound **3.2** in 88% yield.¹⁷ Later, compound **3.2** was subjected to lithiation using n-BuLi followed by treatment with tributyl tin chloride to afford compound **3.3** in good yield.¹⁷ In the next step, compound **3.3** was coupled to compound **1.4** in Stille coupling conditions in THF using palladium (II) catalyst to give compound **3.4** in decent yields. Deprotection of compound **3.4** with 1M HCl led to compound **1.5** in 73% yield.

Scheme 3: Route II towards key intermediate **1.2**

We expected to obtain key intermediate **1.2** after treatment of compound **1.5** with methyl amine to obtain corresponding imine, followed by reduction using sodium borohydride. Unfortunately, reaction didn't initiate under these conditions and starting materials were recovered as it is. Therefore, we desired to change the

synthetic plan as outlined in **Scheme 3b**. In this case, the same starting material thiophene-2-carboxaldehyde **3.1** first was subjected to imine formation using methyl amine followed by reduction with sodium borohydride to afford compound **3.5** in 60% yield. In the next step, Boc protection of compound **3.5** gave compound **3.6** in 97% yield, and finally compound **3.6** was subjected to lithiation using *n*-BuLi followed by treatment with tributyl tin chloride. Unfortunately, instead of **3.7** we obtained unexpected compound **3.8** as a major product. ¹H NMR spectroscopy shows three protons in aromatic region and one proton at 3.96 ppm corresponding to **3.8**.¹⁸

Another attempt towards key intermediate **1.2** was made as described in route **III** and outlined in **Scheme 4**. The synthesis started from lithiation of methyl thiophene **4.1** with *n*-BuLi, which was further treated with tributyl tin chloride to give compound **4.2** in 64% yield.¹⁹ Subsequently, compound **4.2** was coupled with compound **1.4** in Stille coupling conditions in 1,4-dioxane using palladium (II) catalyst to give compound **4.3** in 83% yield. Next, we were planning partial bromination of compound **4.3** with *N*-bromosuccinimide using free radical initiator azobisisobutyronitrile (AIBN). However, this reaction did not lead to compound **1.6**, instead we observe a complex mixture of side products and had to abandon this scheme (**Scheme 4**).

Scheme 4: Route III towards key intermediate **1.2**

Yet another attempt towards key intermediate **1.4** is outlined in **Scheme 5**, route IV. We used compounds **2.2** and **1.4** as our starting materials and subjected them to Stille coupling in 1,4-dioxane using palladium (II) catalyst to obtain compound **5.1** in 84% yield. Boc-deprotection of the later using trifluoroacetic acid resulted in compound **1.7** in 82% yield. Further, in order to attain key starting material

1.2, compound **1.7** was treated with methyl iodide as a methylating agent and potassium carbonate as a base. Although this step was successful, the yield of compound **1.2** was very poor, only 21%. Such low yield is the result of exclusive formation of over-alkylated product (**Scheme 5**). Therefore, this synthetic pathway was not efficient enough and was abandoned as well.

Scheme 5: Route IV towards key intermediate **1.2**

5.3.2 Photophysical Properties of Compound **1.1**:

To explore utility of the final fluorophore **1.1**, we investigated the photophysical properties of **1.1** in MeOH and MeOH/H₂O solutions. In both solutions, MeOH and MeOH/H₂O fluorophore **1.1** displayed identical absorption maxima at 356 nm and a shoulder at 371 nm (**Figure 1**). Fluorescent emission spectra ($\lambda_{ex}=356$ nm) in both solvents exhibited similar fluorescence bands, with a maximum at 401 nm for **1.1** in MeOH and 403 nm in MeOH/H₂O (**Figure 2**). The solution state quantum yield of **1.1** in MeOH/H₂O ($\Phi_f = 0.26$) was slightly higher than that in MeOH ($\Phi_f = 0.20$), Stokes shift of the new fluorophore **1.1** was 31 nm.

Table 1: Numerical photophysical data of **1.1** in MeOH and MeOH/H₂O at 10^{-5} M

Solvent	λ_{abs} , nm	λ_{em} , nm	Relative Φ_f with respect to quinine sulphate
MeOH	356, 371	401	0.20
MeOH/H ₂ O (50:50)	356, 371	403	0.26
MeOH/H ₂ O (2:98)	356, 371	403	0.25

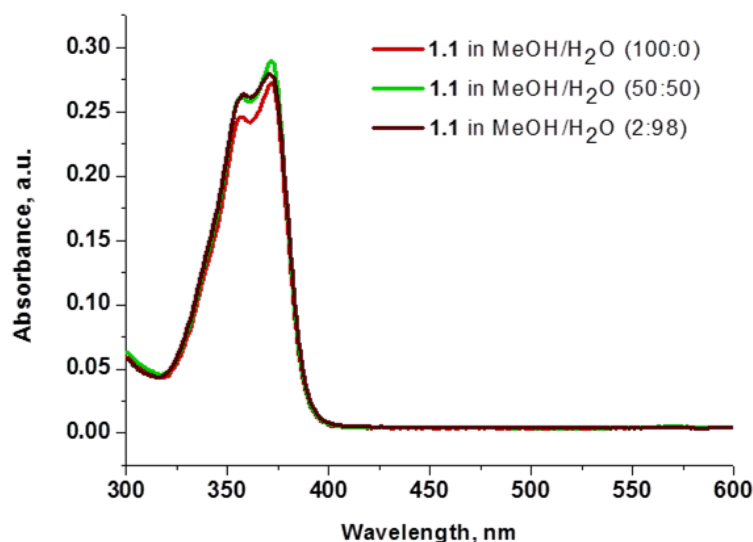


Figure 1: UV-Vis absorption spectra of **1.1** in MeOH and MeOH/H₂O at 10^{-5} M

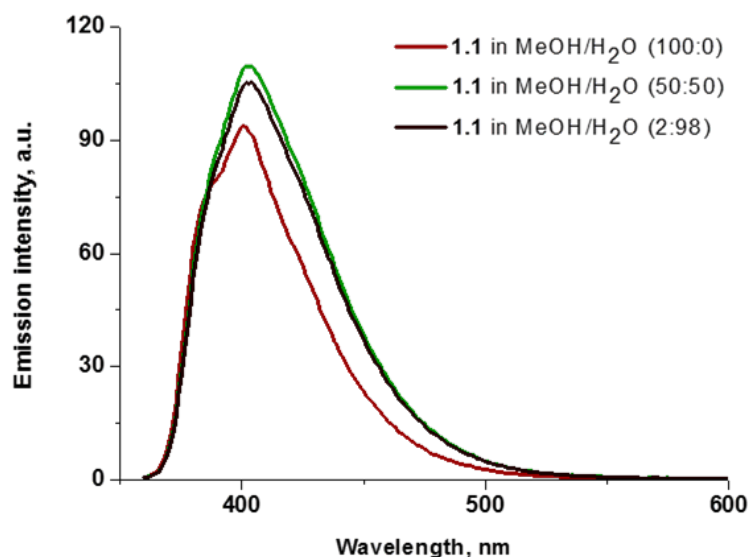


Figure 2: Emission spectra of **1.1** in MeOH and MeOH/H₂O ($\lambda_{\text{ex}} = 356$ nm) at 10^{-5} M

5.3.3 Examination of Binding Ability of **1.1** to Metal Ions:

Fluorescence response of compound **1.1** in presence of various metal ions was investigated in this chapter. The study was carried out in aqueous methanolic buffer at pH 7.5, and metal ions such as Ag^{+} , Zn^{+2} , Cu^{+1} , Mg^{+2} , Pb^{+2} , Cd^{+2} , Hg^{+2} , Li^{+1} and Fe^{+3} were tested. Among them, addition of Hg^{+2} to **1.1** showed a significant decrease of fluorescence intensity by 75% (**Figure 3**). This can be explained by the fact that after coordination to metal ion fluorophore becomes electron deficient, and as a result the PET from proximal tertiary nitrogen to adjacent chromophore increases and the fluorescence intensity of the fluorophore decreases. Fluorescence properties of

compound **1.1** (10^{-5}M) were also studied upon increasing the concentration of Hg^{2+} (1-10 eq), and it was observed that as the concentrations of Hg^{2+} increases fluorescent intensity of **1.1** gradually decreases as shown in **Figure 4**. In order to estimate the binding stoichiometry of naphthridine-boronic acid- Hg^{2+} complex, Job plot experiments were employed.²⁰ In Job method, equal concentrations of Hg^{2+} and **1.1** were prepared, and mixed in different proportions maintaining a total concentration of $10\text{ }\mu\text{M}$. Using the obtained data a graph was plotted between the emission intensity (fixed at 408 nm) and a mole fraction of compound **1.1** (**Figure 5**). The minimum emission intensity was reached when the mole fraction was 0.5. These results indicate that the formation of naphthridine-boronic acid- Hg^{2+} complex in a 1:1 ratio. The association constant (K_a) of naphthridine-boronic acid- Hg^{2+} was calculated from the variation of fluorescence intensity as a function of the concentration of Hg^{2+} by using Benesi-Hildebrand equation²¹ (equation 1) and fitting the emission wavelength at 408 nm. The calculated K_a for **1.1** with Hg^{2+} was $2.842 \times 10^5\text{ M}^{-1}$.

$$\frac{1}{F-F_0} = \frac{1}{K_a(F_{\max}-F_0)[\text{Hg}^{2+}]} + \frac{1}{F_{\max}-F_0} \quad \dots \dots \dots (1)$$

Where F is the fluorescence intensity at 408 nm at any given concentration of Hg^{2+} , F_0 is the fluorescence intensity at 408 nm in the absence of Hg^{2+} , F_{\max} is the fluorescence intensity at 408 nm in the presence of Hg^{2+} in solution and K_a is association constant.

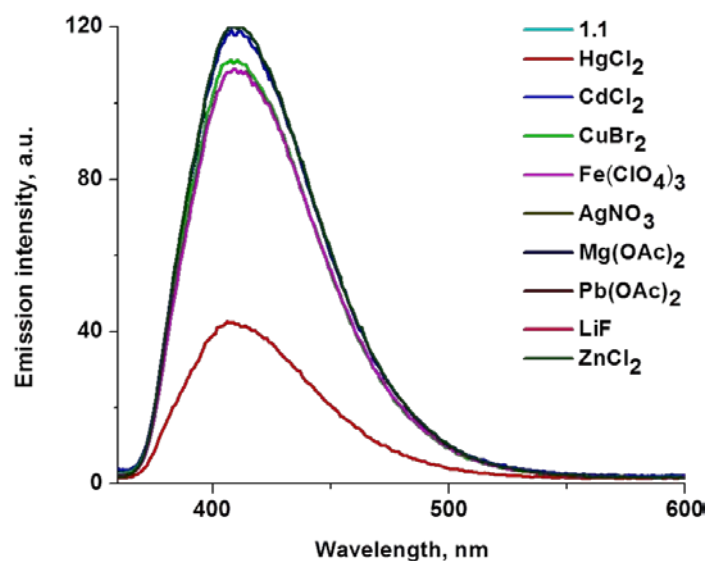


Figure 3: Fluorescence spectra of compound **1.1** (1eq, 10^{-5}M) in $\text{MeOH}/\text{H}_2\text{O}$ ($v/v=1:1$, 5.0 mM PBS, pH 7.50) in presence of various metal ions (1 eq, 10^{-5}M)

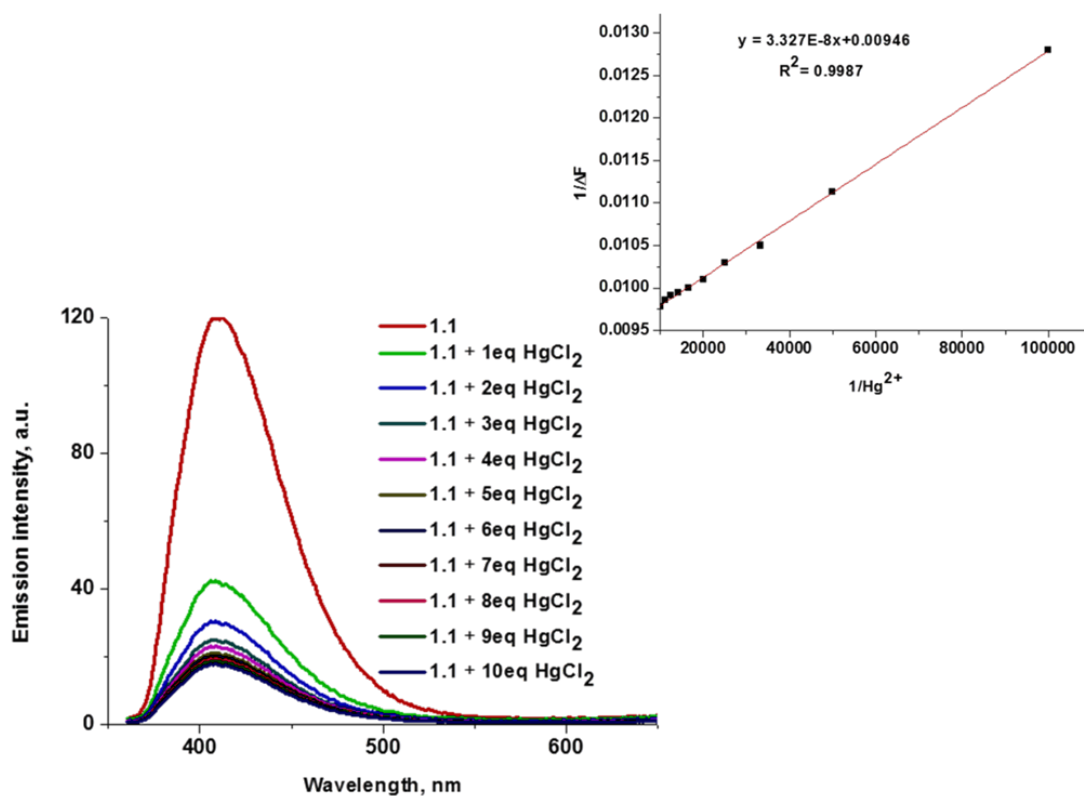


Figure 4: Fluorescence spectra of compound **1.1** (1eq, 10^{-5} M) in MeOH/H₂O (v/v=1:1, 5.0 mM PBS, pH 7.50) in presence of Hg²⁺ at various concentrations (0-10 eq) and inset shows Benesi-Hildebrand plot of the naphthyridine-boronic acid-Hg²⁺ complex in MeOH/H₂O (v/v=1:1, 5 mM PBS, pH 8.20) solutions. The monitored emission wavelength was 408 nm

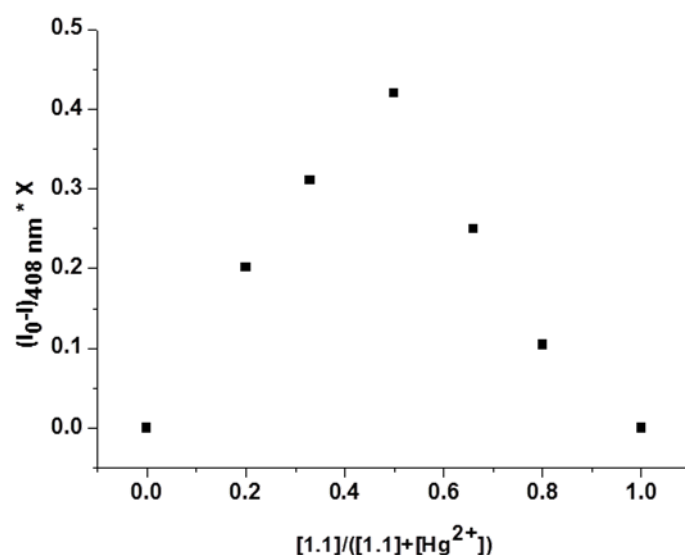


Figure 5: Job plot of naphthyridine-boronic acid-Hg²⁺ complex (total concentration was 10 μ M) in MeOH/H₂O (v/v=1:1, 5.0 mM PBS, pH 7.50). The monitored emission wavelength was 408 nm

In order to understand the structure of naphthyridine-boronic acid- Hg^{2+} complex, proton NMR spectroscopy was employed.²² Addition of Hg^{2+} to the DMSO solution of **1.1** resulted in a downfield chemical shift of the H_a proton from 7.10 ppm to 7.55 ppm, additionally a moderate down field chemical shifts observed for H_e and $\text{H}_{h,i,j}$ (**Figure 6**). These changes indicate that Hg^{2+} interacts mainly with the sulphur atom, which was expected as high affinity of mercury for sulphur atoms is well known, and partly binds to the N_1 and N_8 of the naphthyridine moiety; at the same time there are no interaction with N-methyl nitrogen (no shift observed in NMR spectrum, not shown in **Figure 6**). The decrease of fluorescence intensity (**Figure 5**) or down field chemical shifts of H_a , H_e and $\text{H}_{h,i,j}$ upon addition of Hg^{2+} (**Figure 6**) are due to decrease of electron density after coordination of Hg^{2+} to the respective binding site as shown in **Figure 6**. Therefore, these both observations support the theory of PET mechanism for presented here chemosensor.

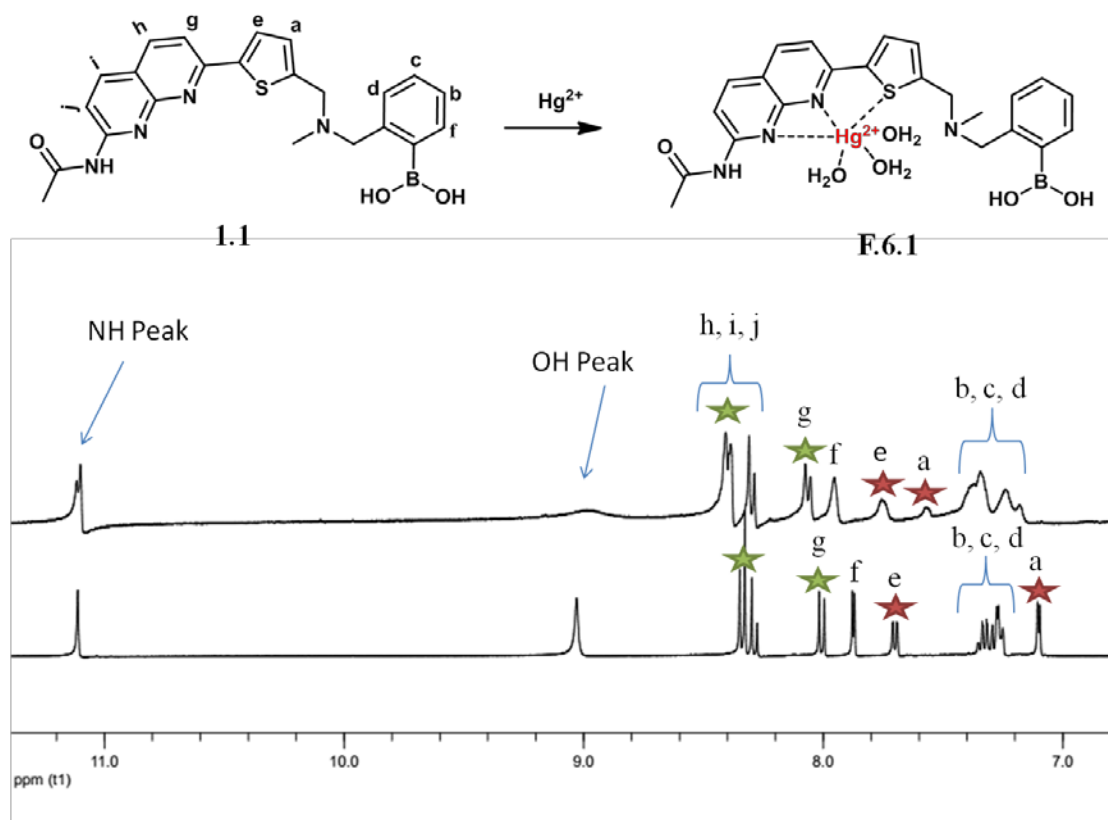


Figure 6: ^1H NMR spectra of compound **1.1** (1 eq) in the presence of Hg^{2+} (3 eq) in $\text{DMSO}-d_6$

5.3.4. Examination of Binding Ability of **1.1** to Monosaccharides:

Fluorescence titration studies of compound **1.1** (10^{-5} M) in presence of various monosaccharides was carried out in aqueous methanolic phosphate buffer at pH 8.20. As expected, the fluorescence intensity of compound **1.1** increased upon increasing of saccharides concentration (D-glucose, D-mannose, D-fructose and D-galactose). As reported by Shinkai *et al.*²³ such fluorescence response explained by the fact that boronic acids (such as compound **1.1**) form cyclic esters with cis 1,2-diol or 1,3-diol of mono saccharides, which leads to increase of the Lewis acidity of the central boron atom. As result B-N (proximal tertiary nitrogen) interactions are strengthening²⁴ and PET from proximal tertiary nitrogen to adjacent fluorophore is suppressed and the fluorescence of the fluorophore is enhancing.^{23,25} The fluorescence enhancement I/I_0 obtained for D-glucose, D-galactose, D-mannose and D-fructose is in the order D-fructose > D-galactose > D-mannose > D-glucose as shown in **Figure 7**.

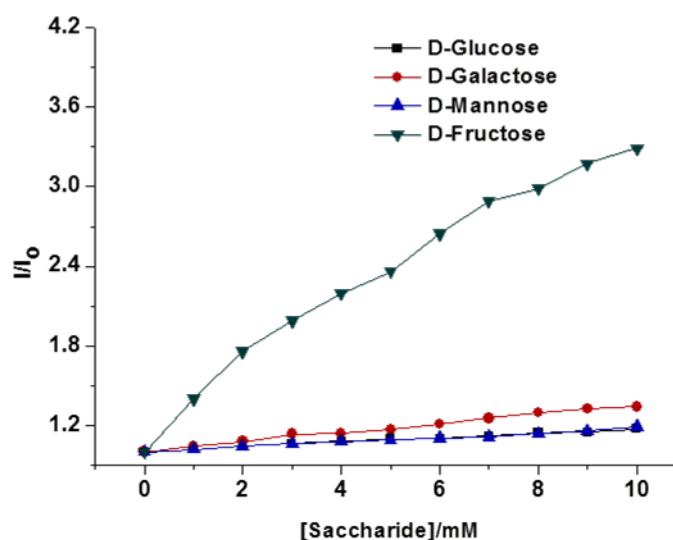


Figure 7: Fluorescence intensity of compound **1.1** (1×10^{-5} M) in MeOH/H₂O (v/v=1:1, 5 mM PBS, pH 8.20) in the presence of D-glucose, D-mannose, D-fructose and D-galactose

The binding selectivity of **1.1** towards D-fructose is around two and half fold higher compared to other monosaccharides (D-galactose, D-mannose, D-glucose) at lower concentrations (< 10 mM) as shown in **Figures 8, 9, 10** and **11**. The association constant (K_a) of naphthridine-boronic acid based fluorescence chemo sensor **1.1** with D-fructose, D-glucose, D-galactose and D-mannose were calculated from the variation of fluorescence intensity as a function of the concentration of D-

monosaccharides, using Benesi-Hildebrand equation²¹ (equation 2) and fitting the emission wavelength at 403, 409, 410 and 408 respectively. The observed association constants (K_a) for **1.1** is D-fructose>D-galactose>D-mannose>D-glucose and the calculated association constant are listed in Table 2-5.

$$\frac{1}{F - F_0} = \frac{1}{K_a(F_{\max} - F_0)[\text{sugar}]} + \frac{1}{F_{\max} - F_0} \quad \dots \dots \dots (2)$$

Where F is the fluorescence intensity at 403/409/410/408 nm at any given concentration of D-fructose/D-galactose/D-mannose/D-glucose respectively, F_0 is the fluorescence intensity at 403/408/409/410 nm in the absence of D-saccharides, F_{\max} is the fluorescence intensity at 403/409/410/408 nm in the presence of D-fructose/D-galactose/D-mannose/D-glucose respectively in solution and K_a is association constant.

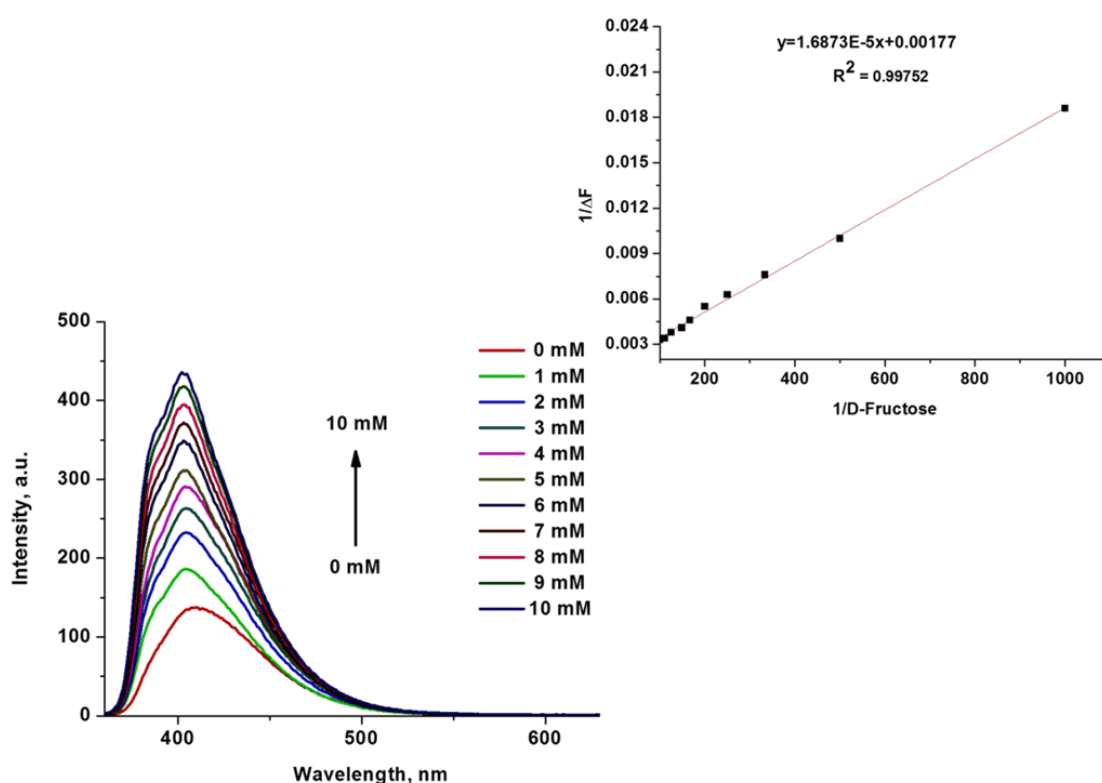


Figure 8: Fluorescence spectra of compound **1.1** (10^{-5} M) in presence of D-fructose at various concentrations (0-10 mM) and inset shows Benesi-Hildebrand plot of the naphthyridine-boronic acid-fructose complex in MeOH/H₂O (v/v=1:1, 5 mM PBS, pH 8.20) solutions. The monitored emission wavelength was 403 nm

Table-II: Benesi-Hildebrand association constant for **1.1** with D-fructose.

IF	IF-IF ₀ (ΔF)	D- Fructo- se (mM)	1/D- Fruct- ose	1/ΔF	K _a 104.91 M ⁻¹	Slope 1.6873E-5
185.489	53.750	0.001	1000	0.0186		
231.690	99.951	0.002	500	0.010		
262.329	130.590	0.003	333.33	0.0076		
289.623	157.884	0.004	250	0.0063		
311.109	179.670	0.005	200	0.0055	IF ₀ 131.739	Intercept 0.00177
348.621	216.882	0.006	166.66	0.0046		
371.462	239.723	0.007	142.85	0.0041		
393.968	262.229	0.008	125	0.0038		
418.180	286.441	0.009	111.11	0.0034		
433.771	302.032	0.10	100	0.0033		

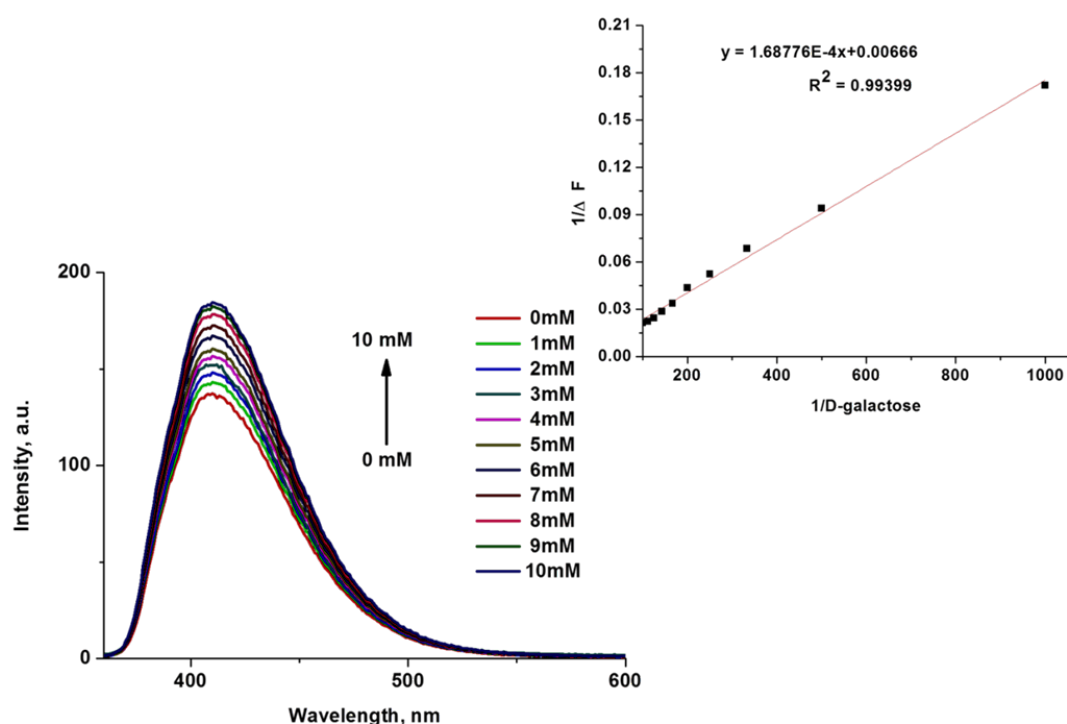


Figure 9: Fluorescence spectra of compound **1.1** (10^{-5} M) in presence of D-galactose at various concentrations (0-10 mM) and inset shows Benesi-Hildebrand plot of the naphthyridine-boronic acid-galactose complex in MeOH/H₂O (v/v=1:1, 5 mM PBS, pH 8.20) solutions. The monitored emission wavelength was 410 nm

Table III: Benesi-Hildebrand association constant for **1.1** with D-galactose.

IF	IF-IF ₀ (ΔF)	D- galactose (mM)	1/D- galactose	1/ΔF	K _a 39.46 M ⁻¹	Slope 1.68776E-4
143.188	5.808	0.001	1000	0.172		
148.000	10.620	0.002	500	0.0941		
151.999	14.619	0.003	333.33	0.0684		
156.438	19.058	0.004	250	0.0524		
160.275	22.895	0.005	200	0.0436	IF ₀ 137.38	Intercept 0.00666
166.896	29.516	0.006	166.66	0.0338		
172.338	34.958	0.007	142.85	0.0286		
178.320	40.94	0.008	125	0.0244		
182.142	44.762	0.009	111.11	0.0223		
184.326	46.946	0.10	100	0.0213		

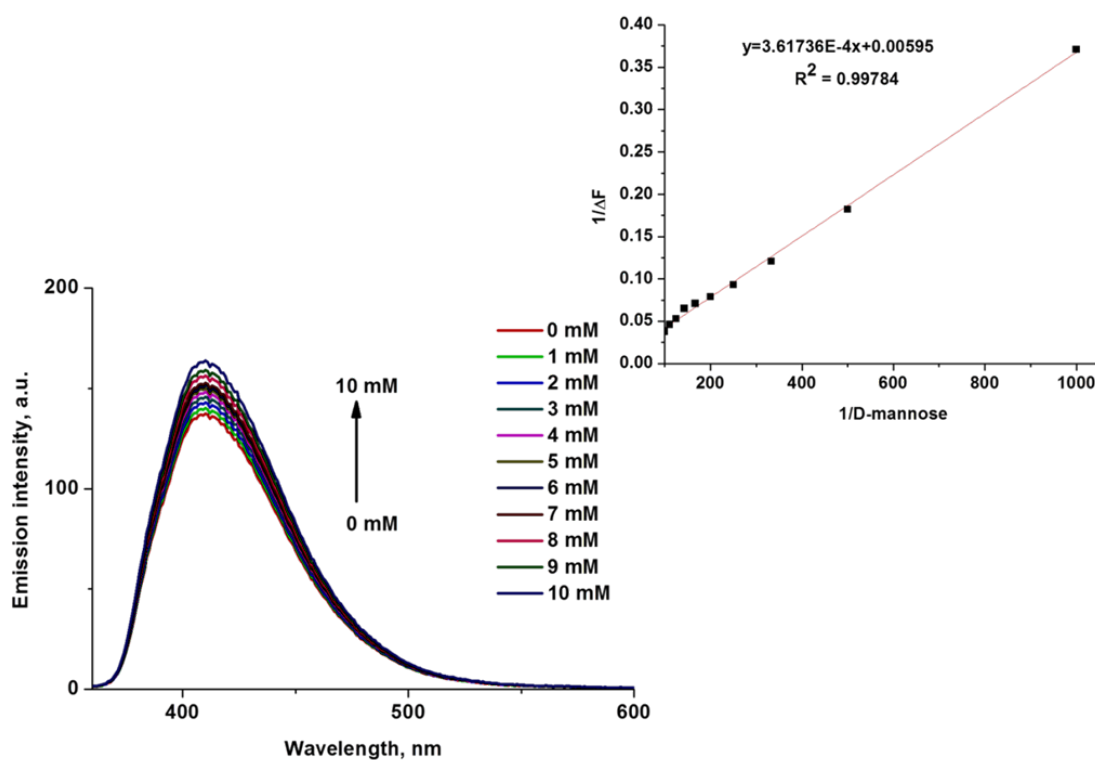
**Figure 10:** Fluorescence spectra of compound **1.1** (10^{-5}M) in presence of D-mannose at various concentrations (0-10 mM) and inset shows Benesi-Hildebrand plot of the naphthyridine-boronic acid-mannose complex in MeOH/PBS (v/v=1:1, 5 Mm PBS, pH 8.20) solutions. The monitored emission wavelength was 408 nm

Table IV: Benesi-Hildebrand association constant for **1.1** with D-mannose.

IF	IF-IF ₀ (ΔF)	D-mannose (mM)	1/D- mannose	1/ΔF	K _a 16.44 M ⁻¹	Slope 3.61736E-4
139.565	5.808	0.001	1000	0.371		
142.364	10.620	0.002	500	0.182		
145.134	14.619	0.003	333.33	0.121		
147.620	19.058	0.004	250	0.093		
149.528	22.895	0.005	200	0.079	IF ₀ 136.87	Intercept 0.00595
150.954	29.516	0.006	166.66	0.071		
152.254	34.958	0.007	142.85	0.065		
155.730	40.94	0.008	125	0.053		
158.609	44.762	0.009	111.11	0.046		
163.180	46.946	0.10	100	0.038		

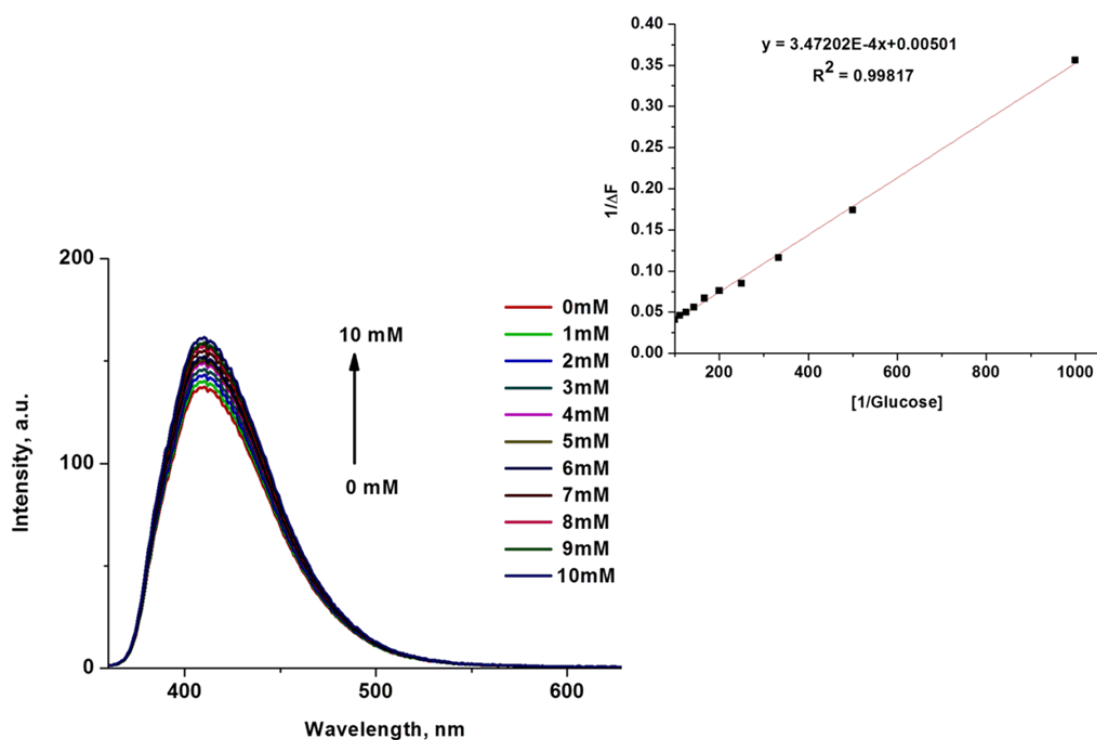
**Figure 11:** Fluorescence spectra of compound **1.1** (10^{-5} M) in presence of D-glucose at various concentrations (0-10 mM) and inset shows Benesi-Hildebrand plot of the naphthridine-boronic acid-glucose complex in MeOH/H₂O (v/v=1:1, 5 mM, pH 8.20) solutions. The monitored emission wavelength was 409 nm

Table V: Benesi-Hildebrand association constant for **1.1** with D-glucose.

IF	IF-IF ₀ (ΔF)	D-glucose (mM)	1/D-glucose	1/ΔF	K _a 14.42 M ⁻¹ IF ₀ 136.64	Slope 3.47202E-4 Intercept 0.00501
139.444	2.804	0.001	1000	0.356		
142.382	5.742	0.002	500	0.174		
145.251	8.611	0.003	333.33	0.116		
148.367	11.720	0.004	250	0.085		
149.730	13.090	0.005	200	0.076		
151.371	14.731	0.006	166.66	0.067		
154.270	17.630	0.007	142.85	0.056		
156.456	19.810	0.008	125	0.050		
158.096	21.450	0.009	111.11	0.046		
160.651	24.010	0.10	100	0.041		

Fluorescence response of the boronic acid based fluorescent chemosensors is usually pH dependent. Therefore, fluorescence response of naphthyridine-boronic acid fluorescent chemosensor **1.1** was measured at different pH, both in the presence and absence of D-fructose. As **Figure 12** displays, in both cases the fluorescent

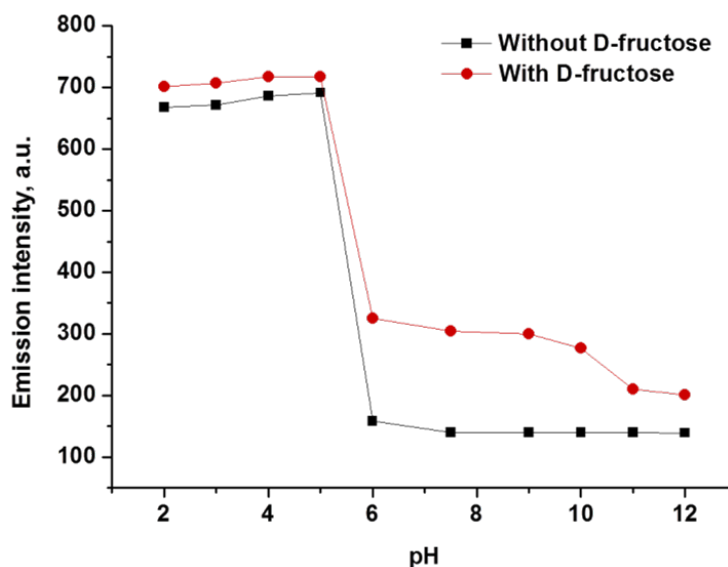


Figure 12: pH vs fluorescent intensity of **1.1** (10^{-5} M) in presence and absence of D-fructose in MeOH/H₂O (v/v=1:1, 5 mM, at various pH) solutions. The monitored emission wavelength was 403 nm

response was similar. Fluorescent intensity was increasing upon pH change from 2 to 5.5 due to protonation of tertiary amine, and was decreasing as pH raised from 5.5 to 12 (**Figure 12**) due to deprotonation of tertiary amine and OH^- adduct formation with boronic acid group.²⁶

5.3.5. Competitive Sensing of Hg^{2+} and D-monosaccharide:

As compound **1.1** has incorporated phenyl boronic acid moiety which is expected to bind to mono-saccharides, its fluorescence response was examined in presence of Hg^{2+} and various D-monosaccharides. It was expected, that cooperative binding of both sugar and metal ion will result in increased sensitivity of the chemosensor to either of analytes, decreasing/eliminating at the same time interference by various factors, which is common for chemosensors acting through “turn-off” mechanism.^{26a} The study was carried out in aqueous methanolic buffer at pH 7.5. Addition of Hg^{2+} to a solution containing both chemosensor **1.1** and D-fructose complex resulted in dramatic decrease of fluorescence intensity by seven folds. This fluorescent response was ~ 2.5 times more in comparison with the one, when compound **1.1** was interacting with mercury without addition of fructose. Till date, there are no reports, where the sensitivity of the chemosensor for metal ions was enhances as result of interaction with fructose, although there are few investigations utilizing metal-sensor coordination in order to improve sensitivity towards sugar.

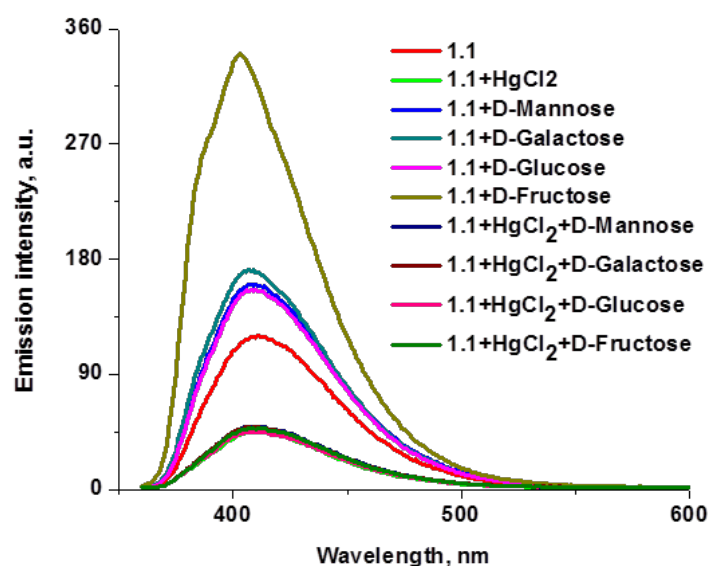


Figure 11: Fluorescence spectra of **1.1** alone (10^{-5} M), **1.1** with Hg^{2+} and **1.1** with Hg^{2+} and D-monosaccharides in MeOH/ H_2O (v/v=1:1, 5 mM, at various pH) solutions

For example, Seiji Shinkai *et al.* reported^{26a} new saccharide receptor for uronic acids, based on two-point interactions of boronic acid and a coordination with zinc (II). Yet another work, employing cooperative binding of fructose and metal ion was performed by group of Tony D. James. In this case, however, the fluorescence response after addition of fructose to chemosensor-Cu (II) complex was negligible.¹³ Thus, presented in this chapter work is the first example of employing boronic acid–diol complexation to achieve significant enhancement of the sensor’s sensitivity towards toxic metal ion.

5.4. Conclusions:

In conclusion, this chapter discloses the design and synthesis of novel fluorescent chemosensor **1.1** [(2-((((5-(7-acetamido-1,8-naphthyridin-2-yl)thiophen-2-yl)methyl)(methyl)amino) methyl)phenyl)boronic acid], its fluorescence properties and interaction with various metal ions and monosaccharides. Chemosensor **1.1** was designed to combine naphthyridine as a fluorescent metal chelating site and phenyl boronic acid as a saccharide recognition unit in one scaffold. The combination of these properties allowed investigation of the sensing abilities of **1.1** over various metal ions and D-monosaccharides. Fluorescence change, mediated by PET mechanism, was utilized as a reporting property of the chemosensor. Compound **1.1** found to have dramatic decrease of fluorescence intensity selectively upon binding to Hg²⁺, probably due to decrease of electron density after coordination of Hg²⁺ to the respective binding site as shown in **F.6.1**. As a result, PET from proximal tertiary nitrogen to adjacent fluorophore enhanced and the fluorescence intensity changed by 3 folds. The binding stoichiometry of the naphthyridine-boronic acid-Hg²⁺ complex was found to be 1:1, according to Job plot experiments. The association constant for **1.1** with Hg²⁺ was found to be $2.842 \times 10^5 \text{ M}^{-1}$. Interestingly, the sensitivity of chemosensor **1.1** greatly improved in the presence of D-fructose at physiological concentration, perhaps as result of the cooperative binding of both D-fructose and mercury ion to the sensor. Presented in this chapter work is the first example of employing boronic acid–diol complexation to achieve significant enhancement of the sensor’s sensitivity towards toxic metal ion. This finding is especially important for applications in food industry, e.g. for detection of mercury contamination of high fructose corn syrup, or for estimation of mercury in polluted biological samples and underground water.

5.5. Experimental Section:

5.5.1. Materials and Methods:

The materials 2-thiophene carboxaldehyde, 2,6-diaminopyridine, n-butyl lithium, tributyltin chloride, bis(triphenylphosphine)palladium(II) dichloride, acetic anhydride, methyl amine (40% aqueous solution), 2-thiophenemethylamine, potassium bis(trimethylsilyl)amide, 2-(bromomethyl)phenylboronic acid and paraformaldehyde were purchased from Sigma Aldrich. N-bromosuccinimide, phosphorus trichloride oxide, azobisisobutyronitrile, di-tert-butyl dicarbonate, trifluoroacetic acid, methyl iodide were purchased from Spectro Chem. Commercial reagents (DL-malic acid, ethane-1,2-diol, sodium borohydride, ammonium bicarbonate, and HCl) were purchased from Merck and Rankem and were used as received. The solvents THF, DMF, toluene, 1,4-dioxane and DCM were distilled and dried before reactions and for extracting purposes. All reactions were carried out under an inert atmosphere with dry solvents, unless otherwise stated. Syringes and needles for the transfer of reagents were dried at 100 °C and allowed to cool in a desiccator over P₂O₅ before use. Reactions were monitored by thin layer chromatography (TLC) on silica gel plates (60 F254), using UV light detection. Merck silica gel (particle size 100-200 mesh) was used for column chromatography. For UV-Vis and fluorescence measurements spectroscopic grade solvents were used.

5.5.2. Buffer Preparation for Fluorescence Studies:

Fluorescence studies were performed using aqueous methanolic buffer (pH 8.20), which was prepared according to Perrin and Dempsey protocol:²⁷ 8 g of NaCl, 0.2 g of KCl, 1.44 g of Na₂HPO₄, 0.24 g of KH₂PO₄ were dissolved in 800 mL of distilled water and adjust pH by adding a solution of 5 M NaOH and finally make a total volume of 1 L with additional distilled water.

5.5.3. Sample Preparation for Fluorescence Binding Studies with Metal Ions:

A known amount of various metal ions (Hg²⁺, Cu⁺, Ag⁺, Mg²⁺, Pb²⁺, Cd²⁺, Hg²⁺, Li⁺ and Fe³⁺) was added from 4.86×10⁻⁴ M stock solution to a solution of compound **1.1** (30 µL of 10⁻³ M). The volume of the prepared solution was adjusted to 3mL with

buffer to achieve final concentration 10 μ M in respect to compound **1.1**. The fluorescence measurements were made for each solution.

5.5.4. Stoichiometry Determination Using Jobs Plot:

In Job method, solutions of Hg²⁺ and **1.1** with equal concentrations were prepared in MeOH/H₂O (v/v=1:1, 5 mM, pH 7.50), and mixed in different proportions maintaining a total volume of 3 mL and total concentration of 10 μ M of the mixture. Then emission of these solutions was recorded, and a graph of the emission intensity (fixed at 408 nm) versus a mole fraction of compound **1.1** was plotted. The stoichiometry of the complex was determined by the point of the maximum emission intensity.

5.5.5. Sample Preparation for Fluorescence Binding Studies with D-Mono Saccharides:

A known amount of D-monosaccharides (D-glucose, D-galactose, D-mannose and D-fructose) was added from 0.3 M stock solution to a solution of compound **1.1** (30 μ L of 10⁻³ M). The volume of the prepared solution was adjusted to 3mL with buffer to achieve final concentration 10 μ M in respect to compound **1.1**. The fluorescence measurements were made for each solution and I/I₀ was plotted at 409, 410, 408 and 403 nm respectively.

5.5.6. Sample Preparation for Fluorescence Binding Studies of D-Fructose at Various pH Solutions:

A known amount of D-fructose was added from 0.3 M stock solution to a solution of compound **1.1** (30 μ L of 10⁻³ M). The volume of the prepared solution was adjusted to 3mL with buffer (pH 2, 3, 4, 5, 7.5, 9, 10, 11, 12 respectively) to achieve final concentration 10 μ M in respect to compound **1.1**. The fluorescence measurements were made for each solution and I/I₀ was plotted at 403 nm.

5.5.7. Sample Preparation for Competitive Binding Studies of D-Monosaccharides and Hg²⁺:

A known amount of D-monosaccharides (from 0.3 M stock solution), Hg²⁺ (from 4.86 \times 10⁻⁴ M stock solution) and 30 μ L of a 10⁻³ M of compound **1.1** was placed in

3mL buffer to give a final concentration of 10 μ M. The fluorescence measurements were made for each solution.

5.5.8. Synthesis of Target Compound 1.1:

Route I; Scheme 2:

Tert-butyl (thiophen-2-ylmethyl)carbamate (2.1):¹⁴

Thiophene-2-methyl amine (0.5 g, 4.42 mmol) was dissolved in dry DCM (20 mL), and triethyl amine (0.95 mL, 6.84 mmol) was added to the solution. Boc-anhydride (1.22 mL, 5.31 mmol) was added portion wise to the above reaction mixture. After complete addition of boc-anhydride the reaction mixture was stirred at room temperature for 4 h. After 4 h, the reaction mixture was washed with water and extracted with DCM. The organic phase was dried with anhydrous sodium sulphate, concentrated under reduced pressure, and the resulting residue **2.1** (0.8 g, 86%) was used without further purification. Spectroscopic data matches with the one from reported procedure. ¹H NMR (CDCl₃, 400 MHz) δ : 7.21 (1H, m), 6.93 (2H, m), 4.87 (1H, brs), 4.47 (2H, d), 1.46 (9H, s).

Tert-butyl ((5-(tributylstannyl)thiophen-2-yl)methyl)carbamate (2.2):¹⁴

To a solution of compound **2.1** (0.4 g, 2.62 mmol) in dry THF (30 mL) was added n-butyl lithium (1.6 M in hexane, 3.58 mL, 5.73 mmol) at -78 °C. After 1 h at -78 °C, tributyl tin chloride (1.57 mL, 5.81 mmol) was added drop wise to the above reaction mixture. After stirring over 6 h at room temperature, the reaction mixture was quenched with 20 mL of saturated aqueous ammonium chloride solution and extracted with THF. The organic phase was dried with anhydrous sodium sulphate, concentrated under reduced pressure, and the resulting residue **2.2** (0.87 g, 93%) was used without further purification. Spectroscopic data matches with the one from reported procedure. ¹H NMR (CDCl₃, 400 MHz) δ : 7.05 (1H, d), 6.99 (1H, d), 4.87

(1H, brs), 4.51 (2H, s), 1.54 (6H, m), 1.46 (9H, s), 1.32 (6H, m), 1.07 (6H, m), 0.89 (9H, m).

Tert-butyl methyl((5-(tributylstannyl)thiophen-2-yl)methyl)carbamate (1.3):

To a solution of compound **2.2** (5.54 g, 11.0 mmol) in 30 mL of dry THF was added 1M KHMDS (22 mL, 22 mmol) dropwise at -10 °C. The reaction was maintained at -10 °C for 1.5 h, and methyl iodide (2.05 mL, 33.0 mmol) was added drop wise. The ice bath was removed and reaction mixture was stirred at room temperature for 4 h. The reaction mixture was washed with brine (4 × 100 mL) and extracted with hexane. The organic layer was collected, dried over anhydrous sodium sulphate, concentrated under reduced pressure to provide compound **1.3** (5.45 g, 96% yield) as a dark brown oil, which was used without further purification. TLC (10% EtOAc in Hexane): R_f = 0.39; ¹H NMR (CDCl₃, 400 MHz) δ: 7.03 (1H, d), 7.01 (1H, d), 4.56 (2H, s), 2.86 (3H, s), 1.65 (2H, m), 1.55 (4H, m), 1.49 (9H, s), 1.33 (6H, m), 1.08 (6H, m), 0.89 (9H, m). ¹³C NMR (CDCl₃, 100 MHz) δ: 155.3, 146.1, 136.7, 134.8, 127.1, 79.9, 47.3, 33.7, 28.9, 28.4, 27.2, 13.6, 10.7. MS (EI, 70ev): *m/z* [M]⁺ calcd for C₂₃H₄₃NO₂SSn: 517.2, found 517.2 [M]⁺. Anal. Calcd for C₂₃H₄₃NO₂SSn: C, 53.50; H, 8.39; N, 2.71; O, 6.20; S, 6.21; Sn, 22.99, found: C, 53.46; H, 8.36; N, 2.75.

7-amino-1,8-naphthyridin-2-ol (2.4):²⁸

2,6-Diaminopyridine **2.3** (1.1 g, 10.07 mmol) and malic acid (1.48 g, 11.07 mmol) were placed in a three necked round bottom flask outfitted with an additional funnel, reflux condenser and mechanical stirrer. The mixture was cooled to 0 °C and conc. H₂SO₄ (5 mL) was added dropwise. After addition of conc. H₂SO₄ was completed, the reaction mixture was slowly heated to 110 °C and stirred for 3 h. The reaction mixture was cooled to 0 °C and the solution was made alkaline (pH=8) by careful addition of aqueous ammonium hydroxide. The crude solid was collected by vacuum

filtration and washed thoroughly with water and methanol to give compound **2.4** as a yellowish solid (1.38 g, 86%). Spectroscopic data matches with the one from reported procedure. ^1H NMR ($\text{DMSO-}d_6$, 400 MHz) δ : 11.91 (1H, s), 7.65 (1H, d), 7.65 (1H, d), 7.03 (2H, s), 6.34 (1H, d), 6.12 (1H, d).

N-(7-hydroxy-1,8-naphthyridin-2-yl)acetamide (2.5):¹⁶

A suspension of compound **2.4** (5.0 g, 15.5 mmol) in 50 mL of acetic anhydride was stirred at 110 °C for 3 h. After 3 h, reaction mixture was cooled to room temperature and the precipitate was collected by vacuum filtration, washed with hexane and dried at reduced pressure to give compound **2.5** as a yellow solid (5.33 g, 89%). Spectroscopic data matches with the one from reported procedure. ^1H NMR ($\text{DMSO-}d_6$, 400 MHz) δ : 11.90 (1H, s), 10.50 (1H, s), 8.02 (1H, d), 7.90 (1H, d), 7.82 (1H, d), 6.40 (1H, d), 2.12 (3H, s).

N-(7-chloro-1,8-naphthyridin-2-yl)acetamide (1.4):²⁹

A mixture of compound **2.5** (10.0 g, 49.25 mmol) and POCl_3 (175 mL) was heated at 100 °C for 2 h. The reaction mixture was cooled to room temperature, and excess of POCl_3 was removed by distillation. The crude residue was dissolved in ice water, and the solution was made alkaline (pH=8) by careful addition of concentrated ammonium hydroxide. The crude solid was collected by vacuum filtration, air-dried, and continuously extracted (Soxhlet extraction) with chloroform for 12 h. Chloroform was removed at reduced pressure, and the crude product was purified using column chromatography on silicagel using MeOH/DCM (1:9) as an eluent to yield compound **1.4** in form of a golden needles (6.47 g, 60%). ^1H NMR ($\text{DMSO-}d_6$, 400 MHz) δ : 8.70 (1H, s), 8.56 (1H, d), 8.20 (1H, d), 8.18 (1H, d), 7.40 (1H, d), 2.30 (3H, S).

Tert-butyl ((5-methyl(7-acetamido-1,8-naphthyridin-2-yl)thiophen-2-yl)methyl) carbamate (2.6):

To a solution of compound **1.3** (6.2 g, 12.0 mmol) in dry 1,4- dioxane (50 mL) were added compound **1.4** (2.0 g, 9.0 mmol) and PdCl₂(PPh₃)₂ (0.315 g, 0.45 mmol) under nitrogen atmosphere. After 12 h at reflux, the solvent was removed under reduced pressure, and the crude residue was dissolved in EtOAc, passed through celite and solvent was evaporated. Crude product was purified by column chromatography using 50% EtOAc in hexane to give **2.6** as yellowish solid (2.5 g, 67%). Mp: 115-118 °C; TLC (50% EtOAc in hexane): R_f = 0.26; ¹H NMR (DMSO-*d*₆, 400 MHz) δ: 11.07 (1H, bs), 8.33 (3H, m), 8.01 (1H, d), 7.87 (1H, d), 7.08 (1H, d), 4.53 (2H, s), 2.80 (3H, s), 2.14 (3H, s), 1.43 (9H, s). ¹³C NMR (CDCl₃, 100 MHz) δ: 169.5, 155.6, 154.6, 153.9, 145.7, 143.5, 139.2, 139.0, 137.0, 126.8, 119.3, 116.9, 114.3, 114.0, 80.2, 48.0, 33.8, 28.4, 24.9. MS (EI, 70ev): *m/z* [M]⁺ calcd for C₂₁H₂₄N₄O₃S: 412.16, found 413.2 [M+1]⁺. Anal. Calcd for C₂₁H₂₄N₄O₃S: C, 61.14; H, 5.86; N, 13.58; O, 11.64; S, 7.77, found: C, 61.26; H, 5.89; N, 13.45.

N-(7-(5-((methylamino)methyl)thiophen-2-yl)-1,8-naphthyridin-2-yl)acetamide (1.2):

Compound **2.6** (0.293 g, 0.71 mmol) was dissolved in TFA: DCM (3 mL: 3 mL) and stirred at RT for 2 h. After 2h solvents were removed and the reaction mixture was treated with sodium bicarbonate solution and extracted with DCM. The organic solvent was removed under reduced pressure and the crude residue was then purified using column chromatography on silicagel using MeOH/DCM (2:8) as an eluent to yield compound **1.2** as a yellowish solid (0.189 g, 85%). Mp: 260-262 °C; TLC (20% MeOH in DCM): R_f = 0.21. ¹H NMR (DMSO-*d*₆, 400 MHz) δ: 11.08 (1H, bs), 8.32 (3H, m), 8.01 (1H, d), 7.86 (1H, d), 7.08 (1H, d), 3.93 (2H, s), 2.35 (3H, s), 2.14 (3H,

s). ^{13}C NMR (DMSO- d_6 , 100 MHz) δ : 170.5, 155.2, 154.9, 154.8, 143.8, 139.6, 138.0, 127.9, 127.5, 119.2, 116.8, 114.2, 49.7, 35.2, 24.5. MS (EI, 70ev): m/z $[\text{M}]^+$ calcd for $\text{C}_{16}\text{H}_{16}\text{N}_4\text{OS}$: 312.1, found 313.1 $[\text{M}+1]^+$. Anal. Calcd for $\text{C}_{16}\text{H}_{16}\text{N}_4\text{OS}$: C, 61.52; H, 5.16; N, 17.93; O, 5.12; S, 10.26, found: C, 61.42; H, 5.23; N, 17.85.

(2-((((5-(7-acetamido-1,8-naphthyridin-2-yl)thiophen-2-yl)methyl)(methyl)amino)methyl)phenyl)boronic acid (1.1):

Anhydrous K_2CO_3 (0.176 g, 1.32 mmol) was added to a stirred suspension of compound **1.2** (0.14 g, 0.44 mmol) in dry DMF (2 mL). After 30 min, a solution of 2-(bromomethyl) phenylboronic acid (0.096 g, 0.44 mmol) in DMF (2 mL) was added, and the reaction mixture was stirred at room temperature for 12 h. DMF was removed under reduced pressure, and the crude residue was washed with water, hexane and toluene to yield compound **1.1** as a white solid (0.14 g, 70%). Mp: 210-212 °C. ^1H NMR (DMSO- d_6 , 400 MHz) δ : 11.12 (1H, s), 9.03 (2H, brs), 8.30 (3H, m), 8.0 (1H, d), 7.87 (1H, d), 7.70 (1H, m), 7.29 (3H, m), 7.10 (1H, d), 3.75 (2H, s), 3.70 (2H, s), 2.14 (3H, s), 2.13 (3H, s). ^{11}B NMR (CD_3OD , 130 MHz) δ : 26.5. ^{13}C NMR (CD_3OD , 100 MHz) δ : 170.5, 155.2, 154.9, 154.8, 143.8, 139.6, 138.0, 127.9, 127.5, 119.2, 116.8, 114.2, 49.7, 35.2, 24.5. MS (EI, 70ev): m/z $[\text{M}]^+$ calcd for $\text{C}_{23}\text{H}_{23}\text{BN}_4\text{O}_3\text{S}$: 446.1, found 447.1 $[\text{M}+1]^+$. Anal. Calcd for $\text{C}_{23}\text{H}_{23}\text{BN}_4\text{O}_3\text{S}$: C, 60.38; H, 4.73; N, 18.78; O, 5.36; S, 10.75, found: C, 61.76; H, 5.12; N, 12.65.

Route-II; Scheme 3a:

2-(thiophen-2-yl)-1,3-dioxolane (3.2):¹⁷

Thiophene-2-carbaldehyde **3.1** (1.35 g, 12.05 mmol), ethylene glycol (2.68 mL, 48.2 mmol) and p-toluenesulfonic acid (0.01 g, 0.06 mmol) were dissolved in toluene (60 mL) in one neck round bottom flask. A Dean Stark apparatus was fitted and the

reaction mixture was heated at 160 °C for 16 h. The reaction mixture cooled to room temperature and washed with 10% NaOH solution and extracted with DCM. The organic phase was dried with anhydrous sodium sulphate, filtered and solvent was evaporated to provide compound **3.2** as brown oil (1.64 g, 88%) which was used without further purification. Spectroscopic data matches with the one from reported procedure. ¹H NMR (CDCl₃, 400 MHz) δ: 7.33 (1H, d), 7.17 (1H, d), 7.01 (1H, m), 6.13 (1H, s), 4.11 (2H, m), 4.01 (2H, m).

(5-(1,3-dioxolan-2-yl)thiophen-2-yl)tributylstannane (3.3):³⁰

To a solution of compound **3.2** (0.9, 5.76 mmol) in dry THF (30 mL) was added n-butyl lithium (1.6 M in hexane, 7.25 mL, 11.6 mmol) at -78 °C. After 1 h at -78 °C, tributyl tin chloride (2.81 mL, 8.64 mmol) was added drop wise to the above reaction mixture. After stirring for 24 h at room temperature, the mixture was quenched with 20 mL of saturated aqueous ammonium chloride solution and extracted with hexane. The organic phase was dried with anhydrous sodium sulphate, concentrated under reduced pressure, and the resulting residue **3.3** was used without further purification (1.08 g, 43%). Spectroscopic data matches with the one from reported procedure. ¹H NMR (CDCl₃, 400 MHz) δ: 7.27 (1H, d), 7.04 (1H, d), 6.15 (1H, s), 4.16 (2H, m), 4.02 (2H, m), 1.56 (6H, m), 1.32 (6H, m), 1.09 (6H, m), 0.91 (9H, m).

N-(7-(5-(1,3-dioxolan-2-yl)thiophen-2-yl)-1,8-naphthyridin-2-yl)acetamide (3.4):

Compound **3.3** (5.32 g, 12 mmol), compound **1.4** (2.0 g, 9 mmol) and PdCl₂(PPh₃)₂ (0.630 g, 0.9 mmol) were taken in a two necked round bottom flask, degassed with nitrogen and dry 1,4- dioxane (100 mL) under nitrogen atmosphere was added. The reaction mixture was refluxed for 3 h, after that the solvent was removed under reduced pressure, and then the crude residue was dissolved in EtOAc, passed through

celite and the solvent was evaporated. The crude residue was purified by column chromatography using 1:1 EtOAc:hexane to give pure compound **3.4** as a yellowish solid (2.0 g, 65%). Mp: 180-190 °C. TLC (50% EtOAc in Hexane): $R_f = 0.26$. ^1H NMR (DMSO- d_6 , 400 MHz) δ : 11.11 (1H, s), 8.34 (3H, m), 8.04 (1H, d), 7.91 (1H, d), 7.27 (1H, m), 6.0 (1H, s), 4.06 (2H, m), 3.96 (2H, m), 2.15 (3H, S). ^{13}C NMR (CDCl₃, 100 MHz) δ : 170.3, 155.1, 154.5, 154.2, 146.1, 144.8, 139.0, 137.0, 132.0, 131.9, 128.4, 128.3, 126.9, 126.4, 119.3, 116.8, 115.0, 24.8. MS (EI, 70ev): m/z [M]⁺ calcd for C₁₇H₁₅N₃O₃S: 341.0, found 342.0 [M+1]⁺. Anal. Calcd for C₁₇H₁₅N₃O₃S: C, 59.81; H, 4.43; N, 12.31; O, 14.06; S, 9.39, found: C, 59.73; H, 4.41; N, 12.29.

N-(7-(5-formylthiophen-2-yl)-1,8-naphthyridin-2-yl)acetamide (1.5):

1M HCl (2 mL) was added dropwise to a solution of compound **3.4** (0.16 g, 0.46 mmol) in dry acetone (30 mL). After complete addition of HCl the reaction mixture was stirred at room temperature for 6 h, then the solvent was removed under reduced pressure and crude residue was extracted with EtOAc. The organic phase was dried with anhydrous sodium sulphate, concentrated under reduced pressure, and the resulting residue **1.5** was used without further purification (0.1 g, 73%). Mp: 270-274 °C. TLC (50% EtOAc in hexane): $R_f = 0.24$; ^1H NMR (DMSO- d_6 , 400 MHz) δ : 11.20 (1H, s), 9.98 (1H, s), 8.44 (3H, m), 8.22 (2H, m), 8.12 (1H, d), 2.18 (3H, s). ^{13}C NMR (DMSO- d_6 , 100 MHz) δ : 185.2, 170.6, 155.4, 154.6, 153.8, 153.3, 145.2, 139.7, 139.2, 138.8, 128.7, 120.3, 117.5, 115.4, 24.5. MS (EI, 70ev): m/z [M]⁺ calcd for C₁₅H₁₁N₃O₃S: 297.0, found 298.1 [M+1]⁺. Anal. Calcd for C₁₅H₁₁N₃O₃S: C, 60.59; H, 3.73; N, 14.13; O, 10.76; S, 10.78, found: C, 60.45; H, 3.68; N, 14.06.

Route-II; Scheme 3b:

N-methyl-1-(thiophen-2-yl)methanamine (3.5):³¹

Thiophene-2-carboxaldehyde **3.1** (0.54 g, 4 mmol) and 40% aqueous methyl amine (0.74 g, 20 mmol) were dissolved in MeOH (20 mL). After 1 h, sodium borohydride

was added portion wise at 0 °C to the reaction mixture. The resulting mixture was stirred at room temperature for 3-4 days. The crude residue was taken up in 200 mL water and extracted with DCM. The organic phase was dried with anhydrous sodium sulphate, concentrated under reduced pressure, and the resulting residue was subjected to column chromatography using 70% EtOAc in hexane to give compound **3.5** (0.30g, 60%). Spectroscopic data matches with the one from reported procedure. ¹H NMR (CDCl₃, 400 MHz) δ : 7.17 (1H, m), 6.91 (2H, m), 3.90 (2H, s), 2.43 (3H, s), 2.18 (1H, s).

Tert-butyl methyl(thiophen-2-ylmethyl)carbamate (3.6):³²

Compound **3.5** (0.2 g, 1.57 mmol) and sodium bicarbonate (0.25 g, 3.14 mmol) were dissolved in dry THF. Boc₂O (0.68 g, 3.14 mmol) was added dropwise to the reaction mixture. The resulting mixture was stirred at room temperature for 3 h. The crude residue was taken up in 100 mL water and extracted with EtOAc. The organic phase was dried with anhydrous sodium sulphate, concentrated under reduced pressure, and the resulting residue was subjected to column chromatography using 10% EtOAc in hexane to give compound **3.6** which was used without further purification (0.34g, 97%). Spectroscopic data matches with the one from reported procedure. ¹H NMR (CDCl₃, 400 MHz) δ : 7.22 (1H, m), 6.94 (2H, m), 4.54 (2H, s), 2.85 (3H, s), 1.52 (9H, s).

Tert-butyl methyl((5-(tributylstannyl)thiophen-2-yl)methyl)carbamate (3.7):¹⁹

n-Butyl lithium (1.6 M in hexane, 2.4 mL, 3.85 mmol) was added to a solution of compound **3.6** (0.4 g, 1.76 mmol) in dry THF (30 mL) at 0 °C. After 1 h at 0 °C, tributyl tin chloride (1.26 g, 3.88 mmol) was added to the above reaction mixture. After stirring for 12 h at room temperature, the reaction mixture was quenched with

20 mL of saturated aqueous ammonium chloride solution and extracted with hexane. The organic phase was dried with anhydrous sodium sulphate, concentrated under reduced pressure. Spectroscopic data matches to compound **3.8** (0.58 g, 64%) instead of **3.7**. ^1H NMR (CDCl_3 , 400 MHz) δ : 6.99 (1H, d), 6.87 (1H, dd), 6.59 (1H, d), 3.96 (1H, s), 2.91 (3H, s), 1.47 (9H, s), 1.34 (12H, m), 0.89 (15H, m).

Route-III; Scheme 4:

Tributyl(5-methylthiophen-2-yl)stannane (4.2):¹⁹

n-Butyl lithium (1.6 M in hexane, 3.81 mL, 6.11 mmol) was added to a solution of compound **4.1** (0.5 g, 5.09 mmol) in dry THF (30 mL) at 0 °C. After 1 h at 0 °C, tributyl tin chloride (1.65 mL, 6.11 mmol) was added drop wise to the above reaction mixture. After stirring over 12 h at room temperature, the reaction mixture was quenched with 20 mL of saturated aqueous ammonium chloride solution and extracted with hexane. The organic phase was dried with anhydrous sodium sulphate, concentrated under reduced pressure, and the resulting residue **4.2** was used without further purification (1.26 g, 64%). Spectroscopic data matches the one from reported procedure. ^1H NMR (CDCl_3 , 400 MHz) δ : 6.96 (1H, d), 6.88 (1H, dd), 2.54 (3H, s), 1.56 (6H, m), 1.33 (6H, m), 1.07 (6H, m), 0.89 (9H, m).

N-(7-(5-methylthiophen-2-yl)-1,8-naphthyridin-2-yl)acetamide (1.6):

Compound **4.2** (2.40 g, 6 mmol), compound **1.4** (1.0 g, 4.5 mmol) and $\text{PdCl}_2(\text{PPh}_3)_2$ (0.149 g, 0.22 mmol) were taken in a two necked round bottom flask, degassed with nitrogen and 1,4- dioxane (50 mL) was added under nitrogen atmosphere. The reaction mixture was refluxed for 2 h, the solvent was removed under reduced pressure, and the crude residue was dissolved in EtOAc, passed through celite and the solvent was evaporated. The crude residue was purified by column chromatography using 1:1 EtOAc:hexane to give compound **1.6** as a yellowish solid (1.1 g, 65%). Mp:

150-152 °C. TLC (50% EtOAc in hexane): $R_f = 0.28$. ¹H NMR (CDCl₃, 400 MHz) δ : 8.44 (1H, d), 8.16 (1H, d), 8.08 (1H, d), 7.75 (1H, d), 7.66 (1H, d), 6.84 (1H, m), 2.57 (3H, s), 2.33 (3H, s). ¹³C NMR (CDCl₃, 100 MHz) δ : 170.5, 156.1, 153.7, 145.83, 145.82, 141.5, 139.9, 136.9, 127.8, 126.8, 118.9, 117.3, 114.1, 24.9, 15.8. MS (EI, 70ev): m/z [M]⁺ calcd for C₁₅H₁₃N₃OS: 283.0, found 284.1 [M+1]⁺. Anal. Calcd for C₁₅H₁₃N₃OS: C, 63.58; H, 4.62; N, 14.83; O, 5.65; S, 11.32, found: C, 63.53; H, 4.63; N, 14.85.

Route-IV; Scheme 5:

Tert-butyl ((5-(7-acetamido-1,8-naphthyridin-2-yl)thiophen-2-yl)methyl)carbamate 5.1:

Compound **1.4** (1.0 g, 4.5 mmol), compound **2.2** (3.0 g, 6 mmol) and PdCl₂(PPh₃)₂ (0.157 g, 0.22 mmol) were taken in a two necked round bottom flask, degassed with nitrogen and dry 1,4- dioxane (100 mL) was added under nitrogen atmosphere. The reaction mixture was refluxed for 1 h, the solvent was removed under reduced pressure, and the crude residue was dissolved in EtOAc, passed through celite and the solvent was evaporated. The crude compound was purified by column chromatography using 60% EtOAc in hexane to give compound **5.1** as a yellowish solid (1.5 g, 84%). Mp: 198-200 °C. TLC (60% EtOAc in hexane): $R_f = 0.24$. ¹H NMR (DMSO-*d*₆, 400 MHz) δ : 11.09 (1H, s), 8.33 (3H, m), 8.01 (1H, d), 7.85 (1H, m), 7.57 (1H, m), 7.01 (1H, d), 4.31 (2H, d), 2.16 (3H, s). ¹³C NMR (DMSO-*d*₆, 100 MHz) δ : 170.4, 156.0, 155.2, 155.0, 154.8, 148.8, 143.5, 139.5, 138.0, 127.7, 126.5, 119.2, 116.7, 114.2, 78.5, 44.0, 28.6, 24.5. MS (EI, 70ev): m/z [M]⁺ calcd for C₂₀H₂₂N₄O₃S: 398.14, found 398.2 [M+1]⁺. Anal. Calcd for C₂₀H₂₂N₄O₃S: C, 60.28; H, 5.56; N, 14.06; O, 12.05; S, 8.05, found: C, 60.15; H, 5.63; N, 14.12.

N-(7-(5-(aminomethyl)thiophen-2-yl)-1,8-naphthyridin-2-yl)acetamide (1.7):

To a solution of compound **5.1** (0.14 g, 0.35 mmol) in dry DCM (2 mL) trifluoroacetic acid (2 mL) was added at 0 °C. The reaction mixture was slowly heated to room temperature and stirred at room temperature for 4 h. After 4 h, reaction mixture was quenched with saturated sodium bicarbonate solution followed by extraction with DCM. The organic phase was dried with anhydrous sodium sulphate, concentrated under reduced pressure, and the resulting residue **1.7** (0.11 g, 82%) was used without further purification. Mp: 172-174 °C. TLC (20% MeOH in DCM): R_f = 0.24. ^1H NMR (DMSO- d_6 , 400 MHz) δ : 11.10 (1H, s), 8.36 (3H, m), 8.26 (2H, s), 8.06 (1H, d), 7.97 (1H, d), 7.30 (1H, d), 4.30 (2H, m), 2.16 (3H, s). ^{13}C NMR (DMSO- d_6 , 100 MHz) δ : 170.5, 158.8, 158.5, 155.1, 154.7, 146.0, 139.8, 138.4, 130.6, 127.9, 119.5, 116.8, 114.6, 37.7, 24.6. MS (EI, 70eV): m/z $[\text{M}]^+$ calcd for $\text{C}_{15}\text{H}_{14}\text{N}_4\text{OS}$: 298.09, found 299.2 $[\text{M}]^+$. Anal. Calcd for $\text{C}_{15}\text{H}_{14}\text{N}_4\text{OS}$: C, 60.38; H, 4.73; N, 18.78; O, 5.36, S, 10.75, found: C, 60.26; H, 4.78; N, 18.65.

5.6. References:

- (1) Hardy, S.; Jones, P. *J. Chromatogr. A* **1997**, 791, 333.
- (2) Morel, F. M. M.; Kraepiel, A. M. L.; Amyot, M. *Annu. Rev. Ecol. Syst.* **1998**, 29, 543.
- (3) Dufault, R.; LeBlanc, B.; Schnoll, R.; Cornett, C.; Schweitzer, L.; Wallinga, D.; Hightower, J.; Patrick, L.; Lukiw, W. J. *Environ. Health* **2009**, 8, 2.
- (4) Danet, A. F.; Bratu, M.-C.; Radulescu, M.-C.; Bratu, A. *Sens. Actuators, B* **2009**, 137, 12.
- (5) Hashemi-Moghaddam, H.; Saber-Tehrani, M. *J. AOAC Int.* **2008**, 91, 1453.
- (6) Butler, O. T.; Cook, J. M.; Harrington, C. F.; Hill, S. J.; Rieuwerts, J.; Miles, D. L. *J. Anal. At. Spectrom.* **2006**, 21, 217.
- (7) (a) Lin, W.; Long, L.; Tan, W. *Chem. Commun.* **2010**, 46, 1503. (b) Wang, D.-H.; Zhang, Y.; Gong, Z.; Sun, R.; Zhao, D.-Z.; Sun, C.-L. *RSC Adv.* **2015**, 5, 50540.
- (8) Hu, J.; Hu, Z.; Cui, Y.; Zhang, X.; Gao, H.-W.; Uvdal, K. *Sens. Actuators, B* **2014**, 203, 452.
- (9) Vedamalai, M.; Wu, S.-P. *Eur. J. Org. Chem.* **2012**, 2012, 1158.
- (10) (a) Djurdjevic, S.; Leigh, D. A.; McNab, H.; Parsons, S.; Teobaldi, G.; Zerbetto, F. *J. Am. Chem. Soc.* **2007**, 129, 476. (b) Suda, H.; Kobori, A.;

- Zhang, J.; Hayashi, G.; Nakatani, K. *Bioorg. Med. Chem.* **2005**, *13*, 4507. (c) Lu, S.-H.; Selvi, S.; Fang, J.-M. *J. Org. Chem.* **2007**, *72*, 117.
- (11) Fang, J.-M.; Selvi, S.; Liao, J.-H.; Slanina, Z.; Chen, C.-T.; Chou, P.-T. *J. Am. Chem. Soc.* **2004**, *126*, 3559.
- (12) (a) Yu, M.-M.; Li, Z.-X.; Wei, L.-H.; Wei, D.-H.; Tang, M.-S. *Org. Lett.* **2008**, *10*, 5115. (b) Chahal, M. K.; Sankar, M. *Anal. Methods* **2015**, *7*, 4552. (c) Liu, X.; Chen, M.; Liu, Z.; Yu, M.; Wei, L.; Li, Z. *Tetrahedron* **2014**, *70*, 658.
- (13) Li, M.; Ge, H.; Arrowsmith, R. L.; Mirabello, V.; Botchway, S. W.; Zhu, W.; Pascu, S. I.; James, T. D. *Chem. Commun.* **2014**, *50*, 11806.
- (14) Harvey, C. P.; Tovar, J. D. *J. Polym. Sci., Part A: Polym. Chem.* **2011**, *49*, 4861.
- (15) Anderson, C. A.; Taylor, P. G.; Zeller, M. A.; Zimmerman, S. C. *J. Org. Chem.* **2010**, *75*, 4848.
- (16) Corbin, P. S.; Zimmerman, S. C.; Thiessen, P. A.; Hawryluk, N. A.; Murray, T. J. *J. Am. Chem. Soc.* **2001**, *123*, 10475.
- (17) Chen, H.; Huang, H.; Huang, X.; Clifford, J. N.; Forneli, A.; Palomares, E.; Zheng, X.; Zheng, L.; Wang, X.; Shen, P.; Zhao, B.; Tan, S. *J. Phys. Chem. C* **2010**, *114*, 3280.
- (18) Mita, T.; Higuchi, Y.; Sato, Y. *Org. Lett.* **2011**, *13*, 2354.
- (19) Palamà, I.; Di Maria, F.; Viola, I.; Fabiano, E.; Gigli, G.; Bettini, C.; Barbarella, G. *J. Am. Chem. Soc.* **2011**, *133*, 17777.
- (20) Yeh, J.-T.; Chen, W.-C.; Liu, S.-R.; Wu, S.-P. *New J. Chem.* **2014**, *38*, 4434.
- (21) (a) Benesi, H. A.; Hildebrand, J. H. *J. Am. Chem. Soc.* **1949**, *71*, 2703(b) Singh, R. B.; Mahanta, S.; Guchhait, N. *J. Mol. Struct.* **2010**, *963*, 92.
- (22) Vedamalai, M.; Wu, S.-P. *Org. Biomol. Chem.* **2012**, *10*, 5410.
- (23) (a) James, T. D.; Sandanayake, K. R. A. S.; Shinkai, S. *J. Chem. Soc., Chem. Commun.* **1994**, 477. (b) James, T. D.; Sandanayake, K. R. A. S.; Shinkai, S. *Angew. Chem. Int. Ed.* **1994**, *33*, 2207.
- (24) (a) Bosch, L. I.; Fyles, T. M.; James, T. D. *Tetrahedron* **2004**, *60*, 11175(b) Zhu, L.; Shabbir, S. H.; Gray, M.; Lynch, V. M.; Sorey, S.; Anslyn, E. V. *J. Am. Chem. Soc.* **2006**, *128*, 1222.
- (25) de Silva, A. P.; Gunaratne, H. Q. N.; Gunnlaugsson, T.; Huxley, A. J. M.; McCoy, C. P.; Rademacher, J. T.; Rice, T. E. *Chem. Rev.* **1997**, *97*, 1515.

- (26) (a) Takeuchi, M.; Yamamoto, M.; Shinkai, S. *Chem. Commun.* **1997**, 1731.
(b) Yang, W.; Yan, J.; Springsteen, G.; Deeter, S.; Wang, B. *Bioorg. Med. Chem. Lett.* **2003**, *13*, 1019. (c) Hosseinzadeh, R.; Mohadjerani, M.; Pooryousef, M. *Luminescence* **2015**, *30*, 549.
- (27) Dempsey, B. *London: Chapman and Hall Ltd* **1974**, 25, 13.
- (28) Varadi, L.; Gray, M.; Groundwater, P. W.; Hall, A. J.; James, A. L.; Orena, S.; Perry, J. D.; Anderson, R. J. *Org. Biomol. Chem.* **2012**, *10*, 2578.
- (29) Jeon, J.-H.; Tanaka, K.; Chujo, Y. *Org. Biomol. Chem.* **2014**, *12*, 6500.
- (30) Shen, P.; Tang, Y.; Jiang, S.; Chen, H.; Zheng, X.; Wang, X.; Zhao, B.; Tan, S. *Org. Electron.* **2011**, *12*, 125.
- (31) Pyun, S. Y.; Lee, D. C.; Seung, Y. J.; Cho, B. R. *J. Org. Chem.* **2005**, *70*, 5327.
- (32) Putey, A.; Joucla, L.; Picot, L.; Besson, T.; Joseph, B. *Tetrahedron* **2007**, *63*, 867.

5.7. Appendix:

5.7.1. NMR Spectra of Synthesized Compounds:

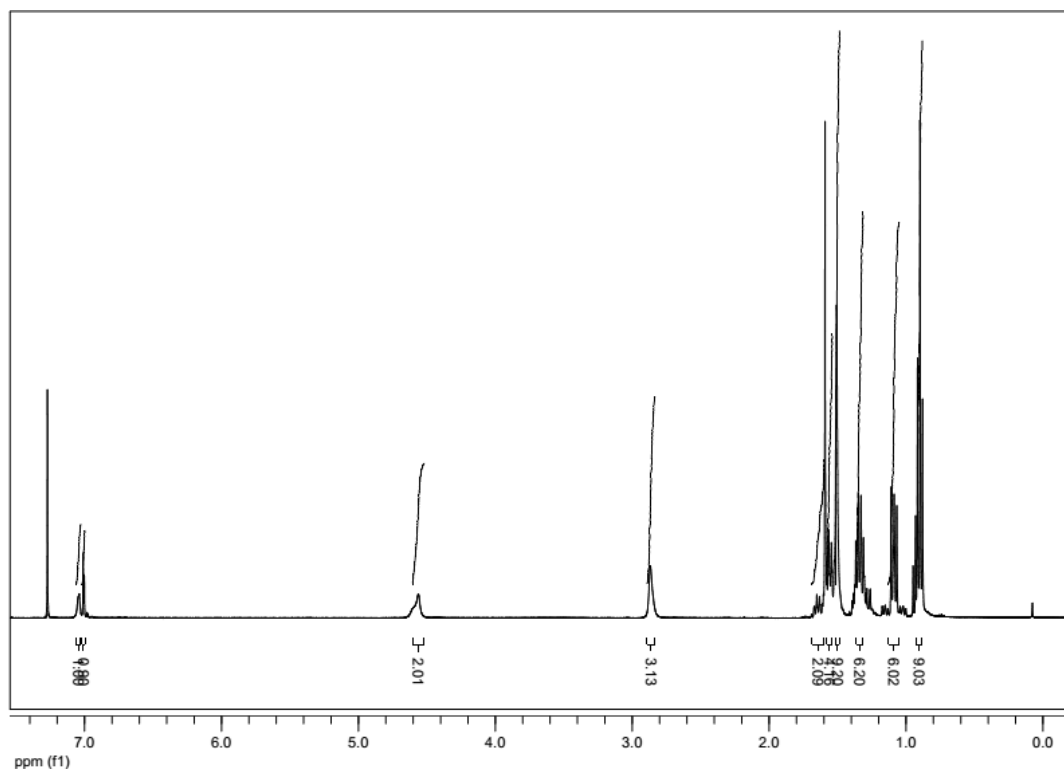


Figure A1: ¹H NMR (CDCl₃, 400 MHz) of compound **1.3**

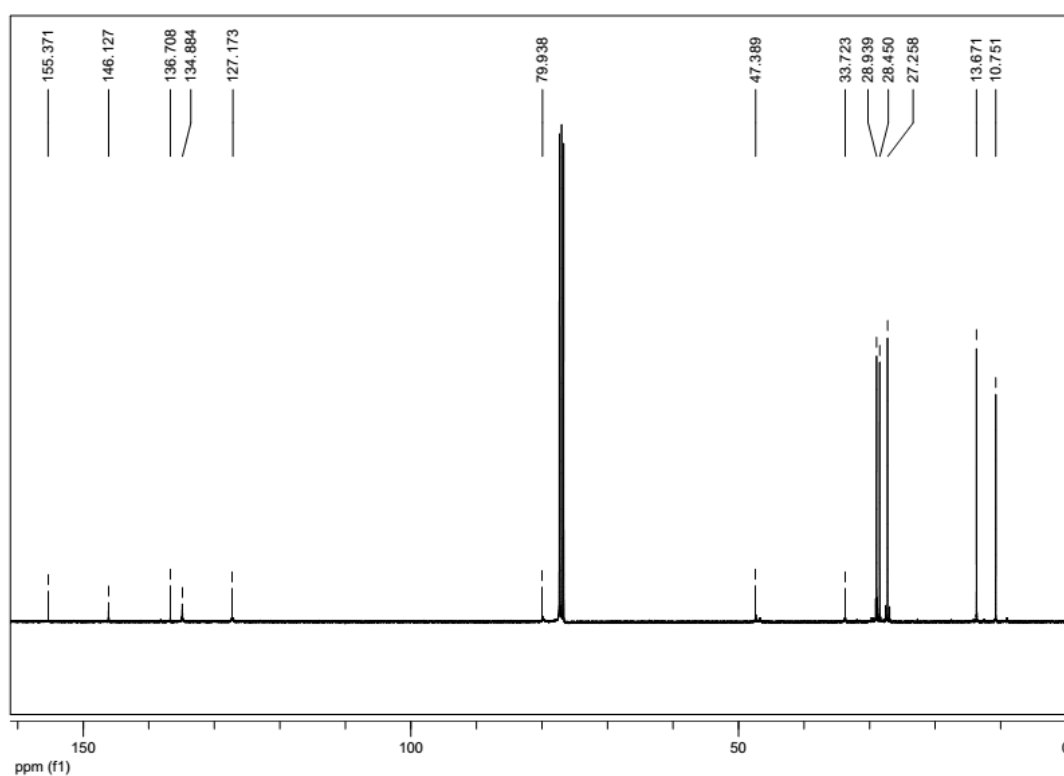


Figure A2: ¹³C NMR (CDCl₃, 100 MHz) of compound **1.3**

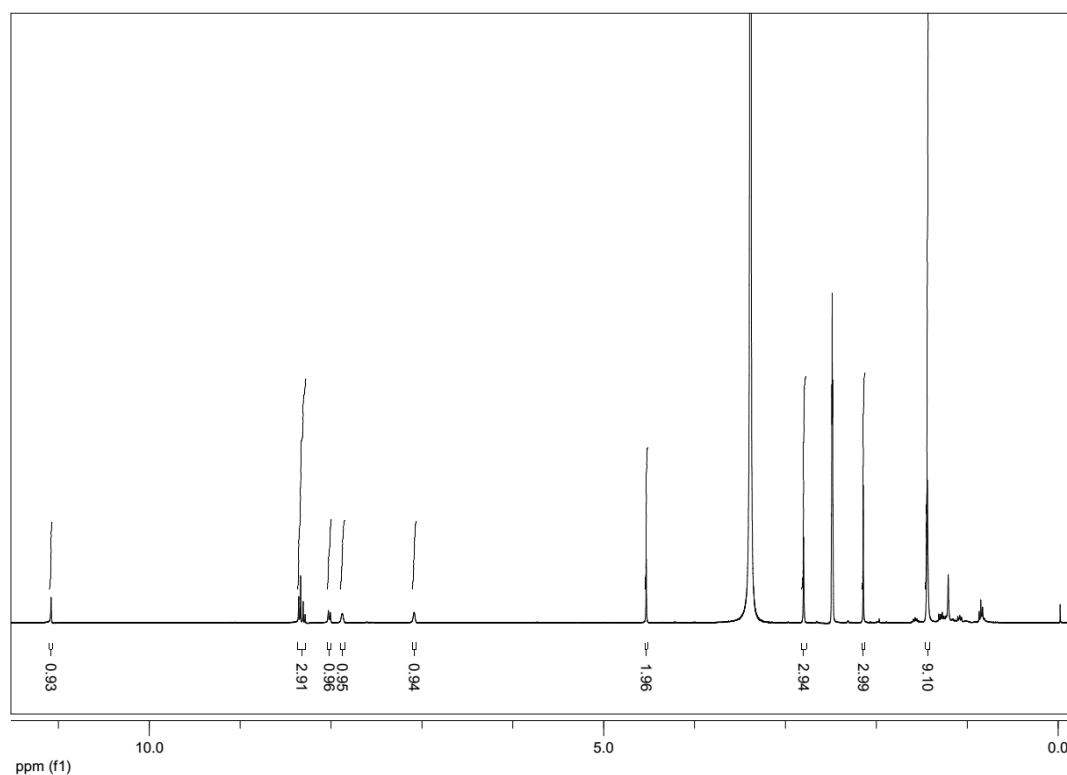


Figure A3: ^1H NMR (DMSO- d_6 , 400 MHz) of compound **2.6**

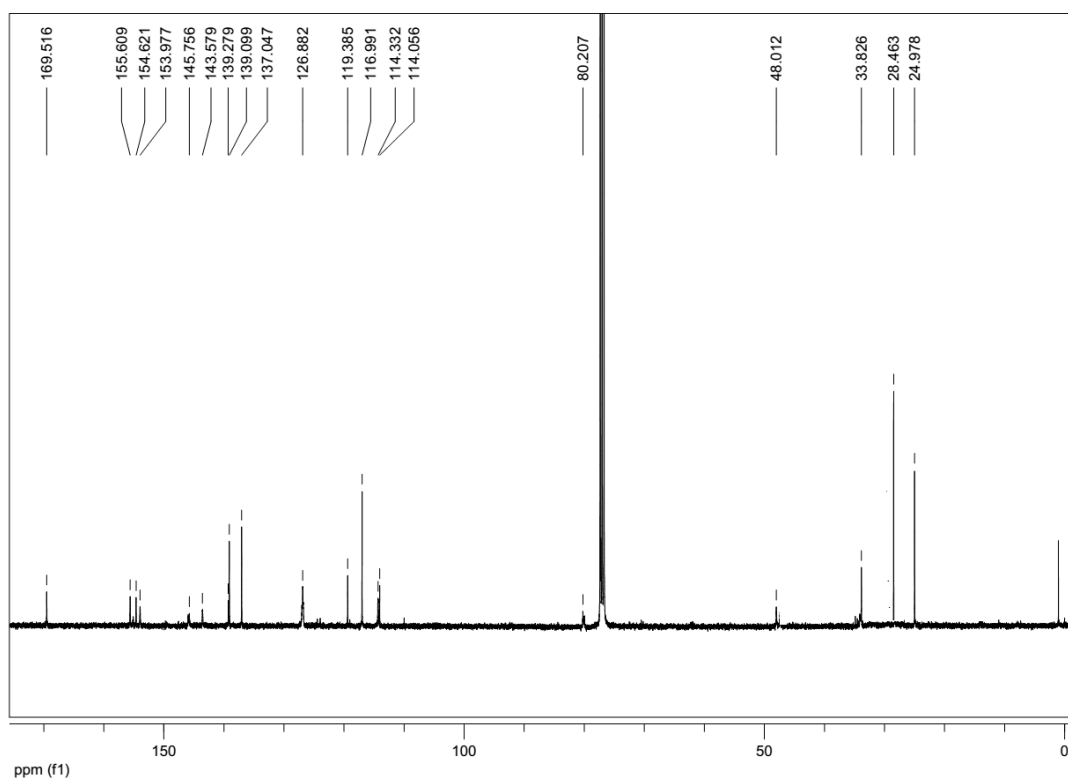


Figure A4: ^{13}C NMR (CDCl $_3$, 100 MHz) of compound **2.6**

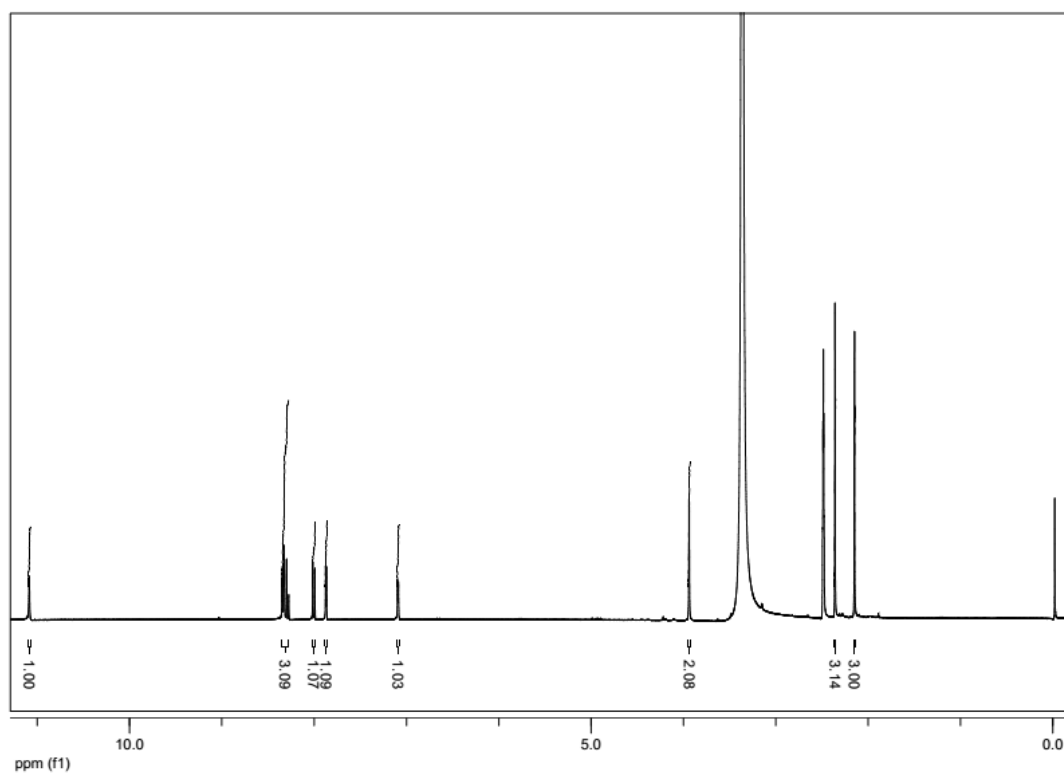


Figure A5: ¹H NMR (DMSO-*d*₆, 400 MHz) of compound **1.2**

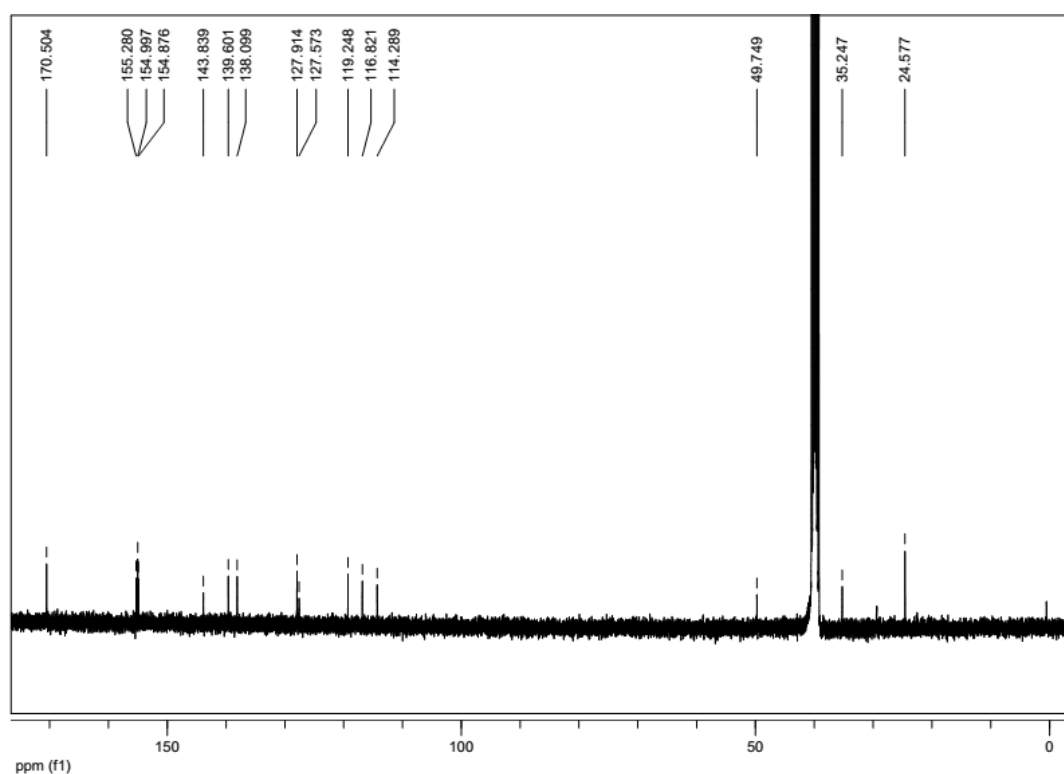


Figure A6: ¹³C NMR (DMSO-*d*₆, 100 MHz) of compound **1.2**

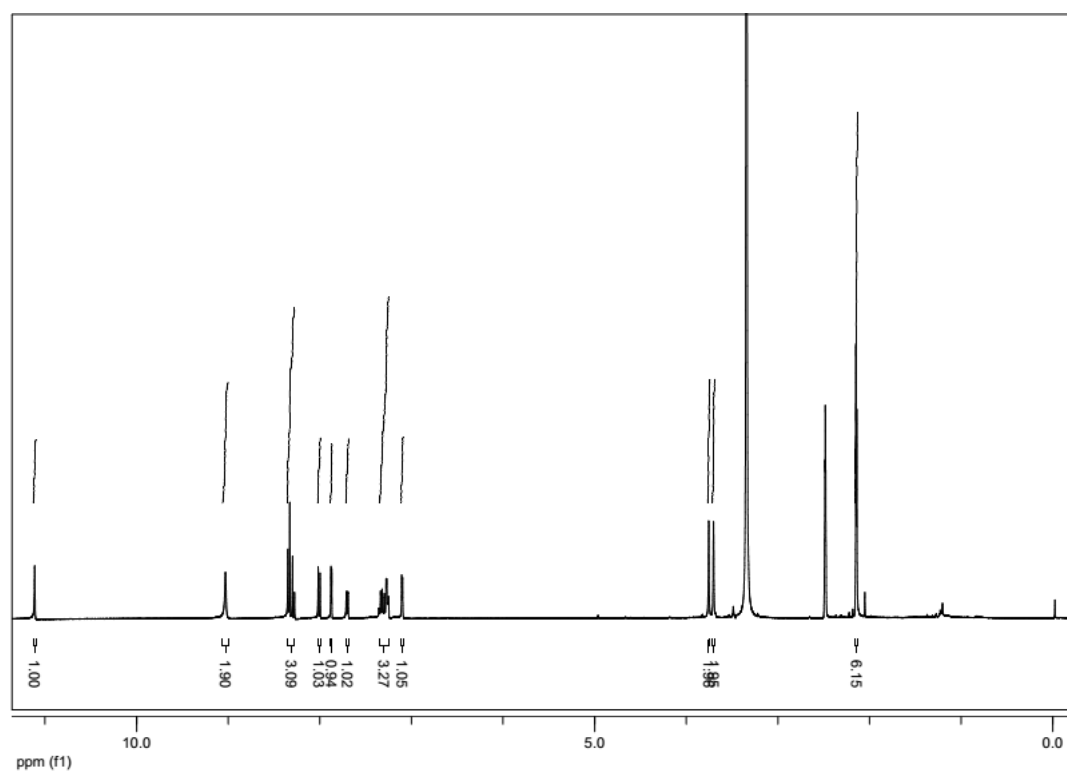


Figure A7: ¹H NMR (DMSO-*d*₆, 400 MHz) of compound **1.1**

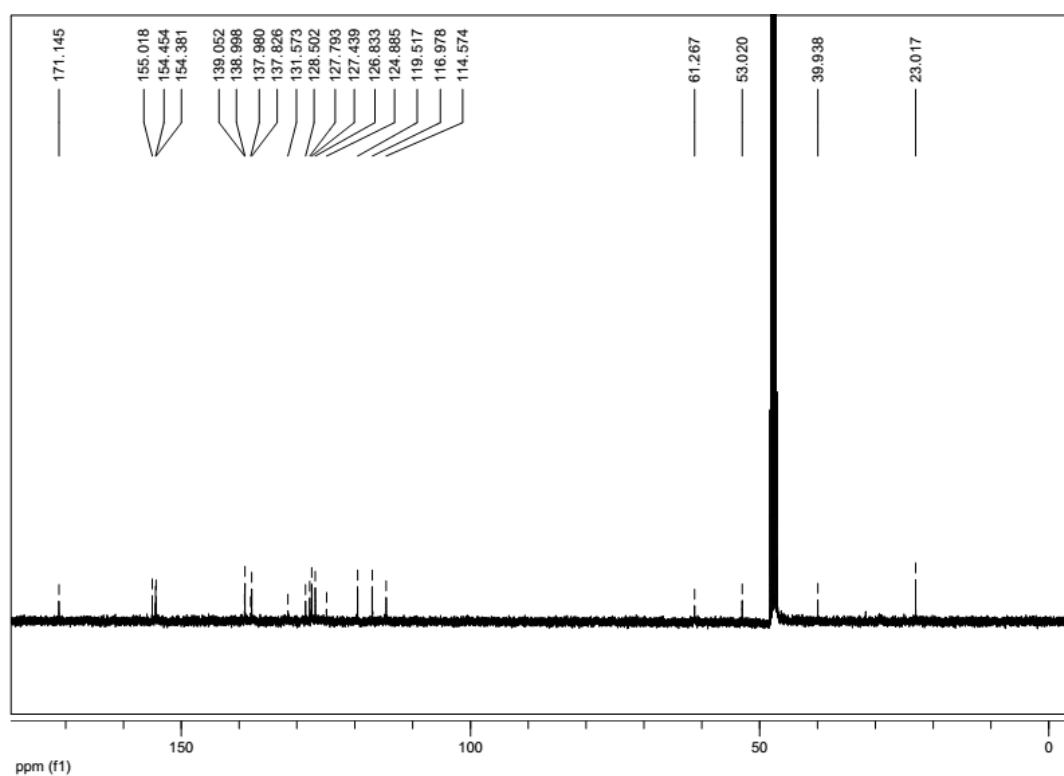


Figure A8: ¹³C NMR (CD₃OD, 100 MHz) of compound **1.1**

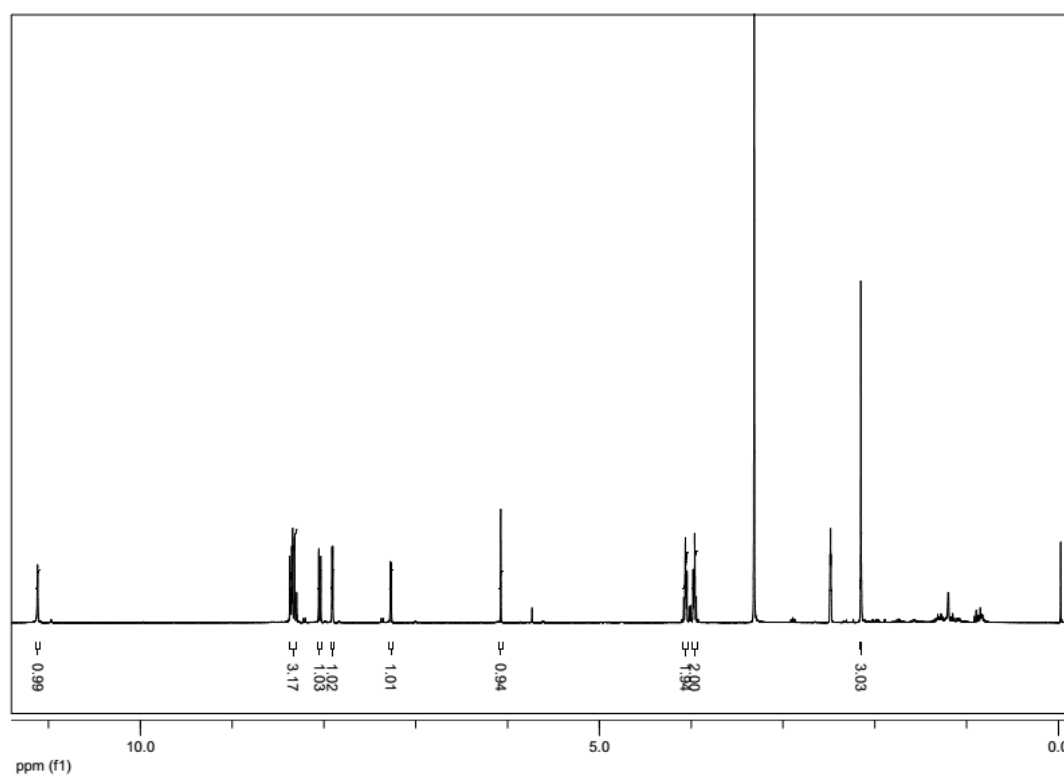


Figure A9: ¹H NMR (DMSO-*d*₆, 400 MHz) of compound **3.4**

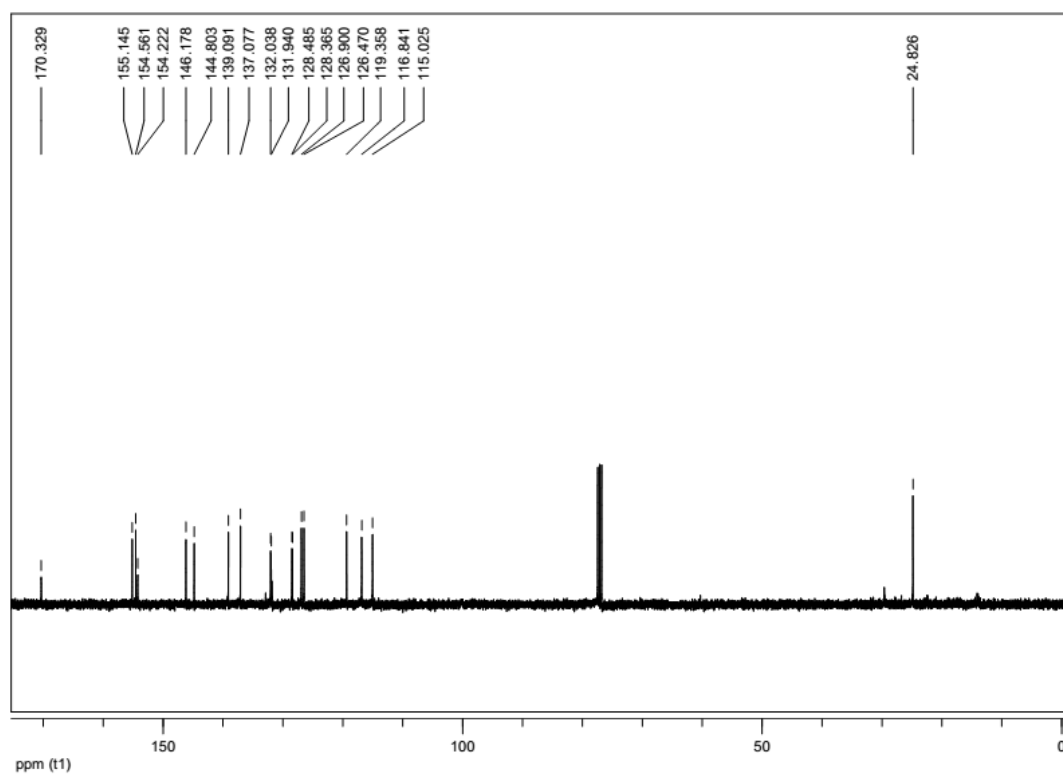


Figure A10: ¹³C NMR (CDCl₃, 100 MHz) of compound **3.4**

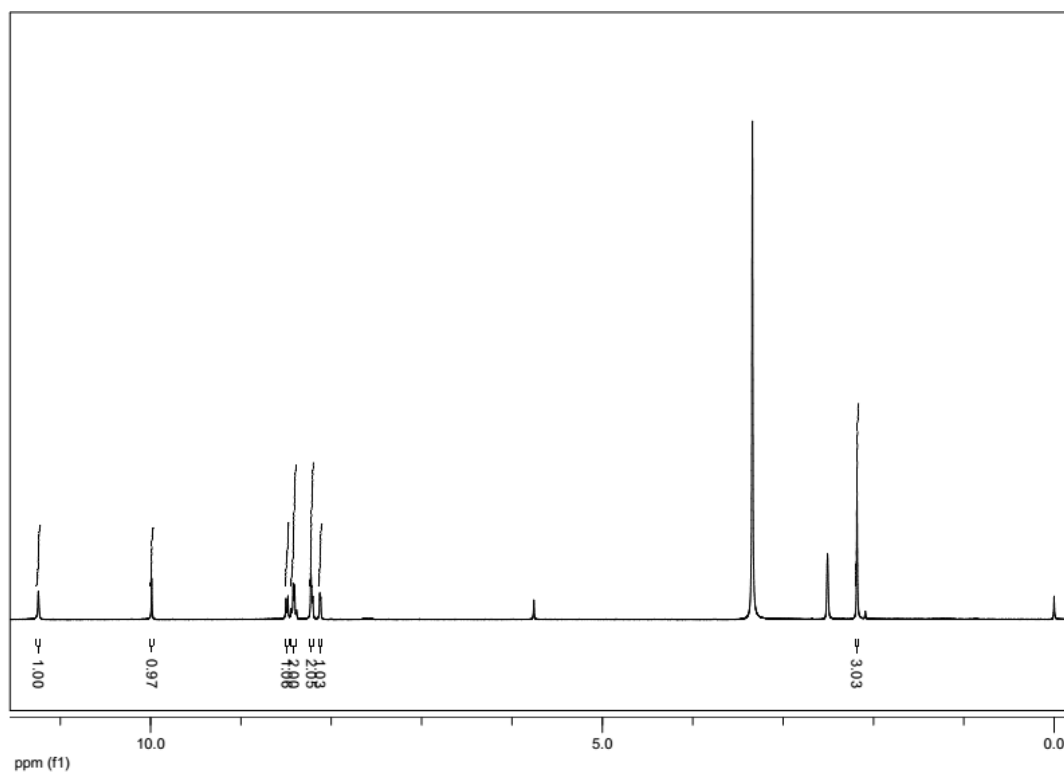


Figure A11: ^1H NMR ($\text{DMSO}-d_6$, 400 MHz) of compound **1.5**

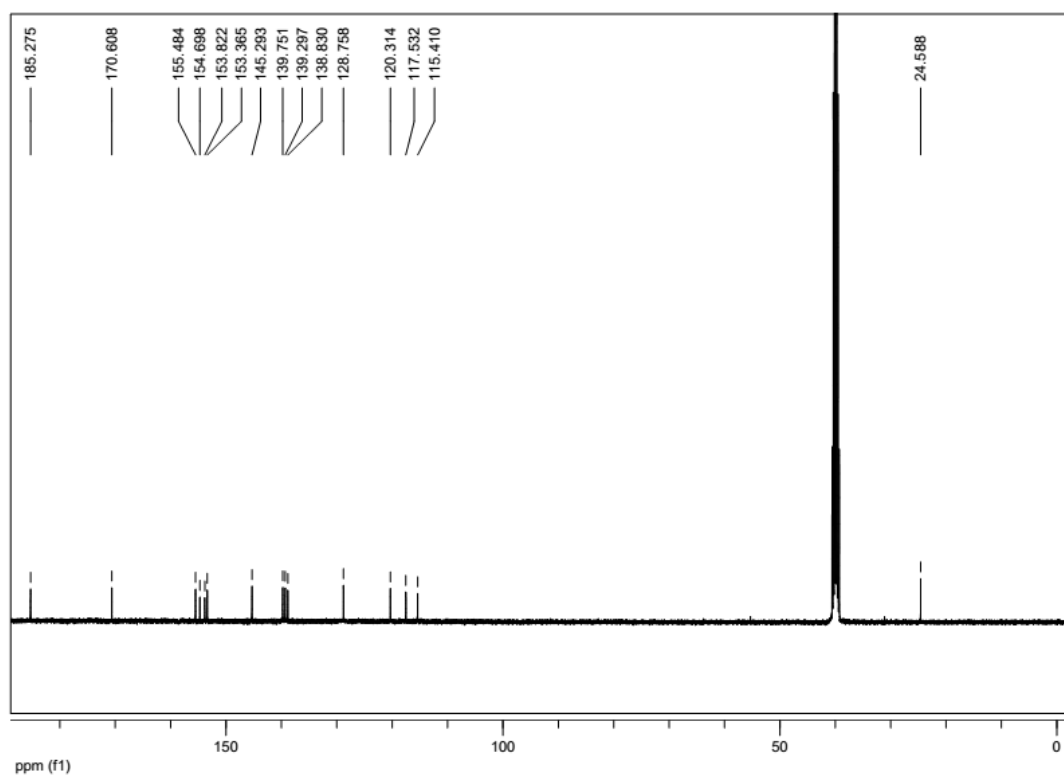


Figure A12: ^{13}C NMR ($\text{DMSO}-d_6$, 100 MHz) of compound **1.5**

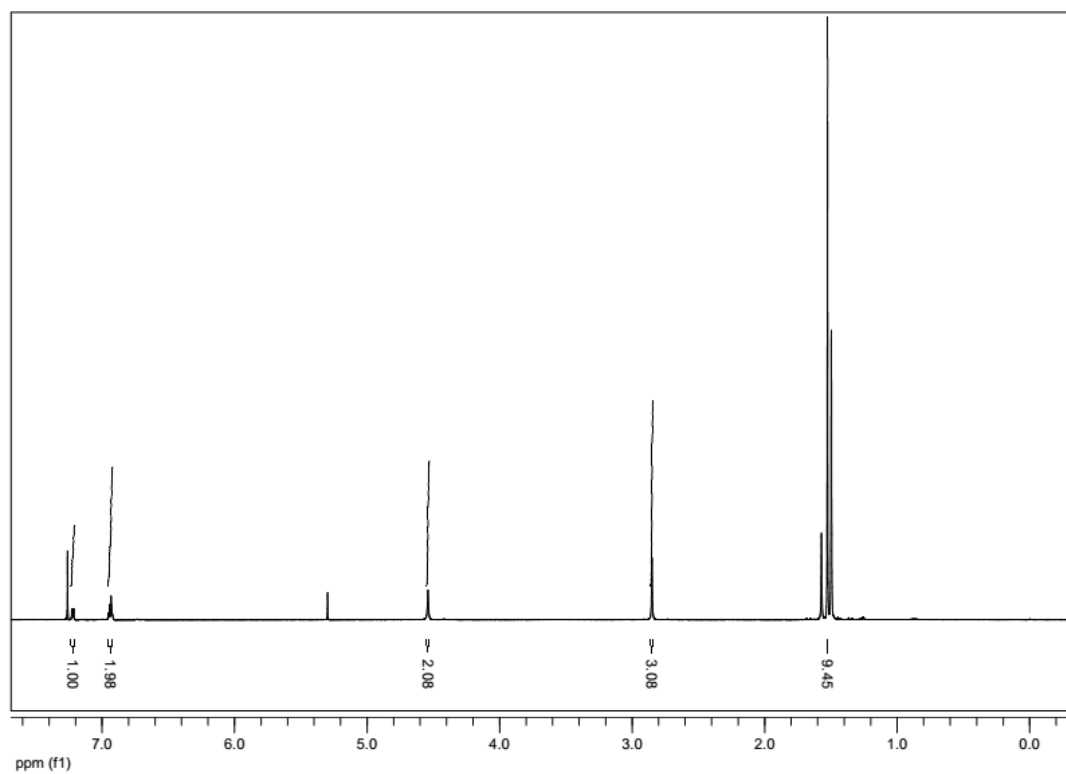


Figure A13: ¹H NMR (CDCl₃, 400 MHz) of compound **3.6**

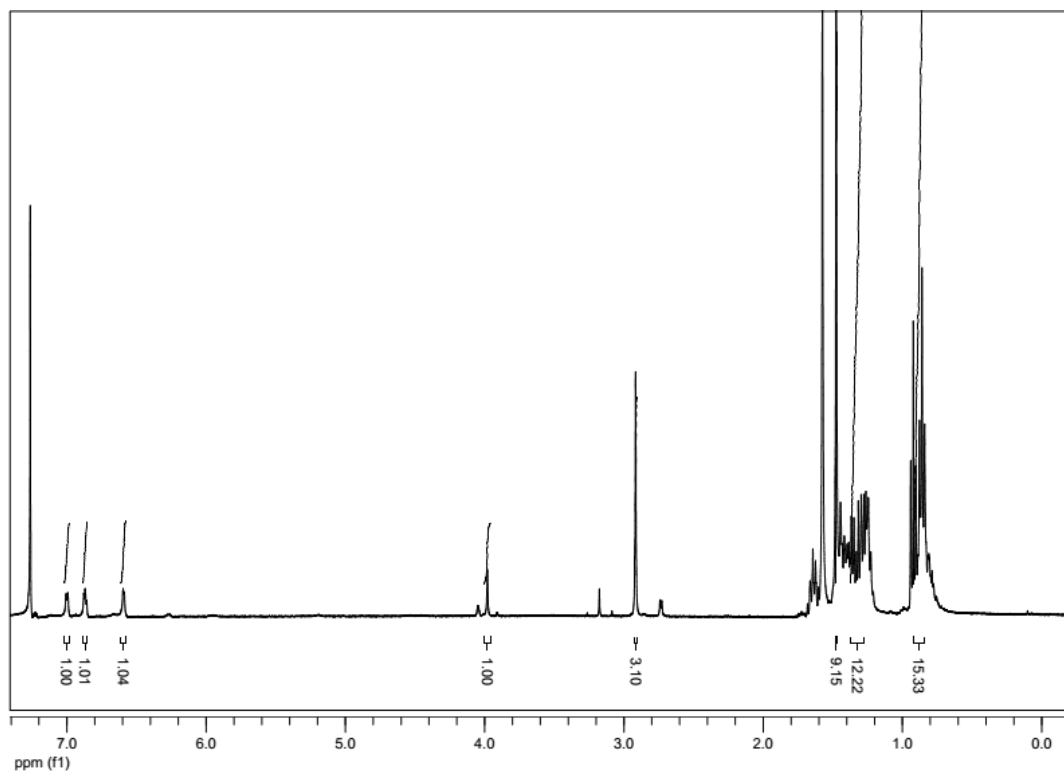


Figure A14: ¹H NMR (CDCl₃, 400 MHz) of compound **3.8**

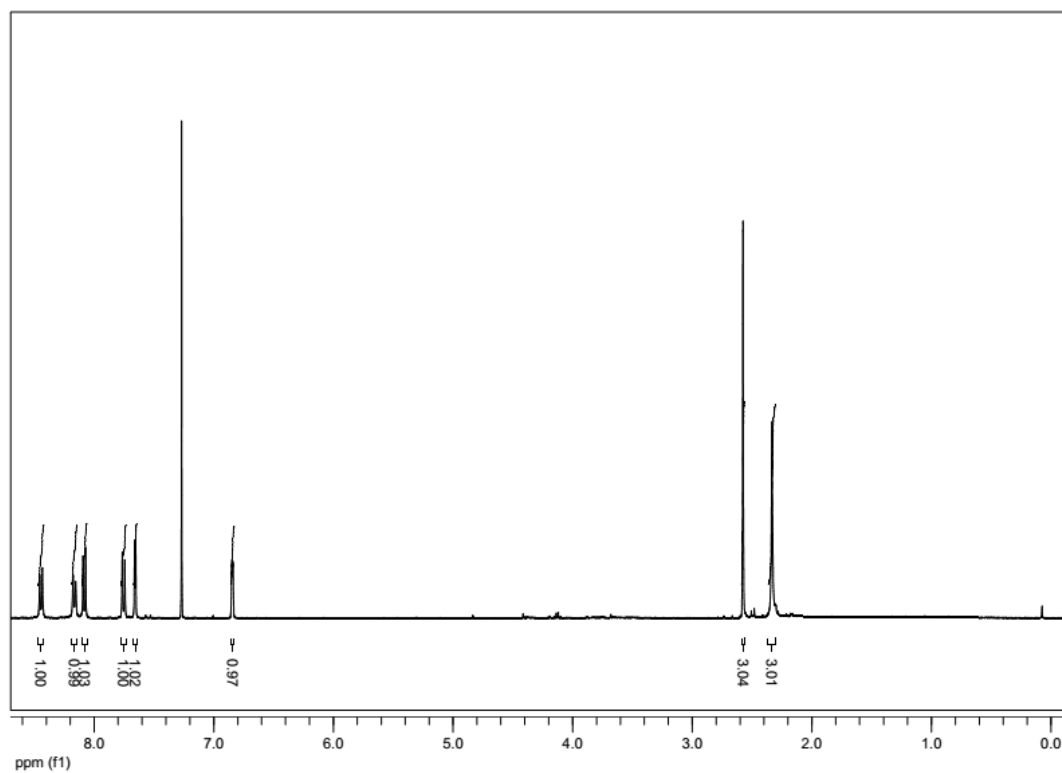


Figure A15: ^1H NMR (CDCl_3 , 400 MHz) of compound **1.6**

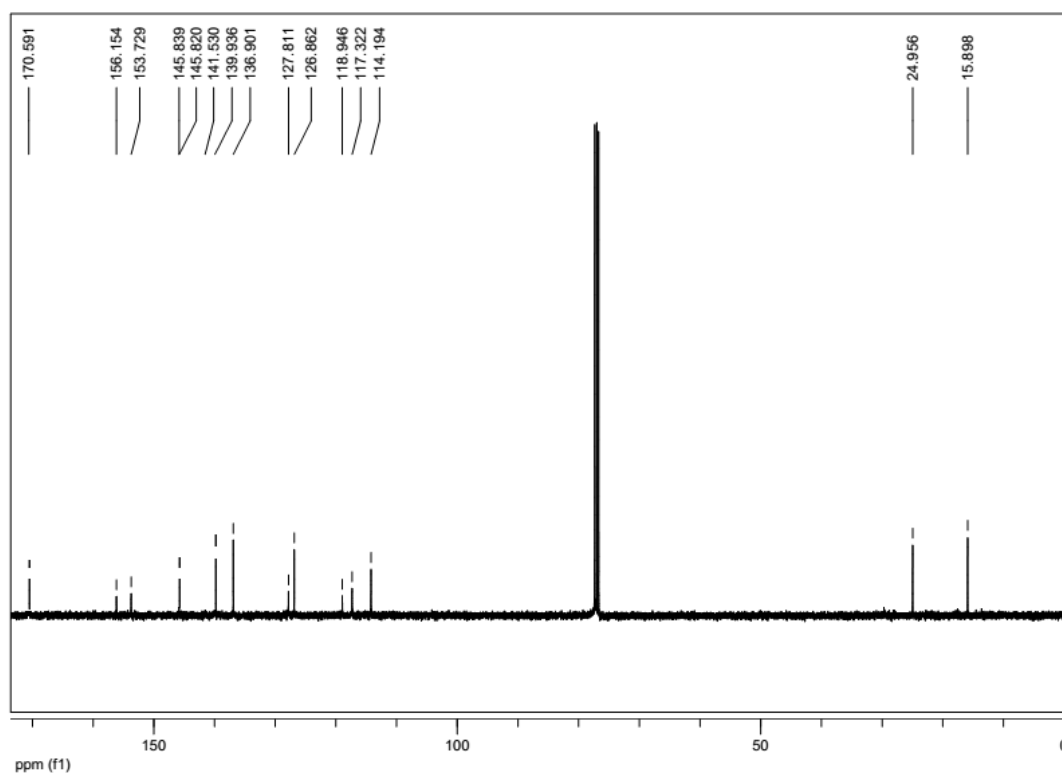


Figure A16: ^{13}C NMR (CDCl_3 , 100 MHz) of compound **1.6**

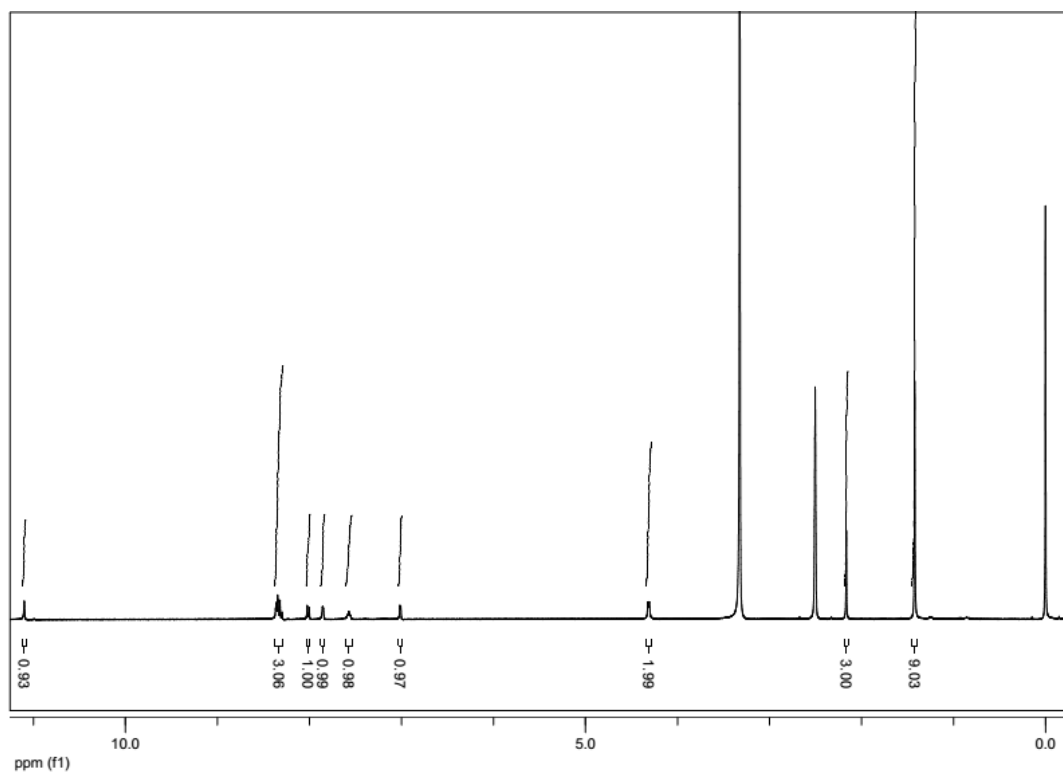


Figure A17: ¹H NMR (DMSO-*d*₆, 400 MHz) of compound **5.1**

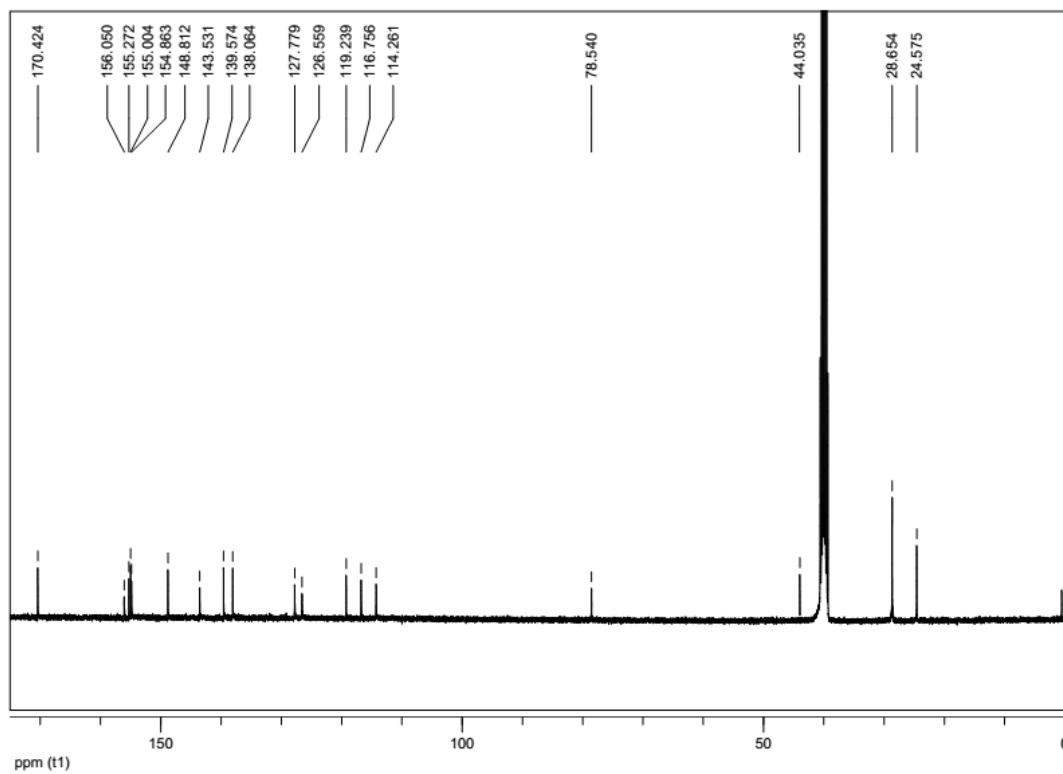


Figure A18: ¹³C NMR (DMSO-*d*₆, 100 MHz) of compound **5.1**

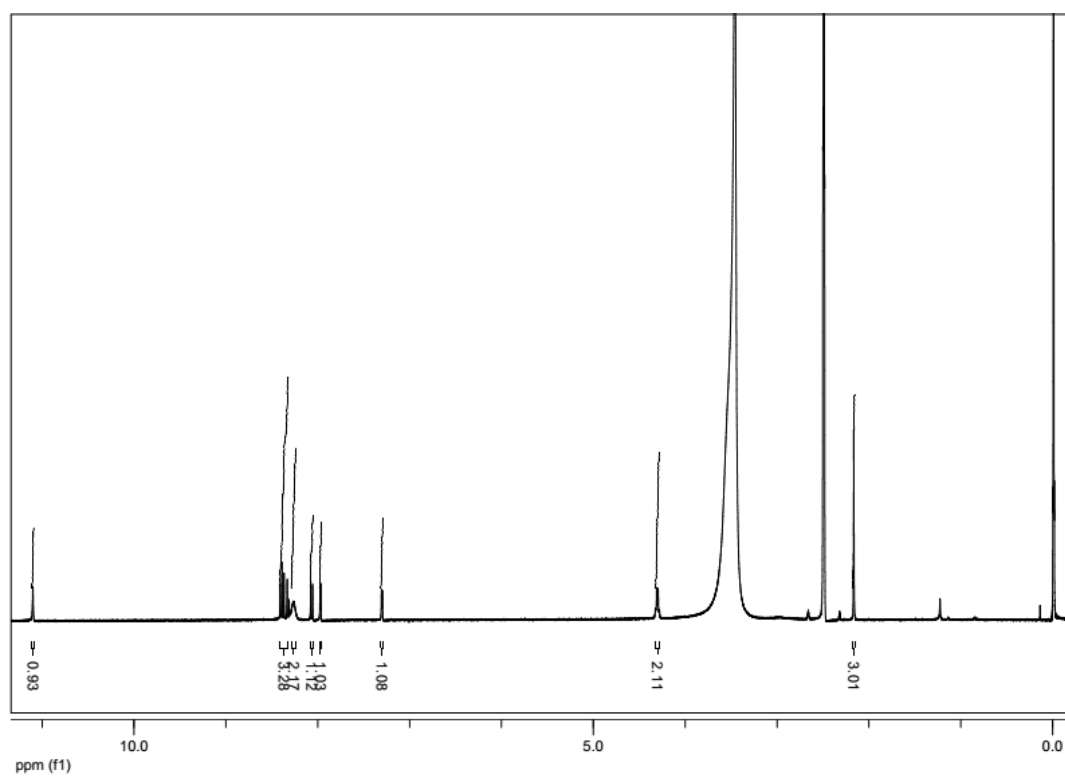


Figure A19: ¹H NMR (DMSO-*d*₆, 400 MHz) of compound **1.7**

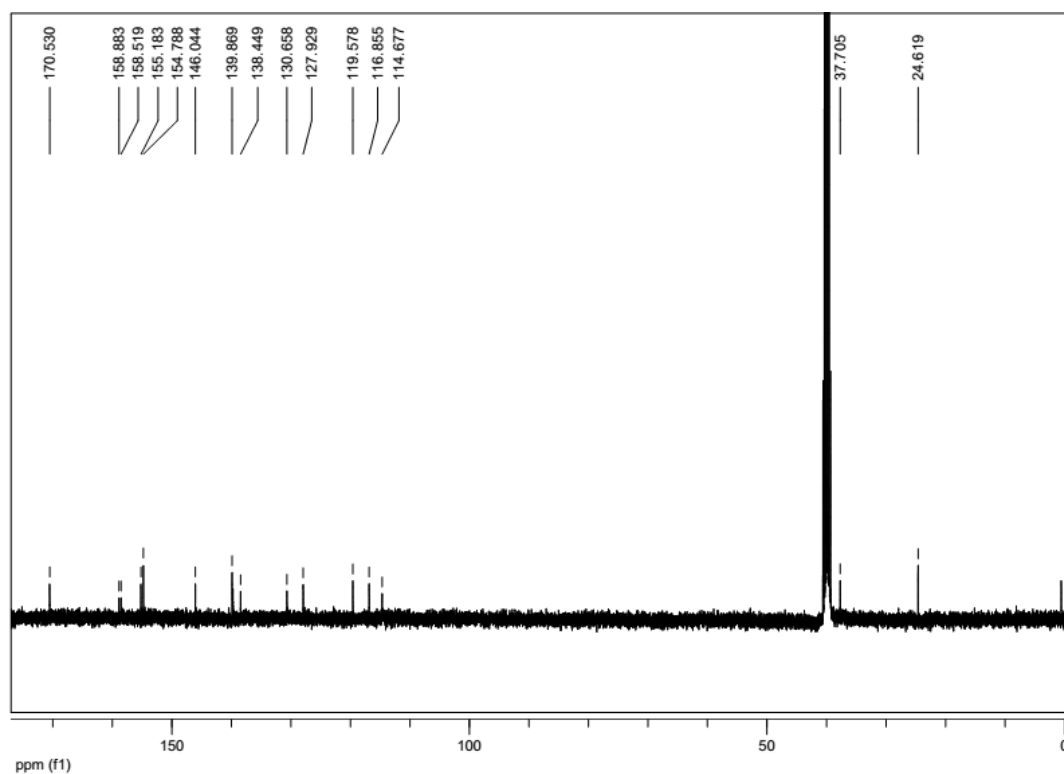


Figure A20: ¹³C NMR (DMSO-*d*₆, 100 MHz) of compound **1.7**

E. Ramanjaneya Reddy

ergamreddy8@gmail.com/ergamreddy@yahoo.com

Personal Details:

Date of Birth : 10/08/1986

Nationality : Indian

Sex : Male

Marital status : Married



Education:

2010-2015: Ph.D in Chemistry, Dr. Reddy's Institute of Life Sciences, University of Hyderabad Campus, Hyderabad, Telangana, India.

2006-2008: M.Sc (Organic Chemistry), School of Chemistry, Sri Venkateswara University, Tirupathi, Andhra Pradesh, India.

2003-2006: B.Sc (M.P.C), Loyola Degree College (YSRR), (Sri Venkateswara University), Tirupathi, Andhra Pradesh, India.

2001-2003: 12th (Inter M.P.C), Govt. Junior College, Pulivendula, Andhra Pradesh, India.

Awards and Recognitions:

- Awarded as senior research fellow (SRF) during the period 2012-2015 from CSIR. New Delhi, India.
- Awarded as junior research fellow (JRF) during the period 2010-2012 from CSIR. New Delhi, India.
- Qualified CSIR-Junior research fellowship conducted by joint council of scientific and industrial research (CSIR) – University grants commission (UGC) national eligibility test (NET) in June 2009 and 2010

List of Publications in Peer Reviewed Journals

1. Selective Multicolour Imaging of Zebrafish Muscle Fibres by Using Fluorescent Organic Nanoparticles. **Ramanjaneya Reddy, E.**; Banote, R. K.; Chatti, K.; Kulkarni, P.; Rajadurai, M. S.* *ChemBioChem* **2012**, *13*, 1889.
2. Organic Nano-Vesicular Cargoes for Sustained Drug Delivery: Synthesis, Vesicle Formation, Controlling “Pearling” states and Terfenadine Loading/Release studies. Botcha, A. K.; Dulla, B.; **Ramanjaneya Reddy, E.**; Chennubhotla, K. S.; Kulkarni, P.; Chandrasekar, R*.; Rajadurai, M. S.* *Journal of Nanotechnology* **2014**, Article ID 369139, 13 pages.
3. Passive Optical Waveguiding Tubular pharmaceutical Solids and Raman Spectroscopy/ Mapping of Nano/Micro Scale Defects. Chandrasekhar, N.; **Ramanjaneya Reddy, E.**; Prasad, M. D.; Rajadurai, M. S*.; Chandrasekar, R.* *CrystEngComm* **2014**, *16*, 4696.
4. Red Fluorescent Organic Nanoparticle Bio-Probes: A Novel Photostable Cytoplasmic Stain for Long Term *In Vitro* and *In Vivo* Visualization. **Ramanjaneya Reddy, E.**; Yellanki, S.; Medishetty, R.; Konada, L.; Alamuru, N. P.; Haldar, D.; Parsa, K. V. L.; Kulkarni, P.; Rajadurai, M.* *ChemNanoMat* **2015**, *16*, 567.
5. Fluorescent 3, 5 and 5 - Substituted Nucleosides Derivatives with Selective Antibacterial Activity. **Ramanjaneya Reddy, E.**; Yaseen, A. M.; Rizvi, A.; Deora, G.; Banerjee, S.; Sevilimedu, A.; Rajadurai, M.* *J. Med. Chem.* **2015**, submitted.
6. 1,8-Naphthyridine-Based Boronic Acid as Fluorescent Chemosensor for Hg^{2+} and D-Fructose Sensing. **Ramanjaneya Reddy, E.**; Rajadurai, M.* **2016**, manuscript is to be submitted shortly.

Presentations in Conferences and Symposiums

- 2012** Attended and presented a poster on “Selective Multicolour Imaging of Zebrafish Muscle Fibres by Using Fluorescent Organic Nanoparticles” at **Frontiers in Chemical Sciences (FICS 2012)**, held in IIT Guwahati campus, Guwahati, Assam, India, December 2-3, 2012.
- 2013** Attended and presented a poster on “Synthesis, Characterization and Application of Fluorescent Organic Nanoparticles for Biological Imaging” at **Symposium in Memory of Dr. K. Anji Reddy**, held in Dr. Reddy’s Institute of Life Sciences, HCU campus, Hyderabad, India, September 23, 2013.
- 2015** Attended and presented a poster on “Novel Fluorescent 3, 5 and’ 5 - Substituted Nucleosides Derivatives with Selective Antibacterial Activity” at **Young Scholar’s Science Cafe Meet**, held in Dr. Reddy’s Institute of Life Sciences, HCU campus, Hyderabad, India, August 10, 2015.